Politecnico di Torino

Master's Degree in Mechanical Engineering
A.Y. 2022/2023

Multi-Body analysis of the elasto-kinematic behaviour of a front double wishbone suspension for Front-Wheel-Drive light-duty commercial vehicles

Supervisor:
Prof. Enrico Galvagno

Co-Supervisor (Iveco Group):
Ing. Vittorio Dal Col

Candidate:
Nicolò Demaestri

Abstract

This Thesis is part of a wider feasibility study concerning the transition from the actual internal combustion engine to an electric motor for a Rear-Wheel-Drive light-duty commercial vehicle. Among the available solutions to implement the transition, the possibility of converting the present Rear-Wheel-Drive to Front-Wheel-Drive is investigated.
This Thesis is focused on the current double wishbone suspension of the front axle, to assess how the drivetrain affects its elasto-kinematic behaviour and provide some guidelines to the manufacturer. Considering that traditionally Rear-Wheel-Drive is the predominant architecture implemented on light-duty commercial vehicles, understanding whether Front-Wheel-Drive allows to take advantage of the design and knowledge of the actual suspension is crucial.
This Thesis is a multi-body analysis performed on Hexagon MSC Software Adams/Car, whose results are processed in MathWorks MatLab. The approach adopted to perform the task is resumed in the workflow below.
Firstly, the present Rear-Wheel-Drive model is arranged to obtain two loading conditions, which are maintained throughout the study, because this kind of vehicles belongs to the same category of passenger cars, but it is subject to a load variability that is one order of magnitude greater.
Secondly, a Front-Wheel-Drive model is derived from the initial vehicle, according to the approach of maintaining as many elements as possible. The model obtained is still powered by the initial powertrain and driveline, the latter being reverted, so that the torque flows to the front wheels. This model is not representative of a real vehicle, because the longitudinal engine layout is uncommon for Front-Wheel-Drive, but it fits the task, that is to isolate the effect of the drivetrain.
Thirdly, a set of suspension tests is performed on both front and rear axles, to validate their behaviours taking as reference the available experimental data. Subsequently, a Ramp Steer test on the initial model provides a comparison with the real vehicle handling.
Then, a set of cornering events called Power-Off Cornering and Throttle-On In-Turn is defined, according to the ISO standards. These are transient maneuvers which involve both longitudinal and lateral dynamics and allow a comparison between Front and Rear-Wheel-Drive vehicles.
At last, the double wishbone suspension of the Front-Wheel-Drive vehicle is optimized according to two different approaches and tested again, to assess the influence of both caster angle and caster moment arm over the steering system response.
A short Appendix is attached at the end of this Thesis. The first document reports the precise parameters and criteria to implement the Power-Off Cornering and Throttle-On In-Turn tests. The second document reports the problems encountered during the development of the Front-Wheel-Drive model and explains the solutions to make it work correctly and consistently.

Table of Contents

List of Figures

List of Tables

1 Introduction

1.1 Case Study

The light-duty commercial vehicle [1] involved in the present study is Iveco Daily 35S. This van has a maximum gross weight equal to 3.5t with single wheels on the rear axle and represents the lightest version of Iveco Daily, which is a wide family of vehicles up to 7.2t realized in many different configurations, each one being designed to accomplish various missions according to the customer's requirements. *Figure 1.1* shows a commercial picture of the vehicle.

Figure 1.1: Iveco Daily 35S [2].

Iveco Daily 35S is a Rear-Wheel-Drive van with a longitudinal internal combustion engine installed on the front axle, along with a 6-ratios (manual transmission) or 8-ratios (automatic transmission) gearbox. The torque is transferred to the rear axle by a propeller shaft and equally split between wheels by an open differential acting as final drive. One renowned advantage of Rear-Wheel-Drive is its ability to climb greater road inclinations, especially when the payload is fully exploited. Actually, this category of vehicles is subject to a load variation that is one order of magnitude greater with respect to passenger cars. The front suspension is a double wishbone, where a transversal leaf spring, commercially known as QuadLeaf, connects the lower control arms of both sides, acting simultaneously as a spring element and an anti-roll bar. This solution ensures compact packaging, along with a reduction in weight and cost with respect to traditional torsion bars, but is restricted to the light versions of this van. The rear suspension is a rigid axle embedding the differential box, with a pair of longitudinal leaf springs and an anti-roll bar. This is a common solution for light-duty commercial vehicles, mainly appreciated for its simple design and payload. However, it is usually associated with a poor elasto-kinematic behaviour due to the limited chances of optimization. The manufacturer offers a more expensive option with active rear suspension where both leaf springs are replaced by air springs.

2 Theoretical Background

2.1 Vehicle Dynamics

A simplified analytical model [3] of a vehicle negotiating a curve is represented in *Figure 2.1.* There are only three degrees of freedom associated with a rigid rotation in the horizontal plane, namely the longitudinal and lateral velocities along with the yaw velocity, which are defined in the vehicle reference frame [4]. Their mathematical definitions are:

$$\mathbf{V}_G = V_x\hat{\mathbf{i}} + V_y\hat{\mathbf{j}} \qquad\qquad \dot{\boldsymbol{\psi}} = r\hat{\mathbf{k}} \tag{2.1}$$

Point G indicates the vehicle centre of gravity, while point C is the instantaneous centre of curvature. The segment connecting these two points, called path radius, can be divided in its components according to the vehicle reference frame, which are respectively known as curvature radius and rotating length (less popular):

$$R = \frac{V_x}{r} \qquad\qquad S = -\frac{V_y}{r} \tag{2.2}$$

As seen in these definitions, the velocity vector is generally angled with respect to the vehicle longitudinal axis, so that a lateral velocity is present. The inclination just mentioned is called sideslip angle, whose value is typically small (less than 10°). Its definition is here reported:

$$\beta = \arctan\frac{V_y}{V_x} \approx \frac{V_y}{V_x} = -\frac{S}{R} \tag{2.3}$$

Sideslip angle literally measures how much a vehicle is slipping in the lateral direction while dealing with a curve. It is clear that a null value corresponds to a neutral condition, where the vehicle is tangential to its circular trajectory in point G, thus implying a null lateral velocity. Conventionally, a positive sideslip angle corresponds to a "nose-out" configuration, meaning that the vehicle front points outwards with respect to its circular trajectory. This behaviour is achieved below a threshold longitudinal velocity. Oppositely, a negative sideslip angle is called "nose-in" and means that the vehicle front is pointing inwards. This condition occurs at higher speeds, once the vehicle has crossed its neutral configuration.

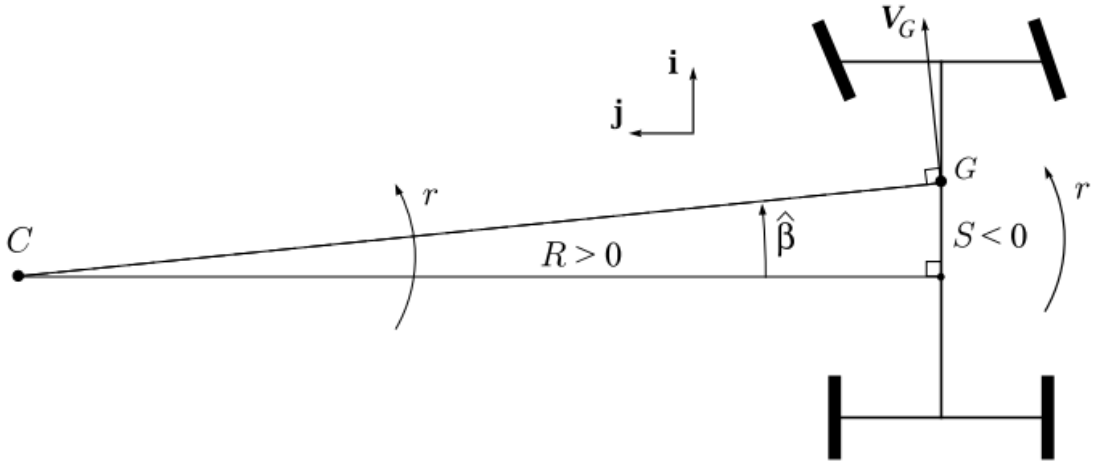

Figure 2.1: Steering - state variables [5].

Longitudinal velocity, sideslip angle and yaw velocity are the state variables commonly adopted to fully describe a vehicle engaged by a curve.

2.1.1 Kinematic Steering

Kinematic or low speed steering is based on the assumption that the vehicle longitudinal velocity is infinitely small, so that the tyres are in pure rolling condition and are not exerting any tangential force (longitudinal or lateral) to the ground. This hypothesis implies that each tyre slip angle is null, meaning that the wheel velocity vector lies in the wheel plane. *Figure 2.2* shows the Ackermann geometry, which prevents the occurrence of slip angles on tyres during a cornering maneuver. To achieve this condition, the inner wheel steer angle is greater than the outer one, so that a unique instantaneous centre of curvature is defined. The advantage is that there is no fight between the front wheels in trying to determine a unique centre of curvature, with a clear reduction in tyres wear. The wheels steer angles are related by the following relationship, involving the front axle track and the vehicle wheelbase:

$$\frac{1}{\tan\delta_{12}} - \frac{1}{\tan\delta_{11}} \approx \frac{1}{\delta_{12}} - \frac{1}{\delta_{11}} = \frac{t_1}{l} \tag{2.4}$$

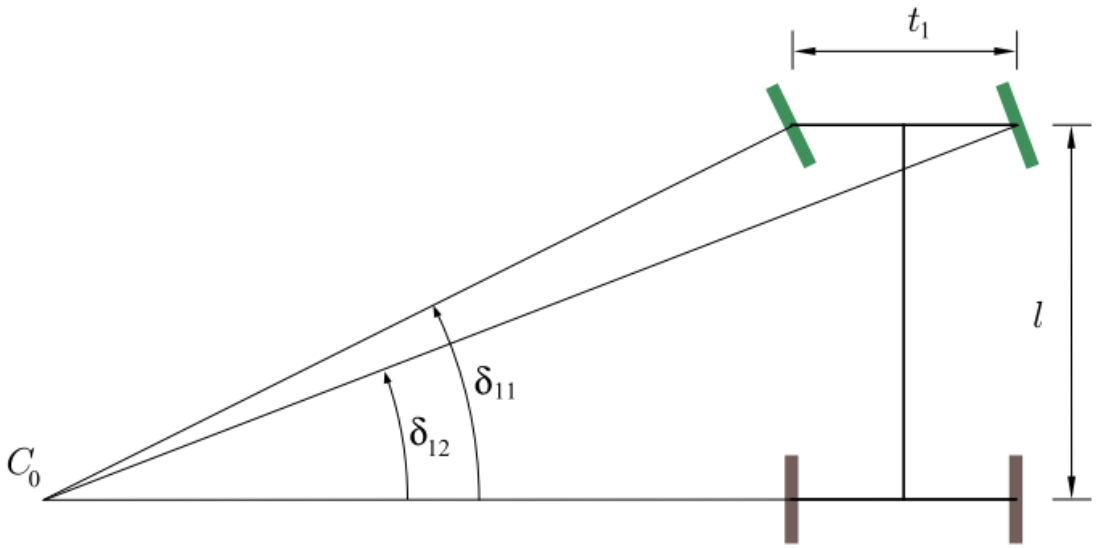

Figure 2.2: Steering - Ackermann geometry [5].

2.1.2 Dynamic Steering

When the vehicle speed is not low enough, the assumptions of kinematic steering lose validity and a dynamic steering model is required. This formulation takes into consideration the wheels slip angles, which are no more null because the pure rolling condition is not ensured, thus allowing the tyres to exert longitudinal and cornering forces. A simple way to discuss it involves the definition of a bicycle model, where the vehicle is reduced to its equivalent single-track representation. The wheels steer and slip angles are averaged between the inner and outer sides of the same axle, to obtain a unique value, as if the vehicle had just two wheels:

$$\delta_F = \frac{\delta_{FI} + \delta_{FO}}{2} \qquad \alpha_F = \frac{\alpha_{FI} + \alpha_{FO}}{2} \qquad \alpha_R = \frac{\alpha_{RI} + \alpha_{RO}}{2} \tag{2.5}$$

Figure 2.3 shows the dynamic steering model described in ISO 8855:2011 [4], which also includes a steering rear axle. Obviously most road vehicles only have steering front wheels, therefore the following condition holds:

$$\delta_F = \delta_A \qquad \delta_R = 0 \tag{2.6}$$

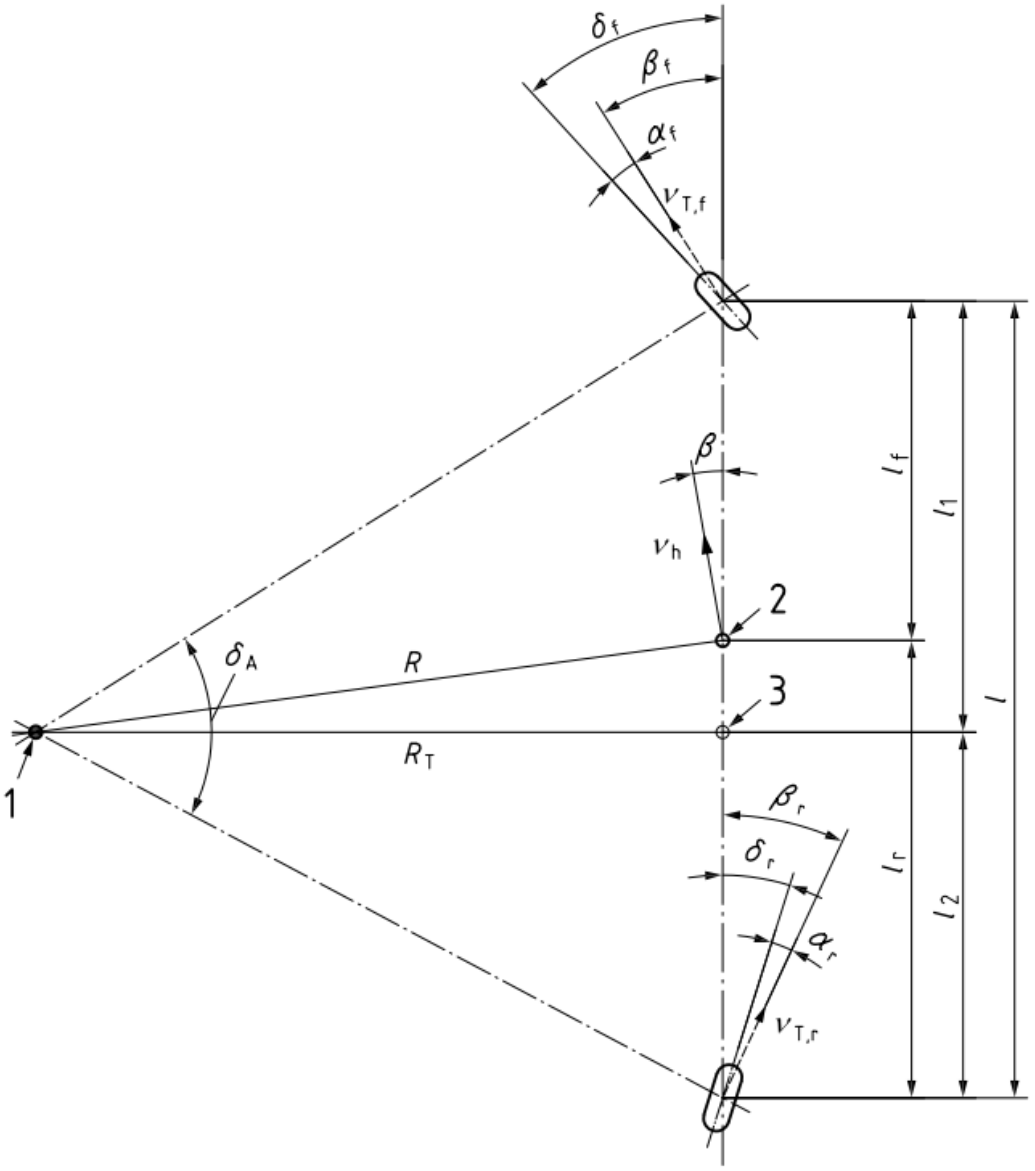

Figure 2.3: Steering - single-track model [4].

The instantaneous centre of curvature is graphically defined intersecting the lines normal to each tyre velocity vector, whose inclination with respect to the wheel plane is measured by its slip angle. The difference between the tyre steer and slip angles defines sideslip angle, which measures the inclination between the tyre velocity vector and vehicle longitudinal axis:

$$\beta_F = \delta_F - \alpha_F \qquad\qquad \beta_R = \alpha_R \tag{2.7}$$

The tyres slip angles allow to evaluate the understeering or oversteering tendency of a vehicle. A neutral behaviour consists in identical slip angles on front and rear tyres and provides a response equal to the kinematic condition, meaning that its path radius is equal to the one in kinematic steering. Nevertheless, the vehicle is not in kinematic condition, because its sideslip angle is not equal to its kinematic value and the wheels sideslip angles are not null. An understeering response corresponds to a predominant front slip angle, thus a farther instantaneous centre of curvature, meaning that the vehicle tends to widen its trajectory. Instead, an oversteering behaviour corresponds to a prevailing rear slip angle and a shorter path radius, meaning that the vehicle tends to close its trajectory and increase yaw velocity.

2.2 Tyre Dynamics

The basic behaviour of compliant tyres interacting with a rigid soil can be explained according to the brush model, where the force is applied in a single point belonging to the contact patch, which is the interface between tyre and ground. As any elastic element, a tyre can generate forces only when its brushes are deformed with respect to the rest position, so that they exert a tangential stress against the ground. Such force is generally made of a longitudinal and a lateral component, defined in the tyre local reference system:

$$\mathbf{F} = F_x\hat{\mathbf{i}} + F_y\hat{\mathbf{j}} \qquad F_x = C_x \cdot s \qquad F_y = C_y \cdot \alpha \tag{2.8}$$

- s: longitudinal slip. It measures the relative longitudinal velocity between tyre and ground. It is null in pure rolling condition and equal to 100% in case of tyre saturation, which is the condition corresponding to locking or spinning, where the tyre exerts its maximum available force, which is affected by both vertical load and friction coefficient
- α: slip angle. As seen in the previous pages, it measures the orientation of the wheel velocity vector with respect to the wheel plane. It is null when the tyre runs straight on a horizontal road or, while cornering, if the kinematic steering condition is ensured
- C_x and C_y: longitudinal and cornering stiffnesses. These are the coefficients multiplying the tyre slip in either longitudinal or lateral directions. They are affected primarily by the vertical load acting on the tyre, according to a less-than-proportional relationship

It is possible to state that a tyre exerts a longitudinal force every time a vehicle is accelerating or braking, while it generates a lateral force when the vehicle negotiates a curve. In real world, tyres are often stressed in both directions simultaneously, thus experiencing a condition called combined slip, where the total available grip is split into two tasks. To understand how the vehicle dynamics and ultimately handling are affected, the understeer gradient is introduced:

$$\alpha_F - \alpha_R = \delta_{sw} - \delta_0 = \left(\frac{m_F}{C_{yF}} - \frac{m_R}{C_{yR}}\right) \cdot a_y = K_{us} \cdot a_y \tag{2.9}$$

As previously anticipated when discussing the single-track model, the difference between front and rear slip angles is indicative of how a vehicle departs from the ideal neutral condition. Particularly, a positive difference corresponds to a wider path radius, which is the definition of understeer itself. An equivalent formulation is the difference between the actual steering wheel angle and its value in kinematic condition, which is again positive in case of an understeering behaviour. The static mass distribution affects the overall behaviour of a vehicle, which tends to suffer understeer when the front axle is more loaded, as in the majority of passenger cars. Instead, commercial vehicles are usually subject to significant mass variations on the rear axle, which can result in neutrality or eventually oversteer when the whole payload is exploited. Besides the static load distribution, it is important to consider the load transfer occurring every time a vehicle is subject to longitudinal accelerations, which involves the cornering stiffnesses of front and rear wheels. Specifically, a braking maneuver loads more the front tyres, which increase their cornering stiffness, while the opposite happens on the rear axle. The overall effect is a reduction in understeer, which eventually turns into oversteer. Instead, a strong acceleration loads more the rear wheels, thus enhancing their cornering stiffness and leading to the opposite phenomenon, which results in additional understeer. These simple considerations explain why a vehicle braking or simply decelerating in curve tends to close its trajectory, while it is likely to widen it when the accelerator pedal is pushed more. The latter observation does not contemplate power oversteer, a behaviour typical of Rear-Wheel-Drive sporty cars.

2.3 Suspensions

Any road vehicle is provided with suspensions, which are part of the chassis [6]. Their task is to connect the wheels to the body, while ensuring an optimal tyre-ground contact and providing a filter against the road irregularities to ensure people's comfort. At the same time, suspensions play a structural role and are responsible for the vehicle road-holding ability during longitudinal and cornering maneuvers, thus affecting both safety and handling. Road vehicles suspensions are classified by the degree of interaction between the wheels belonging to the same axle:

- Dependent: rigid connection through a solid axle, the wheels travels affect each other
- Independent: no rigid connection, a wheel travel does not affect the other one

Dependent suspensions are typically associated to simple designs, low maintenance, almost constant track, uniform tyre wear and huge achievable payloads. On the other hand, such a simplicity leaves no room to setup the wheels and to optimize its elasto-kinematic behaviour, thus generally resulting in lower handling and comfort. Moreover, they are known for their significant contribution to the unsprung mass and their greater cargo height. Solid axles appeared first historically and nowadays are no more employed in passenger cars, but they still represent the standard solution for Rear-Wheel-Drive commercial vehicles and are commonly known as live axles, where a hollow beam embeds the differential box and drive shafts. The case study is provided with single leaf springs, which reduce the hysteresis typical of multi-leaf springs, usually associated with an increase in friction and a poor elasto-kinematic behaviour. The two sides of the suspension are connected by an anti-roll bar, to increase the quite low roll stiffness typical of solid axles. Leaf springs allow to reduce the overall complexity with respect to coil springs, which would require additional mechanical linkages such as a Panhard bar and longitudinal guidance, to compensate their low transversal and longitudinal stiffnesses respectively. Concerning independent suspensions, they exist in a variety of schemes, which obviously represent different compromises in terms of packaging, performance, complexity and cost. It is no secret that the kind of suspensions represents a marketing tool and contributes to define the customers segment a car addresses. The case study is provided with a low double wishbone suspension on the front axle, which is suitable for a longitudinal engine layout, but would probably give some packaging issues in case of a small utilitarian car powered by a transversal engine, where a McPherson or a high double wishbone suspension would be more appropriate. The coil springs are replaced by a transversal single leaf spring, which connects the lower control arms of both sides and acts simultaneously as vertical and roll stiffness. This solution results in lower bulkiness, complexity and cost, but is suitable for small commercial vehicles only, due to the limited weight it is able to carry.

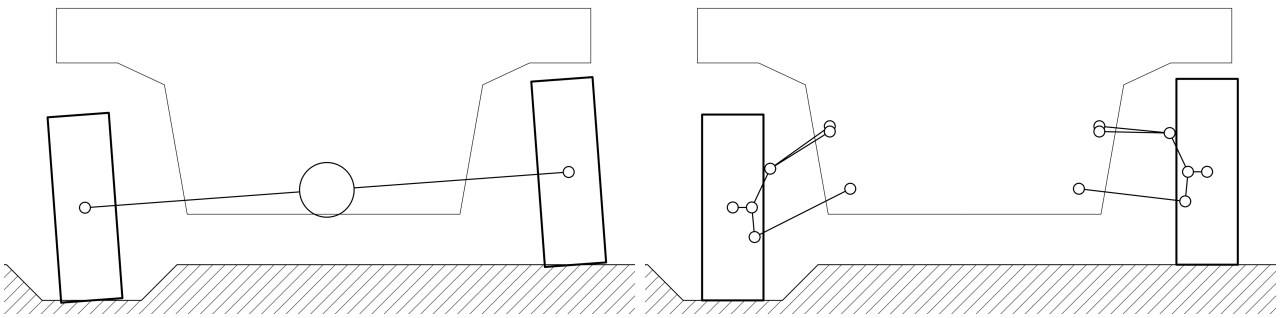

(a) Front View - dependent rear wheels. *(b) Front View - independent front wheels.*

Figure 2.4: Case Study - suspensions reacting to road irregularities.

2.4 Suspensions Parameters

The behaviour of any road vehicle is influenced by a few suspension parameters, which determine the overall setup. Some of these can be modified applying some adjustments to the suspension and steering components, while others are defined by designers and cannot be modified without modifying some mechanical components.

2.4.1 Wheel Setup

The wheels setup parameters affect the orientation of each wheel with respect to the vehicle body. They can affect a vehicle reactivity and its tendency to understeer and become crucial in optimizing the tyres wear. The case study is schematized in *Figure 2.5* and highlights these parameters, whose definitions are reported from Adams Help [7]:

- Toe angle: it is the angle between the longitudinal axis of the vehicle and the line of intersection of the wheel plane, in the top view. It is positive, also known as toe-in, if the wheel front is rotated in towards the vehicle body. On the other hand, a negative angle is called toe-out. *Figure 2.5a* shows a toe-in configuration. On dependent suspensions, the wheels toe angle is usually null and almost insensitive to any bump or rebound motion
- Camber angle: it is the angle the wheel plane makes with respect to the vertical axis of the vehicle. It is positive when the top of the wheel leans outward from the vehicle body. Camber angle should not be confused with the inclination angle, which is identified between the wheel plane and the axis normal to the ground. These two angles coincide when the vehicle body roll angle is null. *Figure 2.5b* shows a positive camber and the corresponding inclination. Dependent suspensions are known for their full camber recovery property, meaning that the body roll does not affect the wheels inclination, so that they keep perpendicular to the ground, apart from the elastic deformations of the solid axle

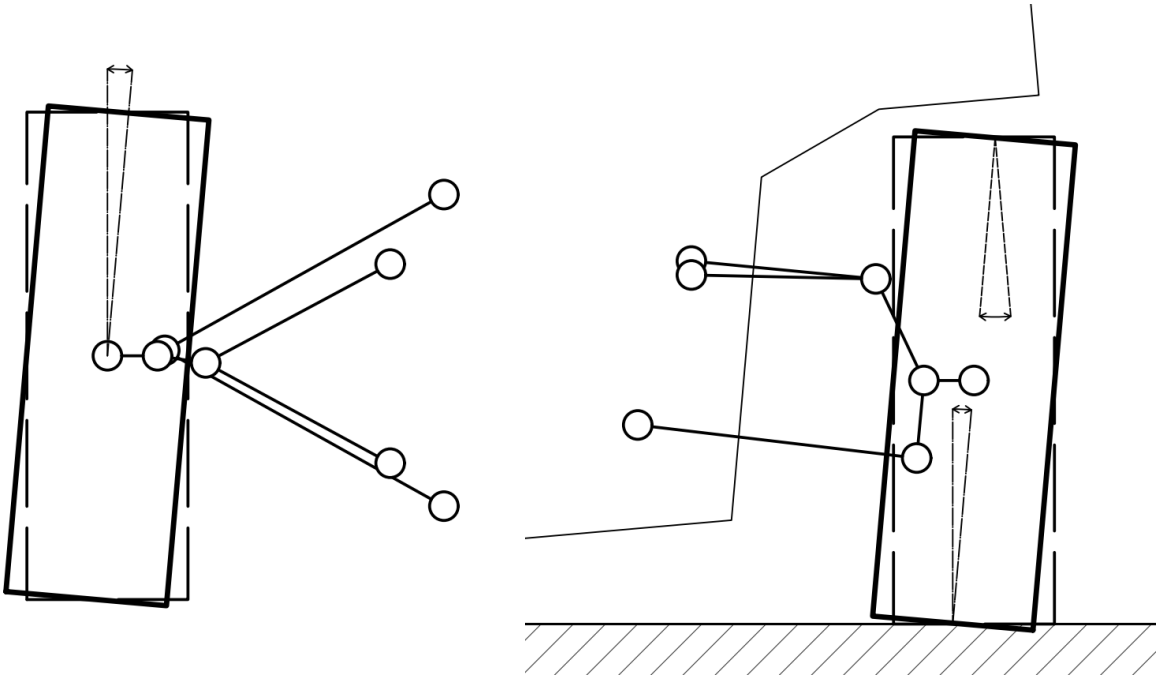

(a) Top View - driving direction upwards. *(b) Front View - driving direction outwards.*

Figure 2.5: Case Study - toe and camber angles.

2.4.2 Steering Geometry

The front suspension of a road vehicle affects the forces exchanged between the wheels and the steering system, which ultimately gives a feedback to the driver. The suspension geometry determines the kingpin axis, around which the wheel steers when the driver rotates the steering wheel. On double wishbone suspensions, the axis is given by the intersection of the spherical joints connecting the upper and lower control arms to the upright. The case study is schematized in *Figure 2.6* and highlights the suspension parameters involving the kingpin axis [7]:

- Caster angle: it is the angle between the kingpin axis and the vertical axis of the vehicle, in the lateral view. It is positive when the kingpin axis is inclined upward and rearward. *Figure 2.6a* shows a positive caster angle, a feature shared by most road vehicles nowadays
- Caster moment arm (mechanical trail): it is the distance from the intersection of the kingpin axis and the road plane to the tyre contact patch measured along the intersection of the wheel plane and road plane, in the lateral view. It is positive when the intersection of the kingpin axis and road plane is forward of the tyre contact patch. *Figure 2.6a* shows a positive mechanical trail, typical of many vehicles thanks to the improved stability
- Kingpin angle: it is the angle between the kingpin axis and the vertical axis of the vehicle, in the front view. It is positive when the kingpin axis is inclined upward and inward. *Figure 2.6b* shows a positive kingpin angle, which is typical of most road vehicles
- Scrub Radius: it is the distance from the intersection of the kingpin axis and the road plane to the tyre contact patch measured along the intersection of the wheel plane and road plane, in the front view. It is positive when the intersection of the kingpin axis and road plane is inboard of the tyre contact patch. *Figure 2.6b* shows a positive scrub radius, which is typically present on double wishbone suspensions, while it can be slightly negative on McPherson architectures to improve stability in case of split-μ braking

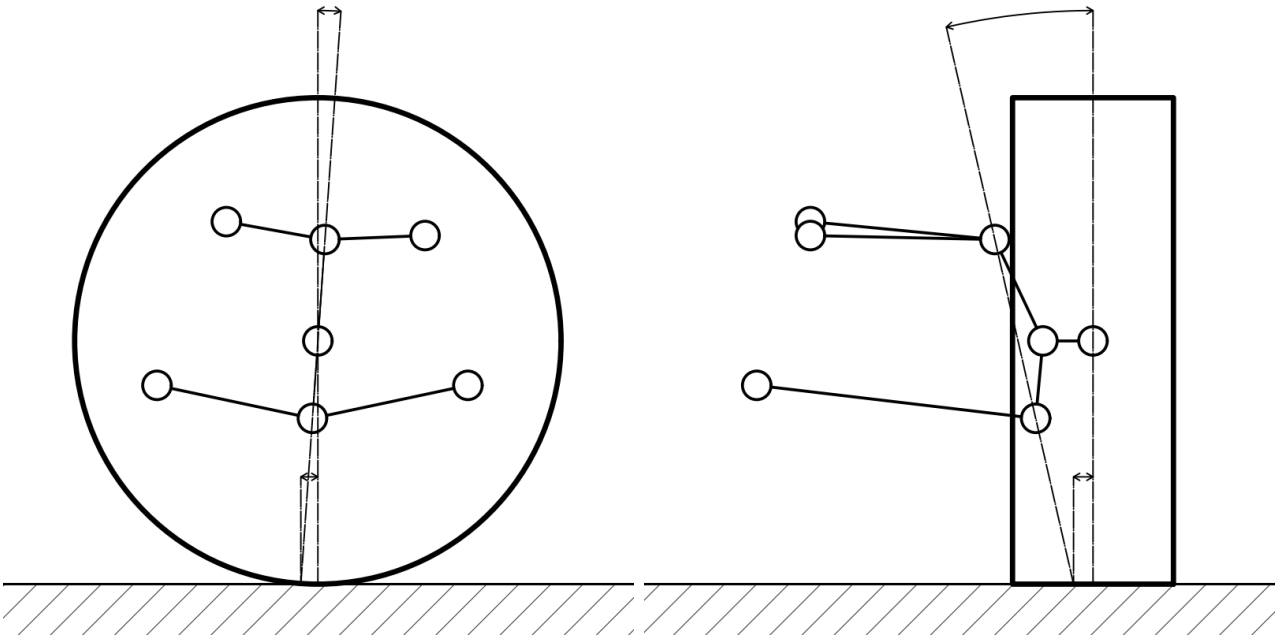

(a) Lateral View - driving direction leftwards. *(b) Front View - driving direction outwards.*

Figure 2.6: Case Study - mechanical trail and scrub radius.

2.5 Drivetrain

Most road vehicles transfer the engine torque to the ground through one pair of wheels belonging to the same axle, which are called driving wheels, while the wheels belonging to the passive axle are known as driven wheels. It is possible to make a simple classification:

- Front-Wheel-Drive: driving front wheels, driven rear wheels
- Rear-Wheel-Drive: driving rear wheels, driven front wheels

Front-Wheel-Drive dominates the market of utilitarian cars, which address the majority of customers thanks to their moderate prices. These vehicles are provided with smaller engine displacements and have compact sizes, which make them ideal for urban driving. Given their nature, the drivetrain must satisfy a few constraints, such as low bulkiness, complexity and cost. These are the reasons why a transversal engine layout in combination with Front-Wheel-Drive is the optimal architecture. These vehicles are not expected to express astonishing performances, because the front wheels must exert both driving and cornering forces to the ground, giving a condition already described as combined slip, which prevents the tyres from fully exploiting their available grip in one of these two fields. This means that during a cornering maneuver, the lateral forces achievable by the front wheels are limited by the simultaneous driving torque they have to apply to the ground. This phenomenon results in an understeering response, where the effective trajectory achieved by the vehicle is wider with respect to the expected one. While this behaviour is not desirable in race cars, it is appreciable in passenger cars, because most people do not have professional driving skills. An understeering vehicle is easier to handle, because the driver can usually avoid troubles just releasing the accelerator pedal. In the field of commercial vehicles, Front-Wheel-Drive is not considered an industrial standard, because it is usually associated with a reduction in the available traction when a longitudinal load transfer towards the rear axle takes place. Such an event occurs every time the vehicle accelerates, climbs a sloped road or simply exploits its entire payload to convey goods. On the other hand, Rear-Wheel-Drive appeared first historically thanks to its mechanical simplicity but is nowadays associated with sporty and luxury cars, which address a small portion of customers due to their high prices. These vehicles are provided with bigger engine displacements and have greater dimensions, which make them ideal for suburban driving. The drivetrain is more complex, because it requires a propeller shaft to connect the engine, typically arranged in a longitudinal layout, to the rear wheels. The shaft also subtracts some space to the cabin and would be hardly implementable in utilitarian cars. These vehicles are generally considered more performing, because the front wheels are dedicated to steering while the rear wheels transfer the driving torque to the ground. The result is a less understeering or eventually oversteering response in cornering maneuvers, meaning that the vehicle is likely to close its trajectory with respect to the expected one. This behaviour is appreciated by passionates and professional drivers, but it is not desirable for most people, who are not trained to safely handle these cars. An unskilled driver facing power oversteer might react reducing the throttle, thus resulting in a complete loss of control. Instead, the opposite reaction together with countersteering would allow to regain control of the vehicle. In the market of commercial vehicles, Rear-Wheel-Drive can be considered the industrial standard, because the longitudinal load transfer towards the rear axle is beneficial to the available traction. Clearly, these vehicles are not designed for sporty driving, but they represent a prosperous field of application of Rear-Wheel-Drive. This Thesis is focused on both drivetrains. The case study is a Rear-Wheel-Drive vehicle, which is converted into a hypothetical Front-Wheel-Drive version to investigate how different drivetrains affect the behaviour of the front suspension. The following pages explain the qualitative response expected during both straight driving and cornering.

2.5.1 Rear-Wheel-Drive

Figure 2.7 shows the front left wheel of the case study to understand how Rear-Wheel-Drive is expected to affect the forces exchanged between the front wheels and the steering system during straight and cornering maneuvers. Looking at the system from the top, two points of interest are highlighted, precisely the tyre-ground contact point, where the tyre forces are applied and the kingpin axis projection on the ground, which acts like a hinge. The former is simply assumed to be placed in the middle of the contact patch, thus neglecting the presence of pneumatic trail, while the latter is given by caster moment arm and scrub radius, which are both positive in the case study. Looking at *Figure 2.7a*, when the engine supplies a driving torque on a straight trajectory, the front wheel applies a resistant torque to the ground, function of the rolling resistance. This longitudinal resistant force generates a counterclockwise torque around the hinge, making the wheel more likely to assume a slight toe-out, while pulling the tie rod. Actually, when the engine supplies a braking torque on a straight trajectory as shown in *Figure 2.7b*, the front axle does not experience any difference, because the rear wheels are the only ones braking the vehicle. Therefore, the front wheel still exerts a longitudinal resistant force, which eventually decreases due to the reduction in vehicle speed, thus relieving the pulling action on the tie rod and allowing the wheel to partially recover from toe-out. Clearly, the behaviour of the front suspension during straight line driving is mainly influenced by the scrub radius, which is the arm giving a torque due to the longitudinal tyre force. Instead, the caster moment arm plays a role when the vehicle negotiates a curve, because it affects the moment exerted by the wheels around the kingpin axis, meaning that it contributes to the vehicle stability and handling. If the front suspension had a null caster moment arm, the driver would feel an empty steering wheel and would not receive any feedback from the wheels, leading to the impossibility to understand their actual steer angle. Moreover, the wheels would be sensitive to any road irregularity, making the driver struggle to keep them in the desired position. Concerning the suspension behaviour in cornering maneuvers, here schematized in *Figures 2.7c and 2.7d*, on Rear-Wheel-Drive vehicles it is possible to neglect the longitudinal resistant force with respect to the lateral component, because there is at least one order of magnitude of difference. Having a positive and quite relevant caster moment arm results in a clockwise torque due to the cornering force, which is barely affected by a driving or braking action. The main effect given by a longitudinal maneuver is a change in vehicle speed, which turns into a variation in lateral acceleration which modifies the lateral load transfer, finally resulting in a different cornering force and restoring torque. Clearly, the outer wheel exerts a huge cornering force, especially at greater lateral accelerations and compensates for the kinematic reduction in caster moment arm due to the steer angle typical of double wishbone suspensions. For this reason, the outer wheel is expected to provide the greatest contribution to the restoring torque. The torque mentioned should not be confused with the tyre self-aligning moment, related to the pneumatic trail.

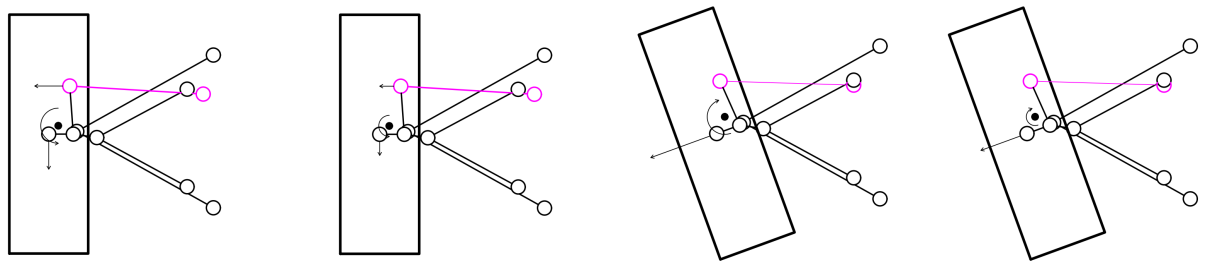

(a) Straight driving. *(b) Straight braking.* *(c) Cornering driving.* *(d) Cornering braking.*

Figure 2.7: Rear-Wheel-Drive - Top View (driving direction upwards).

2.5.2 Front-Wheel-Drive

Figure 2.8 shows the responses expected by a Front-Wheel-Drive vehicle in all four scenarios. When the engine supplies a driving torque on a straight trajectory as shown in *Figure 2.8a*, the front wheel exerts a longitudinal driving force, whose magnitude depends on the engine torque. This force provides a clockwise torque around the hinge which makes the wheel assume a toe-in, along with a pushing action on the tie rod. Looking at *Figure 2.8b*, when the engine supplies a braking torque, the wheel longitudinal force reverts its direction and generates a counterclockwise torque, corresponding to a toe-out and a pulling force on the tie rod. This means that the tie rods work both in compression and traction, while they were expected to work only in traction on a Rear-Wheel-Drive. When considering a cornering maneuver, the assumption made for Rear-Wheel-Drive vehicles is not acceptable, because the tyre longitudinal force is no more negligible with respect to the cornering one, although the latter still prevails. For this reason, when the engine supplies a driving torque, even at constant speed, as in *Figure 2.8c*, the front wheel exerts a greater self-aligning moment with respect to Rear-Wheel-Drive. This happens because the longitudinal and lateral components provide a resultant with greater modulus and arm compared respectively to the cornering force and the caster moment arm alone. When the engine supplies a braking torque as in *Figure 2.8d*, as previously seen in straight maneuvers, the wheels assume a toe-out. The balance of effects on inner and outer sides, along with the suspension elasto-kinematic behaviour cannot be easily predicted, but as it will be possible to see in the Chapter dedicated to Power-Off Cornering, the overall result is a temporary increase in both wheels steer angles, accompanied by a sudden reduction in steering wheel torque required to the driver to hold it in position. Anyway, the progressive decrease in speed, hence in lateral acceleration later leads to a reduction in cornering forces, therefore to a gradual lowering in the restoring torque, as seen in Rear-Wheel-Drive. Instead, when the throttle is pushed further to accelerate the vehicle, the front wheels are expected to load more the tie rods in compression, because they are increasing their toe-in. The opposite combined phenomenon occurs and leads to a progressive reduction in the wheels steer angles, thus to a greater torque required to the driver. The vehicle progressively achieves greater lateral accelerations, so that the cornering forces grow together with the longitudinal ones, giving an overall increase in the restoring torque. Overall, during a cornering maneuver a Front-Wheel-Drive vehicle can be assumed to give a similar response to its Rear-Wheel-Drive counterpart, but it should be interested by a transient missing on the latter, due to the combined effect of longitudinal and cornering forces. The longitudinal component can be highly variable in short times when the driver exerts a pushing or releasing action on the accelerator pedal and therefore it gains relevance faster with respect to the lateral component, which is only depending on the lateral load transfer and clearly takes a longer time to balance the effects of throttle modulation.

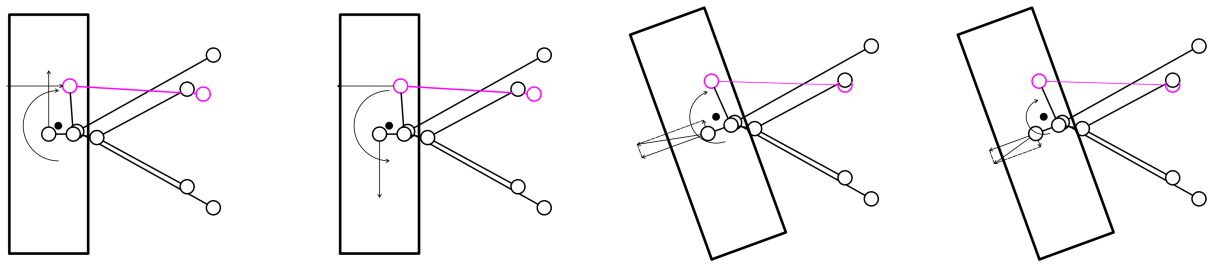

(a) Straight driving. *(b) Straight braking.* *(c) Cornering driving.* *(d) Cornering braking.*

Figure 2.8: Front-Wheel-Drive - Top View (driving direction upwards).

3 Adams/Car Model

3.1 Rear-Wheel-Drive

The starting point of this study is the current Adams/Car Rear-Wheel-Drive model, which is shown in *Figure 3.1* as provided by the manufacturer. The model requires a few adjustments to implement two different loading conditions and a simple intervention on the steering system, whose detailed explanation is attached in the Appendix. The several subsystems composing the full-vehicle assembly are discussed in the next few pages.

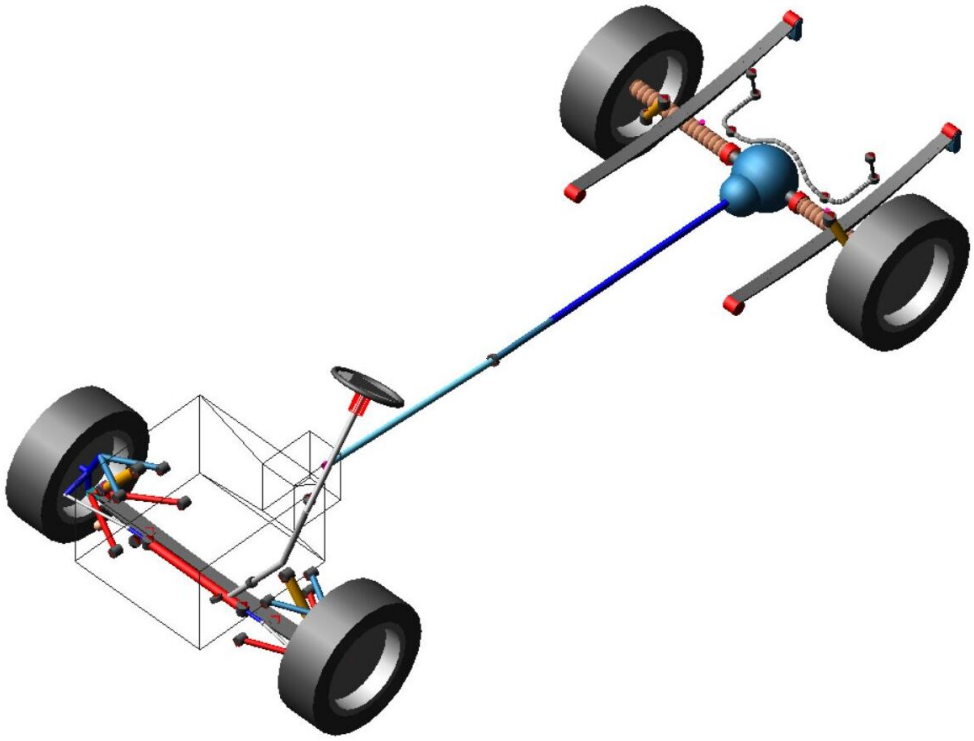

Figure 3.1: Rear-Wheel-Drive - full vehicle.

3.1.1 Front Axle

The front axle is shown in *Figure 3.2a*. It is a double wishbone suspension with a transversal single leaf spring which acts as both the elastic element and anti-roll bar due to the coupling of both sides. The leaf spring is a beam made of 40 discrete elements, 20 per each side starting from its symmetry plane. It has a slightly concave geometry typical of leaf springs and is connected to the lower control arms by one bushing per side. This modelling is not faithful to the real suspension, where the leaf spring is directly resting on the lower control arms, thus giving a contribution to the uncertainty about the cornering stiffness of the front axle. Another pair of symmetric bushings is used to connect the body subsystem to the leaf spring. The mechanical linkages of the suspension (arms, tie rods, upright) are modelled as infinitely rigid. The hinges of both upper and lower control arms are made of bushings, while the connections between the arms and the upright is achieved by spherical joints. Each tie rod is connected to the upright by a spherical joint and by a constant velocity joint to the steering rack. Concerning the spindle, it is made of a spherical joint coincident with a bushing, to properly simulate a bearing. Finally, two hook joints connect the lower strut to the lower control arm and two cylindrical joints couple the upper and lower struts.

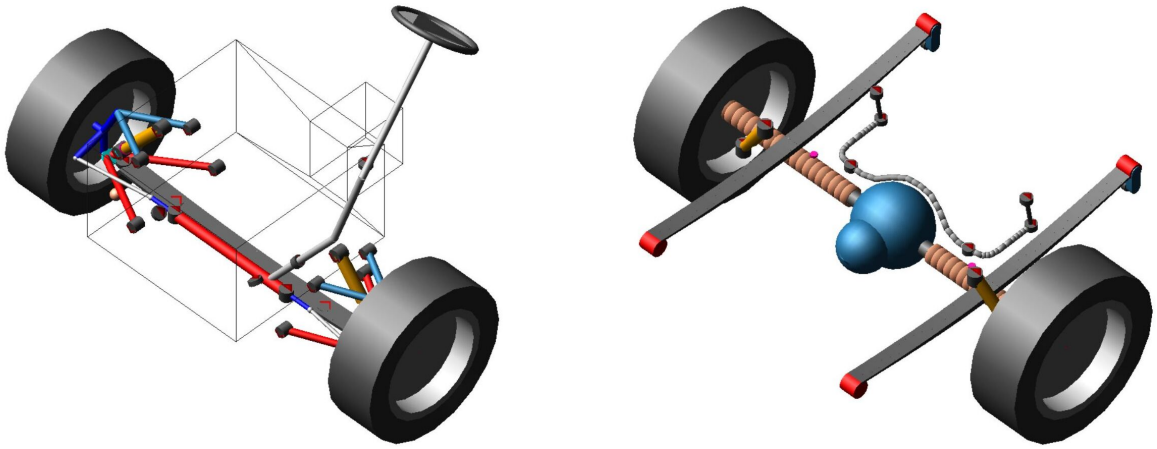

(a) Front axle. *(b) Rear axle.*

Figure 3.2: Rear-Wheel-Drive - front and rear axles.

3.1.2 Rear Axle

The rear axle is shown in *Figure 3.2b*. The rigid axle is modelled as a beam made of 22 discrete elements, 11 per each side. In the middle, the differential box is mounted by two fixed joints to the inner elements of the axle. The spindles are modelled by a spherical joint coincident with a bushing, as in the front axle. A set of hook joints allow the interaction between the rigid axle, the body and the upper and lower struts. These latter are also connected one to each other by cylindrical joints, as in the front axle. The drive shafts and tripots interact with the differential box by constant velocity and translational joints, while another constant velocity joint transmits the motion to the spindle. The leaf springs are both modelled as beams made of 38 elements each. Their ends are connected to the body by sets of bushings and revolute joints. Their elastic deformation is allowed by a shackle, a mechanical component behaving as a rocker, placed on the tail of the chassis. The connection between each leaf spring and the rigid axle is achieved by fixed joints. Finally, the anti-roll bar is made of 26 elements and is connected both to the rigid axle and the chassis by a set of bushings. At last, the damping action is provided by a pair of shock absorbers as in the front suspension.

3.1.3 Steering System

The steering system of the case study has been investigated extensively in [8] and [9]. The model implemented in this Thesis is shown in *Figure 3.3a* and includes a steering wheel, a three-pieces steering column and the rack-pinion mechanism. The steering wheel is connected to the upper shaft by both a revolute and a translational type joints, while each pair of shafts is coupled by constant velocity joints. The lower shaft is connected to the pinion by a perpendicular and a revolute joint, along with a bushing acting as a torsion bar. The torsional damping coefficient of this attachment requires tuning, as explained in detail in the Appendix. The rack housing is connected to the pinion by a revolute joint, to the rack itself by a translational joint and to the chassis by a pair of bushings. Finally, the steering subsystem contains power steering, which can be activated or deactivated by the logical value contained in a dedicated parameter variable. The default configuration is without power steering and will be implemented in all tests concerning the comparison between Front and Rear-Wheel-Drive vehicles. It will be activated only in the last Chapter, which concerns the optimization of the front suspension the Front-Wheel-Drive.

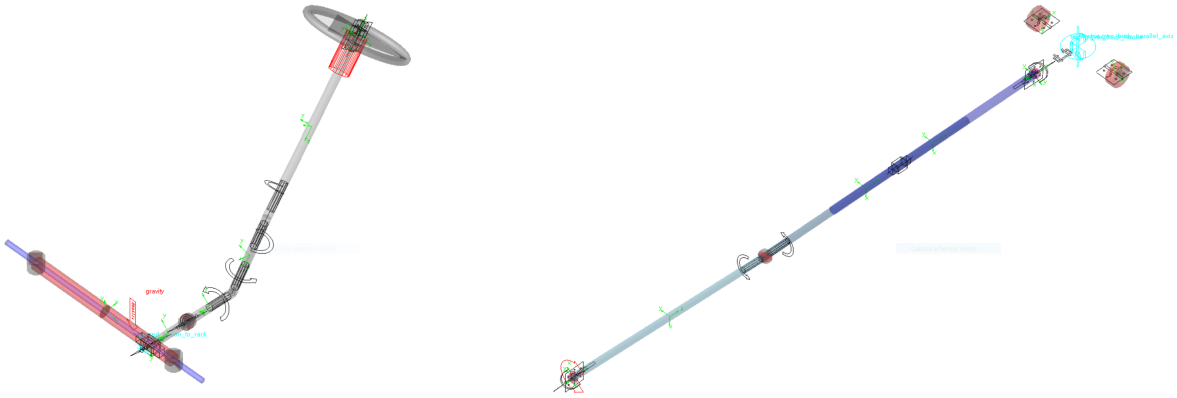

(a) Steering system. *(b) Driveline.*

Figure 3.3: Rear-Wheel-Drive - steering system and driveline.

3.1.4 Driveline

The driveline subsystem is shown in *Figure 3.3b*. It models the propeller shaft and differential outputs. The shaft is made of three elements and connects the gearbox output to the differential box on the rigid axle. It is modelled as infinitely rigid and is mounted to the body by a single bushing. Following the torque flow, the first element is a joint force which communicates the torque arriving from the gearbox. Then, a universal joint connects the gearbox output to the first part of the shaft. The following attachment is the already mentioned bushing. Together with this element, there is a constant velocity joint, coupling the first and the second elements of the shaft. This joint allows a slight relative inclination of the two components. Subsequently, a translational joint connects the second and the third elements of the shaft, allowing an axial clearance. Finally, a universal joint and a coupler allow to split the shaft torque into two equal parts to the differential outputs. These two elements are linked to the drive shafts and tripots of the rear axle by a few communicators, so that their motion is finally transferred to the wheels.

3.1.5 Powertrain

The powertrain subsystem contains data about engine (engine characteristic, revolution speed limits), gearbox (gear ratios), clutch (stiffness, damping, inertia) and final drive. An additional engine subsystem is used to model the inertia properties of the powertrain and is connected by three bushings to the body. This is the third greatest contribution to the sprung mass.

3.1.6 Body

The body subsystem includes a cab and a van, which represent the main contributions to the sprung mass and the chassis, which is made of two longitudinal beams crossing the vehicle. The inertia properties and centre of gravity locations of the two former elements are modified to obtain different loading conditions according to the available experimental data:

- Unladen: empty vehicle, front axle more loaded, greater centre of gravity height. It is the testing condition where the van is carrying nothing
- Laden: full payload, rear axle slightly more loaded, lower centre of gravity height. It is the testing condition where the van is loaded with sandbags

The body parts are modelled as infinitely rigid and connected one to each other by a set of bushings. Finally, the body subsystem is also responsible for the aerodynamic resistance.

3.2 Front-Wheel-Drive

The Front-Wheel-Drive full-vehicle assembly is shown in *Figure 3.4*. The reasoning followed to convert Rear-Wheel-Drive to Front-Wheel-Drive is based on mirroring the initial drivetrain, so that the engine longitudinal layout is preserved and the already present transmission can be exploited with a few adjustments. This model allows to preserve the actual internal combustion engine characteristic, together with the existing manual transmission and final drive, hence exploiting the available information without needing to introduce further assumptions. On the other hand, this approach implies that the model is not optimized for Front-Wheel-Drive, meaning that the driveline is not specifically designed to address a real Front-Wheel-Drive vehicle. As previously explained, since this study is primarily focused on the influence of drivetrains over the front suspension behaviour and consequently over vehicle handling, there is no necessity to investigate how to properly implement a Front-Wheel-Drive on a real van. For the same reason, some interferences are taking place on the front suspension, between the transmission and suspension components. Clearly, packaging is not investigated, because this transmission layout is only a matter of functionality, since the entire powertrain will be transformed in case of an electric vehicle. Overall, the main subsystems modified to obtain a Front-Wheel-Drive model are the front and rear suspensions along with driveline, while some adaptations in the logic part of powertrain and body subsystems are needed. The front suspension mainly requires the addition of a driveline and a differential box, while on the rear suspension these elements are obviously removed. About the transmission, together with the modification of its logic, the most relevant intervention concerns the propeller shaft, which must be downsized and changed in both location and orientation. Similarly, powertrain involves the adjustment of a few communicators which need to be matched with the front axle. Finally, the body only requires some additional communicators to match it with the differential box, while the loading conditions are kept identical to the ones already discussed for Rear-Wheel-Drive vehicles. The detailed approach to obtain Front-Wheel-Drive is explained in the next few pages.

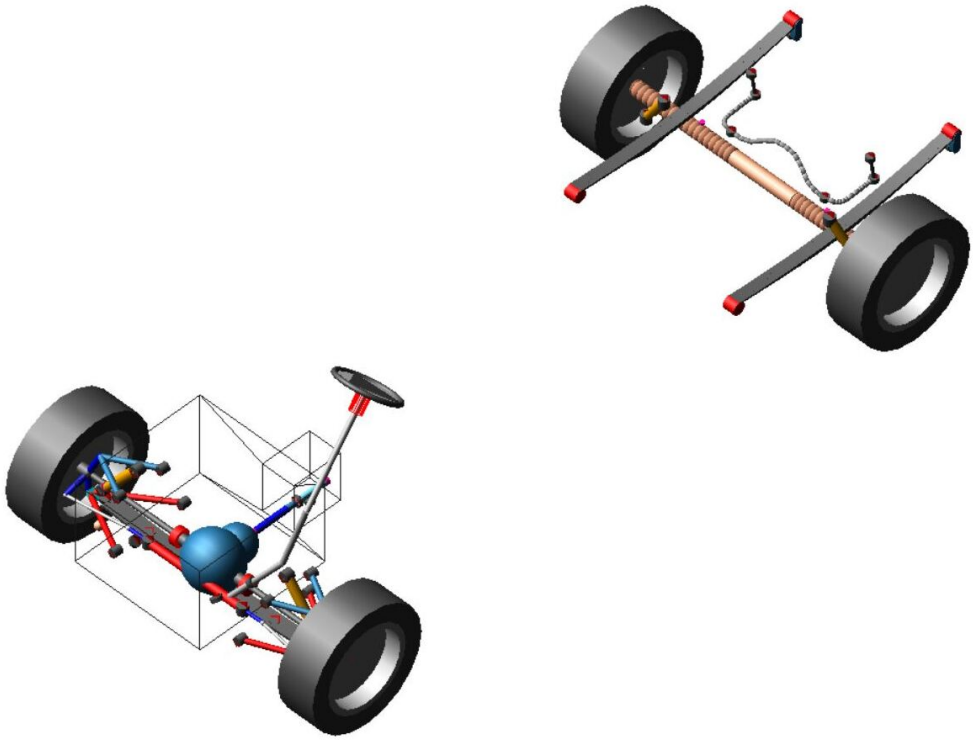

Figure 3.4: Front-Wheel-Drive - full vehicle.

3.2.1 Front Axle

The front axle is shown in *Figure 3.5a*. The suspension geometry is preserved, as well as the steering system and transversal leaf spring. The differential box is derived from the rear suspension and belongs to the front suspension subsystem, but it is no more part of the unsprung mass. Instead, it is connected to the chassis in three non-aligned points, thus becoming part of the sprung mass, as it is in any independent suspension. Clearly, the addition of a differential on the front axle implies a slight shift in the static load distribution, so that the front wheels of this vehicle are a little more loaded with respect to Rear-Wheel-Drive, provided that the body loading configurations are not changed to compensate this slight weight shift. At the same time, the propeller shaft is obviously shortened and leads to a barely noticeable decrease in the overall vehicle mass. The main job involves the front suspension template, which is modified according to the following steps:

1. Parameter variable *pvs_driveline_active*: it is set equal to 1, which corresponds to the activation of group *driveline_active*, already containing the drive shafts and tripots parts along with their joints and communicators. These parts are slightly modified acting on the related hardpoints, so that the drive shafts are coaxial with the wheels centres, hence parallel to the vehicle transversal axis. This layout leads to some interferences with dampers, but prevents the generation of any angle on the constant velocity joints, when the suspension is resting. Finally, the inertia properties of the shafts are inherited from the ones of the rigid axle, provided that they have similar dimensions

2. Input communicators:

   - *cis_diff_to_chassis_left*, *cis_diff_to_chassis_right* and *cis_diff_to_chassis_rear*: these are *mount* communicators with minor role set to *front*. They are automatically generated by the corresponding mount parts and match their output communicators created in the body subsystem, to locate the three above mentioned non-aligned points of connection between the differential box and chassis

3. Output communicators:

   - *cos_differential_housing*: it is a *mount* communicator with minor role set to *inherit*. It is created to match the corresponding input communicator automatically generated in the driveline subsystem, when the mount part *mts_differential_housing* is created. This mount part is necessary to locate the differential box centered between the two differential output parts of the driveline subsystem
   - *col_tripot_to_differential* and *cor_tripot_to_differential*: they are a pair of *location* communicators with minor role set to *front*. They are created to match the corresponding input communicators of the front suspension itself, to connect the position of the differential output parts present in the driveline subsystem with the tripots present in the front suspension subsystem

4. Differential box: this is a part created with both geometry and inertia properties derived from the differential box on the rear axle. Its ellipsoid geometries interfere with the transversal leaf spring and steering rack housing. Since it is aligned with the drive shafts, it is coaxial with the wheels centres when the suspension is resting

Once the template is ready, the corresponding subsystem is created and obviously saved with minor role set to *front*, as in the initial Rear-Wheel-Drive model.

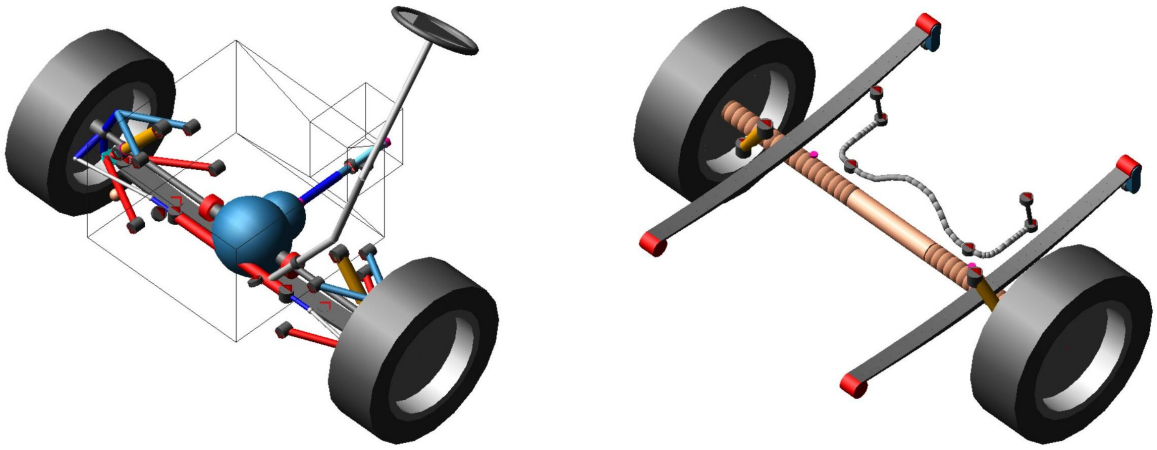

(a) Front axle. *(b) Rear axle.*

Figure 3.5: Front-Wheel-Drive - front and rear axles.

3.2.2 Rear Axle

The rear axle is shown in *Figure 3.5b*. The main intervention consists in removing both drive shafts and differential box. The elastic elements (leaf springs, anti-roll bar) are maintained, as well as the rigid axle. The latter is not recreated as a unique beam, to make its elastic behaviour identical to Rear-Wheel-Drive. Therefore, the void left by differential box is filled with a hollow cylinder, which represents an infinitely rigid connection between the two sides. It behaves like the differential box, but its inertia properties are adjusted to represent a simple piece of hollow beam. This way, the rear axle is lighter with respect to Rear-Wheel-Drive, but its elastic properties are unchanged. As for the front suspension, the procedure to modify the rigid axle starts from its template, which is modified according to the following steps:

1. Parameter variable *pvs_driveline_active*: it is set equal to 0, which corresponds to the deactivation of group *driveline_active*, containing the drive shafts and tripots parts along with their joints and communicators. This simple modification removes the entire driveline, but the differential box is still present, because it is imagined as being part of the rigid axle. However, it gives a massive contribution to the unsprung mass and it is not conceptually correct to keep it on a driven axle

2. Differential box: the part itself is maintained, but the ellipsoid geometries are deleted and replaced by a cylinder, with a diameter equal to the outer one of the rigid axle and a proper length to fill the void left by the differential box and driveline. Its inertia properties are computed referring to a hollow cylinder with both outer and inner radii inherited from the rigid axle. This way, it behaves like an infinitely rigid component, but it has an inertia content coherent with the rest of the rigid axle

Once the template is ready, the rear suspension subsystem is generated and obviously saved with minor role set to *rear*, as in the initial Rear-Wheel-Drive model.

3.2.3 Driveline

The driveline template is modified according to the following steps:

1. Joint-Force *jfs_gearbox_torque*: the sign of the function is reverted. Without this modification, the front wheels spinning direction would make the vehicle move backwards when the engine supplies a driving torque, as a side effect of mirroring
2. Input communicators:
   - *cis_total_axle_torque*: minor role shifted to *front*
   - *cis_diff_ratio*: minor role shifted to *front*
   - *cil_diff_tripot* and *cir_diff_tripot*: minor role shifted to *front*
3. Output communicators:
   - *cos_halfshaft_omega_left* and *cos_halfshaft_omega_right*: minor role shifted to *front*
   - *col_tripot_to_differential* and *cor_tripot_to_differential*: minor role shifted to *front*
4. Propeller shaft: the hardpoints defining the shaft geometry are modified, so that its three constitutive parts are shortened proportionally one to each other and are coaxial. The reason for erasing the angles originally present in Rear-Wheel-Drive is to prevent a torque fluctuation due to excessive phase angles on the universal joints, better explained in the Appendix. The inertia properties of its three parts are scaled down proportionally to their reduction in volume

The driveline subsystem generated from this template is saved with minor role set to *front*. This way, all communicators with minor role set to *any* or *inherit* are automatically shifted and correctly assigned.

3.2.4 Powertrain

The powertrain template is modified according to the following steps:

1. Input communicators:
   - *cis_halfshaft_omega_left* and *cis_halfshaft_omega_right*: minor role shifted to *front*
2. Output communicators:
   - *cos_total_axle_torque*: minor role shifted to *front*
   - *cos_diff_ratio*: minor role shifted to *front*

The powertrain subsystem generated from this template is saved with minor role set to *front*. This way, all communicators with minor role set to *any* or *inherit* are automatically shifted and correctly assigned.

4 Suspension Tests

4.1 Front Axle

Suspension tests are performed on isolated front and rear axles and give information about the elasto-kinematic behaviour of a suspension according to the type of input, thus allowing to separate and isolate each contribution. They are complementary to full-vehicle tests because they give information about single effects and phenomena involving a suspension during usual driving, but they are not sufficient to completely evaluate a vehicle behaviour without the already mentioned full-vehicle tests, which are instead able to capture the overall dynamics. On Adams/Car, they are executed in quasi-static conditions, meaning that each step does not take into account the evolution of the system, thus hiding any hysteretic behaviour that might be detected during a real test. In the present study, the tests performed on both axles are Parallel Wheel Travel, Opposite Wheel Travel and Cornering Force. Specifically, in Parallel Wheel Travel both wheels move vertically with coherent motion direction, hence they follow a compression or extension stroke by the same length. This test is representative of the suspension behaviour when the vehicle faces a road bump. Instead, in Opposite Wheel Travel the wheels have opposite directions, therefore one side of the suspension is subject to compression, while the other one is extending. This test is useful to simulate how the suspension reacts to a lateral load transfer, for example during a cornering maneuver. Finally, the Cornering Force test is a specific case of application of Static Loads, where a lateral force is applied to one wheel, to assess how the loaded wheel reacts to cornering forces and how it affects the other side of the suspension as well. Experimental data from the manufacturer are available for all these tests and allow to check the Adams/Car model reliability.

4.1.1 Parallel Wheel Travel

Figures from 4.1 to 4.5 show the results in terms of toe angle variation, camber angle variation, wheel centre longitudinal displacement, contact point lateral displacement and tyre vertical force as functions of the vertical wheel travel.

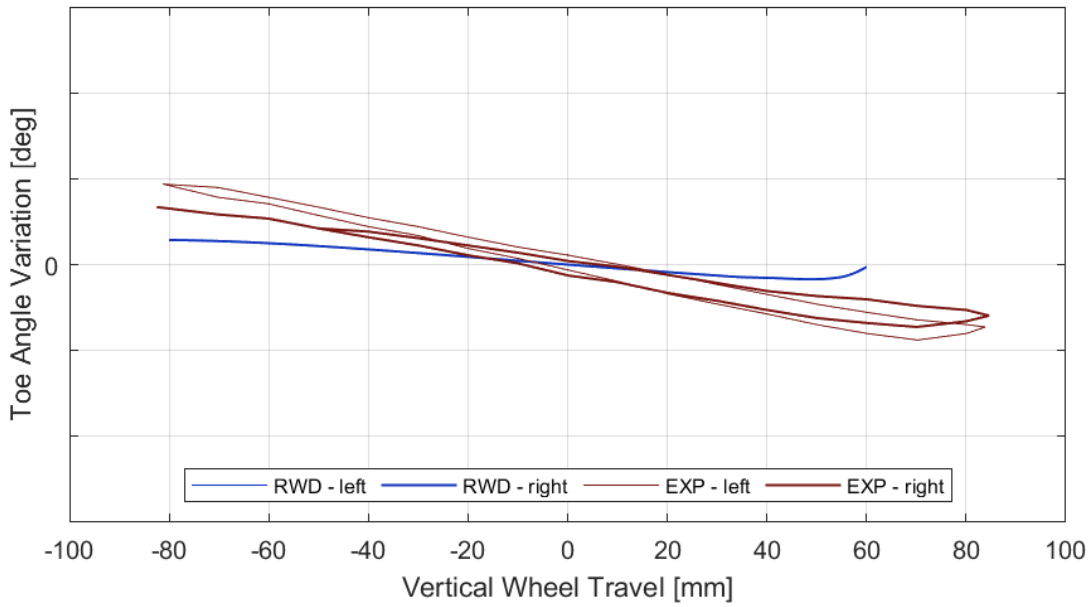

Figure 4.1: Parallel Wheel Travel - toe angle variation vs vertical travel.

Looking at the toe angle, it seems that the model is less sensitive to any variation along the suspension stroke. Qualitatively, the behaviour correctly represents the real suspension, where a compression leads to a toe-out while a rebound produces a toe-in. Turning to camber angle, the data fit is good for a bump travel, where the angle gets negative, but it is less accurate in the extension field, as the angle becomes slightly positive.

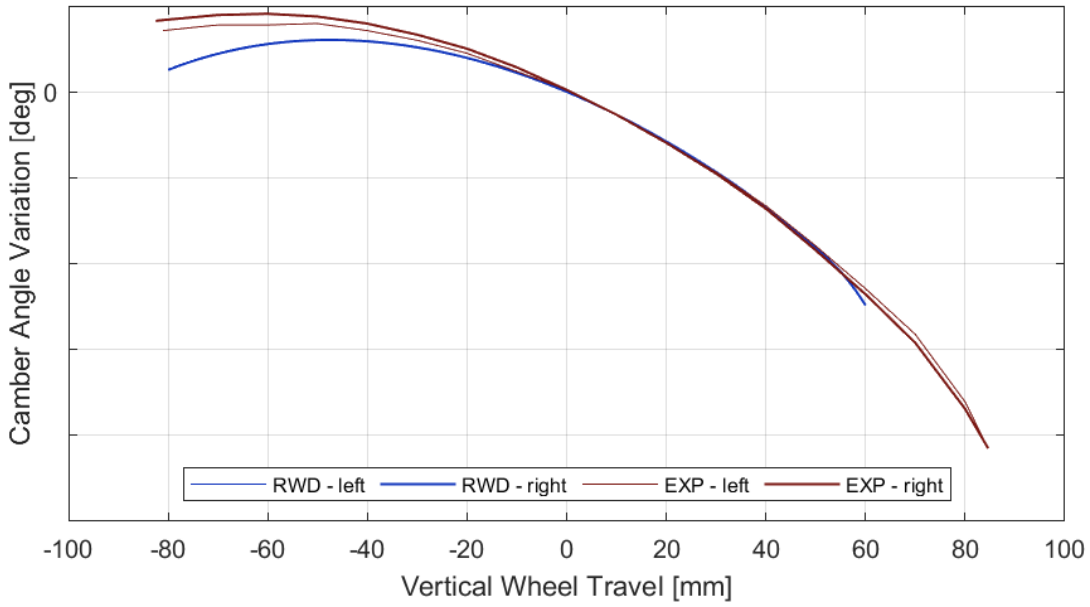

Figure 4.2: Parallel Wheel Travel - camber angle variation vs vertical travel.

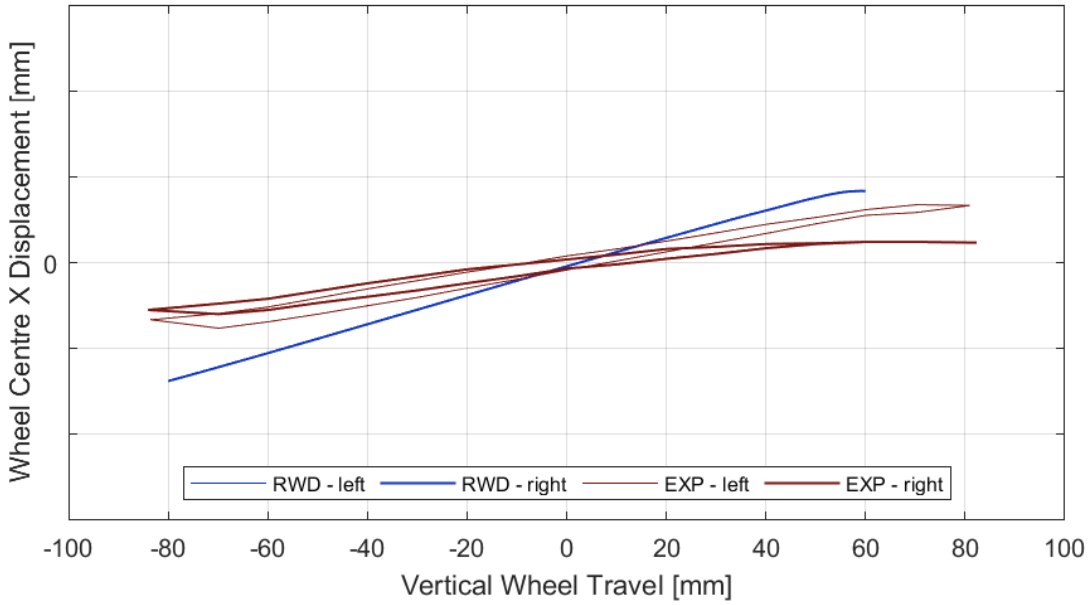

Figure 4.3: Parallel Wheel Travel - wheel centre longitudinal displacement vs vertical travel.

Concerning the wheel centre longitudinal displacement, the virtual model tends to over-estimate it, without considering any asymmetry between the two wheels. A compression stroke generates a backward motion of the wheel centre, meaning that the wheelbase is reduced. Instead, the contact point lateral displacement fits well the real behaviour, where a compression leads to an increase in track, whereas a rebound makes it decrease. At last, the compliance characteristic is well replied by the model, especially in the linear field. This implies that the vertical stiffness of the front suspension is well reproduced on the Adams/Car model.

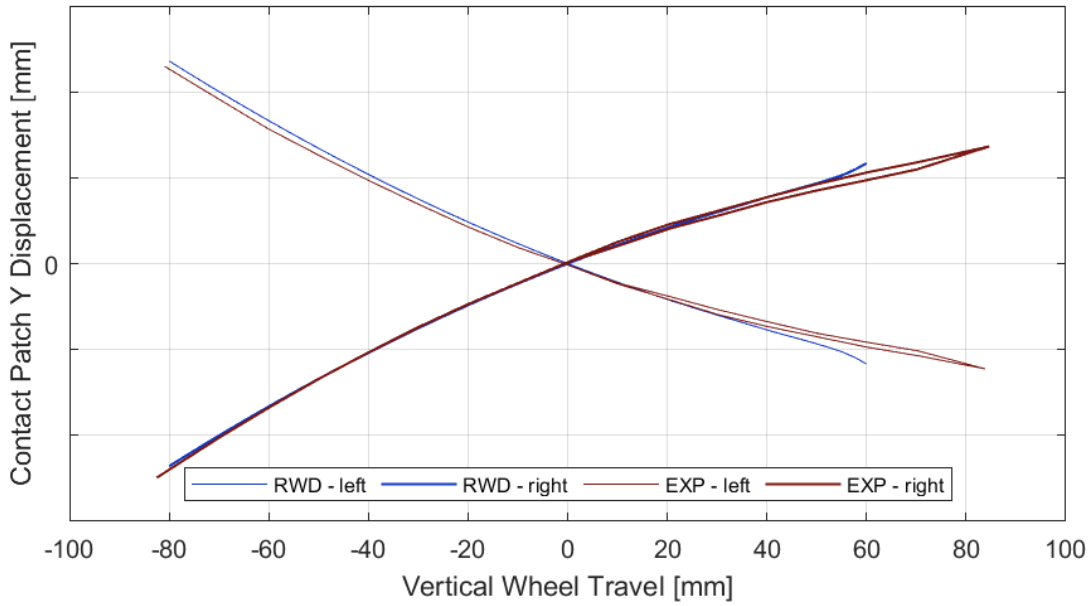

Figure 4.4: Parallel Wheel Travel - contact patch lateral displacement vs vertical travel.

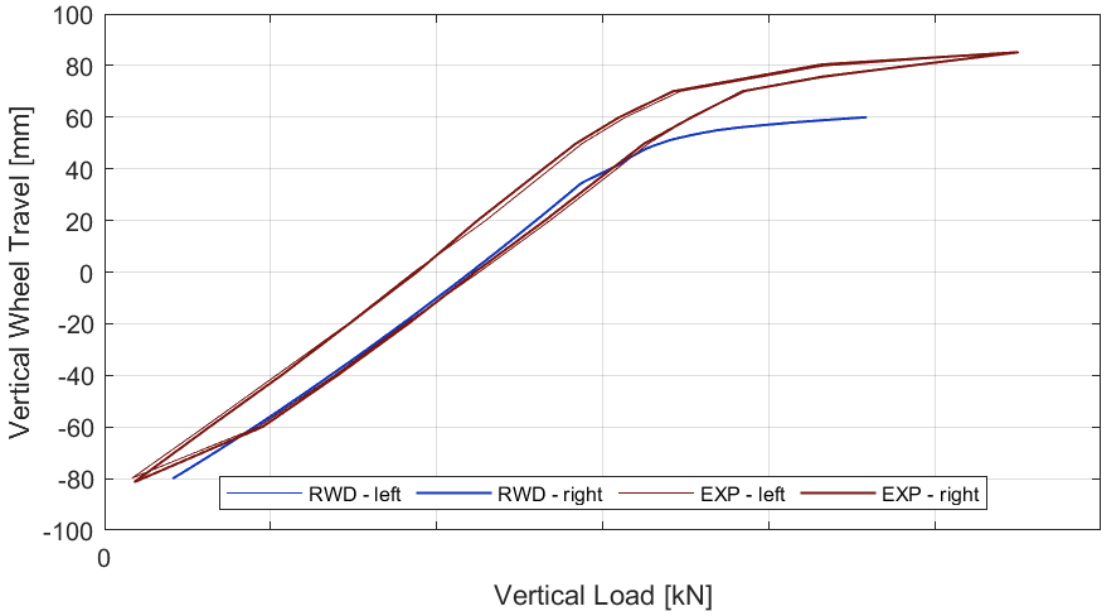

Figure 4.5: Parallel Wheel Travel - vertical wheel travel vs normal load.

4.1.2 Opposite Wheel Travel

The quantities already mentioned in the previous test are reported in *Figures from 4.6 to 4.10*. This time, the differences with respect to the real suspension are more pronounced. Starting from the toe angle, the Adams/Car model detects a strong variation, which seems to couple the actions on the two wheels through the leaf spring, whereas the real suspension keeps the wheels toe angles almost unchanged. Concerning camber angle, similarly to Parallel Wheel Travel, the extended side is underestimating the variation, while the compression stroke shows a better fit.

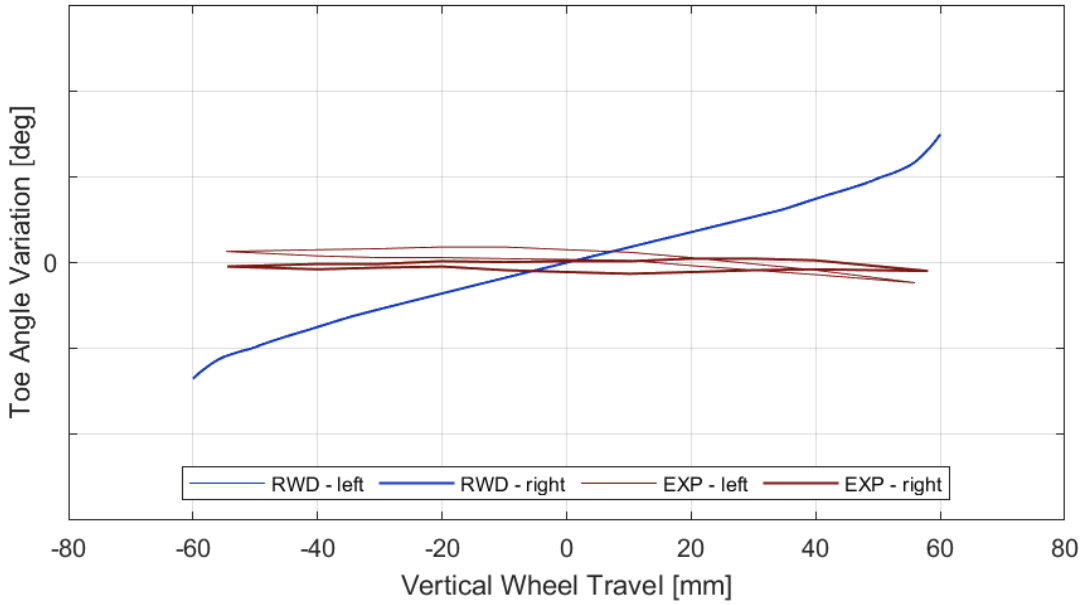

Figure 4.6: Opposite Wheel Travel - toe angle variation vs vertical travel.

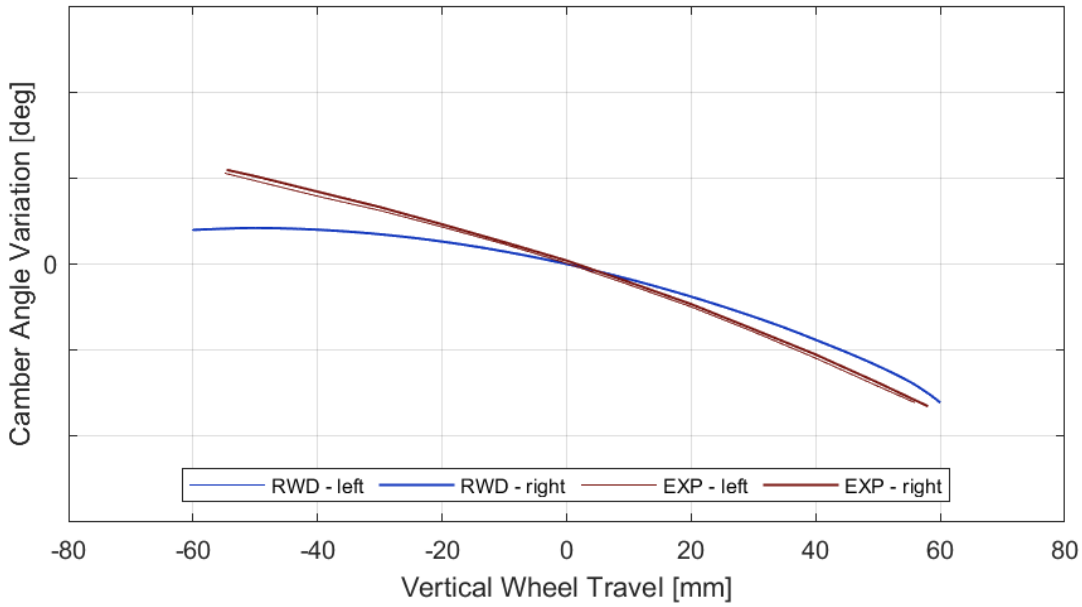

Figure 4.7: Opposite Wheel Travel - camber angle variation vs vertical travel.

About the wheel centre longitudinal displacement, a good fit is overall achieved, with some differences near the bump and rebound stops. Clearly, the wheel undergoing a compression stroke still moves backward and reduces the wheelbase, while the opposite happens on the opposite side of the suspension. Looking at the contact point lateral displacement, the fit is overall good, apart from some differences near the rebound limit. This test leads to a slight decrease in total track, because the transversal motion of the extended side is greater than the one of the compressed side. Finally, the compliance curve seems to have a lower slope, meaning that the model has a greater roll stiffness, with respect to the real vehicle.

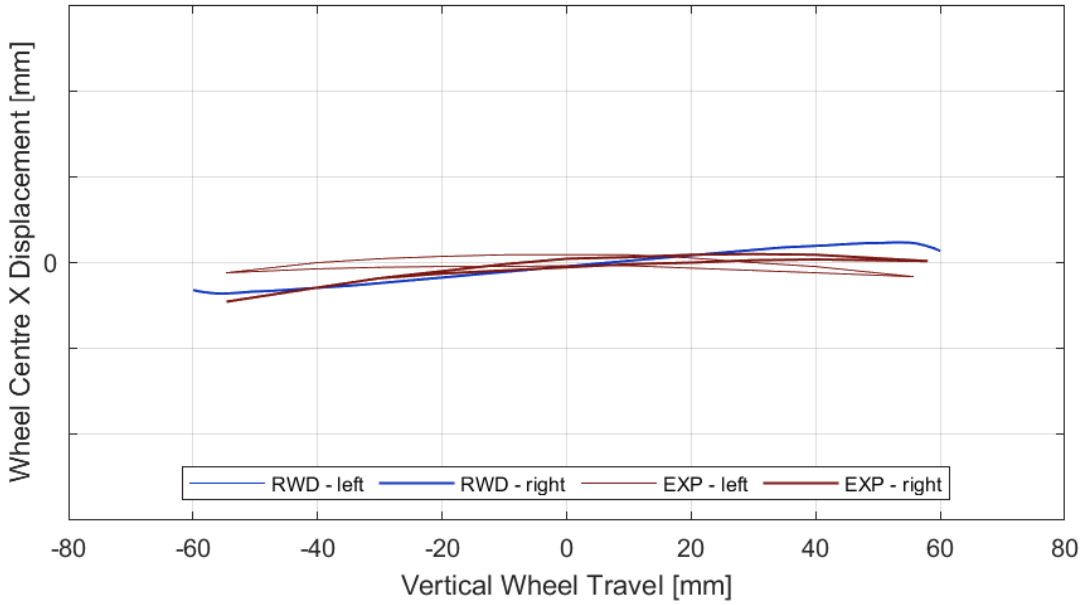

Figure 4.8: Opposite Wheel Travel - wheel centre longitudinal displacement vs vertical travel.

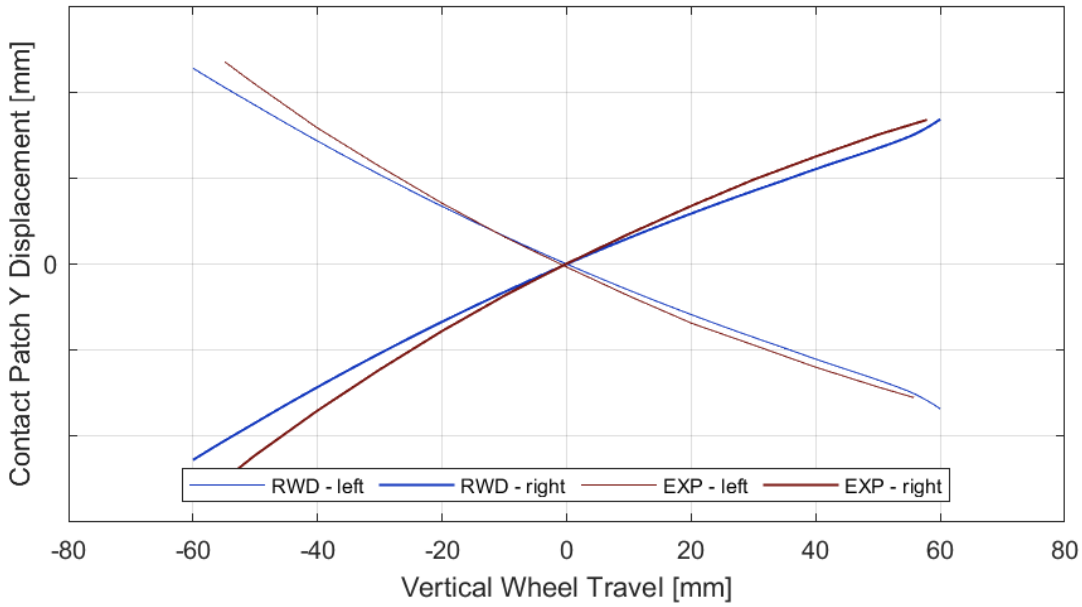

Figure 4.9: Opposite Wheel Travel - contact patch lateral displacement vs vertical travel.

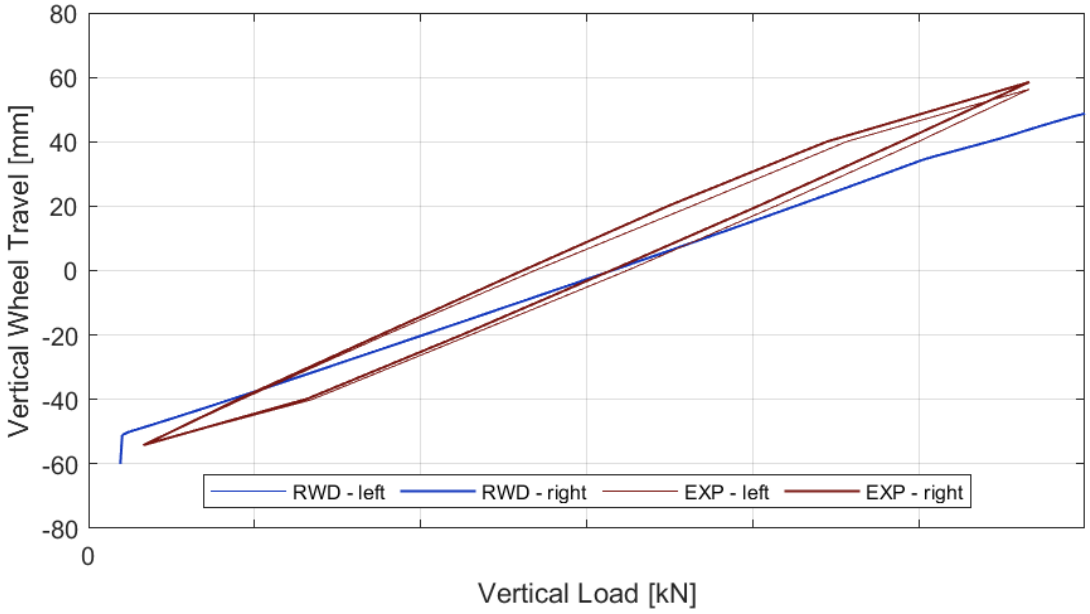

Figure 4.10: Opposite Wheel Travel - vertical wheel travel vs normal load.

4.1.3 Static Load - Cornering Force

The results are reported in *Figures from 4.11 to 4.13* for the cornering force applied to the left wheel. Given the symmetry obtained when applying the force to the right wheel, it is not necessary to report these results as well. The sign convention here adopted for the lateral load is so that a positive force pulls away from the vehicle. Therefore, a cornering force is positive. The toe angle shows huge variations on both wheels, whereas in a real suspension only the loaded wheel is subject to a moderate change. A cornering force makes the loaded wheel assume a toe-out and the opposite one settle to a toe-in, confirming the coupling effect already detected in Opposite Wheel Travel.

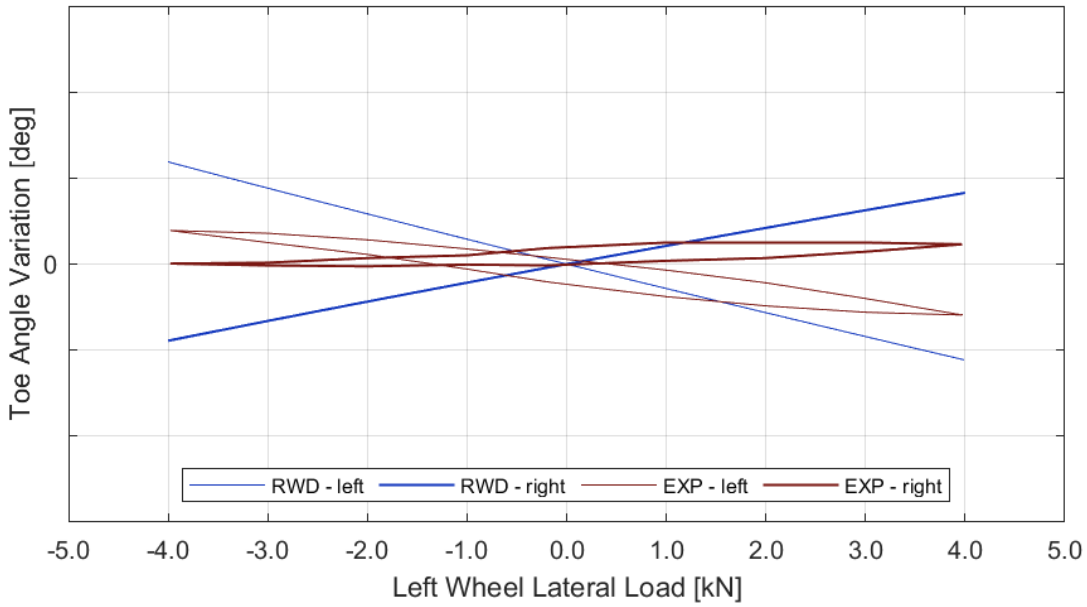

Figure 4.11: Cornering Force - toe angle variation vs lat. load.

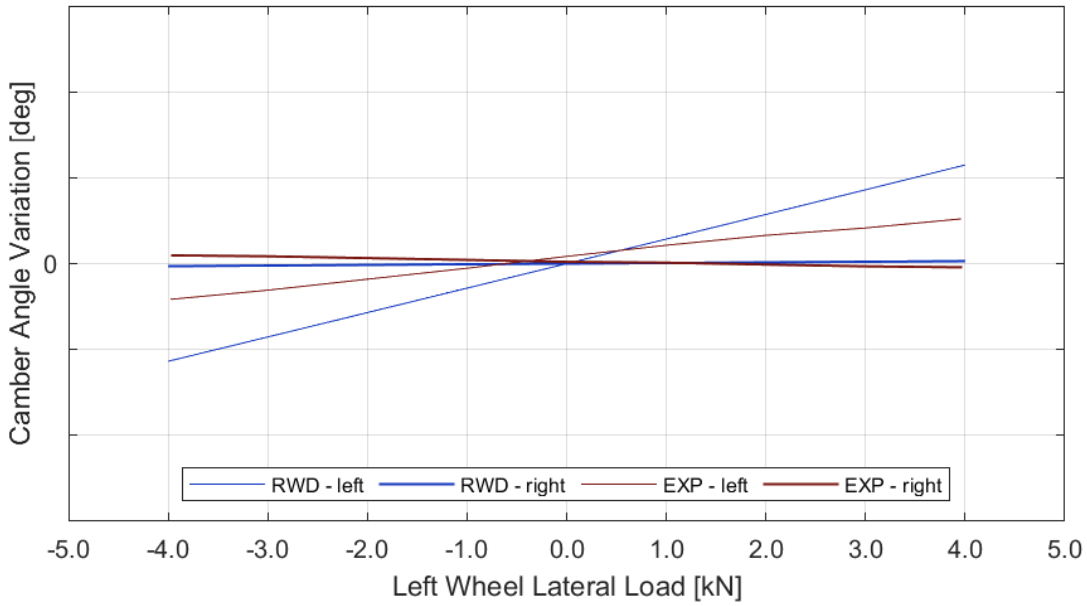

Figure 4.12: Cornering Force - camber angle variation vs lat. load.

Turning to the camber angle, the loaded wheel shows a more compliant behaviour with respect to the real world, with a cornering force resulting in a positive camber, while this time there are no coupling effects with the unloaded wheel, as in the real suspension. At last, the lateral displacement is well represented for the loaded wheel, but the opposite one is insensitive to any change, thus altering the overall track variation detected in the Adams/Car model.

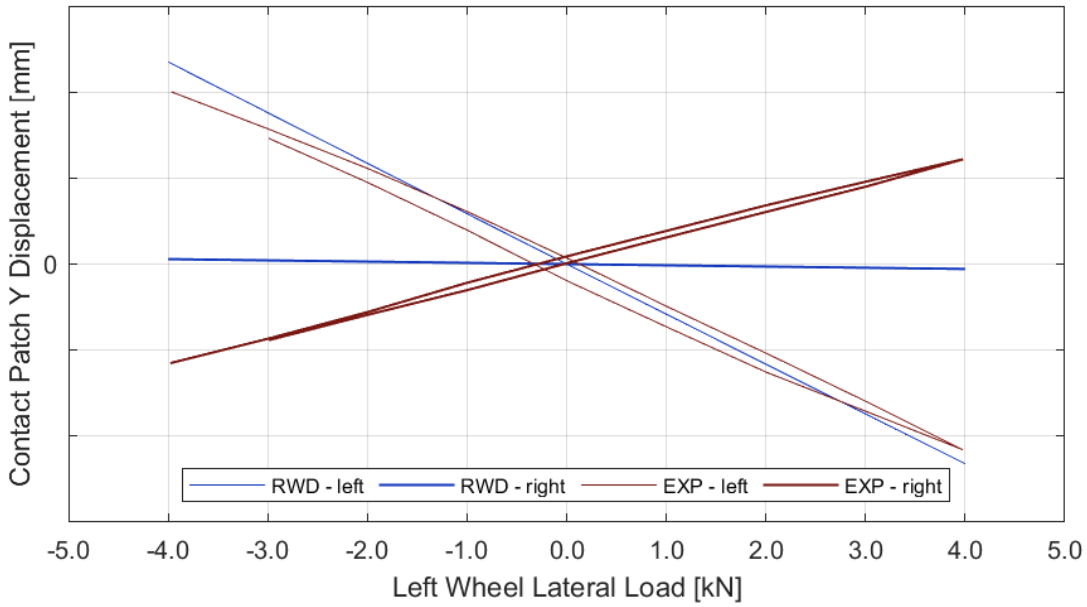

Figure 4.13: Cornering Force - contact patch lateral displacement vs lat. load.

4.2 Rear Axle

4.2.1 Parallel Wheel Travel

Figures from 4.14 to 4.18 report the results of this first test. Both toe and camber angles show good data fit. The former confirms the property of rigid axles, where the wheels are likely to keep a null toe angle. The latter displays a slight variation apparently unexpected, considering the total camber recovery typical of rigid axles. However, the elastic deformation of the axle itself can explain this response, because a compression stroke, indicative of a laden vehicle, forces the wheels to assume a negative camber, coherent with the axle deformation.

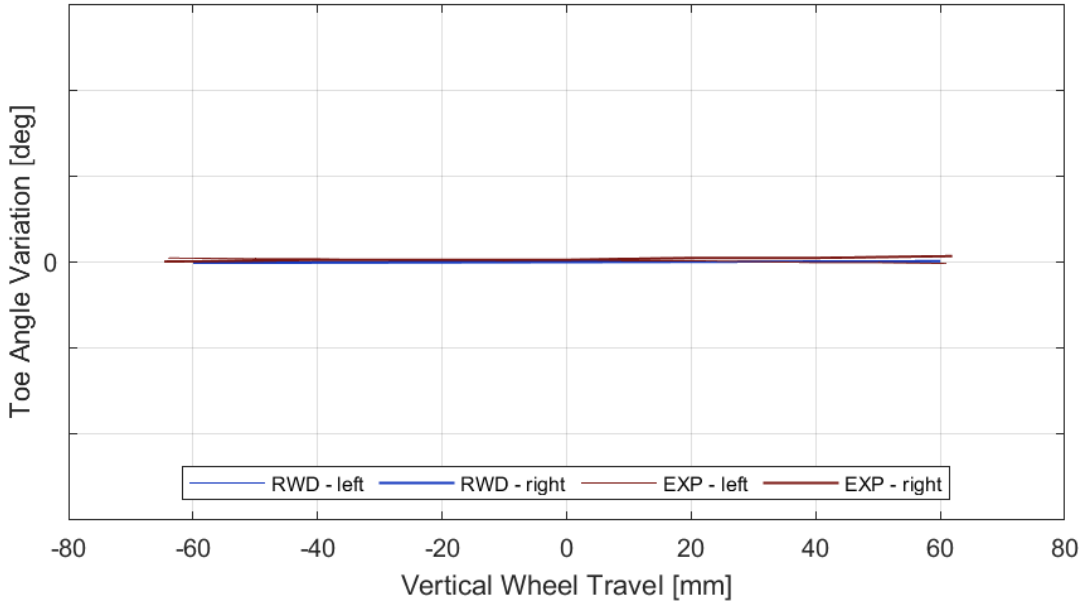

Figure 4.14: Parallel Wheel Travel - toe angle variation vs vertical travel.

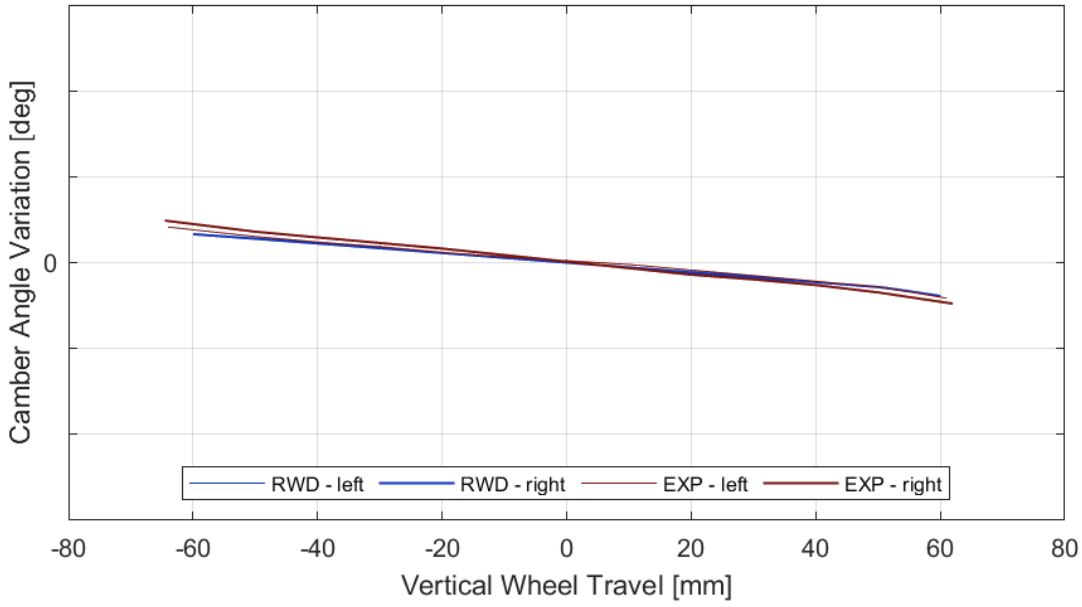

Figure 4.15: Parallel Wheel Travel - camber angle variation vs vertical travel.

Concerning the wheel longitudinal displacement, it is possible to notice some differences between real and virtual vehicles, anyway the overall trend is preserved. During a compression stroke, the wheels tend to translate forward, decreasing the wheelbase. This behaviour is the combined result of the shackles rotation and the leaf springs deflection. About the contact point lateral displacement, a track variation can be detected. This behaviour can be explained uniquely by the camber angle variation previously described, because a compression stroke produces negative camber angles on both wheels, leading to a track increase. At last, the compliance curve shows a good fit, with the Adams/Car model having a slightly lower vertical stiffness.

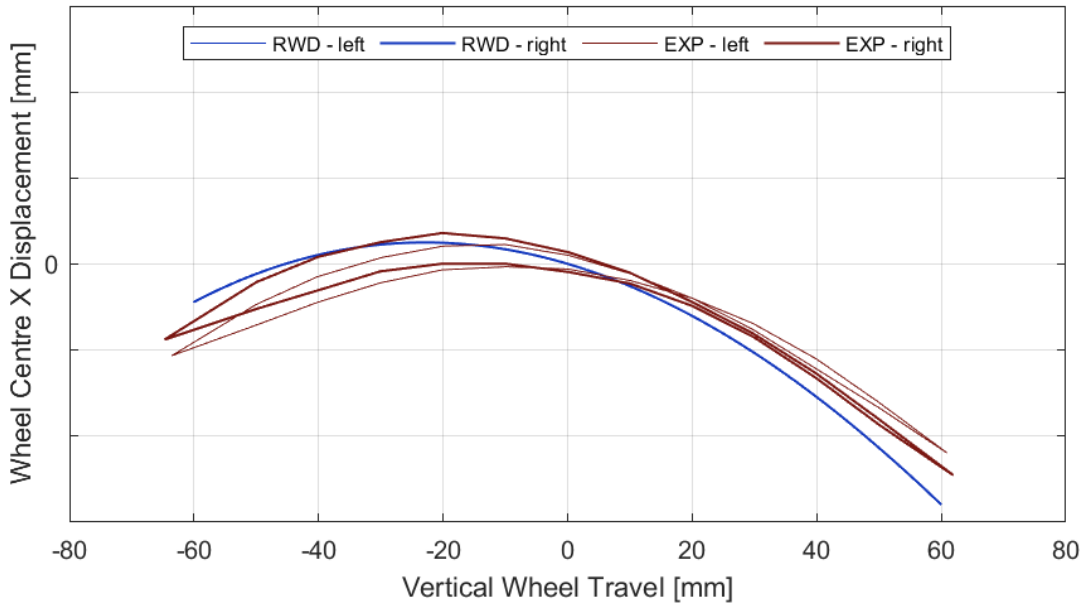

Figure 4.16: Parallel Wheel Travel - wheel centre longitudinal displacement vs vertical travel.

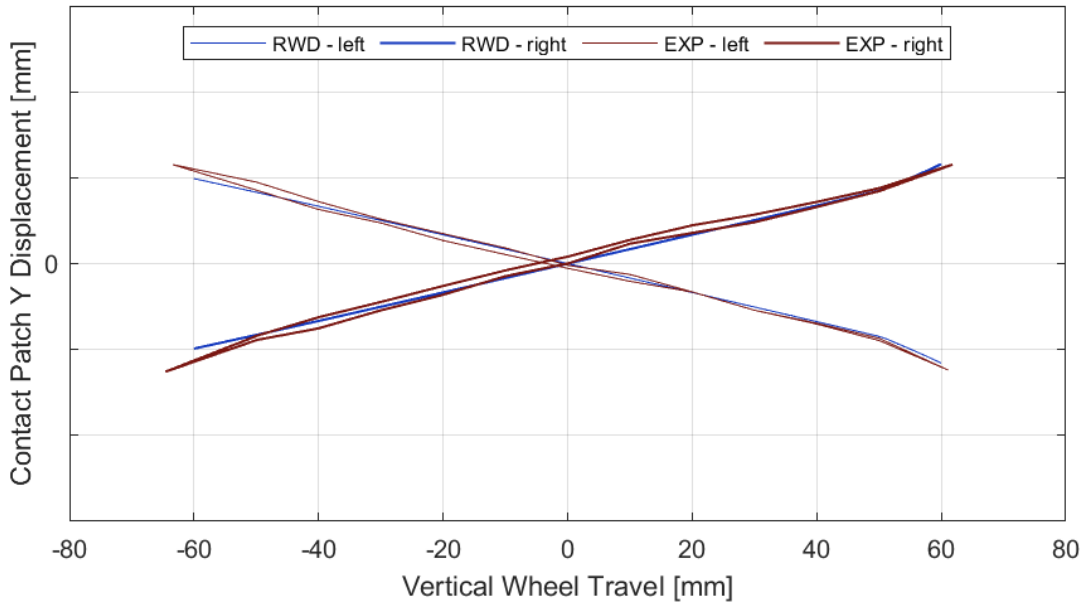

Figure 4.17: Parallel Wheel Travel - contact patch lateral displacement vs vertical travel.

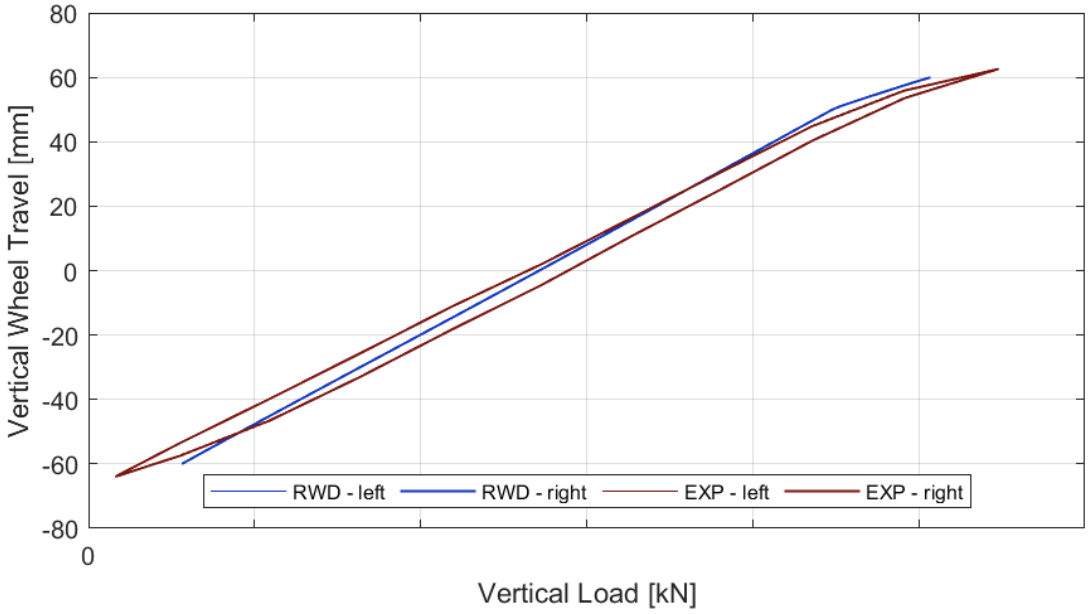

Figure 4.18: Parallel Wheel Travel - vertical wheel travel vs normal load.

4.2.2 Opposite Wheel Travel

The same quantities above mentioned are reported in *Figures from 4.19 and 4.23*. Concerning the toe angle, a good fit is achieved, with the Adams/Car model slightly over-estimating its variation. Clearly, the wheel undergoing compression stroke is forced to move forward as previously seen, while the opposite happens on the other side. Provided the coupling effect of the rigid axle, the former wheel must assume a toe-in, while the latter settles to a toe-out.

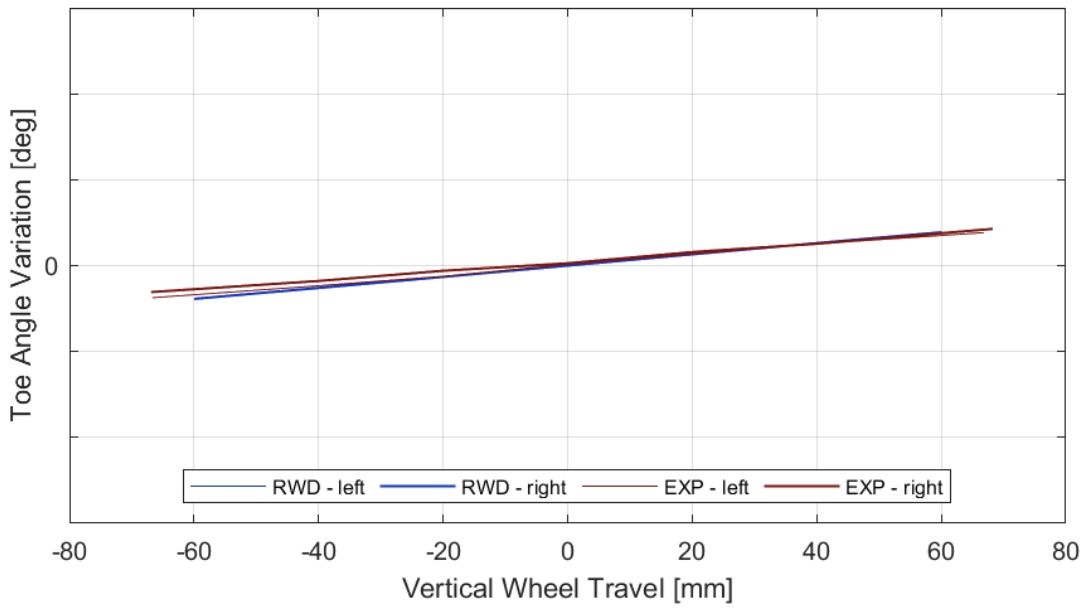

Figure 4.19: Opposite Wheel Travel - toe angle variation vs vertical travel.

Looking at the camber angle, once again the good fit is confirmed and clearly shows the behaviour of a dependent suspension, where the rigid axle forces both wheels to remain coaxial, resulting in huge camber angle variations. Instead, the wheel centre displacement confirms the considerations about the toe angle. Considering the contact point lateral displacement, the response of the suspension is qualitatively similar to the one seen in a Parallel Wheel Travel, but the entity of the motion is one order of magnitude greater. However, this time the two wheels have opposite strokes, therefore the total track is mostly unchanged and the axle translates in the lateral direction.

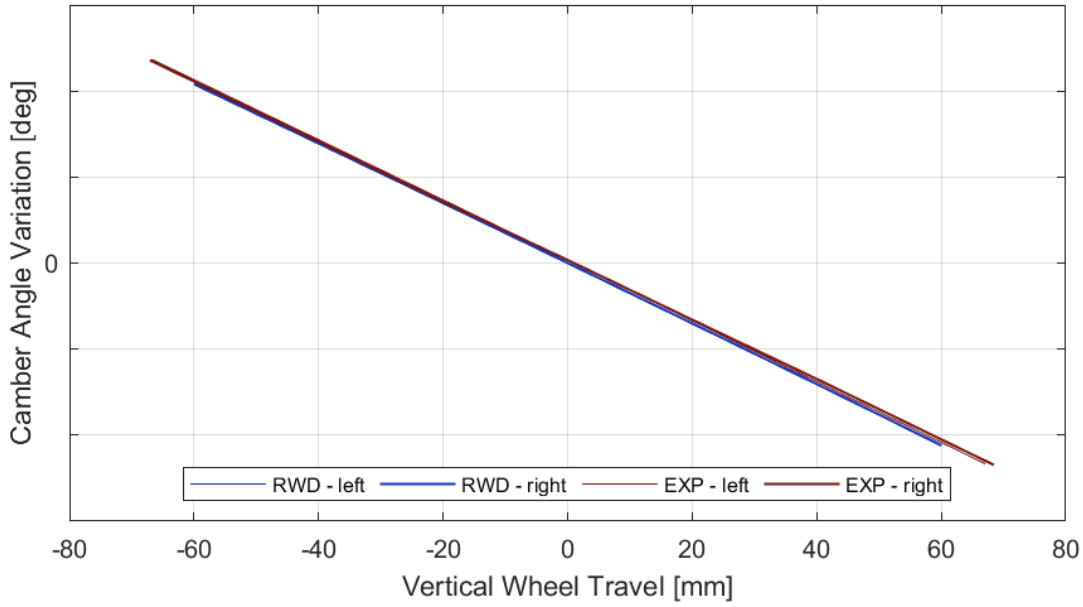

Figure 4.20: Opposite Wheel Travel - camber angle variation vs vertical travel.

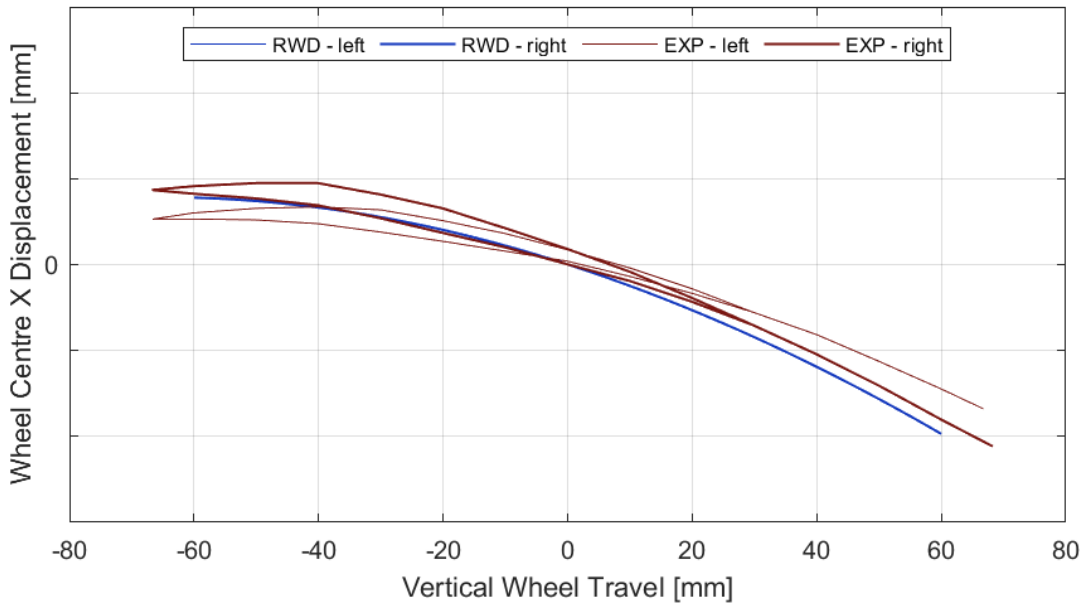

Figure 4.21: Opposite Wheel Travel - wheel centre longitudinal displacement vs vertical travel.

Finally, the compliance curve shows a slope smaller with respect to the previous test. Reminding the meaning of Opposite Wheel Travel, this curve can be interpreted as the compliance to roll motion, hence the rear axle is more sensitive to roll, although an anti-roll bar is installed. The Adams/Car model shows a greater compliance with respect to the real vehicle.

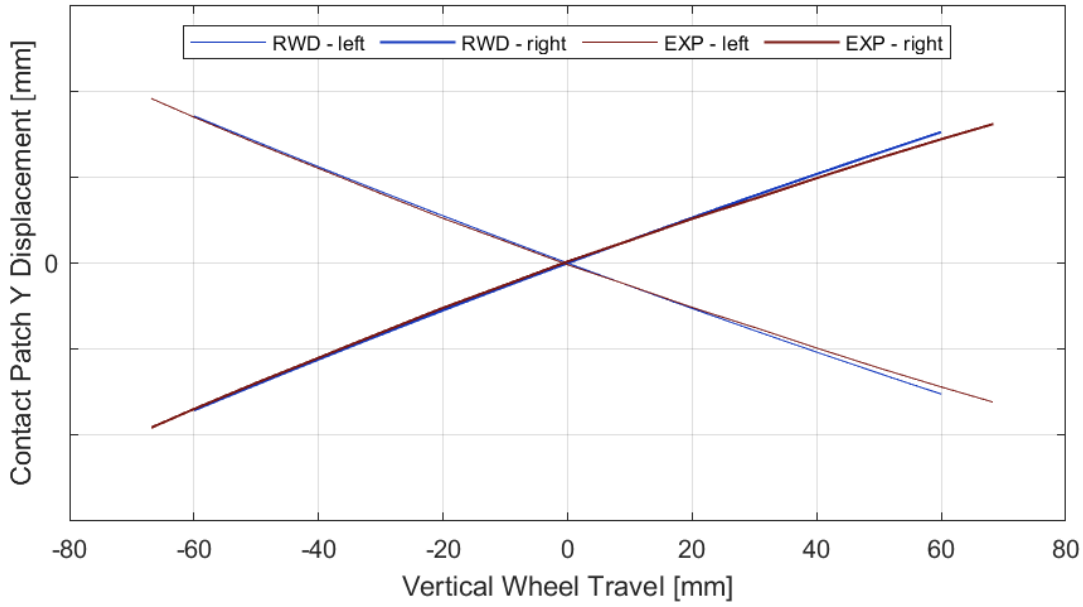

Figure 4.22: Opposite Wheel Travel - contact patch lateral displacement vs vertical travel.

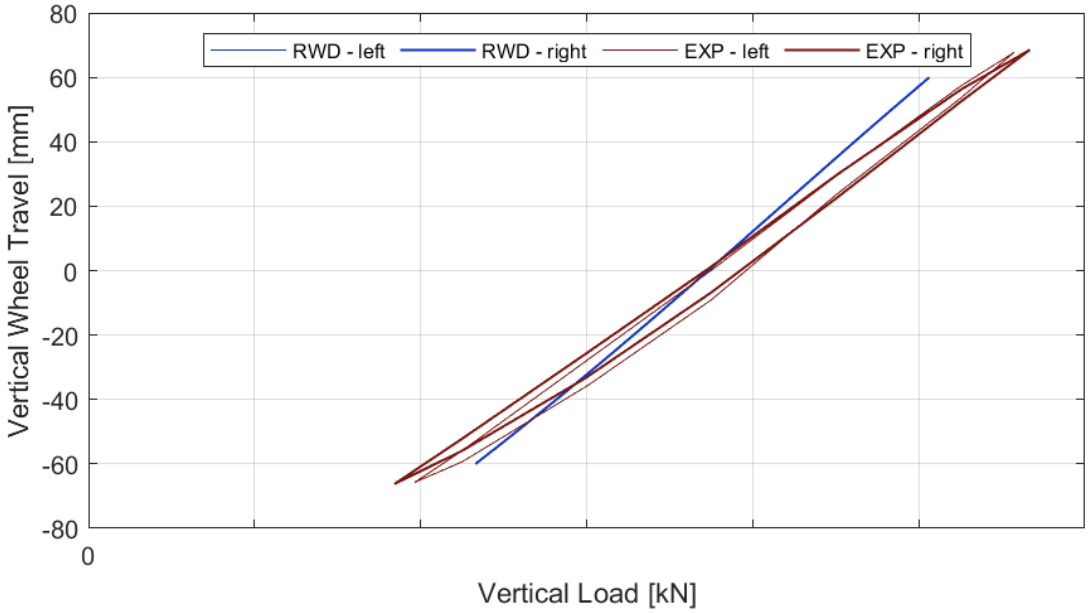

Figure 4.23: Opposite Wheel Travel - vertical wheel travel vs normal load.

4.2.3 Static Load - Cornering Force

The results are reported in *Figures from 4.24 to 4.26* for the left wheel loaded. The results are symmetric, provided the nature of a rigid axle suspension and can be discussed without reporting the test performed on the right wheel. Concerning the sign conventions, a positive lateral load is directed pointing outwards with respect to the vehicle and corresponds to a cornering force.

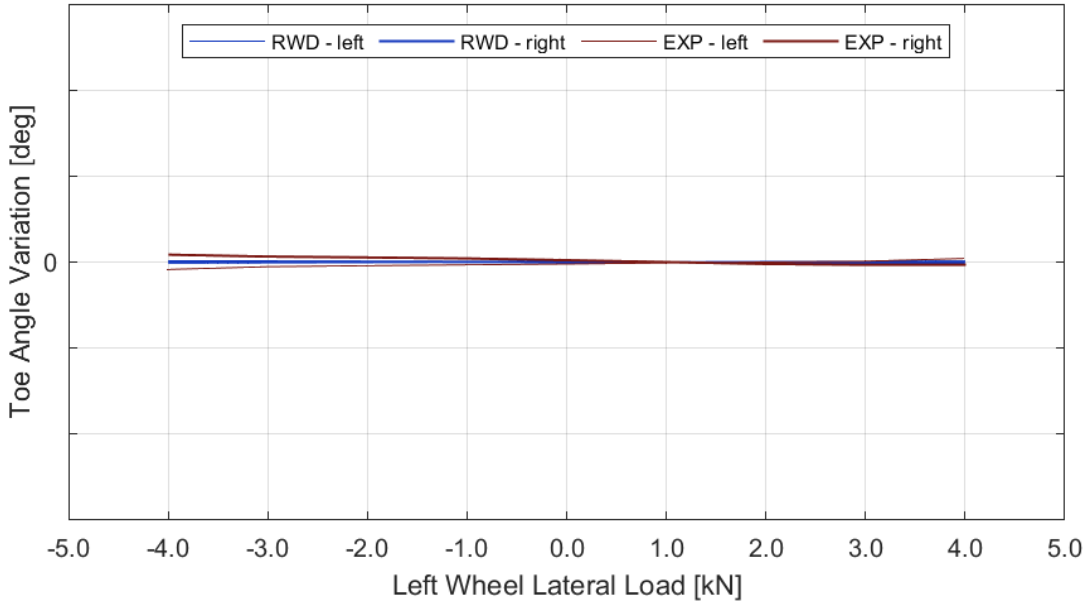

Figure 4.24: Cornering Force - toe angle variation vs lat. load.

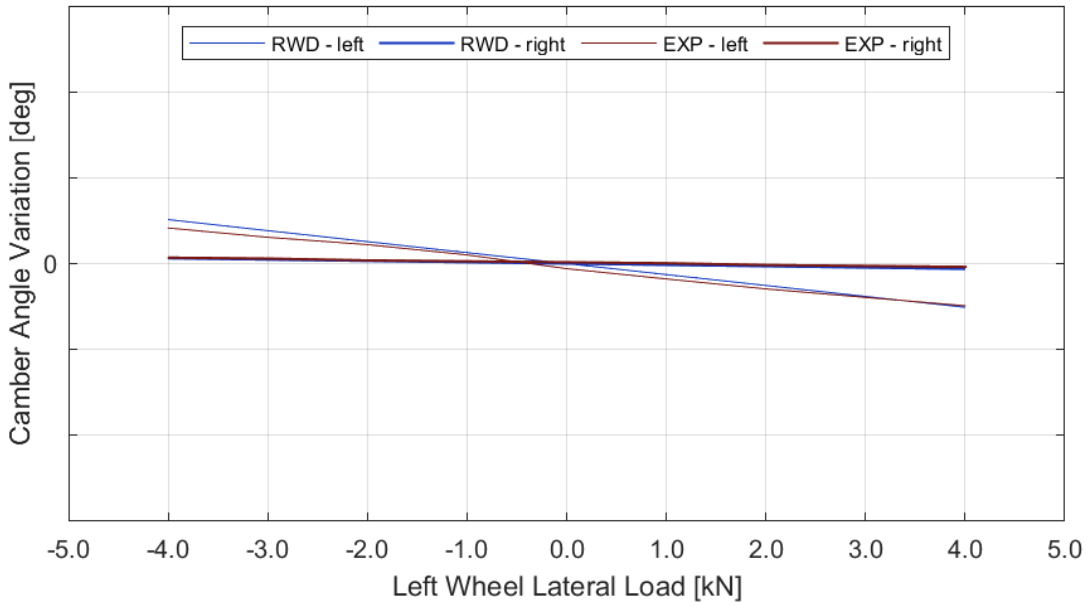

Figure 4.25: Cornering Force - camber angle variation vs lat. load.

Concerning toe angle, its variations are quite negligible. A closer look suggests that the model does not detect any change, while in a real vehicle, the loaded wheel feels a slight toe-in. Anyway, the opposite wheel is insensitive to this effect. Instead, a moderate change on the loaded wheel camber angle is detected, while on the other wheel a negligible variation can be seen. More precisely, a cornering force makes the loaded wheel assume a negative camber and a pulling action is exerted on the rigid axle, forcing it to translate, but also to undergo an elastic deformation in its axial direction. The combination of these two effects acts on the other wheel, which is pulled as well, thus inducing a small negative camber. These considerations lead to the contact point lateral displacement. Since there are no mechanical linkages, such as a Panhard bar, which might play a role in the track variation, the camber angle is the only source of changes. Specifically, the combination of negative camber angles and rigid axle translation makes the wheels move in the direction of the lateral load, with the loaded wheel more subject to motion. At the same time, the opposite wheel undergoes a similar displacement by a reduced amount, therefore a global track increase occurs. The main difference between the Adams/Car model and the real vehicle lies in the wheel that is not loaded, as the former tends to minimize its lateral displacement.

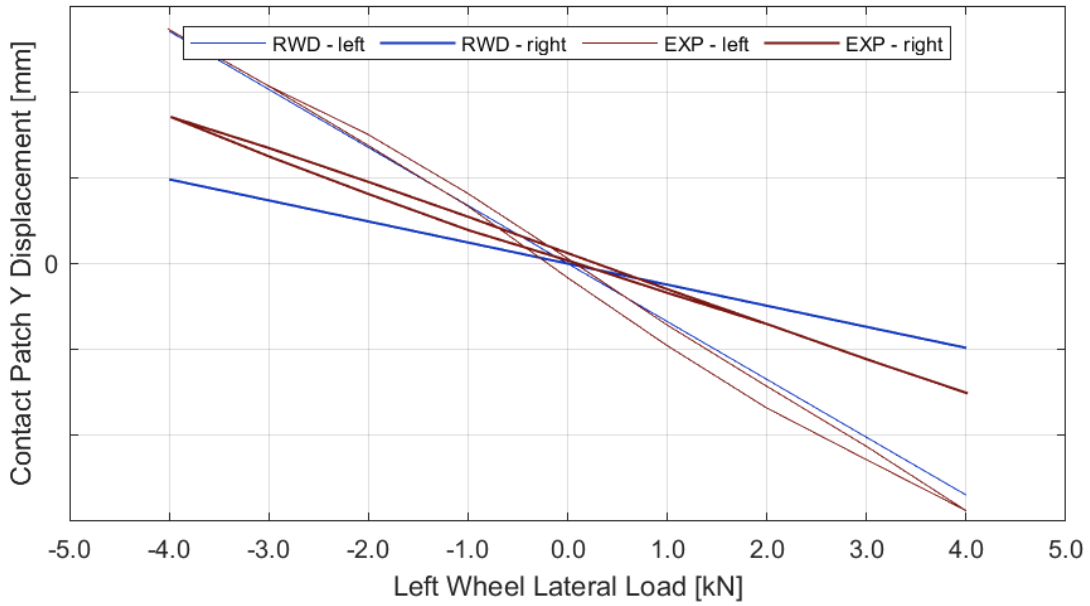

Figure 4.26: Cornering Force - contact patch lateral displacement vs lat. load.

4.3 Conclusions

About the double wishbone suspension, a sufficiently good fit is achieved, however some phenomena are not correctly replied by the Adams/Car model. The errors might be influenced by the choice of modelling all mechanical linkages as infinitely rigid. Moreover, the great number of bushings and joints to be modelled could introduce some misalignments with respect to the real world. Nevertheless, the entity of these differences still makes the model acceptable. Turning to the rigid axle suspension, the Adams/Car model displays a satisfactory repeatability of the empirical results, thanks to the reduced complexity of this subsystem and the choice of modelling the live axle as an elastic beam.

5 Ramp Steer

5.1 Rear-Wheel-Drive vs Experimental

Ramp Steer is an open-loop maneuver based on a gradually increasing steering wheel angle, by a constant rate expressed in °/s. It starts in a steady-state condition where the vehicle is driving on a straight trajectory at constant longitudinal velocity, then the steering wheel is rotated according to the prescribed rate, while acting on the accelerator pedal to keep the vehicle speed as constant as possible. This way, a progressive decrease in path radius occurs, while the lateral acceleration increases, until the vehicle reaches its grip limit. This test is quite common and well described in ISO 4138:2021 [10] and ISO 19364:2016 [11] standards. The former is about a real vehicle testing method, the latter provides the guidelines to validate a simulation tool. In this Chapter, Ramp Steer is firstly used to validate the Adams/Car model with reference to the available handling report provided by the manufacturer. The test is performed in the same conditions adopted in the real world, which consist in a slow ramp at high speed. On the Adams/Car model, power steering is activated, because it is assumed that the real vehicle is provided with it, although it will be deactivated to build the comparison between Front and Rear-Wheel-Drive models. The test parameters are listed in *Table 5.1*.

Ramp	60 °/s
Longitudinal Velocity	100 km/h
Gear Position	4th
Power Steering	Active

Table 5.1: Ramp Steer - Validation - test setup.

The quantities of interest are roll, sideslip and steering wheel angles, which are plotted as functions of lateral acceleration in *Figures from 5.1 to 5.3*. They produce a set of diagrams commonly known as handling curves, because they give an overall idea about the vehicle behaviour perceived by the driver during steady-state cornering. This test is also exploited to determine the static load distribution, which can be easily derived during the initial straight driving mini-maneuver. The comparison in terms of overall mass and static load distribution between the experimental vehicle and Rear-Wheel-Drive model is reported in *Table 5.2*.

	Experimental		Rear-Wheel-Drive	
	Unladen	Laden	Unladen	Laden
Mass (kg)	2340	3480	2340	3480
Front (%)	61.7	46.3	61.3	46.9
Rear (%)	38.3	53.7	38.7	53.1

Table 5.2: Ramp Steer - Validation - mass and static load distribution.

While the overall masses in both loading configurations are correctly represented, it is possible to notice a slight difference in static load distributions between the Rear-Wheel-Drive model and experimental vehicle. Particularly, on Adams/Car the front and rear masses are less emphasized respectively in the unladen and laden conditions, meaning a slight tendency to neutrality with respect to the real van. This is the result pursued during the tuning activity involving the definition of both loading configurations, because the driving idea is to avoid emphasizing the under(over)steer more than the real world.

The body roll angle suggests an optimal data fit, because the centre of gravity height is tuned to proper values for both configurations. Obviously, the laden condition is slightly more prone to roll because, although the centre of gravity height is lower, the huge mass added to the vehicle emphasizes the effect of centrifugal forces. The main difference between real world and Adams/Car model is close to the grip limit, which seems to be reached sooner by the latter.

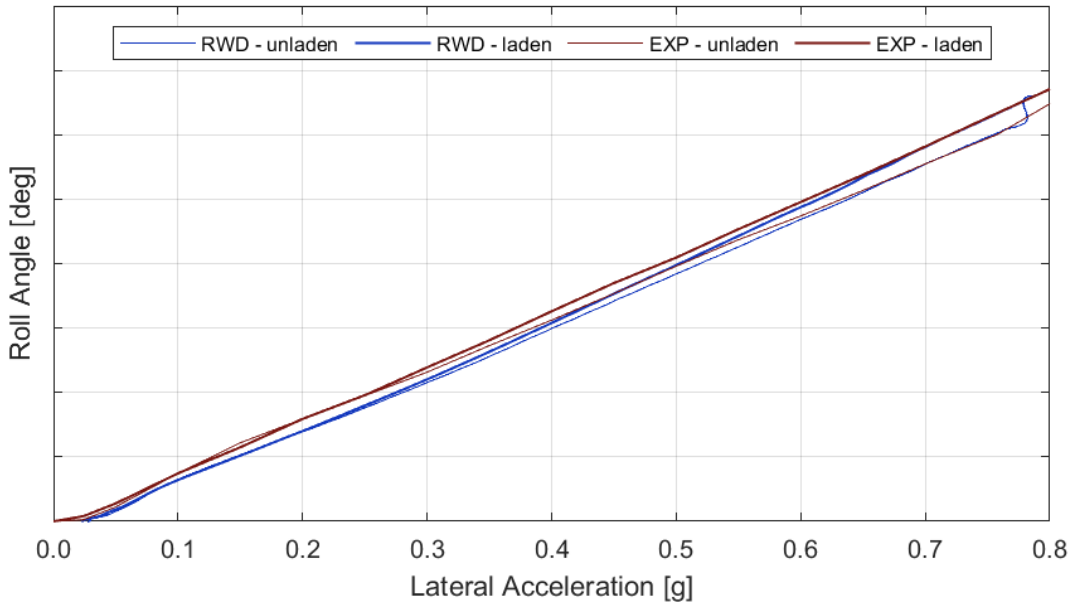

Figure 5.1: Ramp Steer - Validation - roll angle vs lat. acc.

The sideslip angle shows some discrepancies, especially in the unladen vehicle. The laden one is more prone to a "nose-in", meaning that it has a greater sideslip gradient due to the static load distribution towards the rear axle, representative of a lower understeer. The Adams/Car model looks less reliable near the grip limit and moves away from the experimental curves.

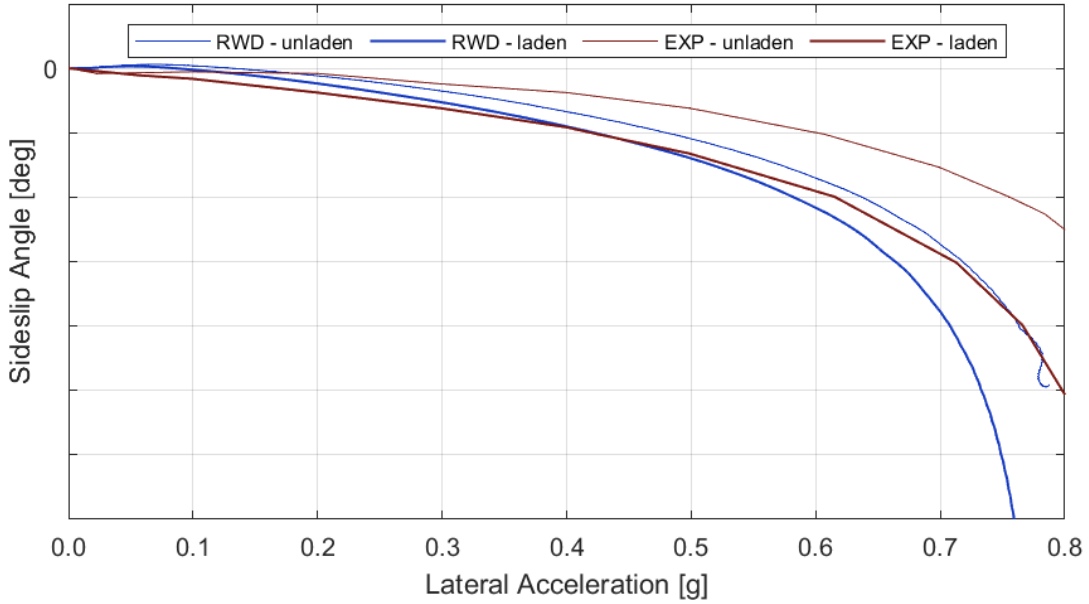

Figure 5.2: Ramp Steer - Validation - sideslip angle vs lat. acc.

Finally, the steering wheel angle shows a good fit in both loading configurations, with the Adams/Car model looking slightly more understeering. The laden vehicle is a little less subject to understeer as previously suggested by the sideslip angle. Moreover, the difference between the two loading conditions is slightly less emphasized in the Adams/Car model, probably due to the static load distributions shown above. The data fit achieved in terms of steering wheel angle is the result of having activated power steering. In the following Section, where it will be deactivated, the angle will experience an increase by 20°-30° and a slight change in the relative behaviours of both loading conditions.

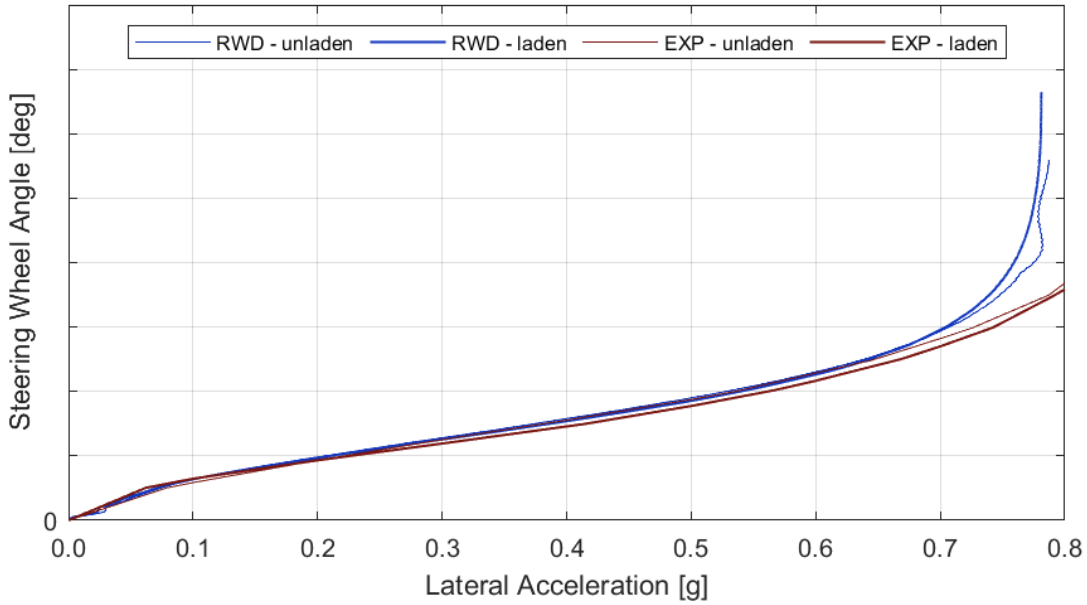

Figure 5.3: Ramp Steer - Validation - steering wheel angle vs lat. acc.

5.2 Front-Wheel-Drive vs Rear-Wheel-Drive

This time, Ramp Steer is used to compare the steady-state behaviours of Front and Rear-Wheel-Drive Adams/Car models. As already announced, power steering is deactivated from now until the last Chapter. The test parameters are identical to the ones adopted in the previous case and are reported in *Table 5.3*.

Ramp	60 °/s
Longitudinal Velocity	100 km/h
Gear Position	4th
Power Steering	Inactive

Table 5.3: Ramp Steer - Drivetrain - test setup.

Table 5.4 shows the mass and static load distribution of all vehicles. A slight mass reduction involves Front-Wheel-Drive, because the propeller shaft is shorter with respect to Rear-Wheel-Drive. At the same time, moving the driveline components to the front axle implies a small variation in mass distribution, so that Front-Wheel-Drive can already be expected to experience a slight additional understeer. This effect is not compensated by rearranging the sprung masses, because it is considered as part of the implementation of Front-Wheel-Drive.

	Rear-Wheel-Drive		Front-Wheel-Drive	
	Unladen	Laden	Unladen	Laden
Mass (kg)	2340	3480	2338	3478
Front (%)	61.3	46.9	64.5	49.0
Rear (%)	38.7	53.1	35.5	51.0

Table 5.4: Ramp Steer - Drivetrain - mass and static weight distribution.

The roll, sideslip and steering wheel angles are shown in *Figures from 5.4 to 5.6*. Additionally, the understeer gradient is reported in *Figure 5.7*.

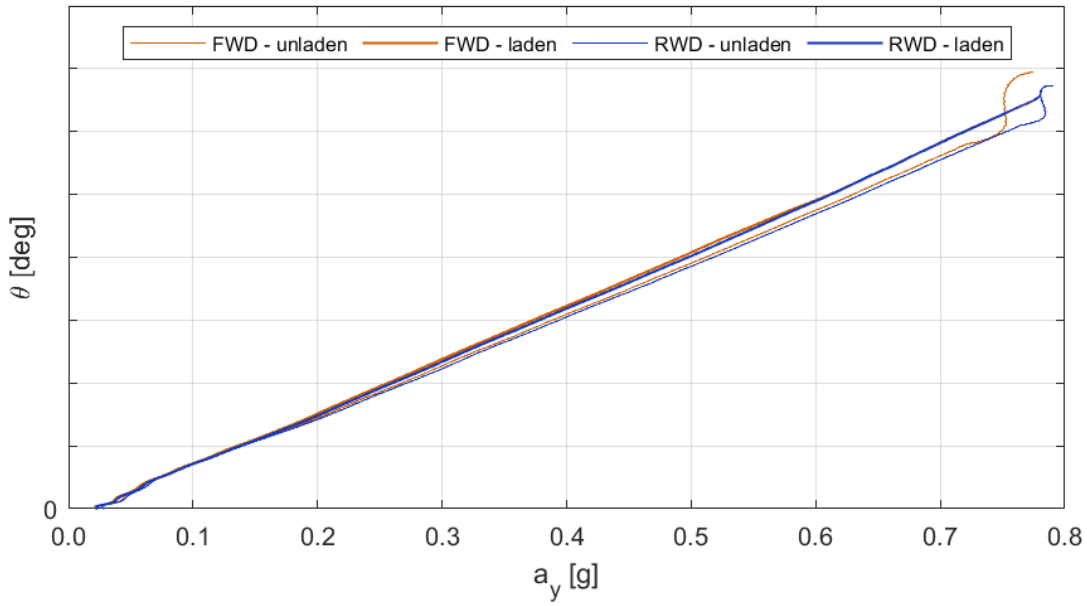

Figure 5.4: Ramp Steer - Drivetrain - roll angle vs lat. acc.

The roll and sideslip angles show many analogies in the laden configuration, while the unladen Front-Wheel-Drive seems less prone to instability when approaching its grip limit. Finally, the steering wheel angle confirms that Front-Wheel-Drive is slightly more understeering in both configurations. Considering the modest entity of this difference, it can be ascribed to the shift in load distribution generated by the rearrangement of the driveline. Clearly, an open-loop test like Ramp Steer is not able to highlight the effects of the drivetrain over handling, because the tyres are subject to cornering forces mainly, while the longitudinal components are negligible at constant longitudinal velocity as far as the pure rolling condition is ensured.

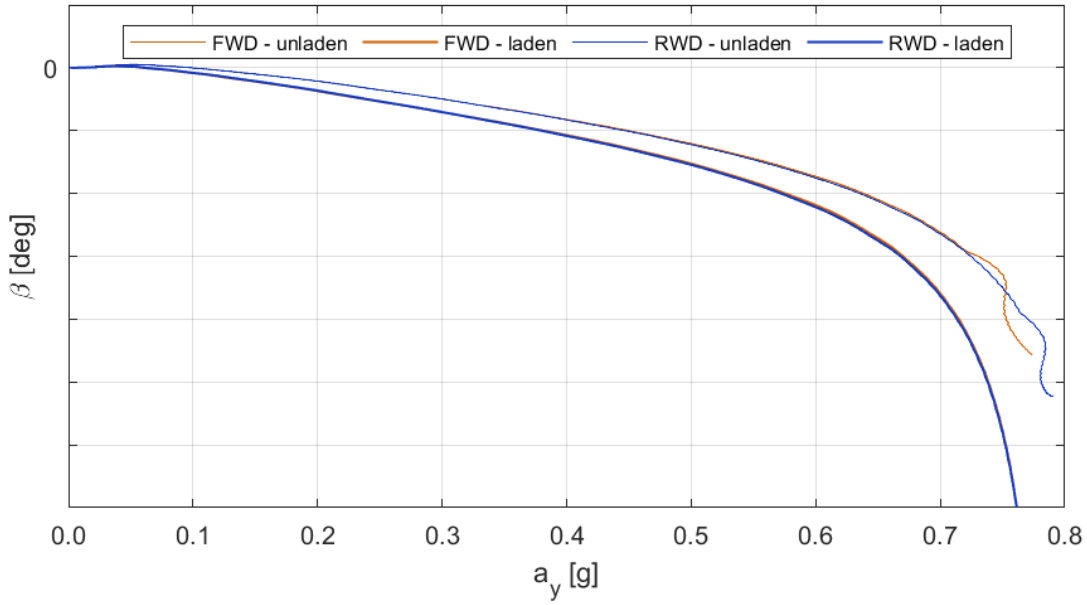

Figure 5.5: Ramp Steer - Drivetrain - sideslip angle vs lat. acc.

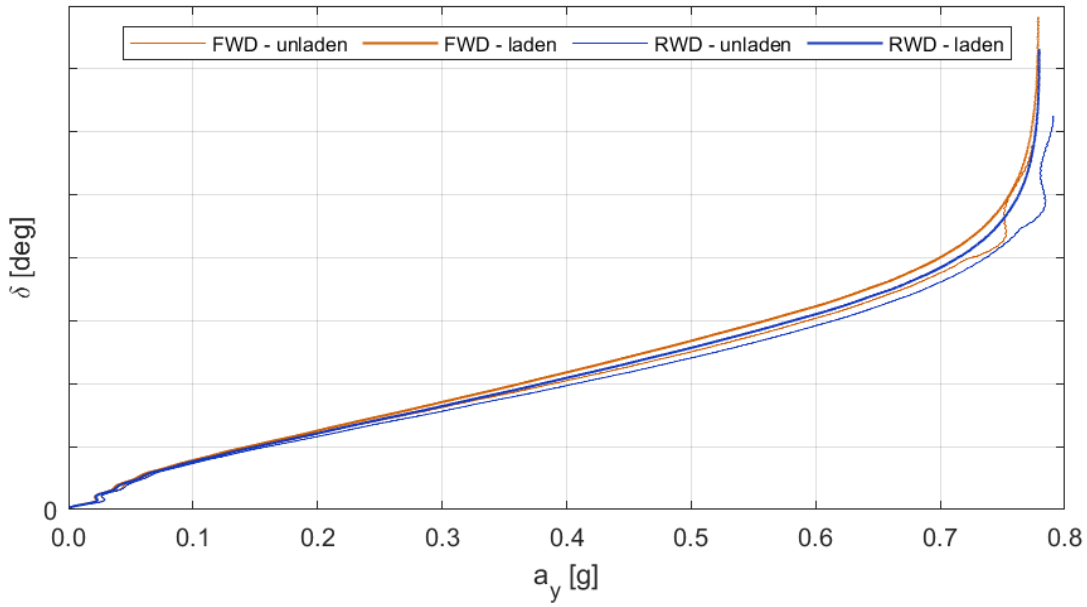

Figure 5.6: Ramp Steer - Drivetrain - steering wheel angle vs lat. acc.

Some additional information is provided by the understeer gradient. As already stated, the unladen configuration is more understeering, because the static load distribution is oriented towards the front axle. Overall, Front-Wheel-Drive always shows a slightly greater understeer, as previously suggested by the steering wheel angle. Interestingly, above 0.7g the unladen van experiences a sudden increase in the understeer gradient. The source of this phenomenon is a loss of contact between the rear inner wheel and the ground, which happens prematurely on Front-Wheel-Drive due to its weight distribution, slightly more advantageous to the front axle. Instead, Rear-Wheel-Drive has a differential box mounted directly on the rigid axle, which gives a small residual load to the rear inner wheel, making it leave the ground only when the vehicle is very close to its grip limit. Clearly, the normal force acting on that tyre is assumed very low, thus leaving room for quick saturation when a driving or braking torque is applied. This phenomenon never happens in the laden condition, which obviously loads more the rear axle and ensures a higher grip on the inner wheel. Despite the expected increase in lateral load transfer and roll angle, the vehicle grip limit is not sufficient to let the lateral transfer unload the rear inner wheel and make it leave the ground, as the loss of control happens first.

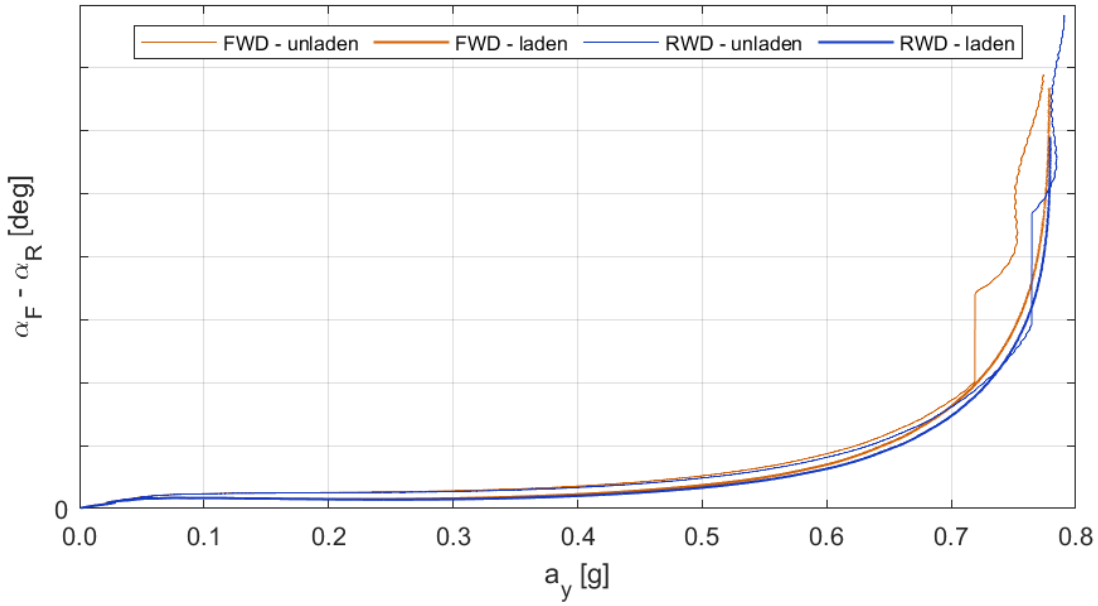

Figure 5.7: Ramp Steer - Drivetrain - understeer gradient vs lat. acc.

6 Power-Off Cornering

6.1 Standard Path Radius

6.1.1 Test Setup

ISO 9816:2018 [12] regulates a test to simulate the vehicle reaction to a sudden release of the accelerator pedal while cornering. It concerns passenger cars and, by extension, light-duty commercial vehicles. Starting from a steady-state condition where an initial lateral acceleration has been achieved, the steering wheel is locked and the throttle is released as fast as possible, while keeping the clutch engaged. The time instant when the accelerator release starts is called power-off instant. In a real-world test, there are two ways to achieve the steady-state initial condition: accelerating the vehicle at a determined path radius or increasing the steering wheel angle at constant longitudinal velocity. Instead, the Adams/Car test works only with the first option. It is built so that in the first mini-maneuver (steering pad), a steady-state condition is achieved and the selected lateral acceleration is achieved. The second mini-maneuver consists in a pedal release, keeping the steering wheel locked. The standard prescribes several quantities to be measured. Their time histories are essential, since this test is describing a transient event, but a complete report includes the definition of some additional variables that are plotted against the initial lateral acceleration. Therefore, a set of successive experiments with an increasing value of this quantity is crucial. Moreover, the standard states to perform the test for both left and right turns. At last, since the vehicle is subject to significant load variations, the unladen and laden configurations are both tested to draw a complete comparison. Concerning the test, there are some rules to be followed. First of all, a proper path radius must be selected. For this first and more robust set of tests, the value adopted is 100 m, which is the standard one. Therefore, the vehicle velocity is the only variable determining its initial lateral acceleration. For this reason, the gear to be selected (excluded the first one) should guarantee the highest engine rotational speed, without exceeding the 80% of its upper limit. This set of conditions determine the vehicle speed in the first mini-maneuver. The data should be recorded for at least 1.5s before power-off and 2.0s after it, but the latter is extended to 4.5s, which is approximately the total duration of the second mini-maneuver in the Adams/Car test and should be sufficient to fully extinguish the transient and settle to a new steady-state response. Concerning the throttle release, a time interval equal to 0.1s is chosen to represent this fast transient. At last, a sampling time interval equal to 0.001s is adopted, as a compromise between computational effort and simulation accuracy. To provide a full spectrum of the vehicle behaviour as required by the manufacturer, the initial lateral acceleration is set in the range from 0.05g to 0.70g, the latter being close to the grip limit shared by all vehicles. The 4th gear is the highest employed, because working with 5th or 6th gears would make the response less reactive and reduce the braking torque available at the wheels. *Table 6.1* resumes these information.

Sampling Time Interval	0.001s
Throttle Release Time Interval	0.1s
Path Radius	100 m
2nd Gear	0.05g - 0.15g
3rd Gear	0.20g - 0.35g
4th Gear	0.40g - 0.70g
Power Steering	Inactive

Table 6.1: Power-Off Cornering - Standard Path Radius - test setup.

Figures from 6.1 to 6.6 show the engine rotational speed time history and the corresponding torque. It is clear that the engine is reacting quickly to the pedal release, but a short transient takes place before settling to an almost linear decrease. This phenomenon is the result of the vehicle pitch inertia and is more visible at lower gears, thanks to the greater braking torque available at the wheels. Similar responses are obtained for FWD and RWD, the latter being slightly more reactive in decreasing its engine speed. This effect is the consequence of the longitudinal load transfer, which is reducing the grip on the rear axle, thus opposing less resistance to the engine, which is slowing down. Concerning the loading condition, a laden van is less prone to decelerate due to its inertia and the engine takes more time to reduce its speed.

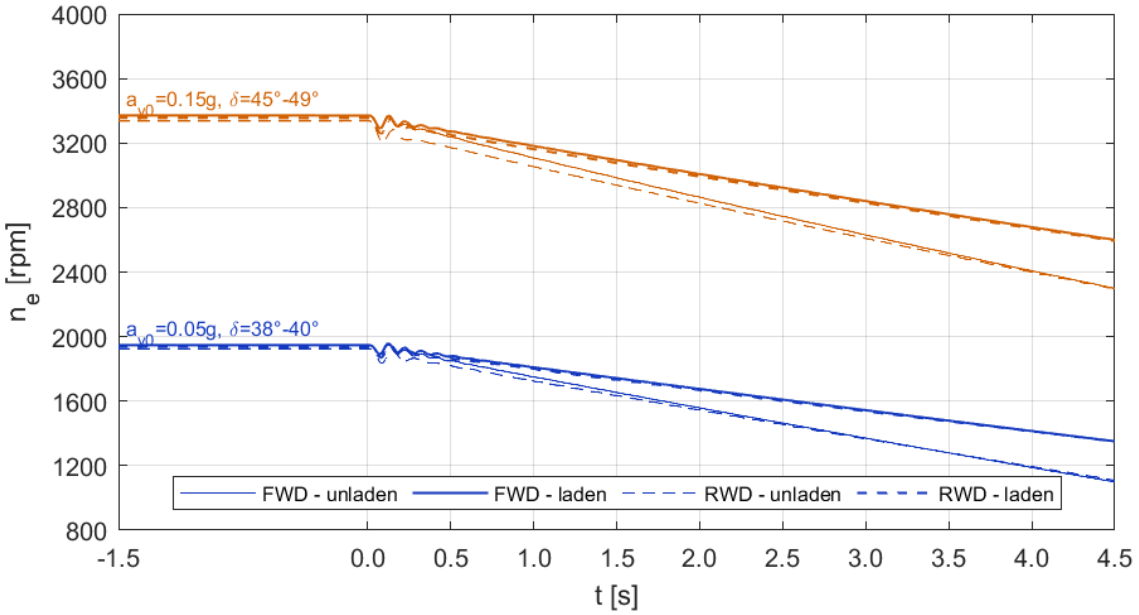

Figure 6.1: Power-Off Cornering - 2nd Gear - engine speed vs time.

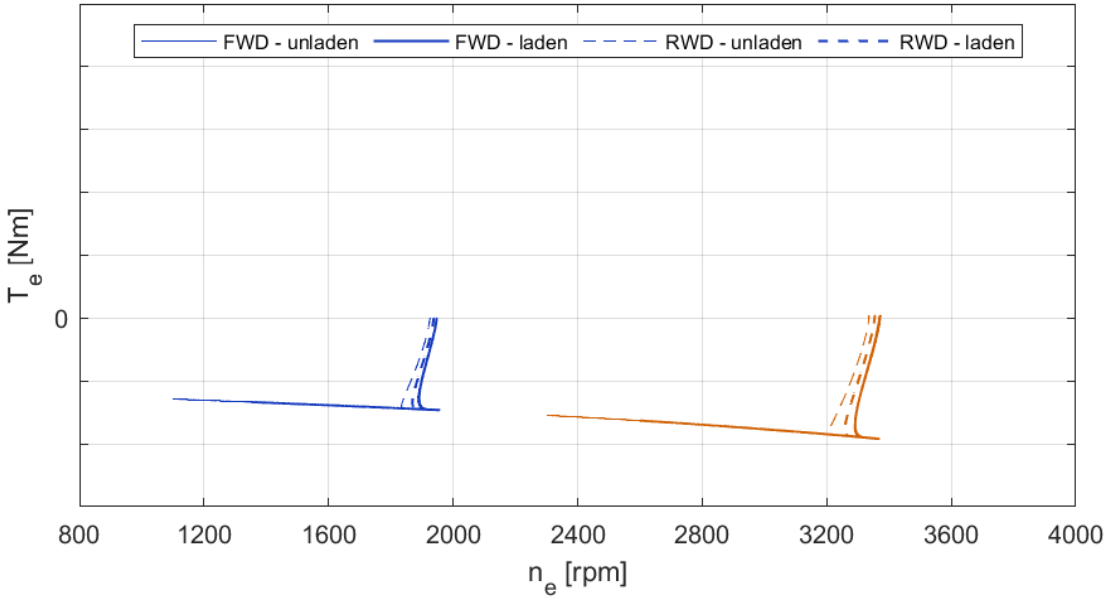

Figure 6.2: Power-Off Cornering - 2nd Gear - engine torque vs speed.

The engine characteristic (torque vs speed) starts from the steady-state working point, where a driving torque is supplied at a given speed, then it drops to the curve corresponding to Throttle @ 0%, where the braking torque is a cubic function of the engine rotational speed. This drop takes place in 0.1s, which is the time to fully release the pedal and corresponds to the overshoot seen in the engine time history. When the braking curve is reached, an almost constant torque is provided, apart from the minor decrease depending on the slowing engine.

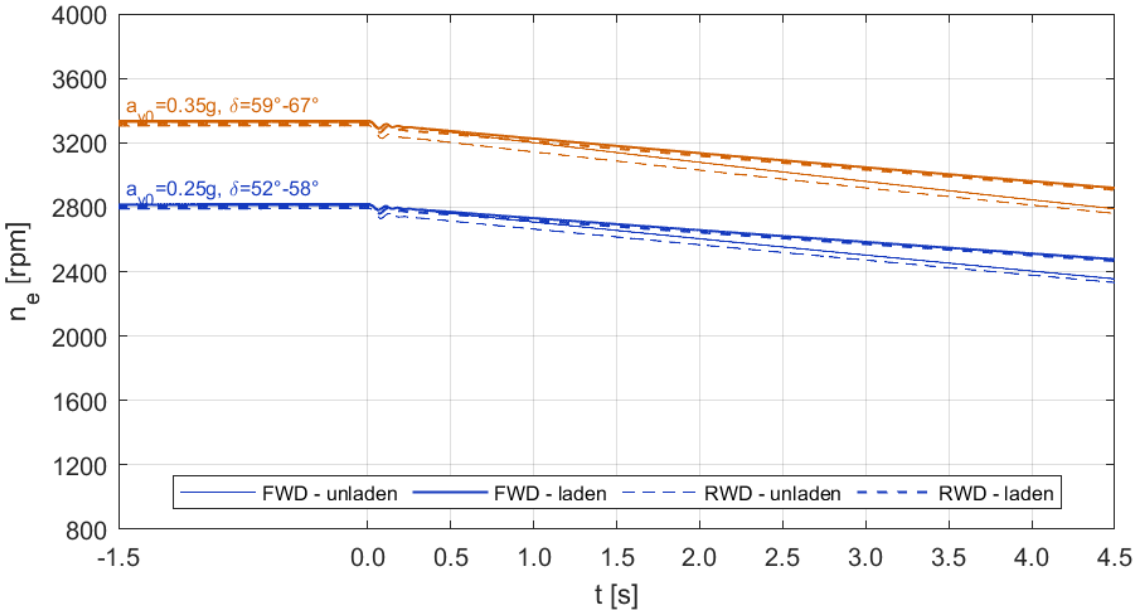

Figure 6.3: Power-Off Cornering - 3rd Gear - engine speed vs time.

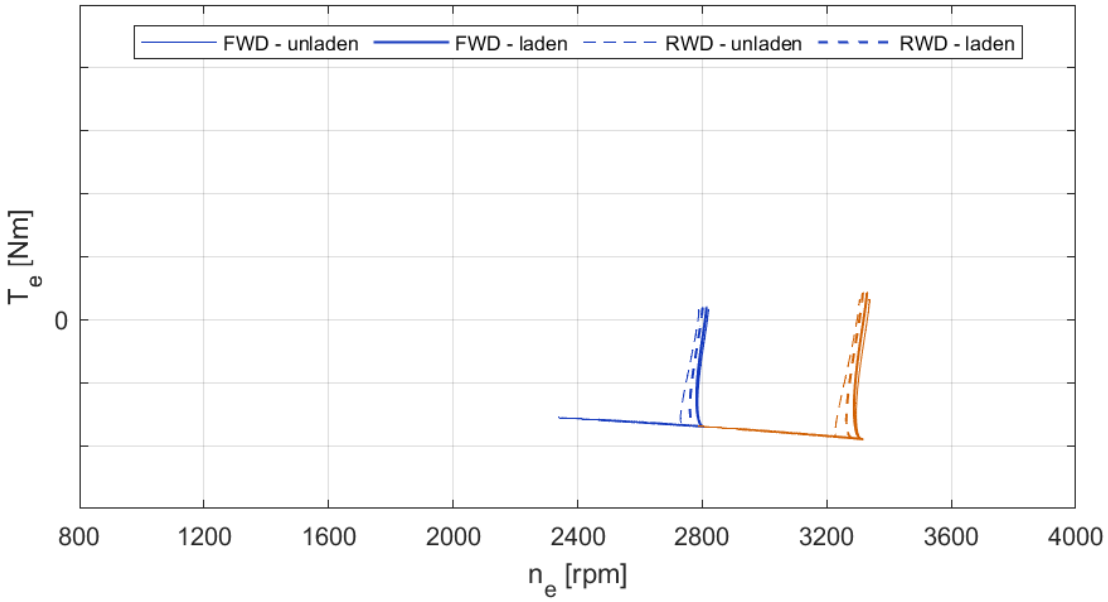

Figure 6.4: Power-Off Cornering - 3rd Gear - engine torque vs speed.

At higher gears, the fast transient disappears and the engine rotational speed settles immediately to the linear decrease. However, the response at 0.65g suggests that RWD is getting unstable, while FWD is keeping a more predictable behaviour. Since the front wheels are taking advantage of the longitudinal load transfer, FWD should be more likely to exert an effective braking torque, even when it gets closer to its grip limit, while RWD can be expected to lose grip on its rear axle, leaving room for tyres saturation and instability. Clearly, the combination of FWD and unladen condition is expected to be the most advantageous to this kind of maneuver, as the front axle is more and more loaded.

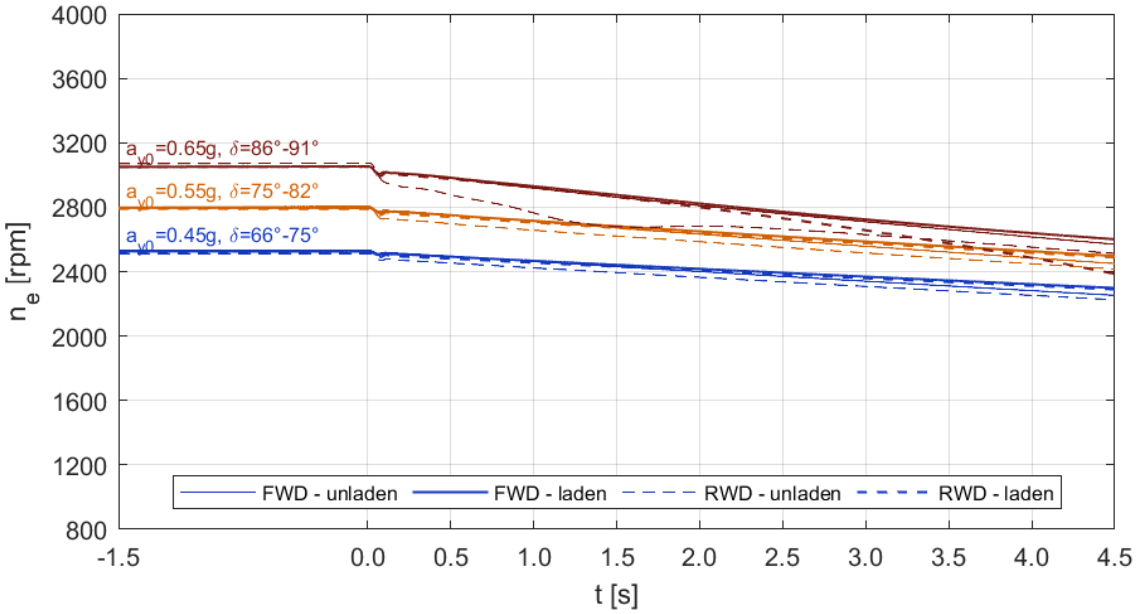

Figure 6.5: Power-Off Cornering - 4th Gear - engine speed vs time.

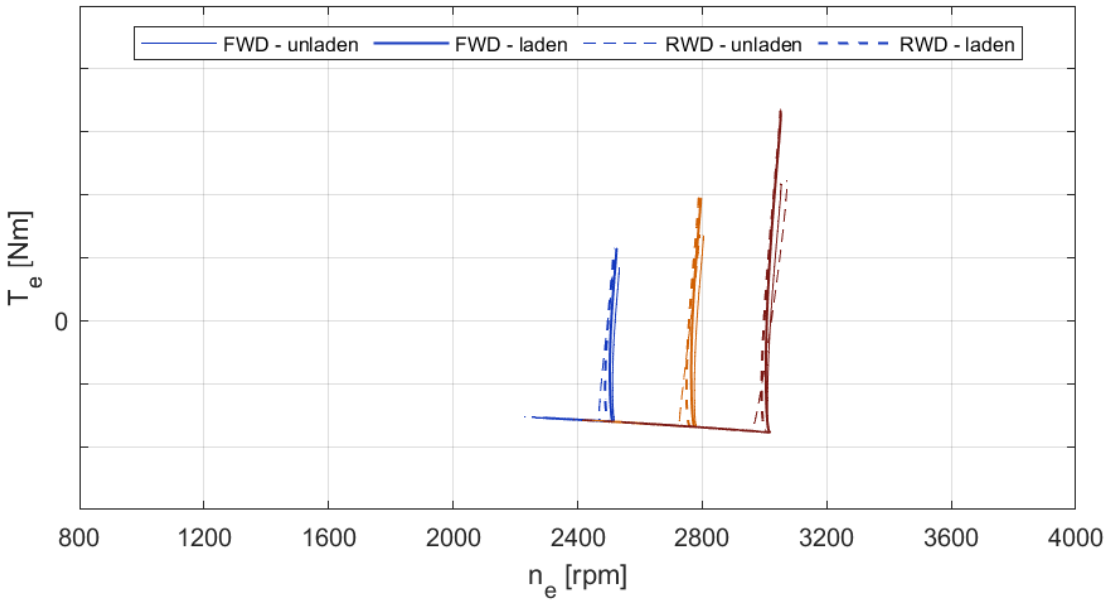

Figure 6.6: Power-Off Cornering - 4th Gear - engine torque vs speed.

6.1.2 Vehicle Dynamics

Figures from 6.7 to 6.9 show the lateral acceleration time history. After the pedal release, in 2nd gear the vehicles show some vibrations, especially on the unladen configuration. These oscillations take a few seconds to be completely damped, especially when starting from greater initial lateral accelerations. Overall, the laden van is slightly less prone to decrease its lateral acceleration, because of its greater inertia which implies a reduced ability to decelerate. Both FWD and RWD seem sensitive to these vibrations, but the former takes more time to properly dampen them. In 3rd and 4th gears, the vibrations become negligible in terms of amplitude and generally solve quickly.

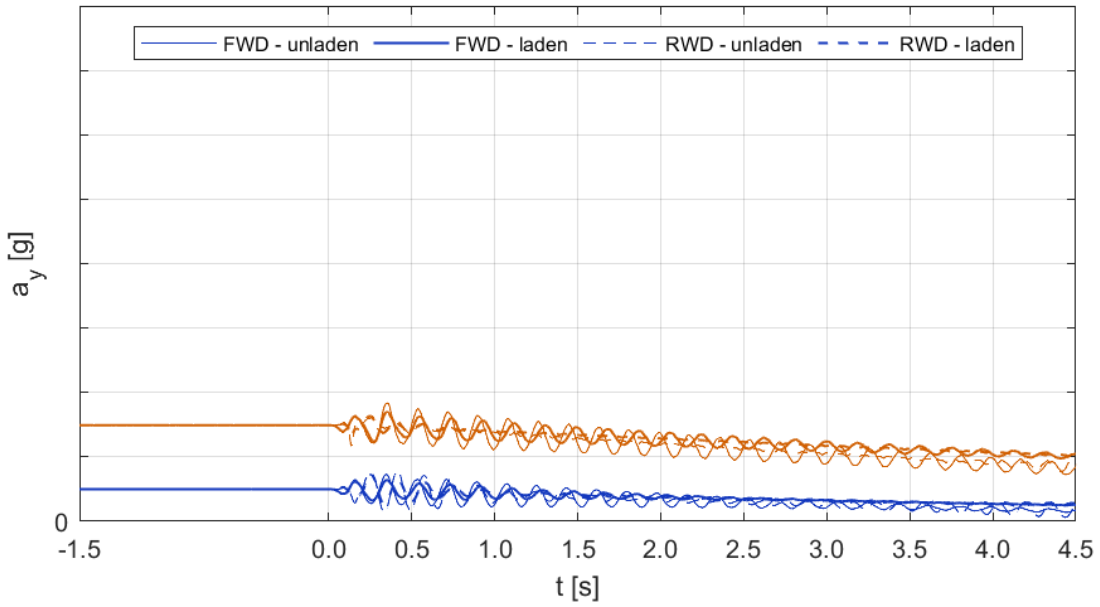

Figure 6.7: Power-Off Cornering - 2nd Gear - lat. acc. vs time.

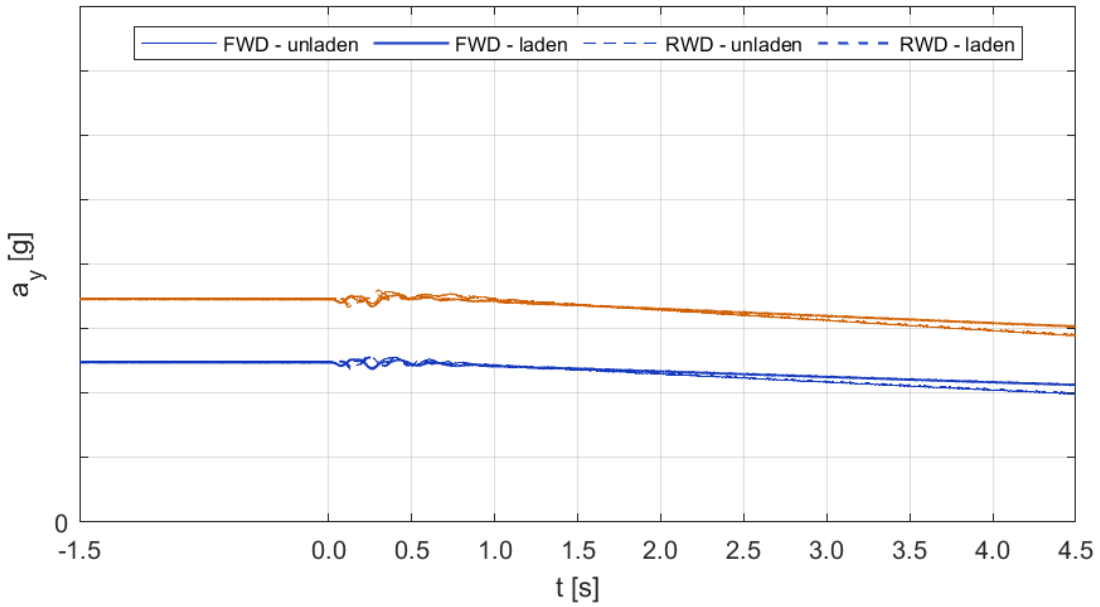

Figure 6.8: Power-Off Cornering - 3rd Gear - lat. acc. vs time.

The exception is represented by the tests close to the vehicle limit, where the transient takes longer and results in different responses. Both loading configurations show that RWD achieves a greater lateral acceleration than FWD, suggesting a tendency to close more its trajectory. However, while the unladen van is able to keep a stable response, the laden configuration tends to increase its lateral acceleration and does not stabilize at the end of the test, as the derivative is still positive, meaning that this working condition cannot restore stability. Instead, FWD provides a response that is different with respect to the predicted one, but is still able to finally reduce its lateral acceleration and stabilize itself.

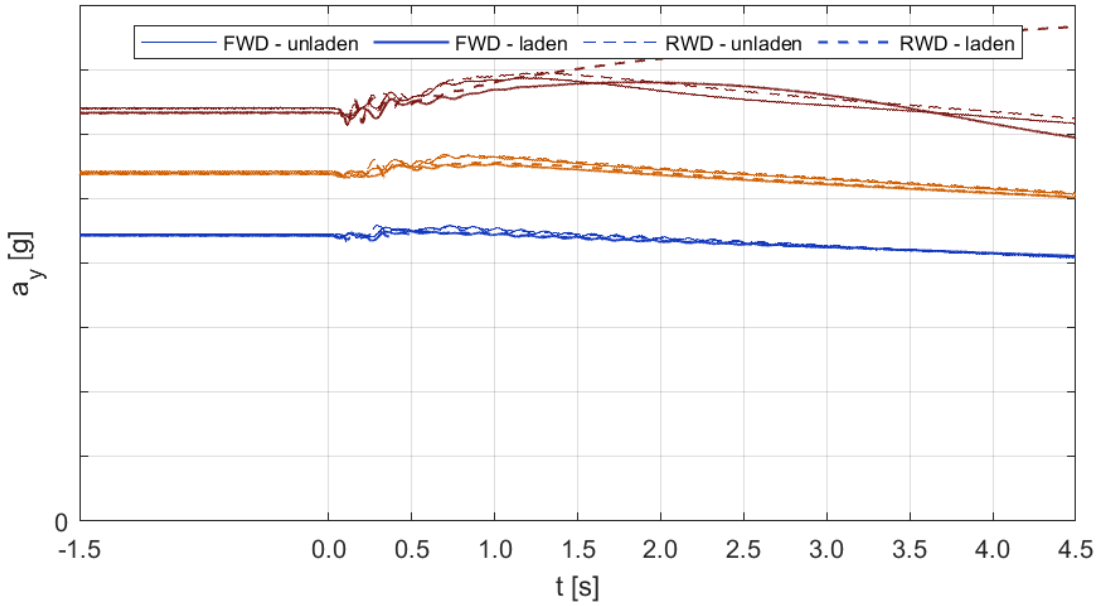

Figure 6.9: Power-Off Cornering - 4th Gear - lat. acc. vs time.

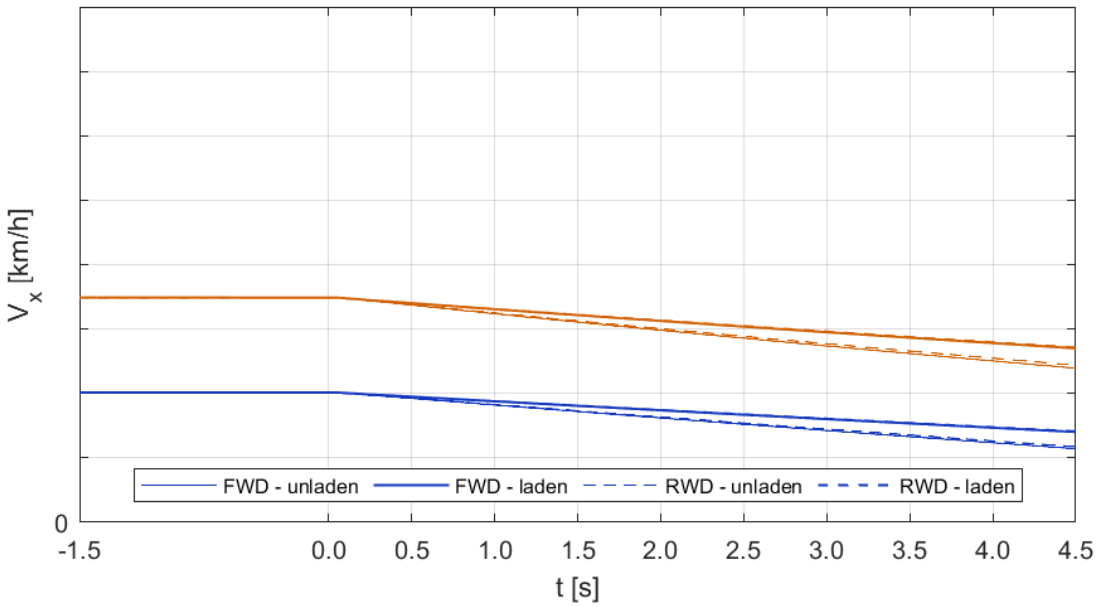

Figure 6.10: Power-Off Cornering - 2nd Gear - long. velocity vs time.

Figures from 6.10 to 6.12 show the longitudinal velocity time history. FWD and RWD show almost identical responses, while the loading condition obviously affects the vehicle inertia, thus making the laden van less sensitive to a decrease in velocity. In 4th gear the loading condition becomes less relevant, apart from the case of laden RWD, which confirms the unstable response already seen in terms of lateral acceleration. The behaviour suggested by these two quantities is that the laden RWD is closing its trajectory excessively.

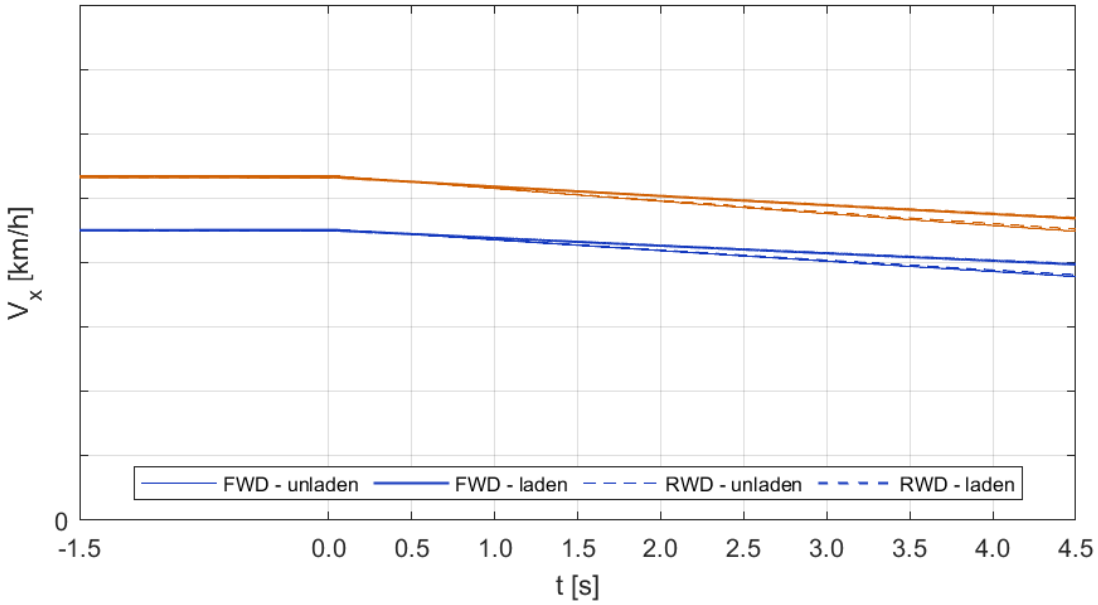

Figure 6.11: Power-Off Cornering - 3rd Gear - long. velocity vs time.

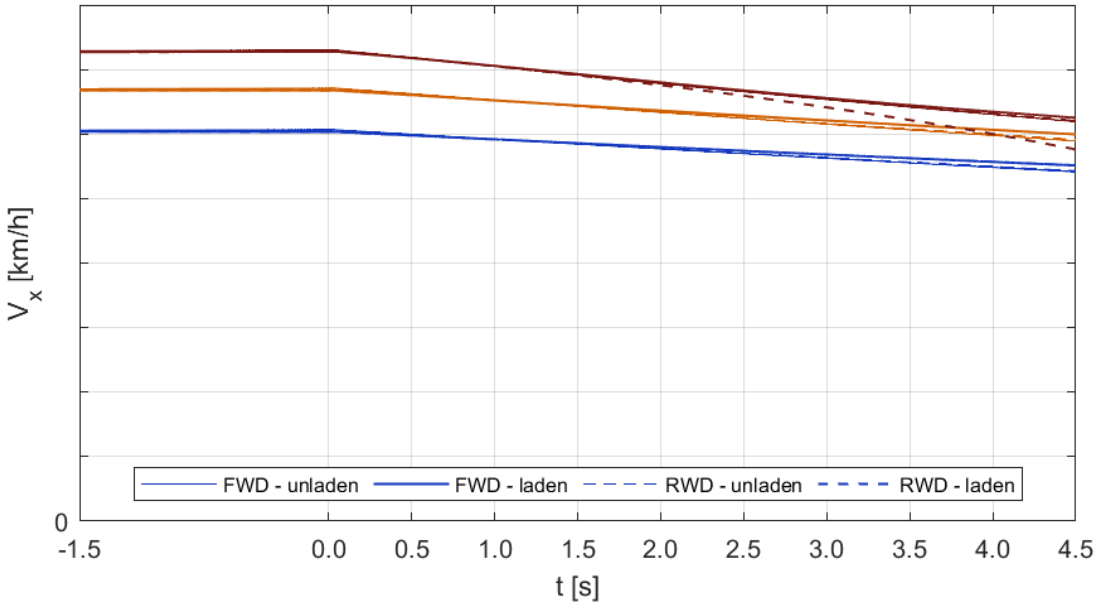

Figure 6.12: Power-Off Cornering - 4th Gear - long. velocity vs time.

Figures from 6.13 to 6.15 show the sideslip angle time history, which leads to similar conclusions. Specifically, in 2nd gear, where the vehicle has a "nose-out" configuration, the vibrations affecting FWD can be noticed, even though they have a minor impact on this quantity. In the field of middle lateral accelerations, achieved in 3rd and 4th gears, the response is almost identical on the two versions of the van. As seen in Ramp Steer, FWD is slightly less prone to a "nose-in" configuration, as a result of its more understeering tendency. The low and middle fields clearly show a progressive settling towards a "nose-out" configuration, coherent with the decrease in longitudinal velocity and the driver's expectations.

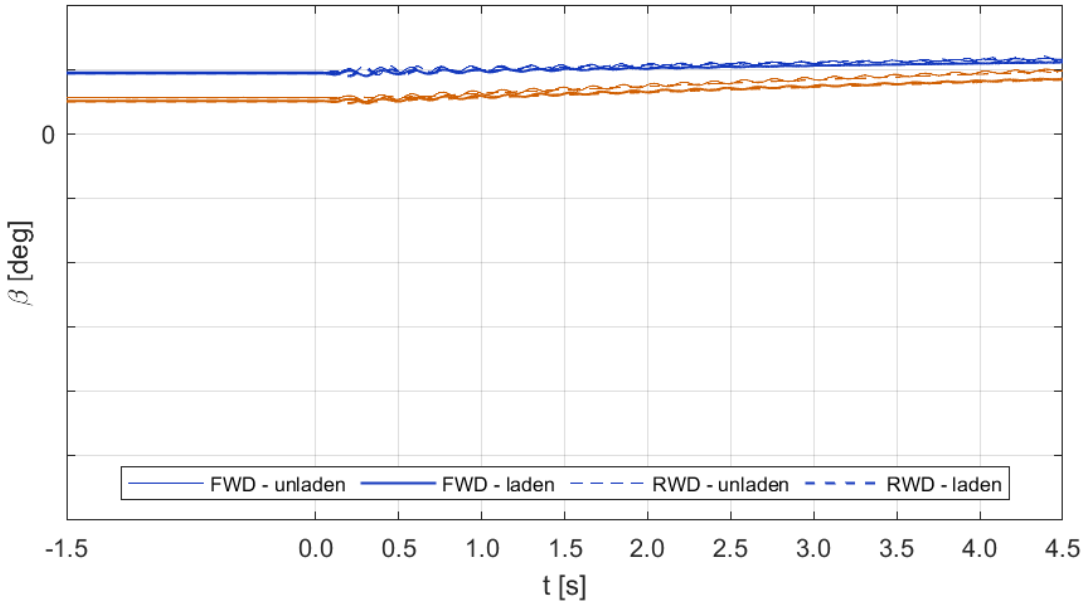

Figure 6.13: Power-Off Cornering - 2nd Gear - sideslip angle vs time.

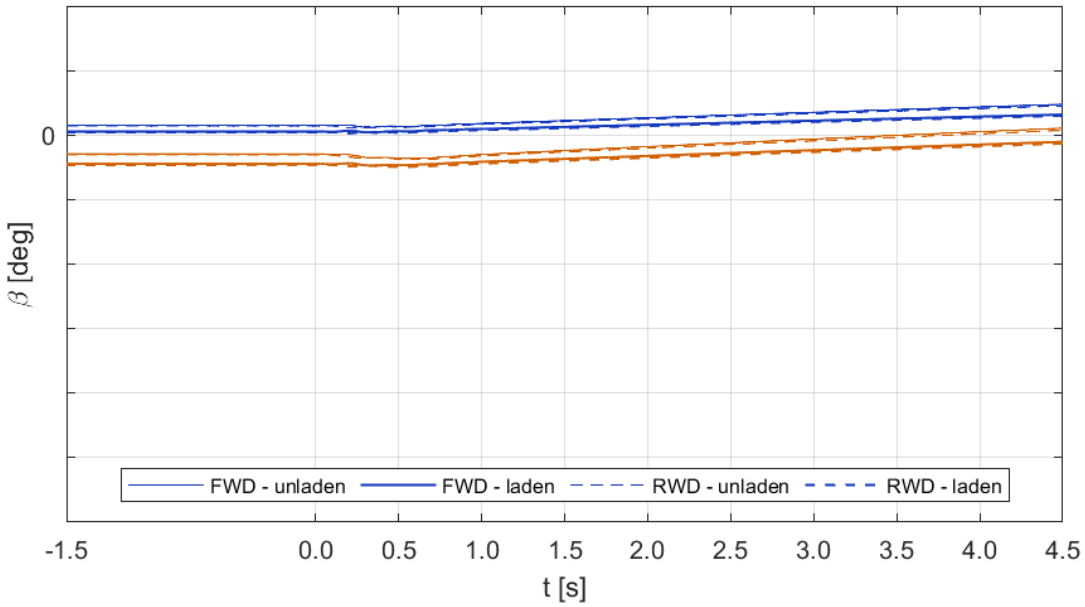

Figure 6.14: Power-Off Cornering - 3rd Gear - sideslip angle vs time.

Only when approaching the vehicle limit, the angle experiences a significant overshoot before slowly restoring its initial value. Clearly, the laden configuration emphasizes the "nose-in" configuration, especially on RWD, where the instability is confirmed by the huge values of sideslip angle reached after the power-off instant. This critical condition shows an inadequate response, as the vehicle is dangerously tilted with respect to its trajectory and, as previously stated, is not able to restore equilibrium.

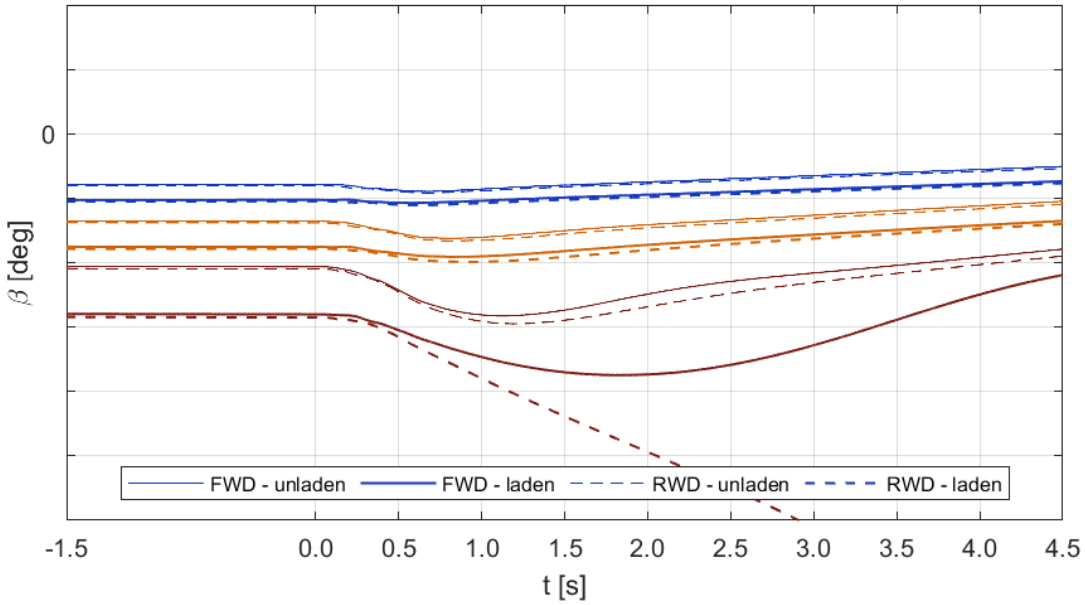

Figure 6.15: Power-Off Cornering - 4th Gear - sideslip angle vs time.

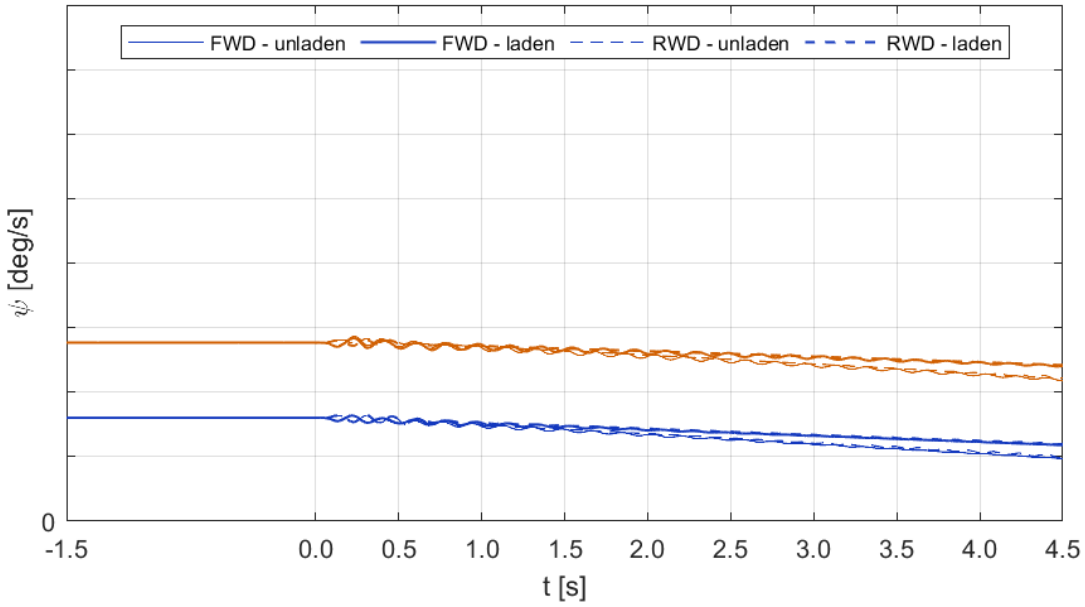

Figure 6.16: Power-Off Cornering - 2nd Gear - yaw velocity vs time.

Figures from 6.16 to 6.18 show the yaw velocity time history. This quantity is useful to highlight and sum up the considerations drawn. In 2nd gear, there is an interesting difference between FWD and RWD, which lies in the value assumed by the quantity after the power-off instant. While FWD shows a decrease in yaw rate, thus a sudden tendency to understeer, RWD manifests an increase, suggesting an immediate oversteering response. Then, an oscillatory transient takes place, with a longer time to be extinguished on FWD. The unladen configuration is slightly more sensitive to this phenomenon.

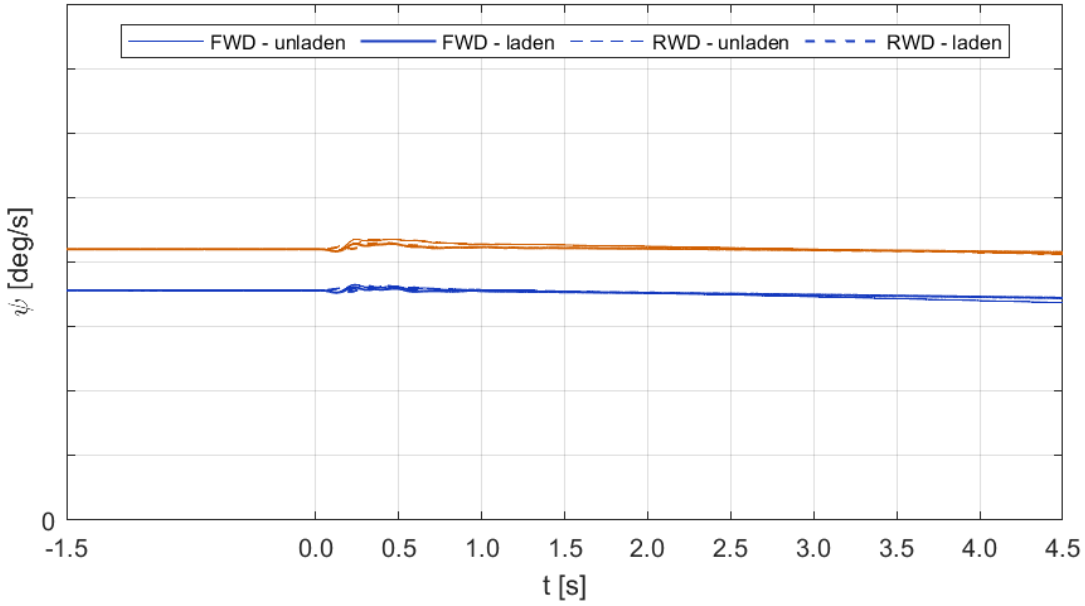

Figure 6.17: Power-Off Cornering - 3rd Gear - yaw velocity vs time.

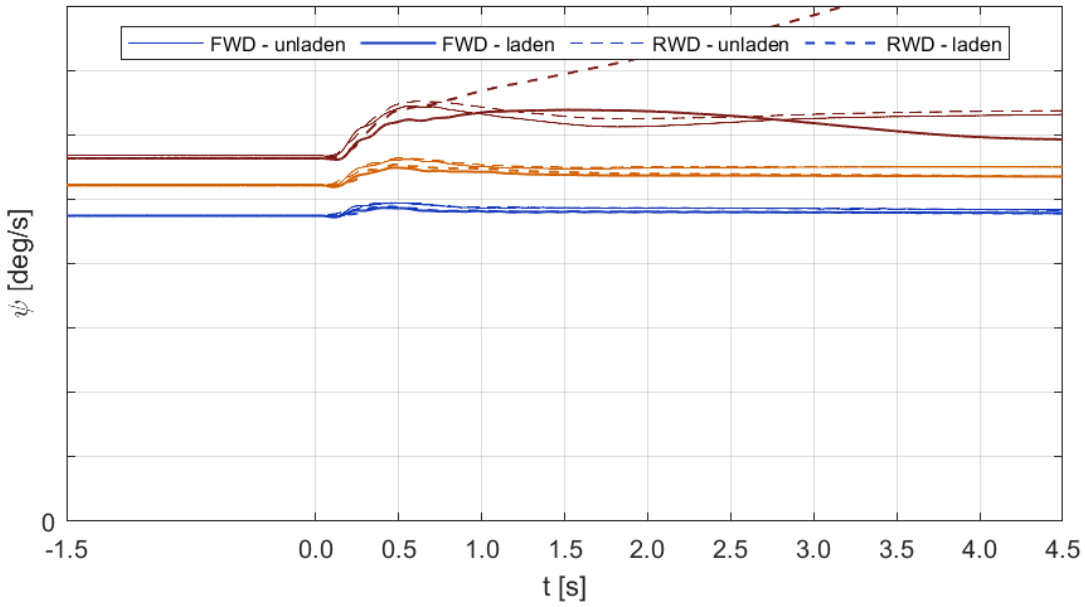

Figure 6.18: Power-Off Cornering - 4th Gear - yaw velocity vs time.

At upper gears, the instantaneous response is similar, but it is no more followed by oscillations. Generally, RWD achieves slightly greater yaw velocities, meaning a less understeering response. Once again, when the vehicle approaches its limit, a trend similar to lateral acceleration can be observed, where the unladen vehicles settle to a new, greater value, while the laden vehicles highlight the ability to recover stability. In addition to the previous prescribed quantities, *Figures from 6.19 to 6.21* report the longitudinal deceleration time history. After the fast transient which reflects the longitudinal load transfer previously considered, it is clear that in 2nd gear FWD is subject to vibrations in the longitudinal direction, as well as in the lateral direction previously seen.

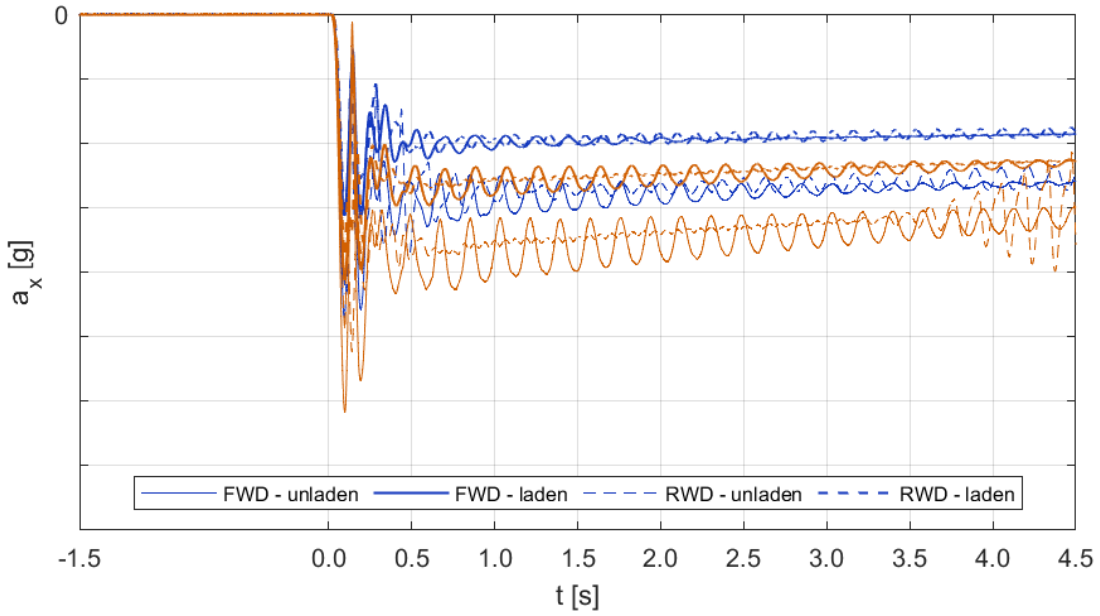

Figure 6.19: Power-Off Cornering - 2nd Gear - long. deceleration vs time.

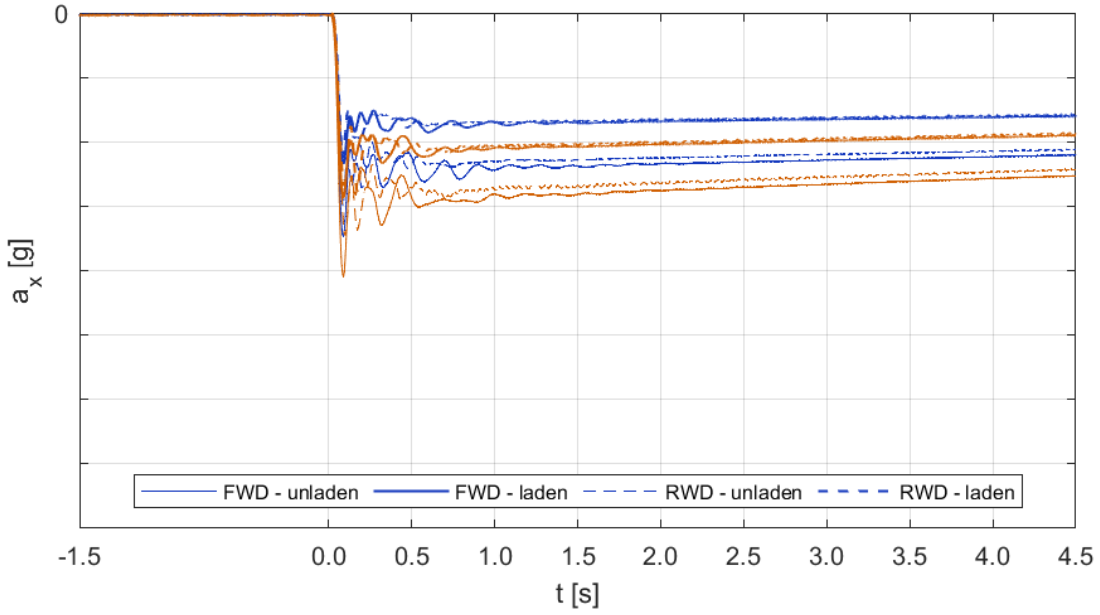

Figure 6.20: Power-Off Cornering - 3rd Gear - long. deceleration vs time.

In 3rd gear, the response is clean for all vehicles, but still FWD is manifesting slightly more significant vibrations during the short transient. Instead, in 4th gear the phenomenon is present when the engine is at lower regimes, but then the field of instability is entered and it is clear that the deceleration felt by the driver dramatically increases, especially on the laden RWD, which is proved to get completely unstable. In contrast, FWD looks less reactive in giving such a deceleration, while it emphasizes its braking ability in the unladen configuration.

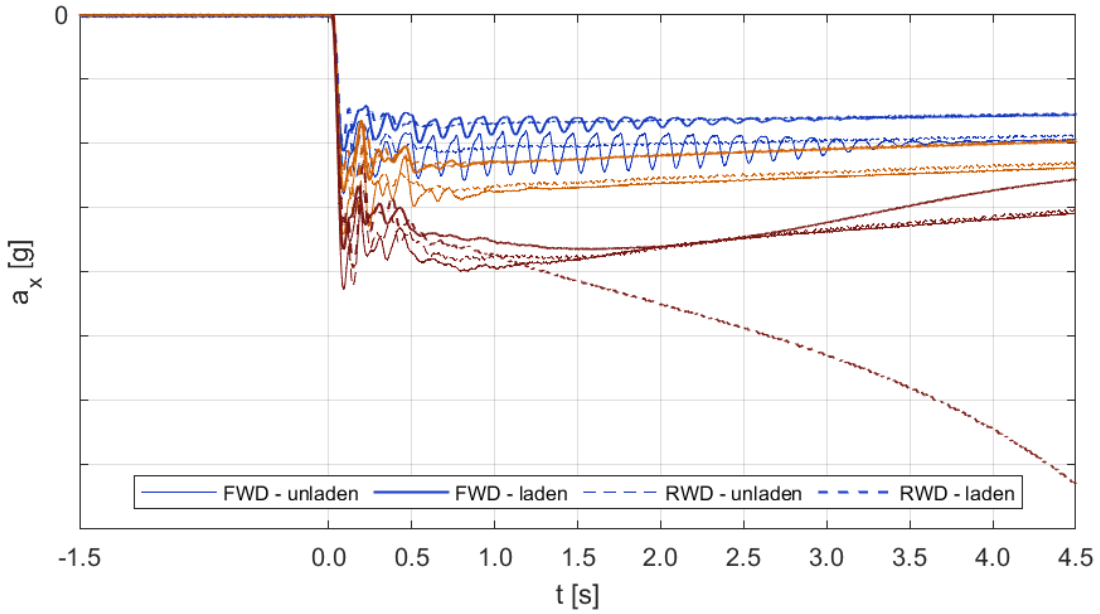

Figure 6.21: Power-Off Cornering - 4th Gear - long. deceleration vs time.

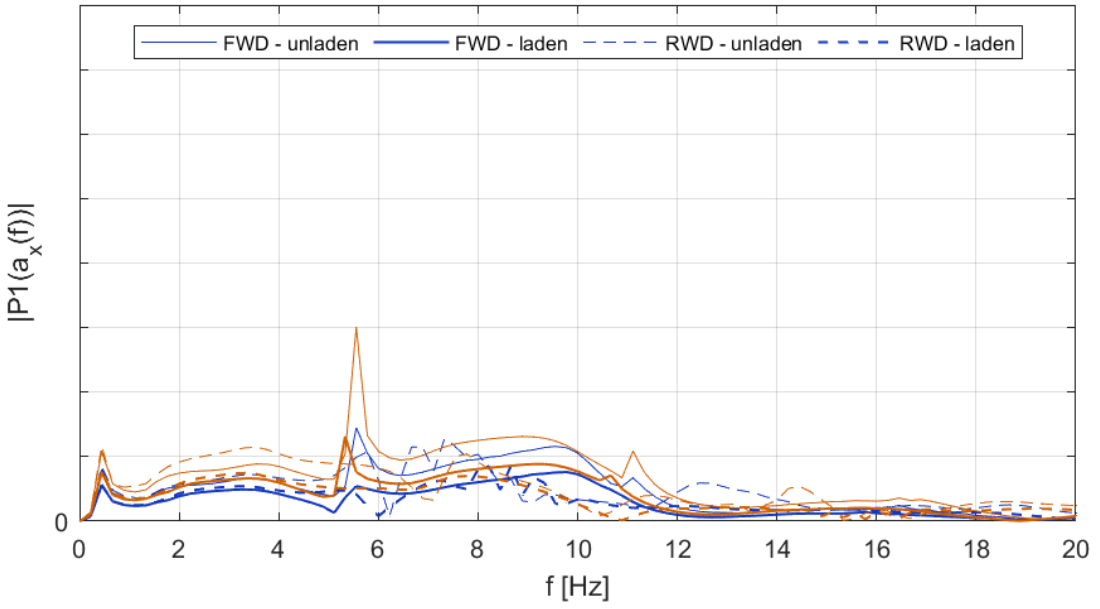

Figure 6.22: Power-Off Cornering - 2nd Gear - PSD of long. acceleration.

In terms of driver's comfort, the previously discussed longitudinal and lateral accelerations are now investigated by computing their power spectral density. *Figures 6.22 and 6.23* show the results to identify the frequency of excitation transmitted to the human body when the vehicle is cornering in 2nd gear. It is clear that the unladen FWD is the most critical, with a frequency between 5 and 6 Hz, falling in the field of resonance of chest and abdomen.

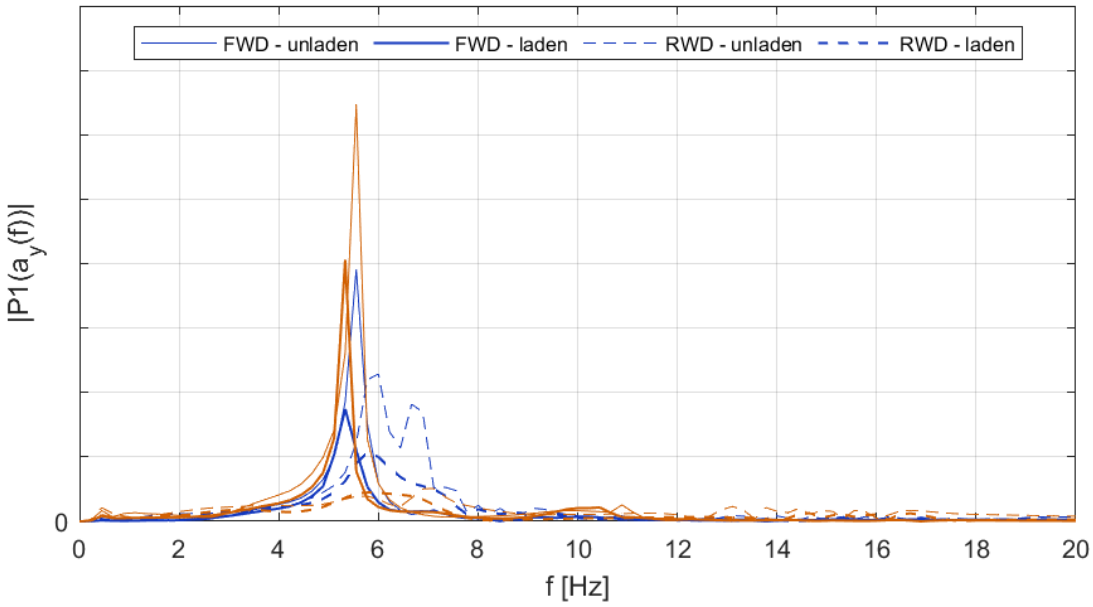

Figure 6.23: Power-Off Cornering - 2nd Gear - PSD of lat. acc.

6.1.3 Tyres Dynamics

Figures from 6.24 to 6.29 show the lateral load transfer on front and rear axles, with respect to their initial steady-state value. This definition allows to isolate the contribution to load transfer due to the cornering event, without taking into account the effect of lateral acceleration. On RWD, the reaction torque generates a fast positive peak on the rear axle. Since this is a left turn, given the clockwise spinning of the propeller shaft when looking at the vehicle from the front, a braking torque loads more the right wheel, resulting in a positive load transfer. This phenomenon is not present on FWD, since the differential box is mounted on the body subsystem, which is part of the unsprung mass.

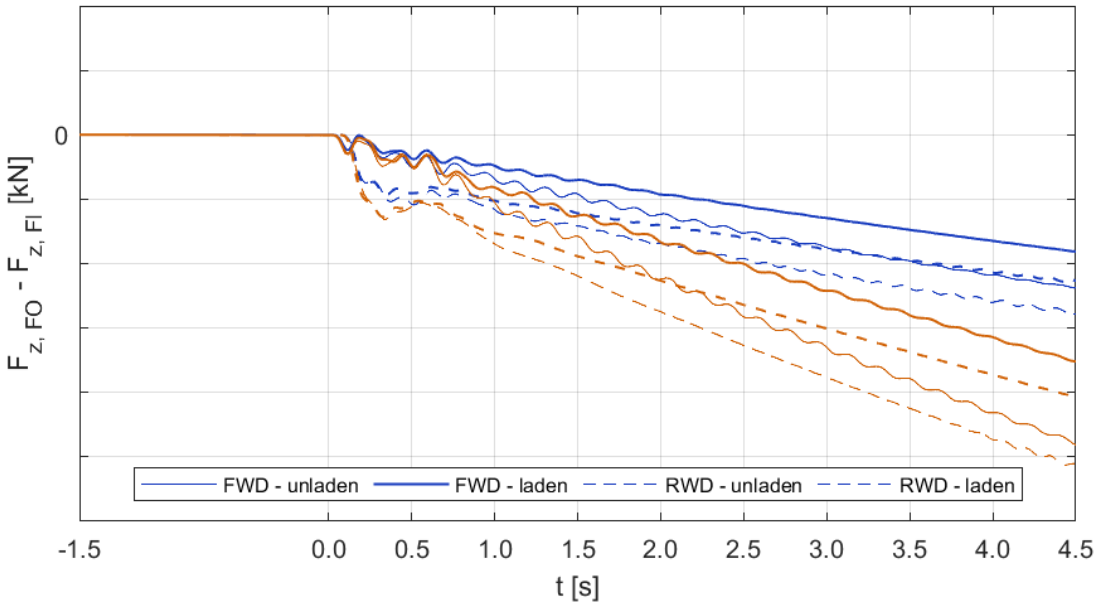

Figure 6.24: Power-Off Cornering - 2nd Gear - front lateral transfer vs time.

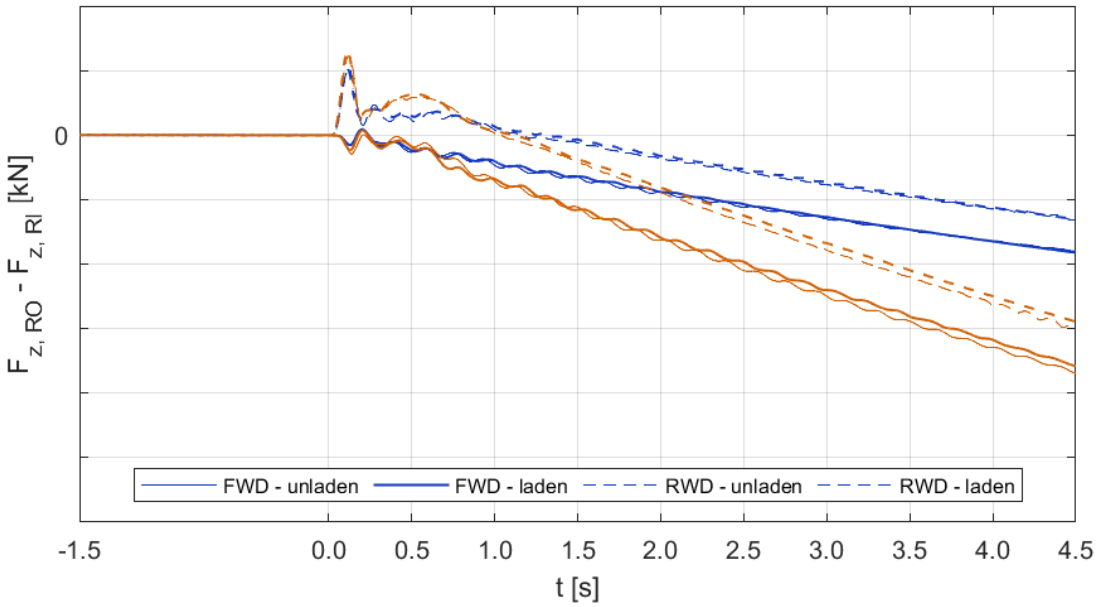

Figure 6.25: Power-Off Cornering - 2nd Gear - rear lateral transfer vs time.

Clearly, the peak reaction torque on the rear axle gains relevance as the initial lateral acceleration increases, because the engine is starting from a greater rotational speed, meaning a higher braking torque. For all tests, RWD keeps a moderate lateral load transfer on the rear axle, even after the initial peak, because the braking torque transferred to the rigid axle is still acting against the load transfer provided by the decreasing lateral acceleration, which would load more the inner wheel. Of course, a right turn would instead boost this lateral load transfer on RWD, leading to asymmetric responses, not present in FWD. Clearly, the front axle reacts to the reaction torque taking place on the rigid axle and loads more the inner wheel. Instead, on FWD both axles behave similarly, as the inner wheels are more loaded.

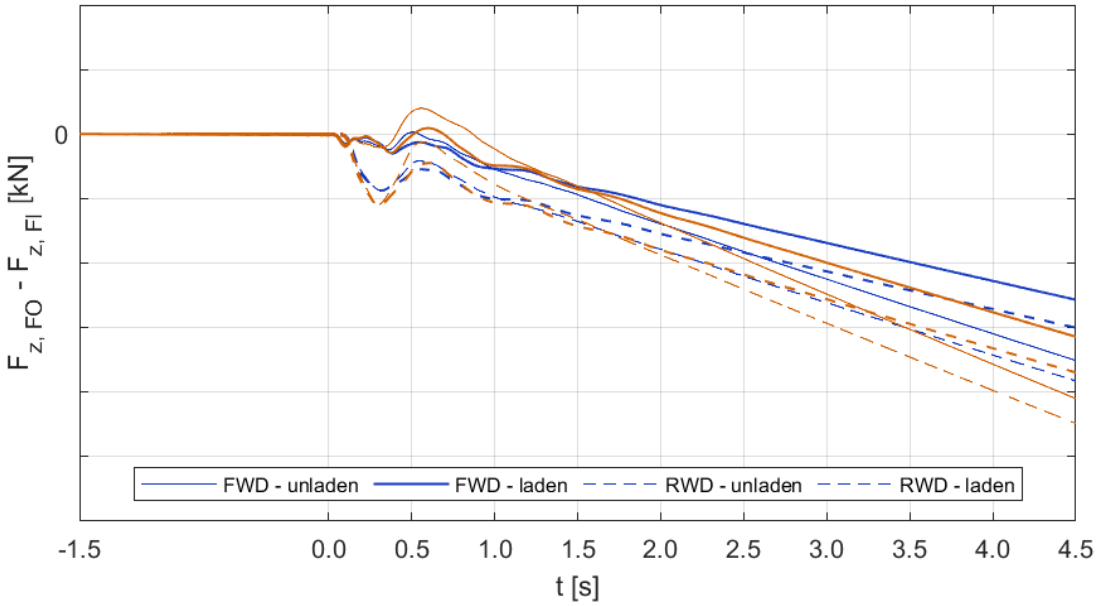

Figure 6.26: Power-Off Cornering - 3rd Gear - front lateral transfer vs time.

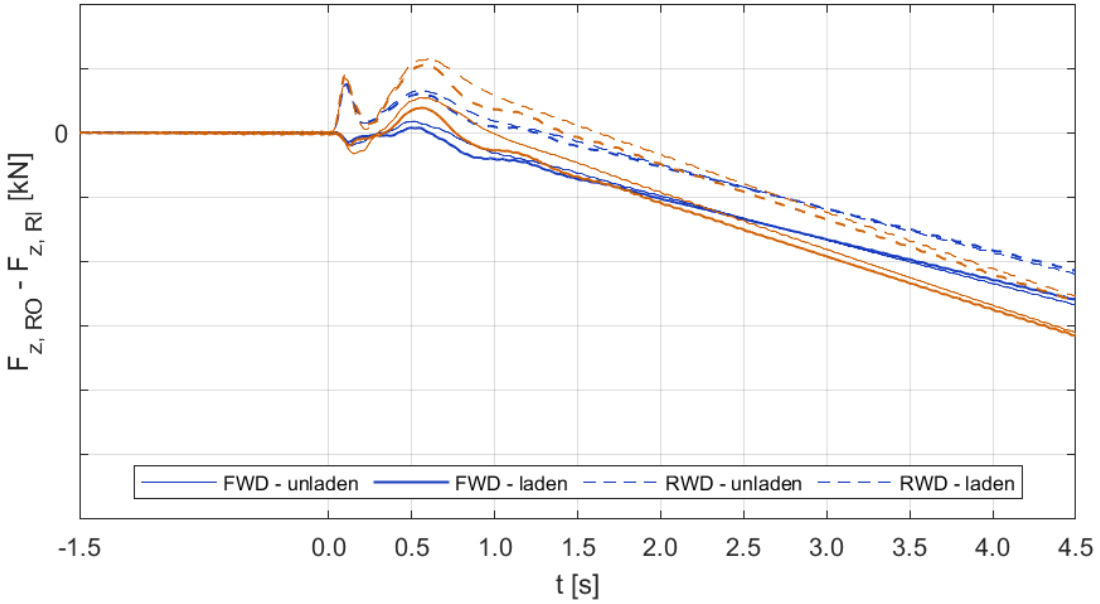

Figure 6.27: Power-Off Cornering - 3rd Gear - rear lateral transfer vs time.

When the vehicle is tested in 4th gear, hence at greater initial lateral accelerations, there is a tendency to show a positive lateral load transfer, especially on the rear axle, before going back to the negative field. This suggests that the van is reaching its limits, because it takes longer to effectively reduce its lateral acceleration and load more the inner wheel. Close to the limit, specifically at 0.65g, different responses are achieved. When the vehicle is unladen, both FWD and RWD still show the ability to recover the expected response, after a few seconds where the outer side is more loaded. However, the laden configuration shows that RWD gets completely unstable and is booming the load transfer on its outer side, without recovering it. Instead, FWD is still able to recover stability after a longer transient.

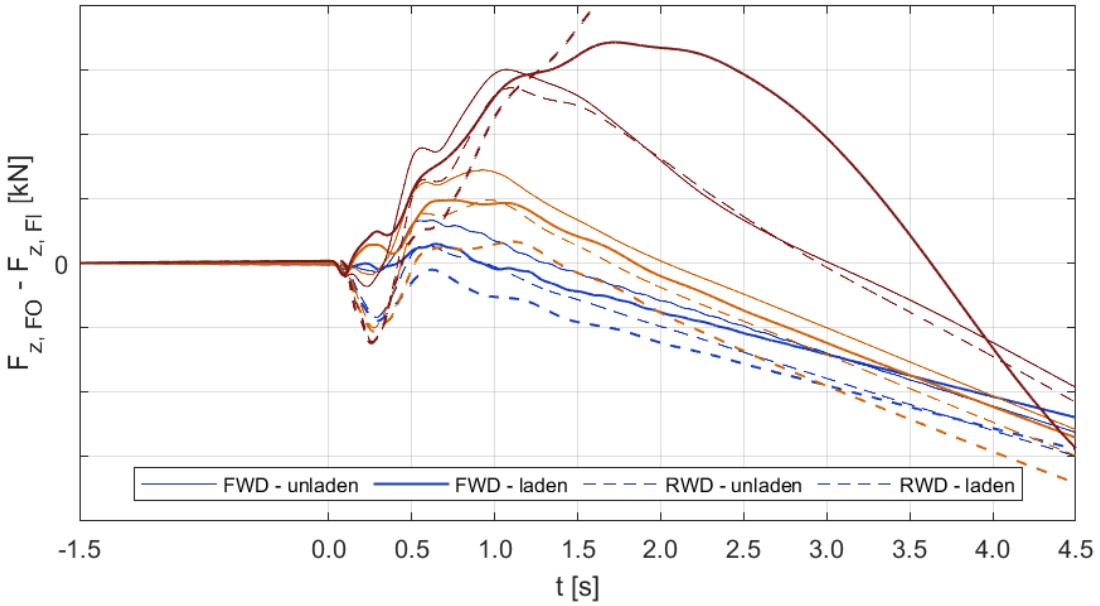

Figure 6.28: Power-Off Cornering - 4th Gear - front lateral transfer vs time.

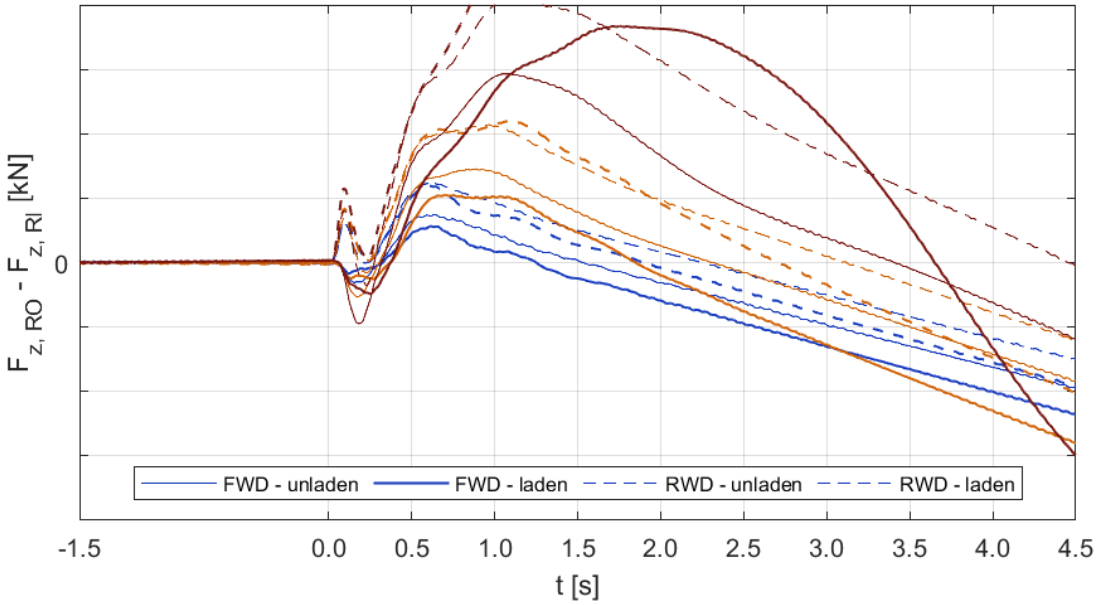

Figure 6.29: Power-Off Cornering - 4th Gear - rear lateral transfer vs time.

Figures 6.30 and 6.31 resume the lateral load transfer as function of the initial lateral acceleration at time instant t_1, hence 1.0s after the power-off instant. On the rear axle, FWD is achieving moderate load transfers, which are slightly negative in the low and middle field of lateral accelerations, meaning that the vehicle quickly reacts to the maneuver by reducing its lateral acceleration. Instead, in 4th gear it shows a positive transfer, because the high level of lateral acceleration makes the vehicle less reactive to power-off. Both axles show similar responses, but an anomalous behaviour takes place at 0.7g. RWD instead confirms the presence of the reaction torque, which loads more the right wheel on the rear axle, resulting in different responses for left and right turns. Consequently, the front axle reacts and behaves oppositely.

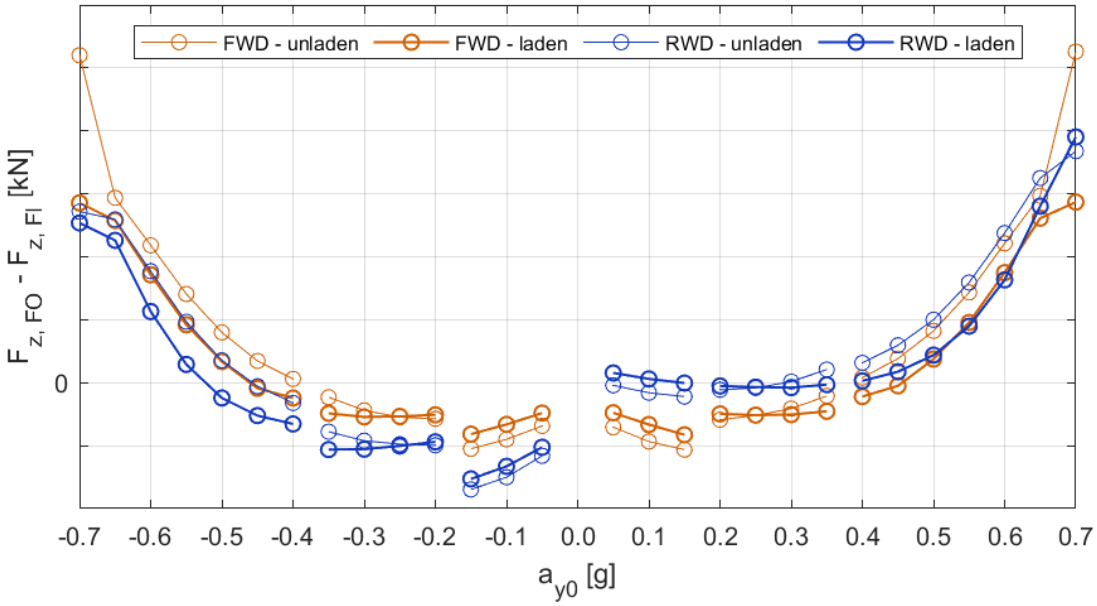

Figure 6.30: Power-Off Cornering - front lateral transfer vs in. lat. acc. @ t_1.

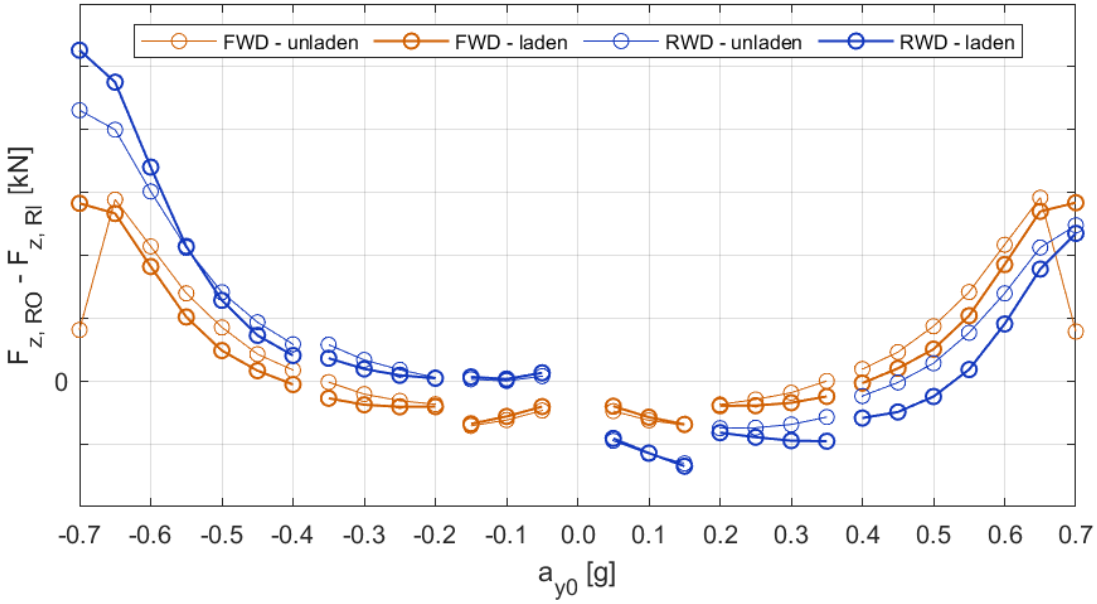

Figure 6.31: Power-Off Cornering - rear lateral transfer vs in. lat. acc. @ t_1.

Figures from 6.32 to 6.34 show the longitudinal load transfer time history, defined as the difference between rear and front axles loads, with respect to their initial steady-state value. This time, the only steady-state load transfer to be excluded is the static weight distribution. The entity of longitudinal load transfer is moderate, since the engine ability to break is about one fifth of its maximum driving torque. These diagrams clarify the oscillations previously detected on the engine rotational speed. Due to the vehicle pitch motion, a sudden forward motion loads more the front axle, which is immediately followed by the reaction of the suspension to its bounce, forcing the body to pitch backwards. This phenomenon is repeated a few times with varying amplitude, until an overshoot with respect to the new steady-state value takes place.

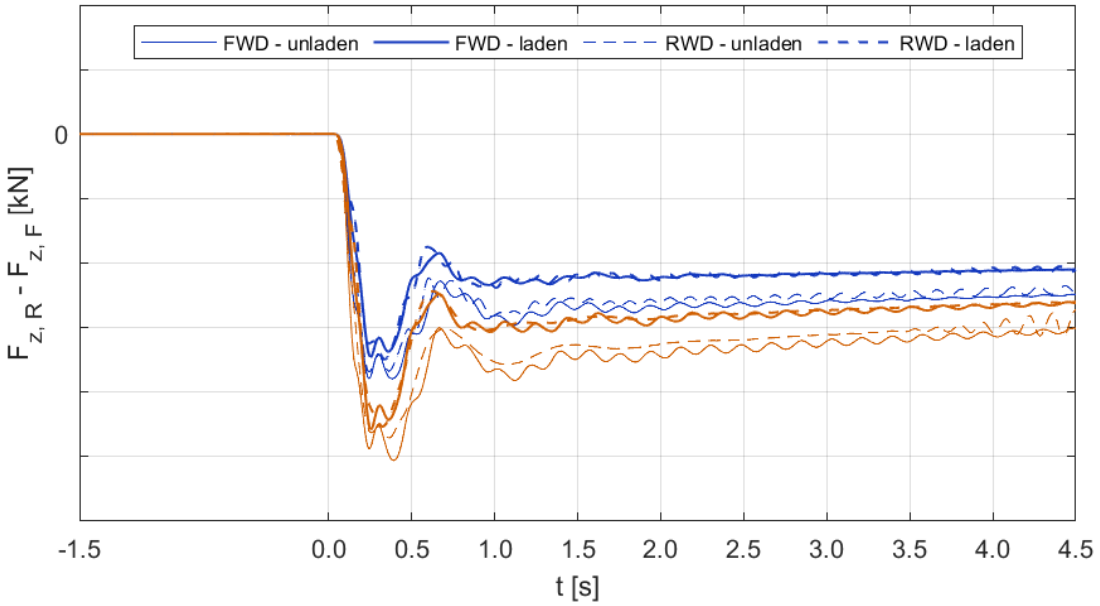

Figure 6.32: Power-Off Cornering - 2nd Gear - long. transfer time.

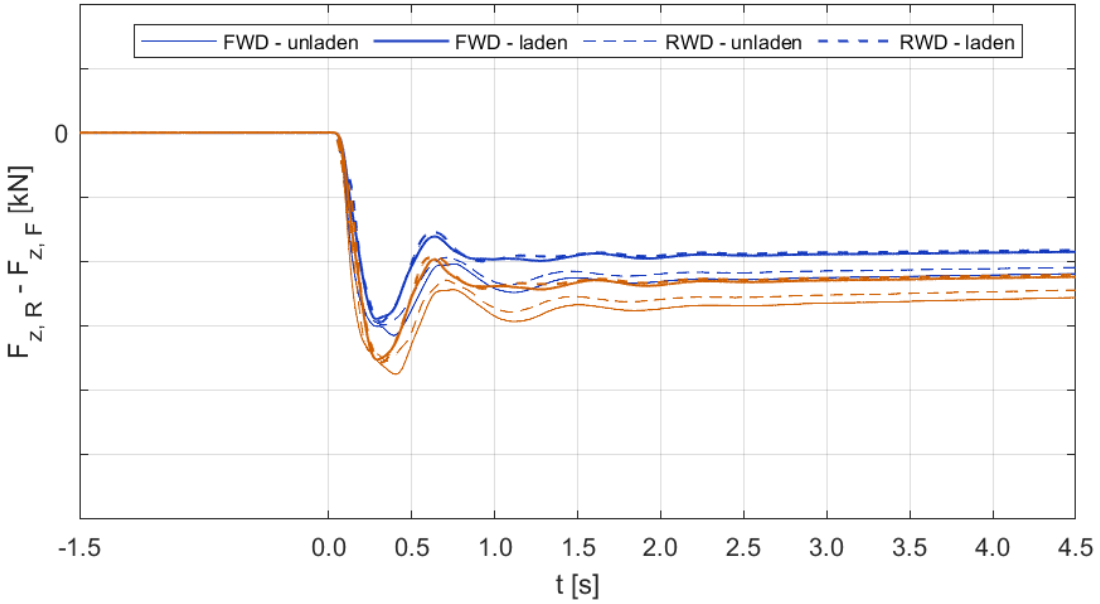

Figure 6.33: Power-Off Cornering - 3rd Gear - long. transfer time.

Overall, FWD and RWD provide similar responses, the former being subject to some little vibrations, especially when the 2nd gear is engaged. Moreover, FWD shows some slightly more pronounced negative peaks during the transient, because the front axle is taking advantage of the load transfer and applies a more effective braking torque to the ground. Clearly, the small shift in load distribution towards the front axle due to the transmission components can be beneficial to the grip of the front axle, even though in a minor amount. Concerning the loading conditions, when the vehicle is running in 2nd and 3rd gears, the laden configuration seems less reactive to a longitudinal load transfer, mainly due to its lower CG height. Instead, in 4th gears the differences given by the loading condition are less noticeable. Only when the vehicle is close enough to its limit, the laden van looks more sensitive to a longitudinal load transfer. Here, the overshoot amplitude is wider, confirming that the vehicle is struggling to settle to a new steady-state condition.

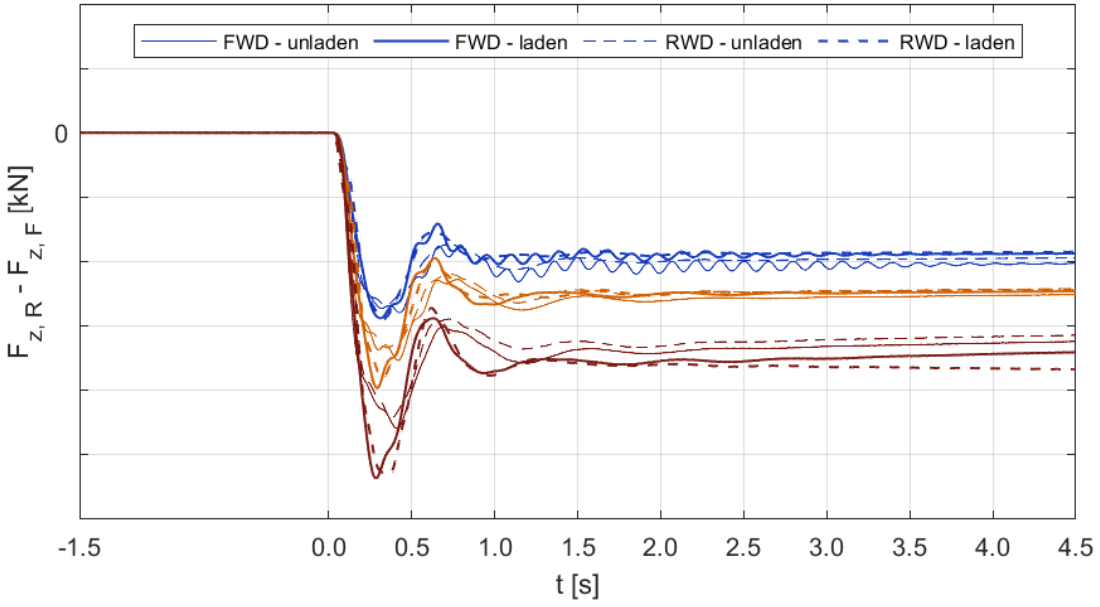

Figure 6.34: Power-Off Cornering - 4th Gear - long. transfer time.

Figure 6.35 reports the longitudinal load transfer as function of the initial lateral acceleration at time instant t_1. The overall fitting between FWD and RWD is confirmed, as well as the fact that an unladen vehicle is more sensitive to load transfer, especially in the field of low and middle lateral accelerations. When the vehicle approaches its limit, the laden configuration becomes more sensitive, but still provides similar results for both FWD and RWD. Instead, the unladen RWD seems to lose sensitivity towards load transfer, suggesting that its braking ability is stressed to the limit when cornering at 0.7g. This response can be better clarified monitoring the wheels longitudinal slip. *Figures 6.36 and 6.37* show the slip achieved on the inner and outer drivetrain as a function of the initial lateral acceleration, again at a time instant equal to 1.0s after the power-off instant. Overall, the slip is less than 5%, thus very close to the pure rolling condition. Only when the vehicle gets close to its limit, the inner wheel of the unladen RWD van is showing a huge slip, which later results in complete saturation at 0.7g. This phenomenon confirms how the rear axle is getting critical, because the combination of unladen configuration, reaction torque and longitudinal load transfer are dangerously unloading the inner wheel, especially during a left turn, leaving room for 100% slippage. Instead, when turning to the right, the reaction torque offers a partial resistance to tyre slipping. This response does not take place on FWD. Finally, as expected, the outer driving wheel never suffers slippage.

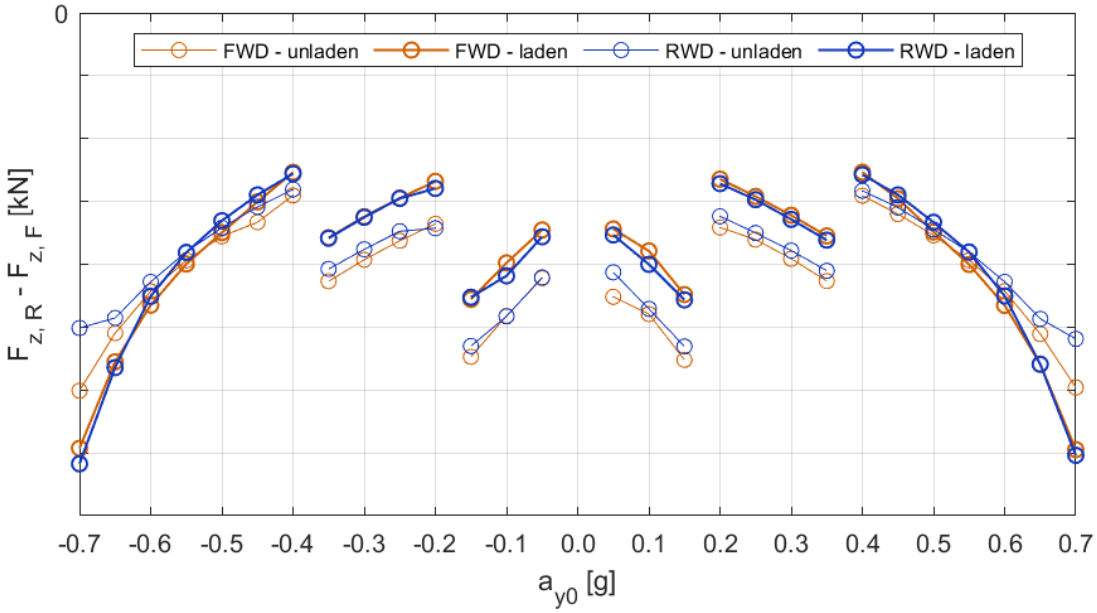

Figure 6.35: Power-Off Cornering - long. transfer vs in. lat. acc. @ t_1.

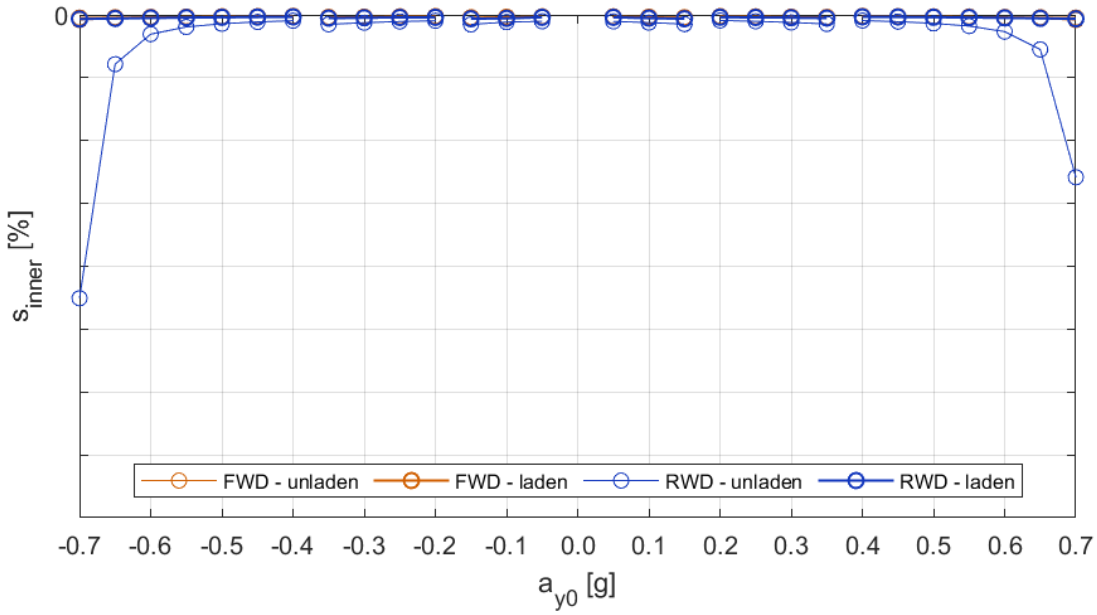

Figure 6.36: Power-Off Cornering - inner slip vs in. lat. acc. @ t_1.

Figures from 6.38 to 6.41 report the slip angle achieved on each wheel as function of the initial lateral acceleration at time instant t_1. This quantities allow to completely understand the tyres dynamics, which involve both longitudinal and lateral forces in this kind of maneuver. Overall, FWD and RWD show similar results, the latter tending to slightly greater angles when approaching the limit. Obviously, the front inner wheel shows the greatest slip angle, due to its steering angle. Similarly, on the rear axle the inner wheel has a slightly greater slip angle, due to its lower turning radius with respect to the outer wheel.

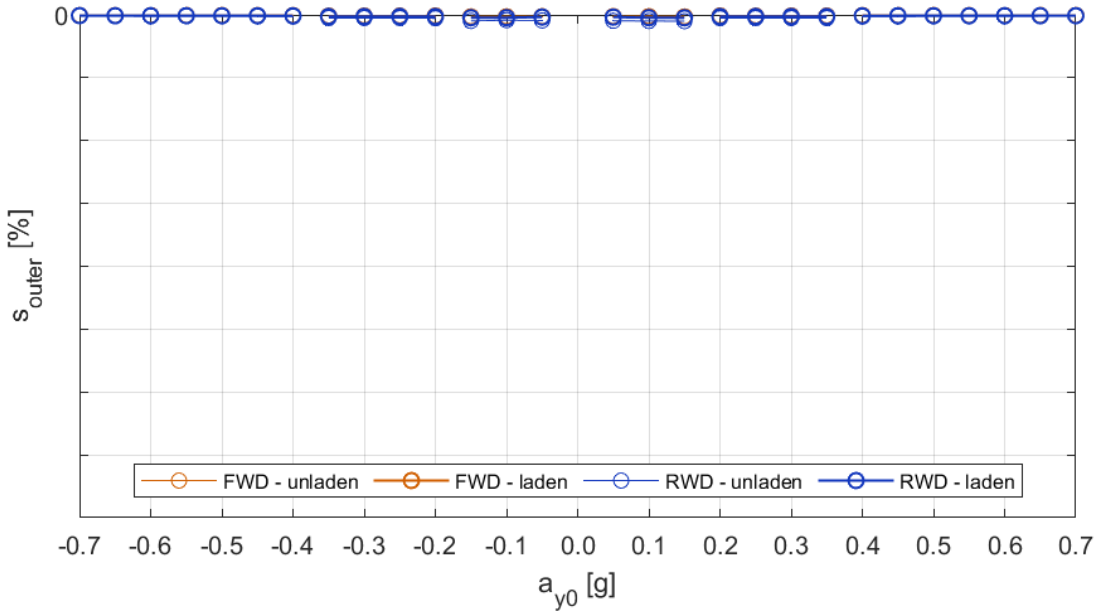

Figure 6.37: Power-Off Cornering - outer slip vs in. lat. acc. @ t_1.

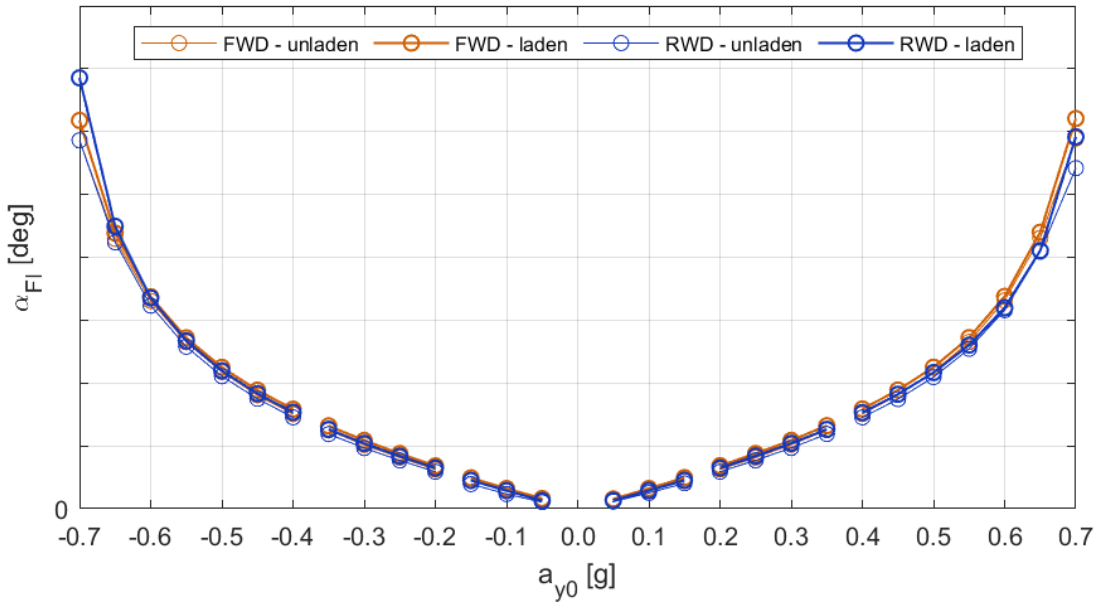

Figure 6.38: Power-Off Cornering - fr. in. slip angle vs in. lat. acc. @ t_1.

The most interesting result is represented by the unladen FWD at 0.7g, where the rear inner wheel achieves a null slip angle during the transient, meaning it is losing contact with the ground. This phenomenon does not occur on RWD, but the previous diagrams about longitudinal slip confirm that the rear inner wheel is saturating. These two results suggest that the van is not able to properly manage this kind of maneuver at 0.7g, because the combination of lateral and longitudinal load transfers dangerously unloads the rear inner wheel. The different response between FWD and RWD is influenced by the entity of the longitudinal load transfer, which is greater in case of FWD. For this reason, FWD forces the wheel to leave the ground, while RWD leaves a residual normal force which allows it to saturate without losing contact.

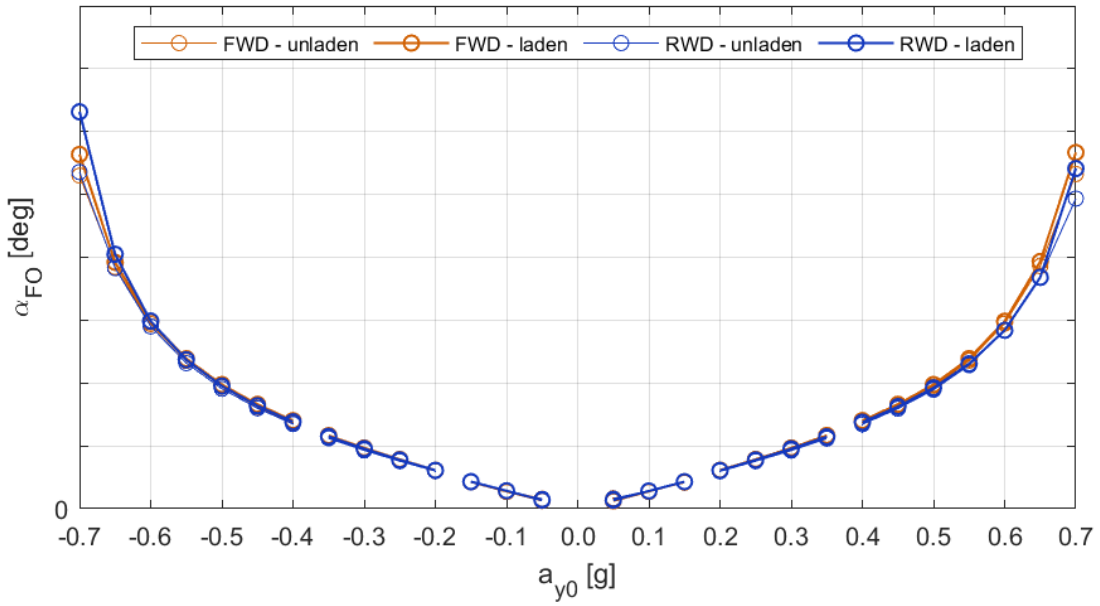

Figure 6.39: Power-Off Cornering - fr. out. slip angle vs in. lat. acc. @ t_1.

Figure 6.42 shows the understeer gradient, defined as the difference between the average front and rear slip angles as function of the initial lateral acceleration, at time t_1. Both loading configurations indicate FWD as more understeering, hence less reactive to the maneuver. The huge value achieved by the unladen van at 0.7g is explained by the phenomenon involving the rear inner wheel. This means that, during a limit maneuver, the unladen FWD would temporarily become insensitive to power-off itself, delaying the action of closing its trajectory. The symmetric response provided by FWD is not confirmed by RWD, which shows a more understeering behaviour when turning to the left, because the rear right wheel is experiencing an enhanced grip due to the reaction torque, thus providing an asymmetric braking action.

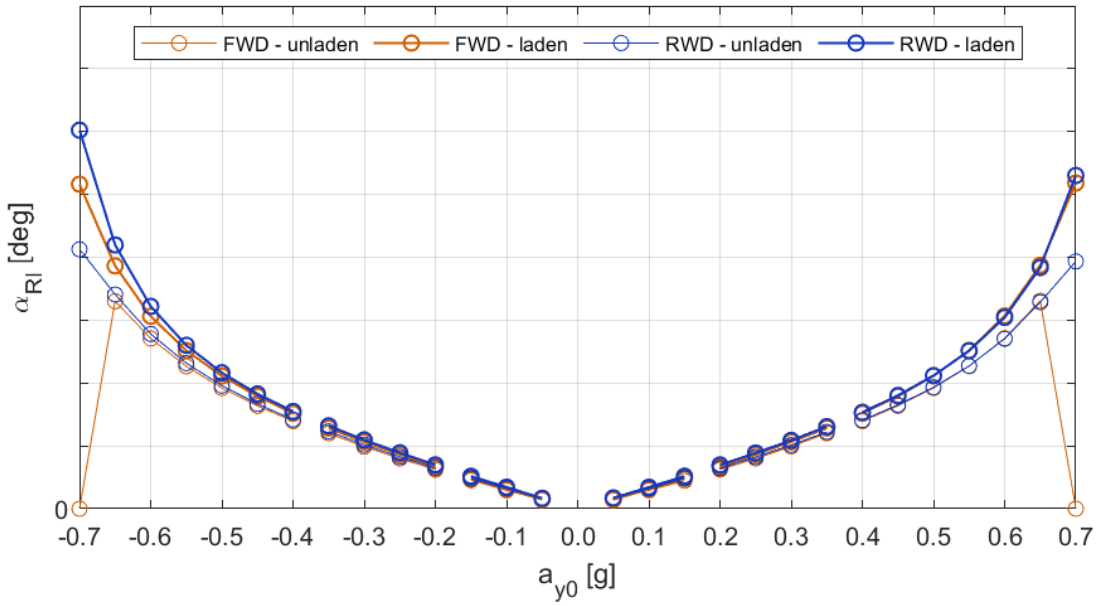

Figure 6.40: Power-Off Cornering - rr. in. slip angle vs in. lat. acc. @ t_1.

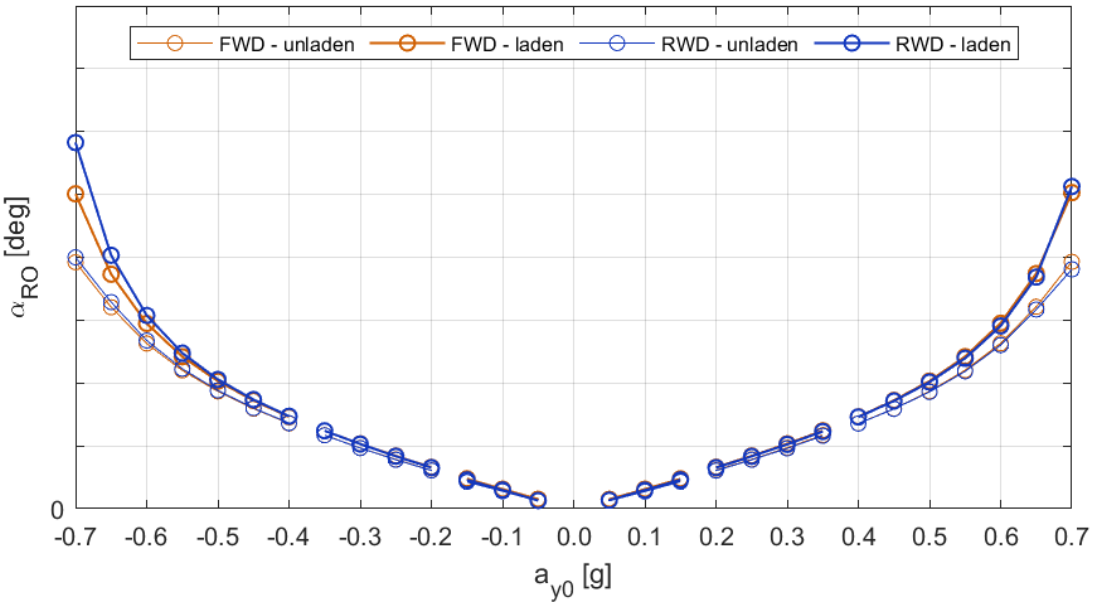

Figure 6.41: Power-Off Cornering - rr. out. slip angle vs in. lat. acc. @ t_1.

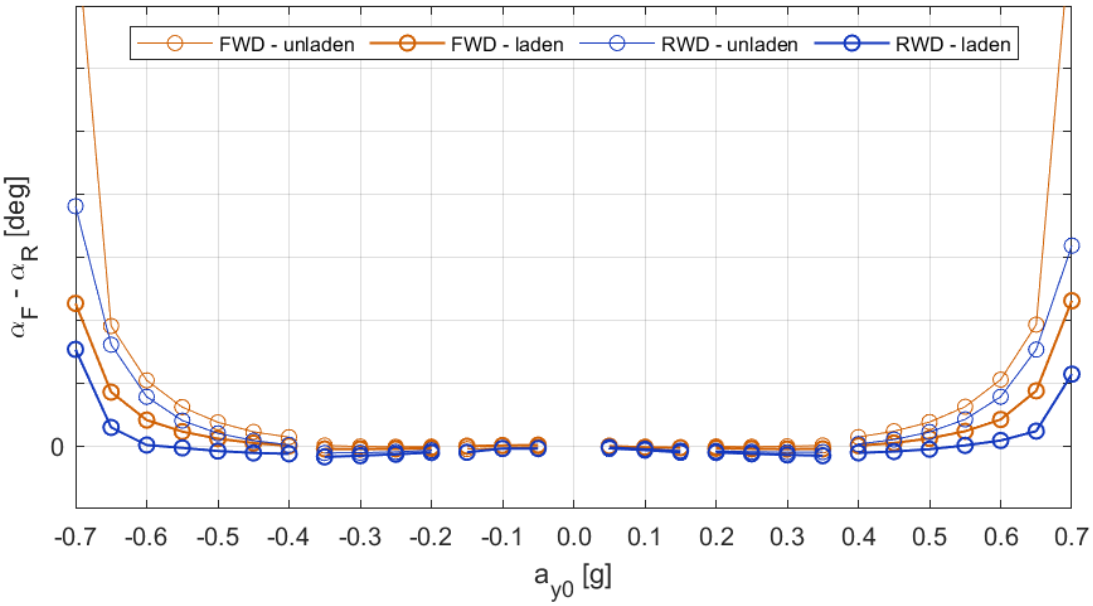

Figure 6.42: Power-Off Cornering - understeer gradient vs in. lat. acc. @ t_1.

6.1.4 Steering System

Figures from 6.43 to 6.51 show the steering wheel torque, front wheels total self-aligning moment and steering rack stroke time histories. These quantities provide information about the steering chain from the front wheels to the steering wheel, hence the driver's point of view. According to the sign conventions used in Adams/Car, a negative steering wheel torque is directed counterclockwise from the driver's viewpoint, thus coherent with a left turn. At the same time, the self-aligning torque on the wheels is negative when directed clockwise, thus effectively providing an aligning action during a left turn. Finally, the steering rack stroke is measured as the travel with respect to the neutral position.

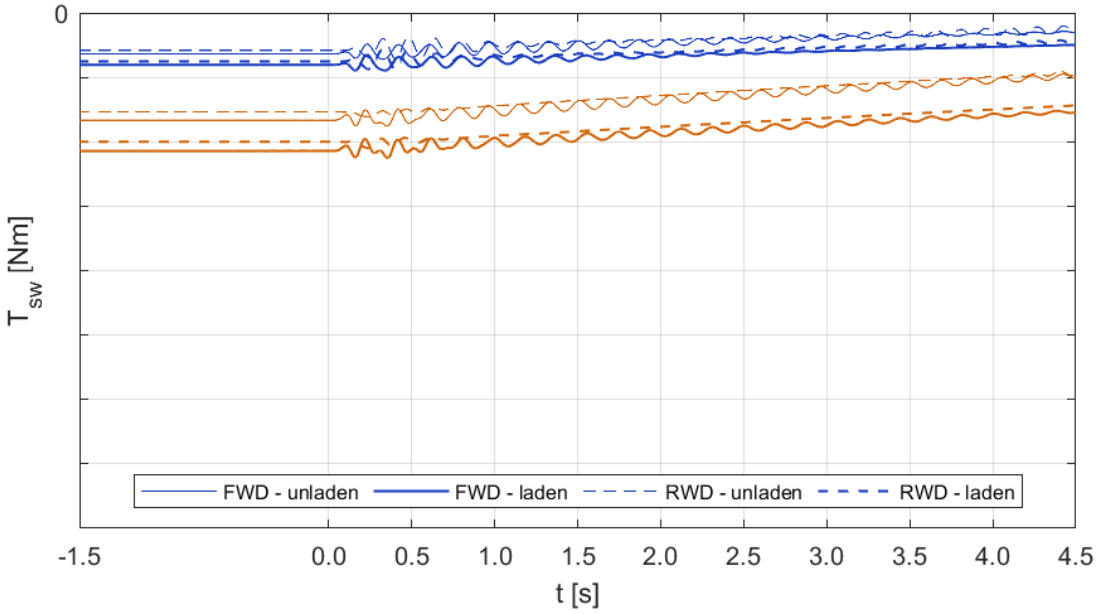

Figure 6.43: Power-Off Cornering - 2nd Gear - steering wheel torque vs time.

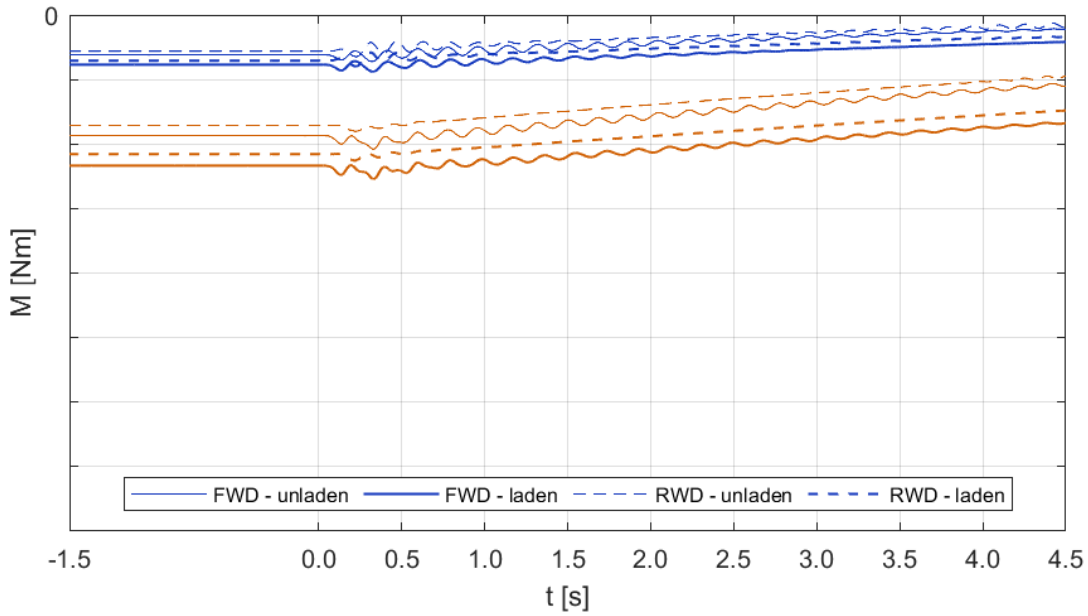

Figure 6.44: Power-Off Cornering - 2nd Gear - self-aligning moment vs time.

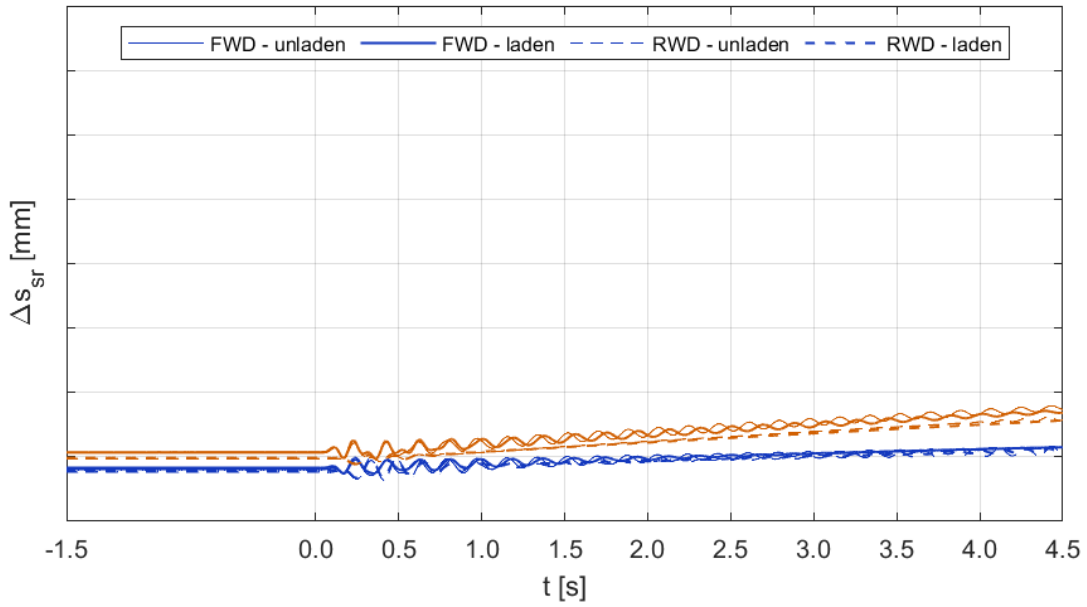

Figure 6.45: Power-Off Cornering - 2nd Gear - rack stroke vs time.

Overall, FWD is slightly more understeering than RWD, as confirmed by the steering wheel torque and rack stroke. In 2nd gear, some vibrations take place on the whole steering chain and are felt by the driver, especially on FWD, for the entire range of lateral accelerations. Instead, RWD shows some vibrations only at very low lateral accelerations and is able to dampen them more quickly. The three quantities allow to understand the immediate reaction to power-off. Specifically, FWD experiences an increase in the self-aligning moment, along with an increase in the rack stroke and a decrease in the steering wheel torque. This means that the driver will suddenly feel a reduction in the resistance opposed by the wheels, which are increasing their steering angle, followed by some vibrations for the next few seconds.

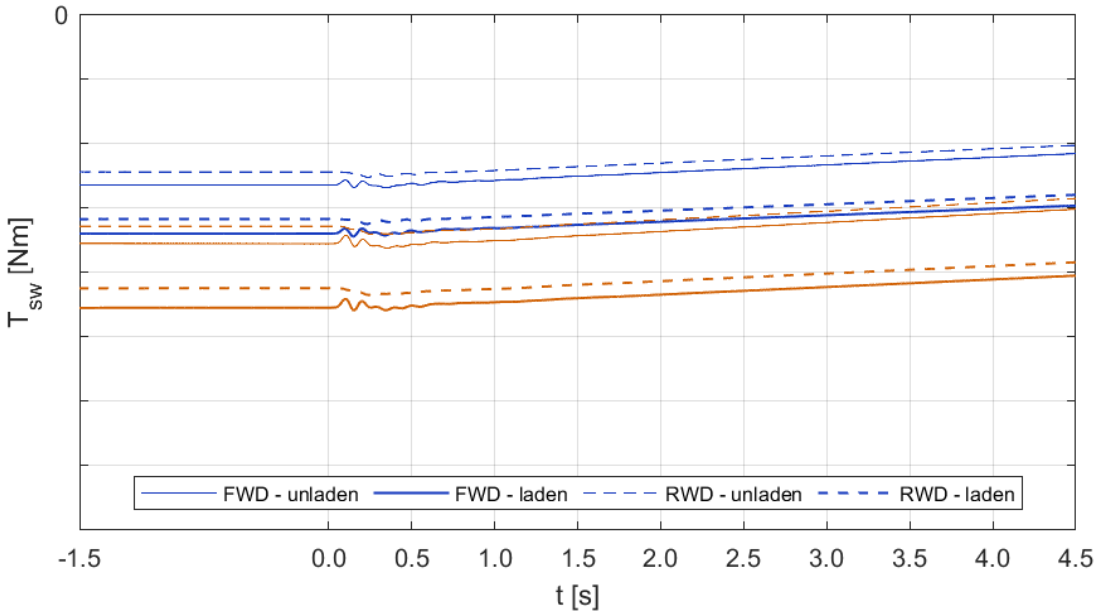

Figure 6.46: Power-Off Cornering - 3rd Gear - steering wheel torque vs time.

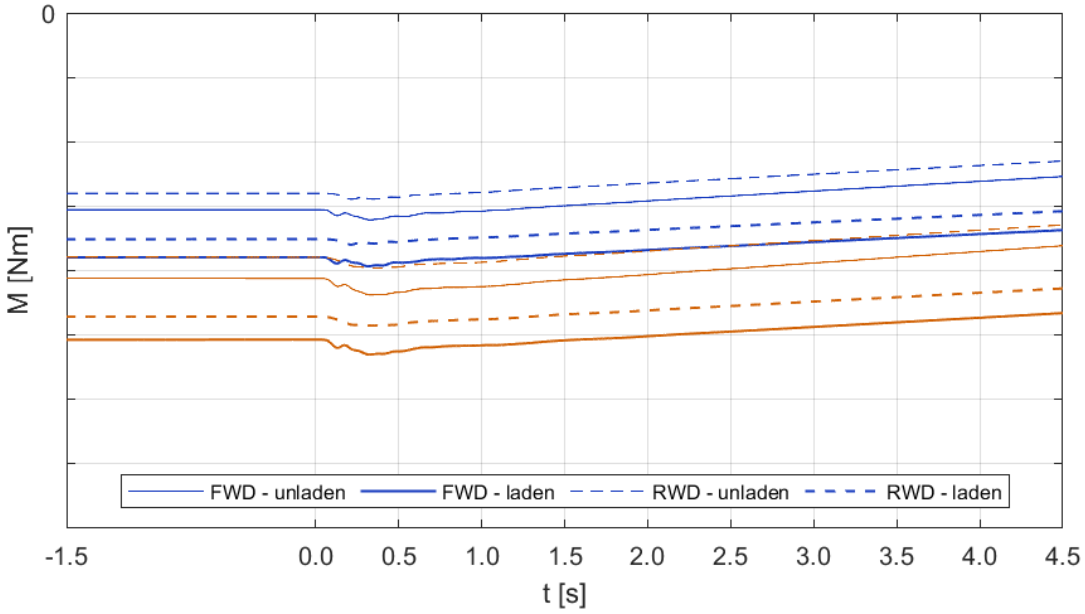

Figure 6.47: Power-Off Cornering - 3rd Gear - self-aligning moment vs time.

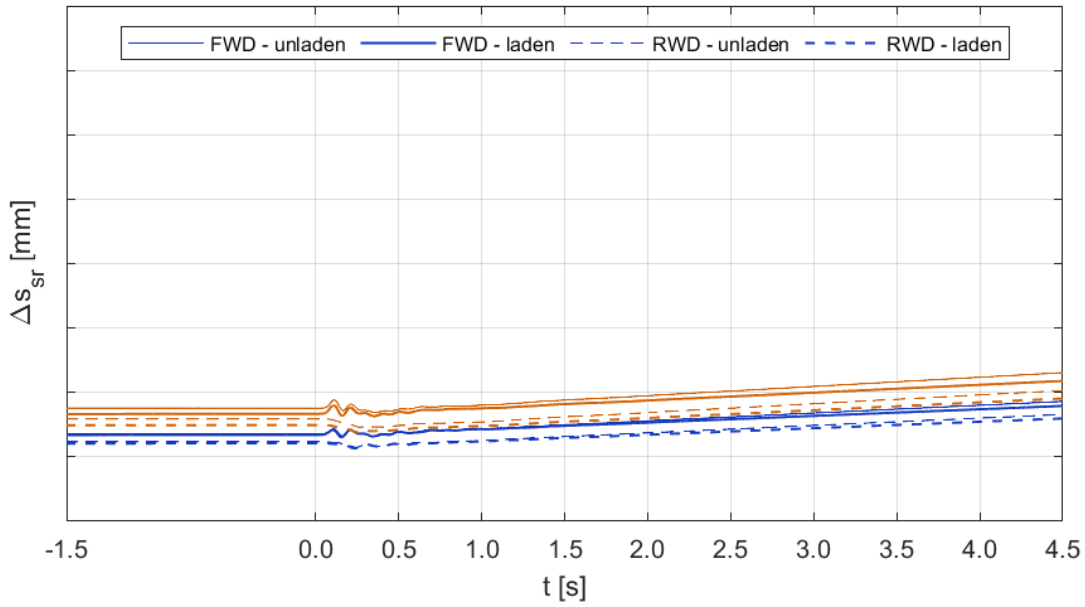

Figure 6.48: Power-Off Cornering - 3rd Gear - rack stroke vs time.

In 3rd gear, the oscillatory phenomena previously seen disappear completely and the steering system takes less than 0.5s to extinguish the transient. The response, even if shortened provides the same sensations to the driver, who is feeling a sudden reduction in the weight of the steering wheel, which corresponds to a slight oversteering action on the front wheels. These phenomena are not seen on RWD, which shows no transient neither in 2nd or 3rd gears. Its unique response is in steady-state, where the progressive reduction of the steering wheel torque is the consequence of reducing the vehicle speed and lateral acceleration. Obviously, FWD follows a very similar steady-state response, once the transient has been extinguished.

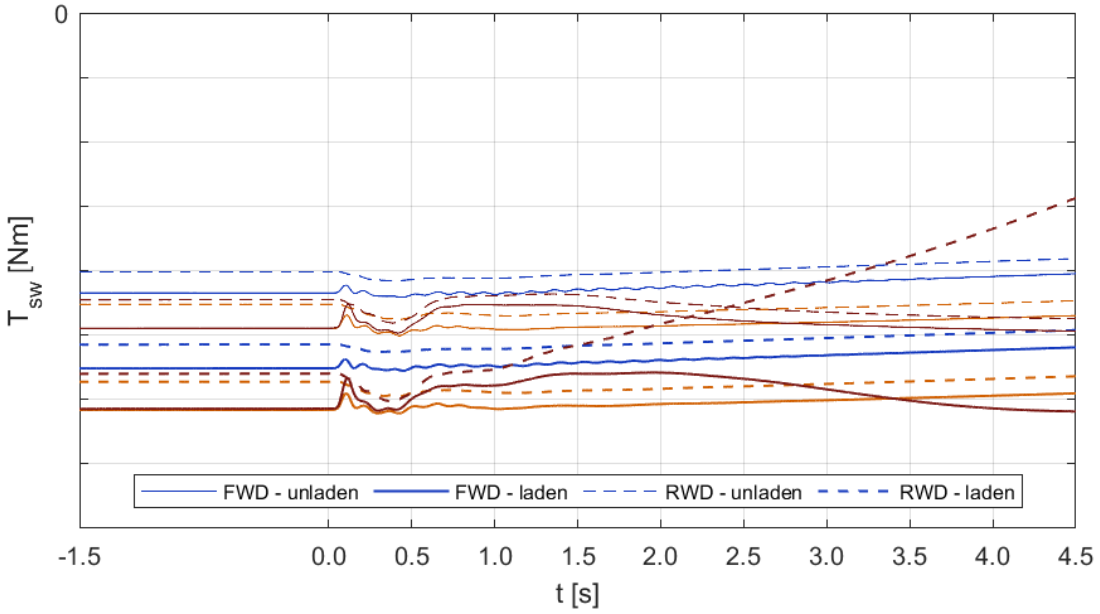

Figure 6.49: Power-Off Cornering - 4th Gear - steering wheel torque vs time.

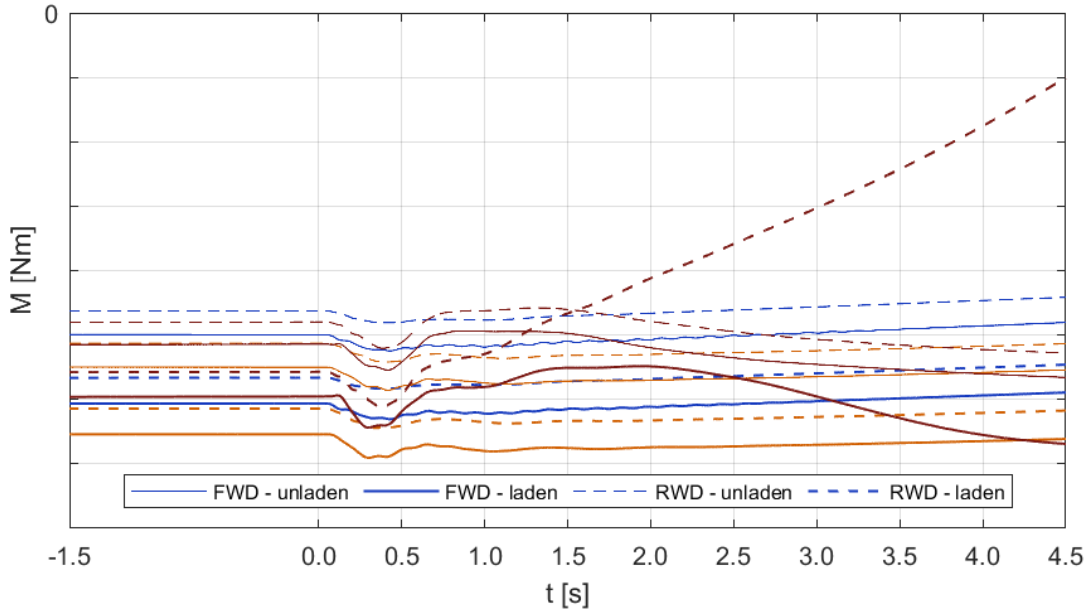

Figure 6.50: Power-Off Cornering - 4th Gear - self-aligning moment vs time.

The most interesting phenomena take place when the vehicle approaches its limit in 4th gear. In terms of steering wheel torque, FWD gives a sudden reduction as in the previous cases. The following reaction of the wheels in terms of self-aligning moment forces the driver to increase the torque, because the wheels are trying to restore their initial angle, as indicated by the rack stroke. After the transient, FWD and RWD still show similar responses when unladen, but they give a completely different feedback when they are laden. RWD makes the front wheels increase their steering angle and invert their moment, giving a sensation of empty steering wheel to the driver and resulting in the already investigated oversteering response. Instead, FWD behaves similarly to the unladen configuration and does not provide critical responses.

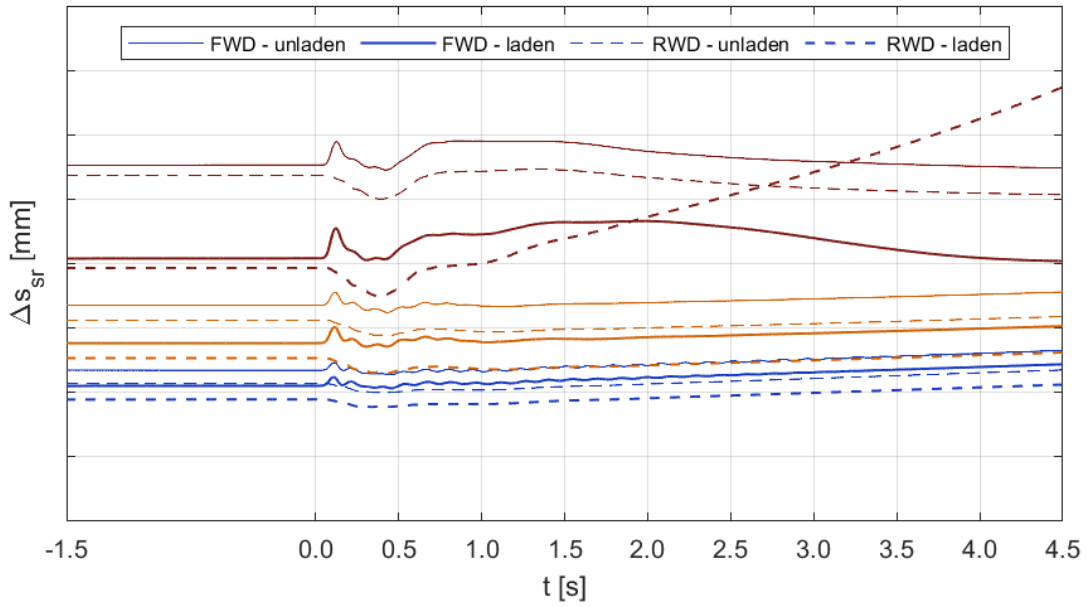

Figure 6.51: Power-Off Cornering - 4th Gear - rack stroke vs time.

6.1.5 Functions of Initial Lateral Acceleration

The last step prescribed by ISO 9816:2018 consists in reporting a few functions of initial lateral acceleration at a specific time instant of interest. The two time instants specifically required are t_1 and t_2, which are respectively 1.0s and 2.0s after the power-off instant. The former corresponds to the transients being extinguished, the latter should represent the new steady-state. *Equation 7.1* defines the mean longitudinal deceleration in the time range of interest for the test, hence 2.0s starting from the power-off instant. It is shown in *Figure 6.52*.

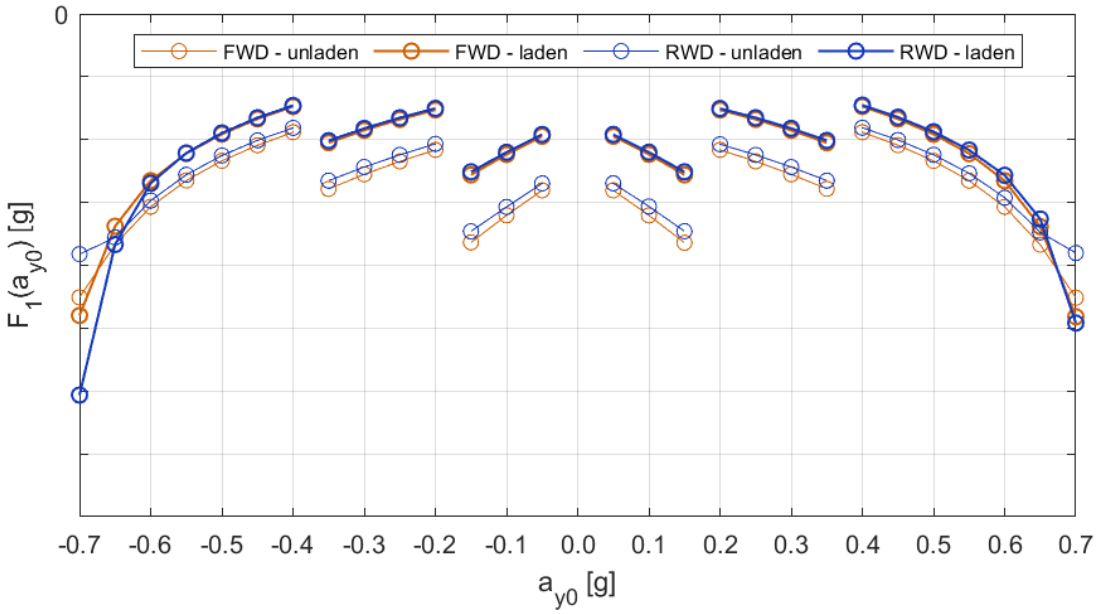

Figure 6.52: Power-Off Cornering - F_1 vs in. lat. acc.

$$f_1(a_{y0}) = a_{x,t_2} = -\frac{V_{x,t_0} - V_{x,t_2}}{t_2 - t_0} \tag{6.1}$$

The function tells that FWD usually has a slightly greater ability to decelerate, thanks to the longitudinal load transfer that is beneficial to the front axle. The unladen configuration obviously decelerates more, thanks to its lower inertia. When the vehicle reaches its limit, FWD still shows similarities between the two loading conditions, while RWD undergoes a huge deceleration when it is laden, as previously seen in the longitudinal velocity time history.

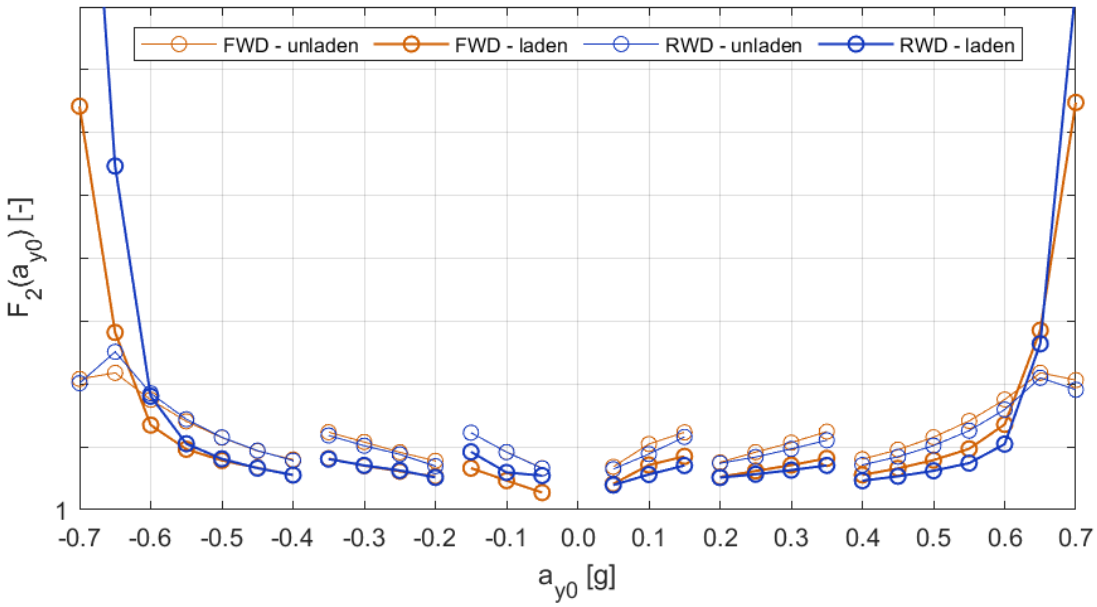

Figure 6.53: Power-Off Cornering - F_2 vs in. lat. acc. @ t_2.

Equation 7.2 defines the ratio between yaw velocity and reference yaw velocity, defined as the yaw velocity the vehicle would have if it maintained the initial path radius with its actual velocity, both at time t_2. It is shown in *Figure 7.53*.

$$f_2(a_{y0}) = \frac{\dot{\Psi}_{t_2}}{\dot{\Psi}_{ref,t_2}} \qquad \dot{\Psi}_{ref,t_2} = \frac{V_{x,t_2}}{R_0} \tag{6.2}$$

Overall, this function shows similar responses between FWD and RWD, with greater differences occurring near the limit, where RWD gets unstable in the laden configuration. The response of RWD is slightly asymmetric due to the reaction torque and does not allow a unique comparison with FWD. *Equation 7.3* defines the ratio between maximum yaw velocity and reference yaw velocity at the time instant corresponding to the maximum yaw velocity. It is shown in *Figure 7.54*. This function is similar to the previous one, meaning that the yaw velocity is maximum when close to t_2. In 2nd gear, some asymmetries between left and right turns involve all vehicles and can be related to the oscillations previously observed.

$$f_3(a_{y0}) = \frac{\dot{\Psi}_{max}}{\dot{\Psi}_{ref,t_{max}}} \tag{6.3}$$

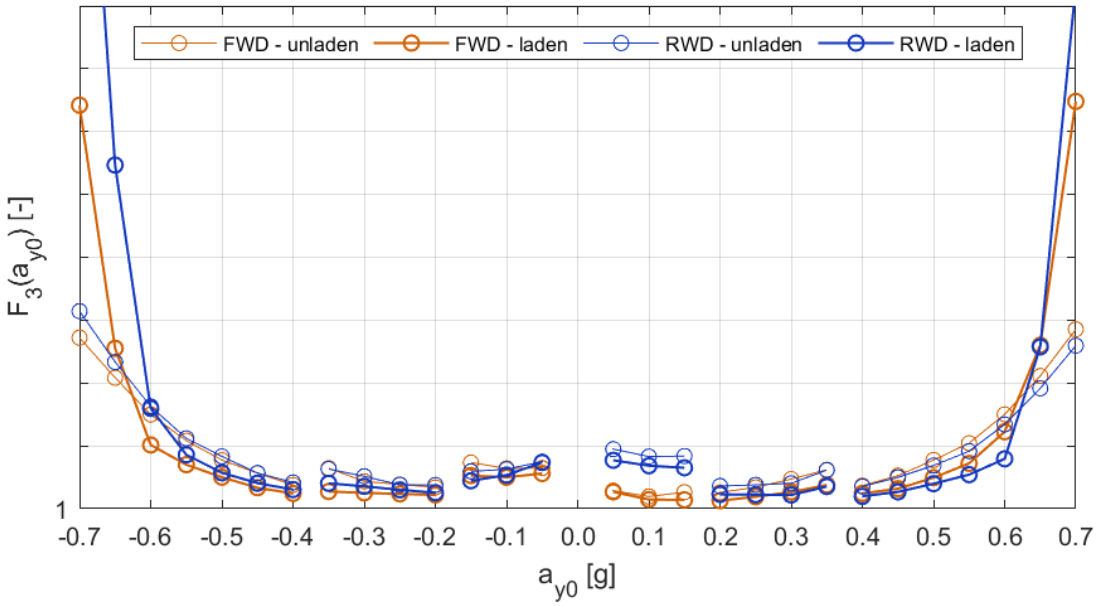

Figure 6.54: Power-Off Cornering - F_3 vs in. lat. acc.

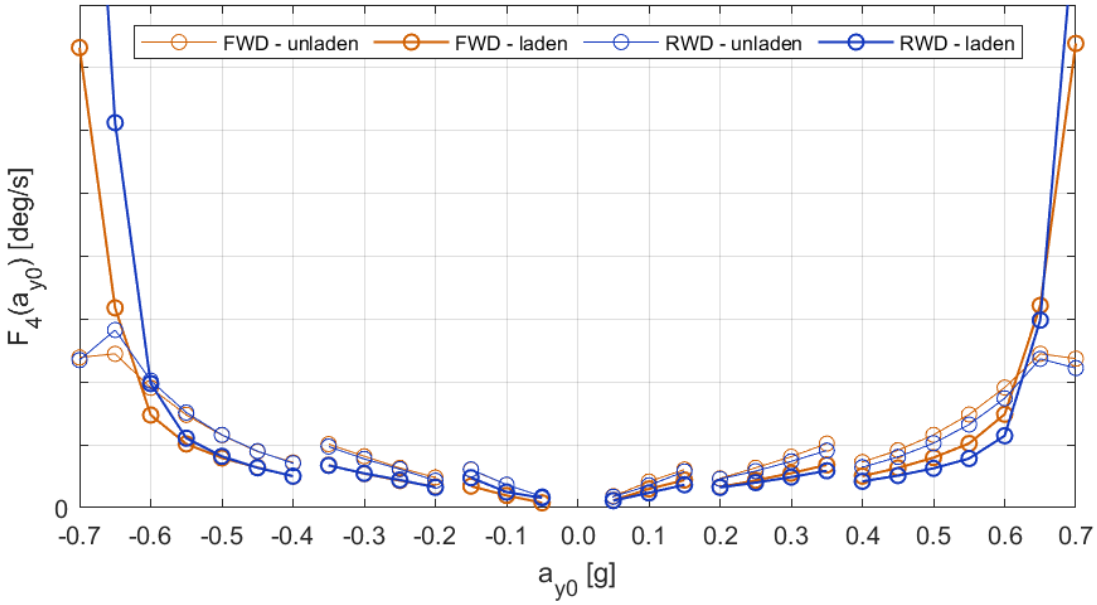

Figure 6.55: Power-Off Cornering - F_4 vs vs in. lat. acc. @ t_2.

Equation 7.4 defines the difference between yaw velocity and reference yaw velocity, both evaluated at time t_2. It is shown in *Figure 7.55*.

$$f_4(a_{y0}) = \dot{\Psi}_{t_2} - \dot{\Psi}_{ref,t_2} \tag{6.4}$$

Equation 7.5 defines the maximum difference between yaw rate and reference yaw rate through the time range of the test. It is shown in *Figure 7.56*.

$$f_5(a_{y0}) = \Delta\dot{\Psi}_{max} = (\dot{\Psi}_t - \dot{\Psi}_{ref,t})_{max} \tag{6.5}$$

These two functions provide results that are qualitatively similar to the previous pair of diagrams. It is worth noticing that the order of magnitude of these differences is generally one tenth of the yaw velocity and gains relevance only when approaching the vehicle limit.

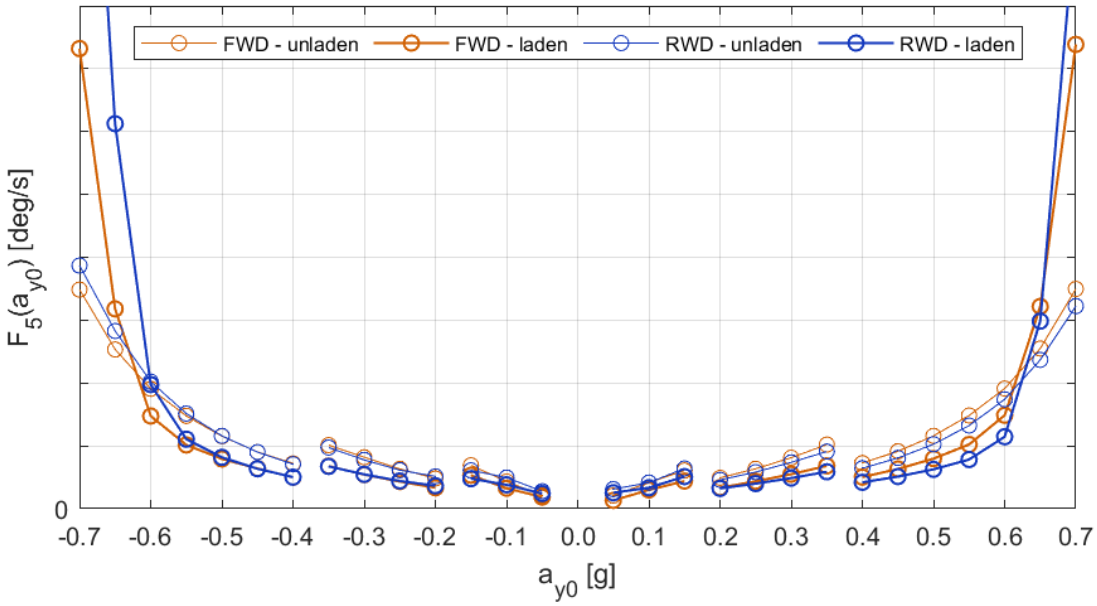

Figure 6.56: Power-Off Cornering - F_5 vs in. lat. acc.

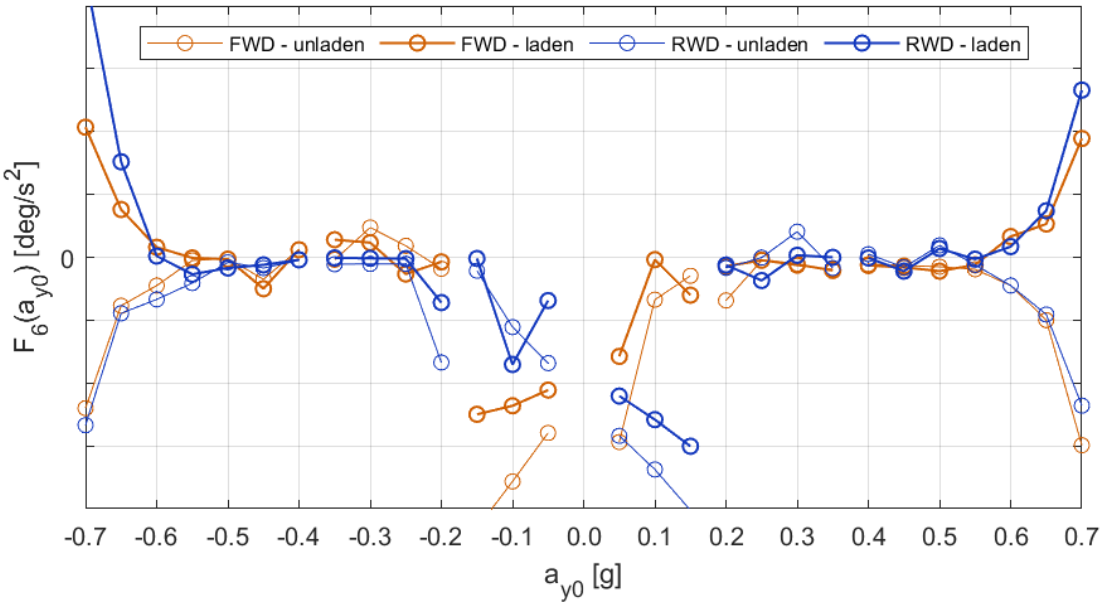

Figure 6.57: Power-Off Cornering - F_6 vs in. lat. acc. @ t_1.

Equation 7.6 defines the instantaneous yaw acceleration, 1.0s after the power-off instant. It is shown in *Figure 7.57*.

$$f_6(a_{y0}) = \ddot{\Psi}_{t=1.0s} = \left(\frac{d\dot{\Psi}}{dt}\right)_{t=1.0s} \tag{6.6}$$

This function represents the yaw acceleration while the transient is being extinguished and clarifies how the vibrations are affecting the quantity. While in 2nd gear there is an apparently chaotic response that is coming from the vibrations already discussed, at middle lateral accelerations the yaw acceleration is almost null, meaning that 1.0s after the power-off instant is a time sufficient to dampen all the vibrations generated by the maneuver.

Instead, near the vehicle limit, the loading condition affects the sign of the function. while the unladen vans have a negative acceleration, corresponding to a negative slope in yaw velocity, the laden vehicles are still increasing it, as shown by the huge positive acceleration. This significant difference is the result of a longer transient experienced by the laden configuration, before restoring the initial equilibrium or getting unstable. The next function prescribed by ISO 9816:2018, namely f_7, is by its mathematical definition identical to f_2, because it represents the ratio between ideal and actual curvature radii, so no further considerations are needed and its graph is not reported. Its definition is given by *Equation 7.7*.

$$f_7(a_{y0}) = \frac{a_{y,t_2}}{a_{y,ref,t_2}} = \frac{R_0}{R_{t_2}} \qquad a_{y,ref,t_2} = \frac{V_{x,t_2}^2}{R_0} \tag{6.7}$$

Equation 7.8 defines the maximum absolute value of sideslip angle and the corresponding time instant at which it is achieved. These twin functions are evaluated in the time range from t_0 to t_2 as usual and are shown in *Figures 7.59 and 7.60*.

$$f_{8-1}(a_{y0}) = |\beta_{max}| \qquad f_{8-2}(a_{y0}) = t_{\beta_{max}} \tag{6.8}$$

These two functions show that the sideslip angle turns from a "nose-out" to a "nose-in" configuration at a value of lateral acceleration around 0.25g. In the field of low lateral accelerations, the maximum sideslip angle is achieved at t_2, because the vehicle is starting from a "nose-out" and the deceleration maneuver obviously enhances this configuration. Instead, in the field of middle lateral accelerations, the maximum is achieved close to the power-off instant, because from a "nose-in" the vehicle is going back to a neutral configuration. Only in the field of greater lateral accelerations, some significant differences between unladen and laden vehicles take place. The former reaches the overshoot at around t_1 and later recovers a value close to the initial steady-state, while the latter takes a longer time, up to t_2, to reach its maximum before slowly settling to the steady-state condition. The maximum sideslip angle also shows the symmetric response typical of FWD and the critical responses given by RWD near the limit.

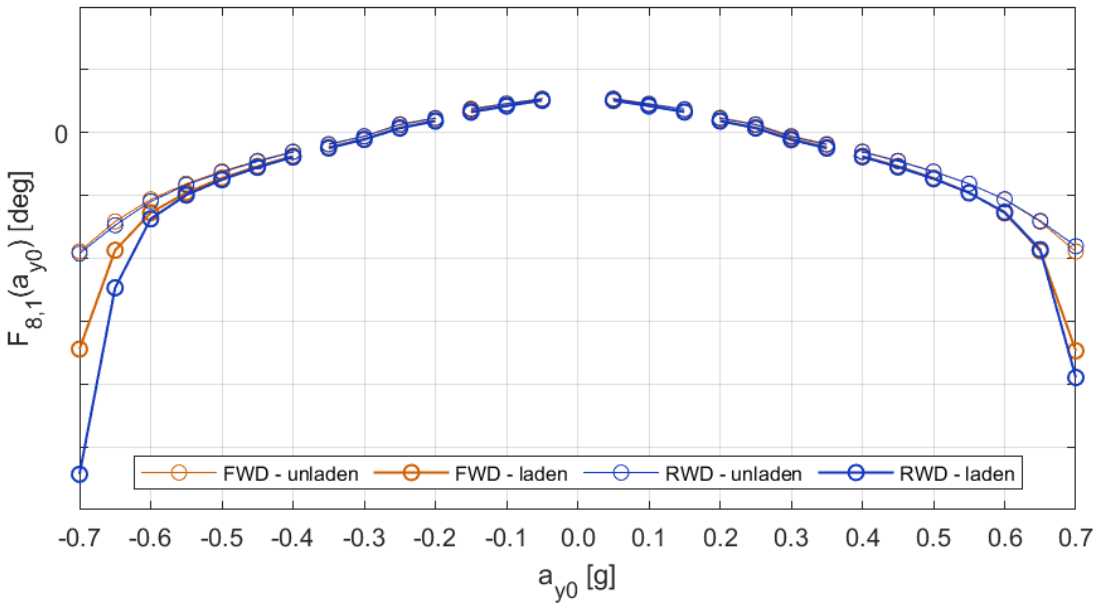

Figure 6.58: Power-Off Cornering - $F_{8,1}$ vs in. lat. acc.

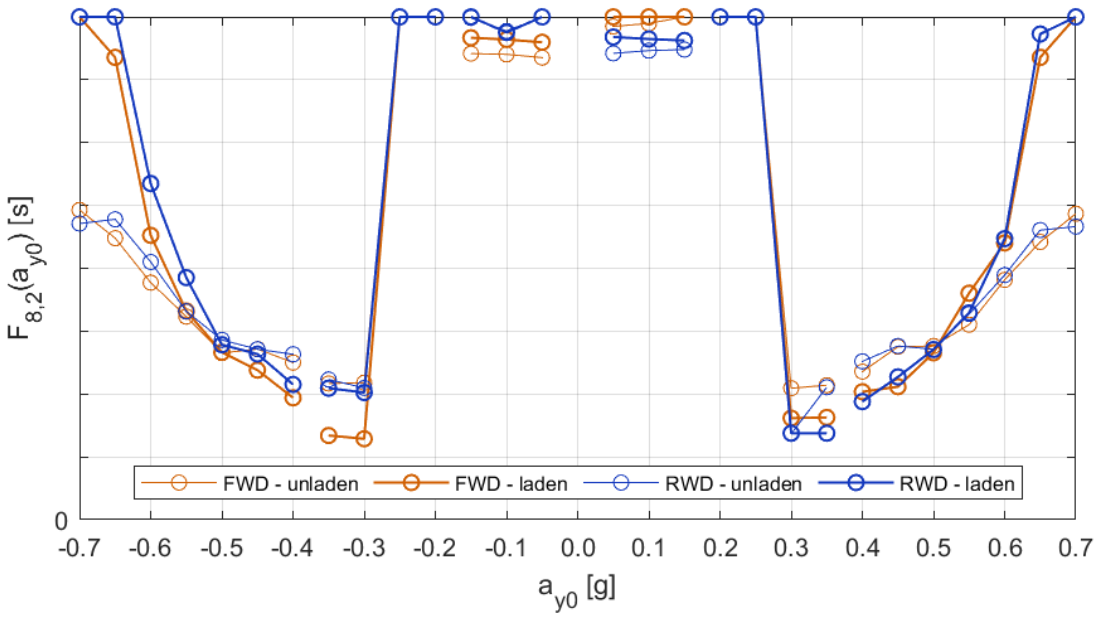

Figure 6.59: Power-Off Cornering - $F_{8,2}$ vs in. lat. acc.

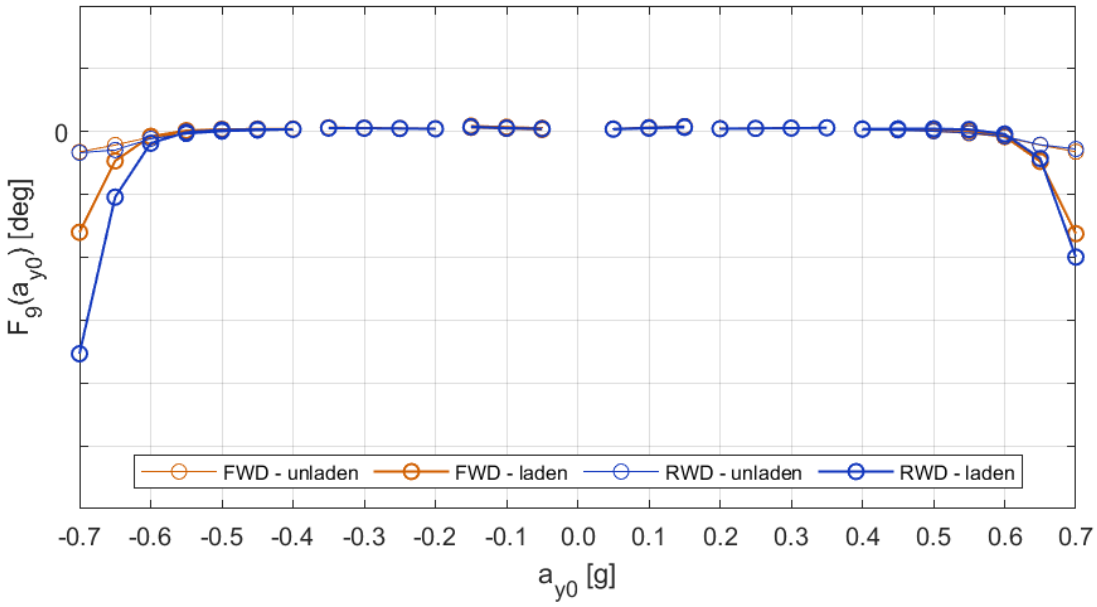

Figure 6.60: Power-Off Cornering - F_9 vs in. lat. acc. @ t_2.

Equation 7.9 defines the difference between sideslip angle 2.0s after the power-off instant and initial steady-state sideslip angle. It is shown in *Figure 7.61*.

$$f_9(a_{y0}) = \beta_{t_2} - \beta_0 \tag{6.9}$$

Equation 7.10 defines the difference between maximum sideslip angle and initial steady-state sideslip angle. It is shown in *Figure 7.62*.

$$f_{10}(a_{y0}) = \beta_{max} - \beta_0 \tag{6.10}$$

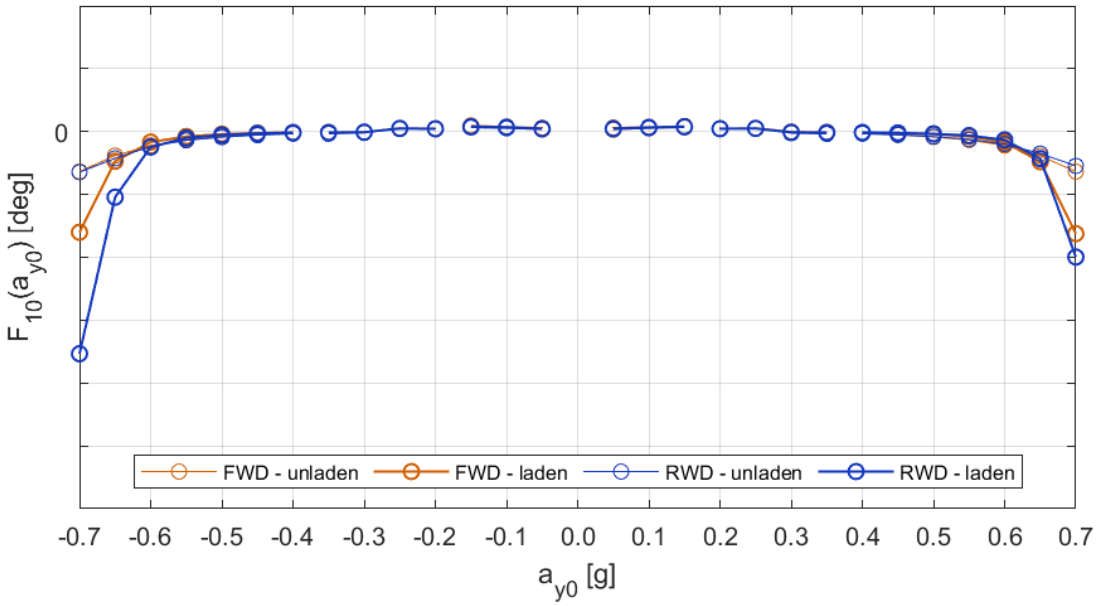

Figure 6.61: Power-Off Cornering - F_{10} vs in. lat. acc.

These two functions are very effective in highlighting the vehicle ability to restore its initial steady-state condition. Until 0.55g, the van goes back to the initial sideslip angle in less than 2.0s. When it approaches its limit, it assumes a configuration that is more "nose-in" than the beginning. While the unladen vehicles are comparable, the laden RWD clearly shows its oversteering tendency, reaching an angle that is doubled with respect to its FWD counterpart.

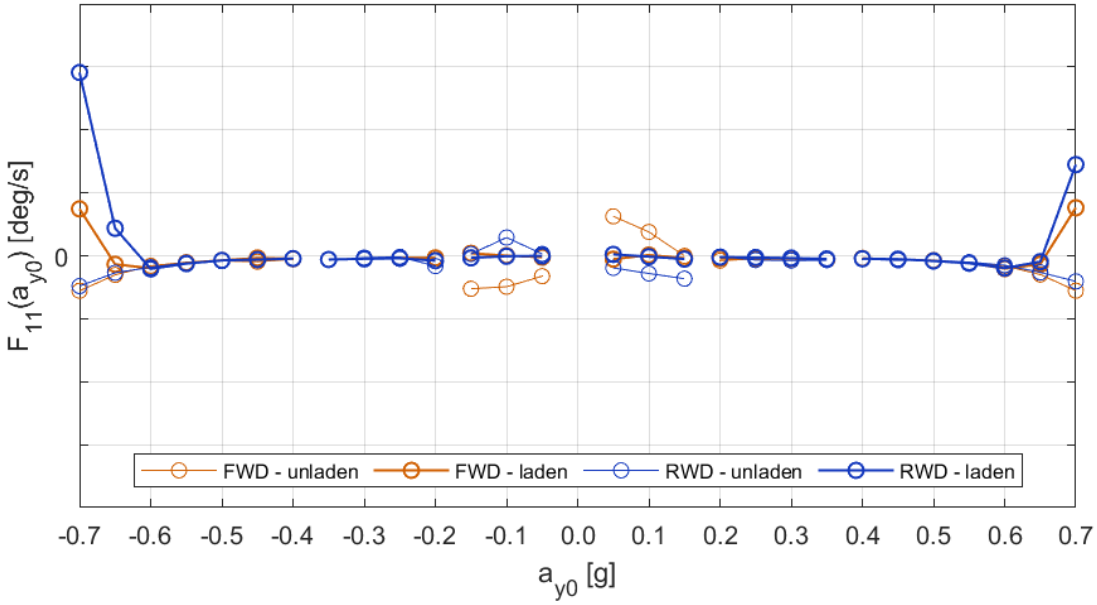

Figure 6.62: Power-Off Cornering - F_{11} vs in. lat. acc. @ t_2.

Equation 7.11 defines the difference between yaw velocity and calculated yaw velocity, both 2.0s after the power-off instant. It is shown in *Figure 7.63*.

$$f_{11}(a_{y0}) = \dot{\beta}'_{t_2} = \dot{\Psi}_{t_2} - \frac{a_{y,t_2}}{V_{x,t_2}} \tag{6.11}$$

This function represents the sideslip angle velocity uncorrected for the effects of the sideslip angle itself and the deceleration. The comparison between the actual yaw velocity and the one unaffected by sideslip angle gains relevance at low lateral accelerations, as well as close to the limit. The first result involves the unladen vehicle, which is more sensitive to vibrations, especially in the FWD version. Instead, near the grip limit the laden condition shows some critical responses, with RWD experiencing a remarkable increase in the quantity, confirming its sensitivity to the maneuver and the huge contribution given by sideslip angle.

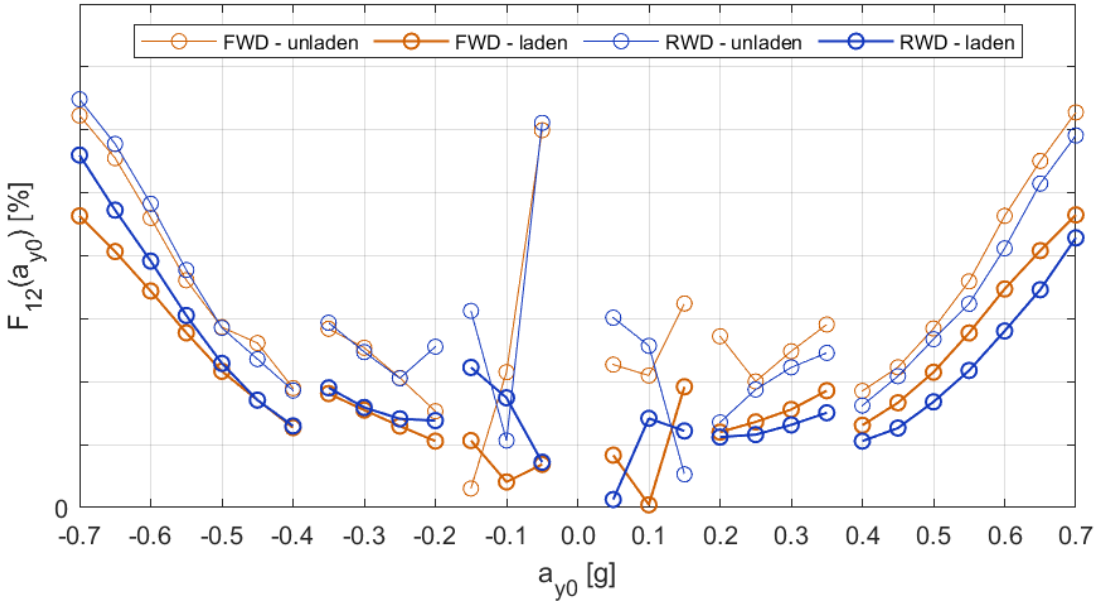

Figure 6.63: Power-Off Cornering - F_{12} vs in. lat. acc. @ t_2.

Equation 7.12 defines the percentage deviation as the radial distance between vehicle reference point and initial circular path, 2.0s after the power-off instant. It is shown in *Figure 7.64*.

$$f_{12}(a_{y0}) = \Delta s_{y,t=2.0s} = \frac{R_0 - R_{t_2}}{R_0} \tag{6.12}$$

In 2nd gear, the unladen FWD tends to close its trajectory more than RWD, as confirmed by its yaw sensitivity, but at greater lateral accelerations its more understeering and symmetric behaviour is revealed, meaning that it will be less prone to close its trajectory.

6.2 Minimum Path Radius

6.2.1 Test Setup

Power-Off Cornering tests performed up to this point make reference to a unique path radius equal to 100 m, which is the standard value prescribed in ISO 9816:2018. However, this test setup stresses the differences between Front and Rear-Wheel-Drive vehicles mainly in 4th gear, especially at great lateral accelerations, while at lower gears the vehicle handling is not completely emphasized. To add further knowledge of the maneuver, a restricted set of tests is now performed adopting the criterion of minimizing path radius while keeping the initial engine rotational speed maximum. The driving idea is to enhance both longitudinal and lateral forces exerted by tyres to the ground and assess whether saturation takes place and how drivetrains are involved. Concerning path radius, ISO 9816:2018 allows a minimum permissible value equal to 30 m, which is chosen for the test in 2nd gear, while the initial lateral acceleration is selected to maintain the allowed 80% of maximum engine rotational speed. In 3rd gear, path radius needs to be increased up to 50 m, otherwise the vehicle cannot ensure grip while running the engine at its allowed threshold. About 4th gear, the previous Section contains a test at 0.70g, which already corresponds to the minimum path radius achievable at the 80% of engine maximum rotational speed, therefore the same test is here reported and examined more in depth. This set of tests can be considered as a seek for the minimum path radius the vehicle can manage assuming the engine is running at the allowed threshold. *Table 6.2* resumes the combinations of gear position, path radius and initial lateral acceleration. Power steering is still inactive, while the throttle release time interval is maintained equal to 0.1s. The results are reported in terms of time histories only, because the adoption of different path radii would make the comparison of different lateral accelerations meaningless.

Sampling Time Interval		0.001s
Throttle Release Time Interval		0.1s
2nd Gear	Path Radius	30 m
	Lateral Acceleration	0.50g
3rd Gear	Path Radius	50 m
	Lateral Acceleration	0.65g
4th Gear	Path Radius	100 m
	Lateral Acceleration	0.70g
Turn Direction		Left
Power Steering		Inactive

Table 6.2: Power-Off Cornering - Minimum Path Radius - test setup.

6.2.2 Vehicle Dynamics

Figures 6.64 and 6.65 show the lateral acceleration and longitudinal velocity time histories. Looking at the latter, the unladen FWD is able to decelerate slightly more than RWD, thanks to the longitudinal load transfer beneficial to the front wheels. Instead, the laden condition shows closer behaviours or eventually a stronger deceleration for RWD, which has already proved to get unstable more quickly in the previous Section. Concerning the lateral acceleration, all vehicles show a sudden drop after power-off, which is slightly sharper for RWD and starts a fast oscillatory transient. This vehicle is more prone to increase its lateral acceleration after this transient, especially in 3rd and 4th gears, thus exhibiting a greater tendency to oversteer.

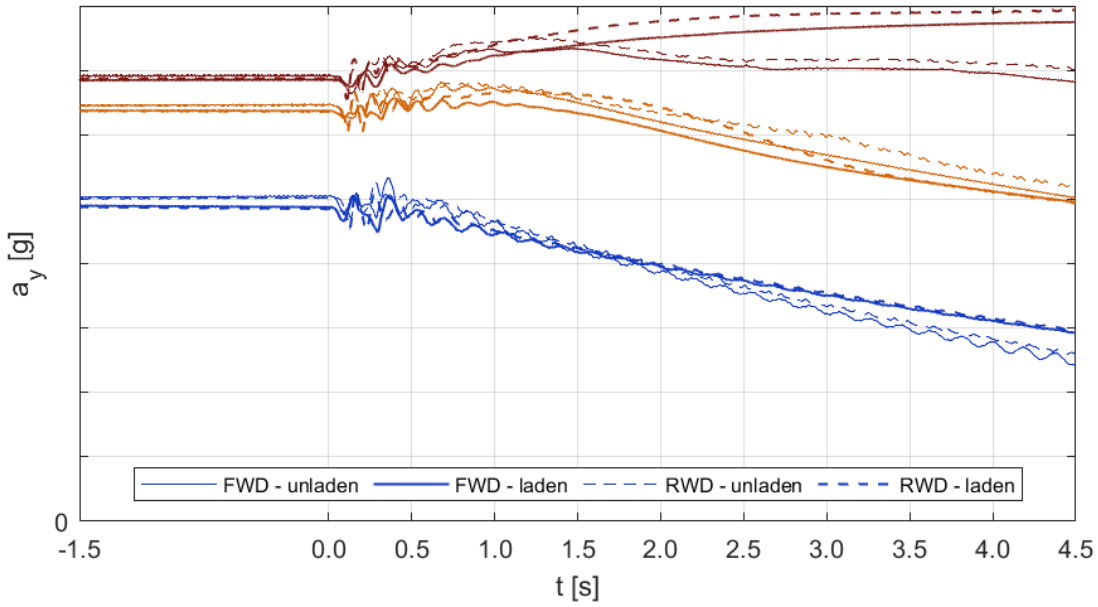

Figure 6.64: Power-Off Cornering - Minimum Path Radius - lat. acc. vs time.

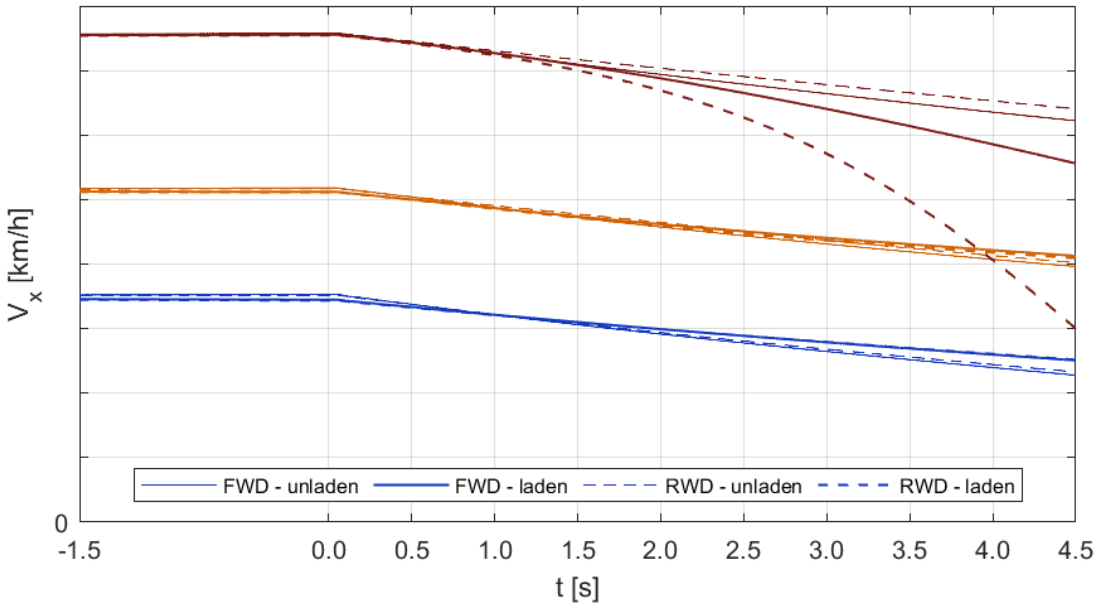

Figure 6.65: Power-Off Cornering - Minimum Path Radius - long. velocity vs time.

Figures 6.66 and 6.67 show the sideslip angle and yaw rate time histories. The tendency of RWD vehicles to oversteer more than FWD is confirmed, especially in the laden condition. RWD is more sensitive to the longitudinal load transfer, which happens quickly after power-off and leads to a drop in cornering stiffness on the rear axle, making the vehicle oversteer. Instead, the unladen RWD is not really effective in transferring the wheels braking torque to the ground. Yaw velocity confirms the previous observations and suggests that FWD experiences a slight drop after power-off, which should be assumed as a temporary additional understeer. In 4th gear, approaching the grip limit, both FWD and RWD enter oversteer, but the former takes a longer time to get unstable and gives the driver enough time to correct the maneuver.

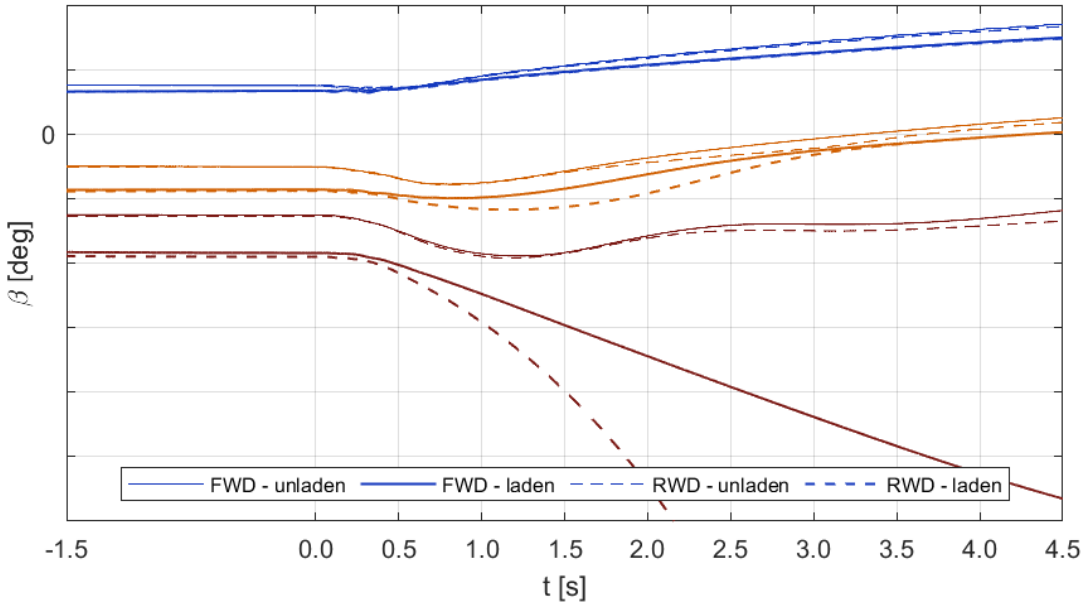

Figure 6.66: Power-Off Cornering - Minimum Path Radius - sideslip angle vs time.

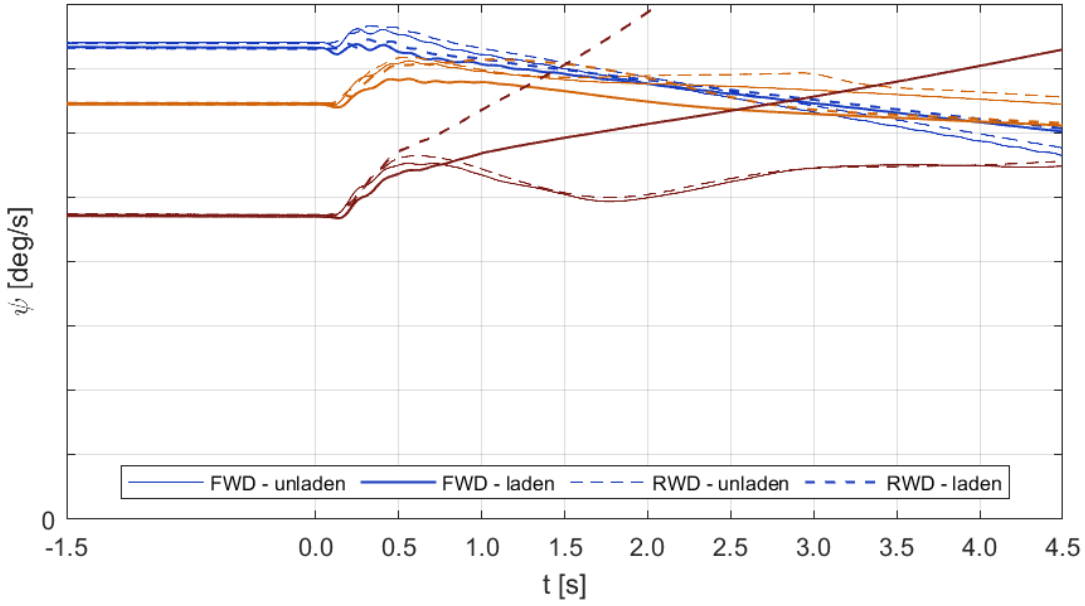

Figure 6.67: Power-Off Cornering - Minimum Path Radius - yaw velocity vs time.

6.2.3 Tyres Dynamics

Figures 6.68 and 6.69 show the lateral load transfers on front and rear axles, with respect to their initial steady-state values. The effects of reaction torque are huge in 3rd and 4th gears for RWD and leave room for slippage on the rear inner wheel in case of unladen vehicle. FWD is always faster in transferring the lateral load to the inner side, given its immunity to the phenomenon. In 4th gear, the unladen FWD shows a strange response on the rear wheels, where the lateral load transfer keeps almost null. As confirmed by the following quantities, the rear inner wheel is leaving the ground due to an insufficient residual normal load. At last, the laden vehicles in 4th gear confirm their instability, as the lateral transfers never get negative.

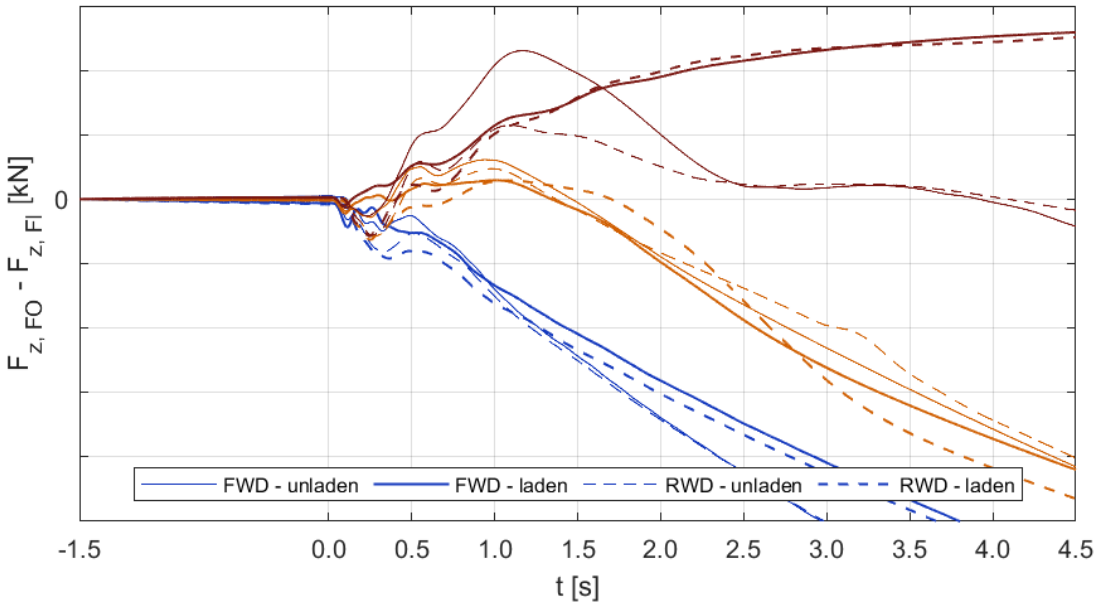

Figure 6.68: Power-Off Cornering - Minimum Path Radius - front lateral transfer vs time.

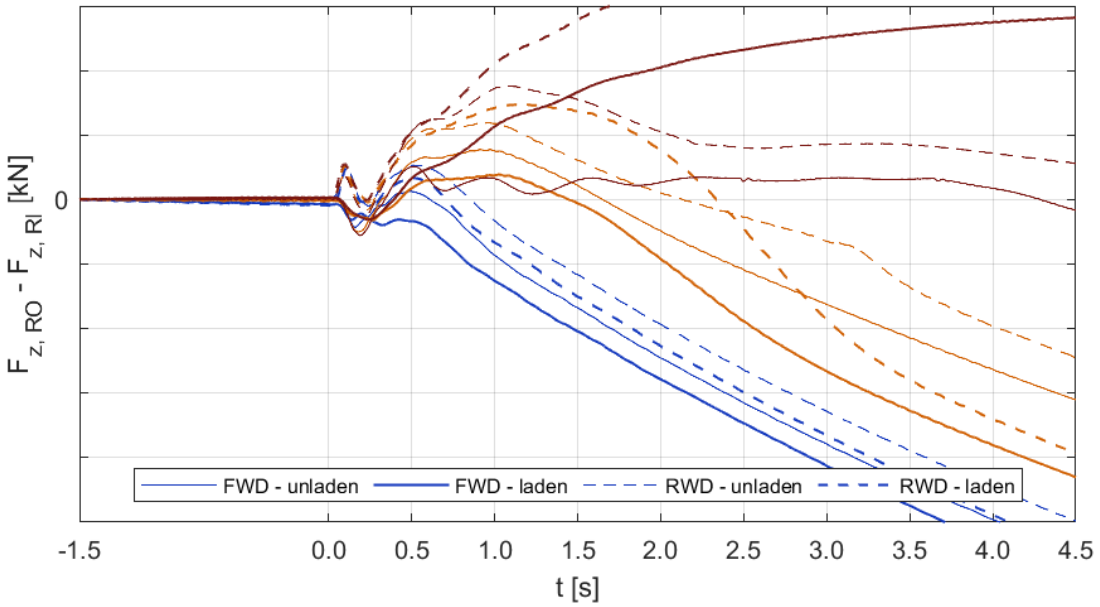

Figure 6.69: Power-Off Cornering - Minimum Path Radius - rear lateral transfer vs time.

Figure 6.70 shows the longitudinal load transfer time history, defined as the difference between rear and front axles normal loads, with respect to their initial steady-state values. The maximized braking torque leads to a significant overshoot immediately following power-off. Generally, the unladen FWD exhibits a greater load transfer due to its enhanced grip on the front tyres, while RWD shows a temporary reduction in braking capabilities. The laden condition shows results that are closer for both drivetrains. *Figures 6.71 and 6.72* show the slips achieved on the driving wheels as functions of time. These two graphs confirm the difficulties experienced by RWD in braking at high lateral accelerations. The inner wheel reaches great slip or complete saturation in 3rd and 4th gears, while on the outer wheel, no slippage occurs.

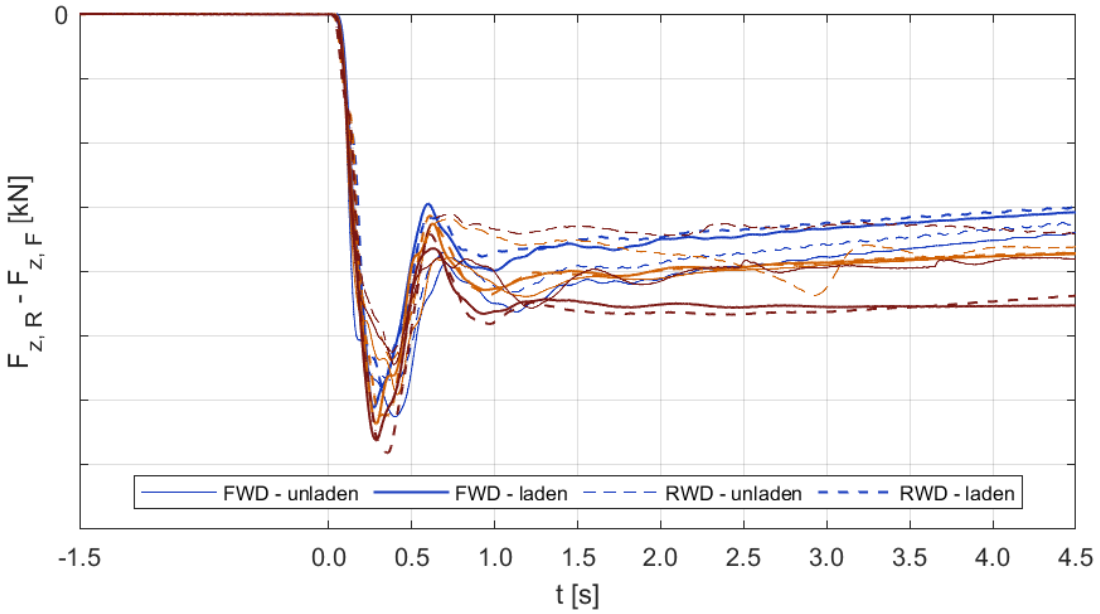

Figure 6.70: Power-Off Cornering - Minimum Path Radius - long. transfer time.

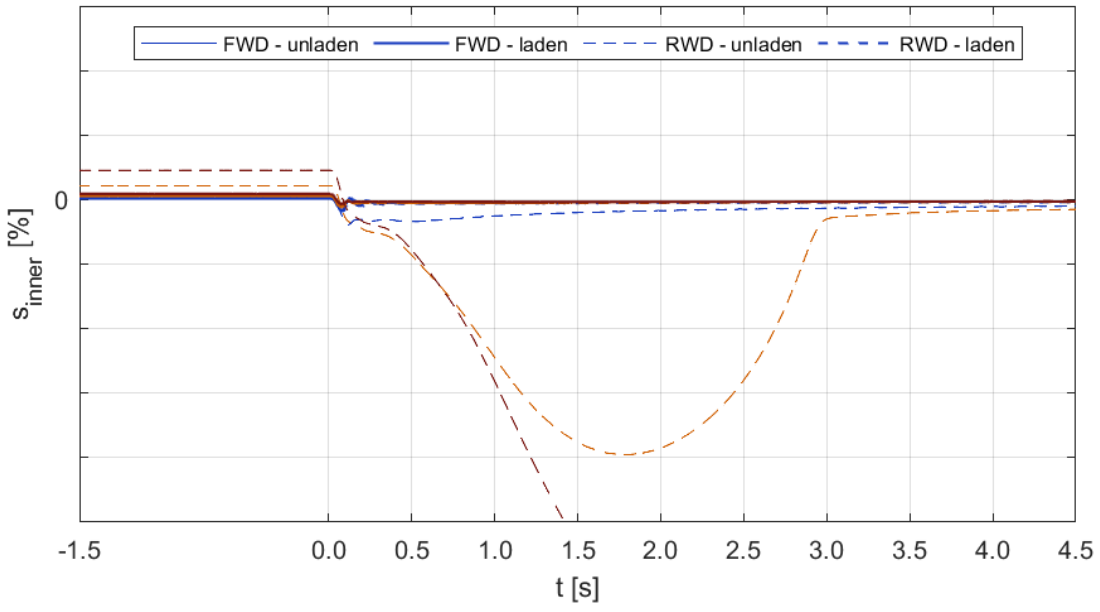

Figure 6.71: Power-Off Cornering - Minimum Path Radius - inner slip vs time.

On the unladen FWD, the rear inner wheel shows no slip because it loses contact with the ground, as confirmed by the understeer gradient shown in *Figure 6.73*. The phenomena involving this wheel induce understeer in both unladen vehicles, but in two different ways. While RWD loses its ability to decelerate due to saturation, which explains a greater path radius, FWD enhances braking and induces additional understeer because that wheel is leaving the ground. Instead, the laden vehicles are both prone to close the trajectory, with FWD able to delay instability and reduce oversteer. Apart from these limit cases in 4th gear, FWD is always more understeering with respect to RWD, with an interesting sudden step in the gradient occurring after power-off. This phenomenon involves the steering system as well.

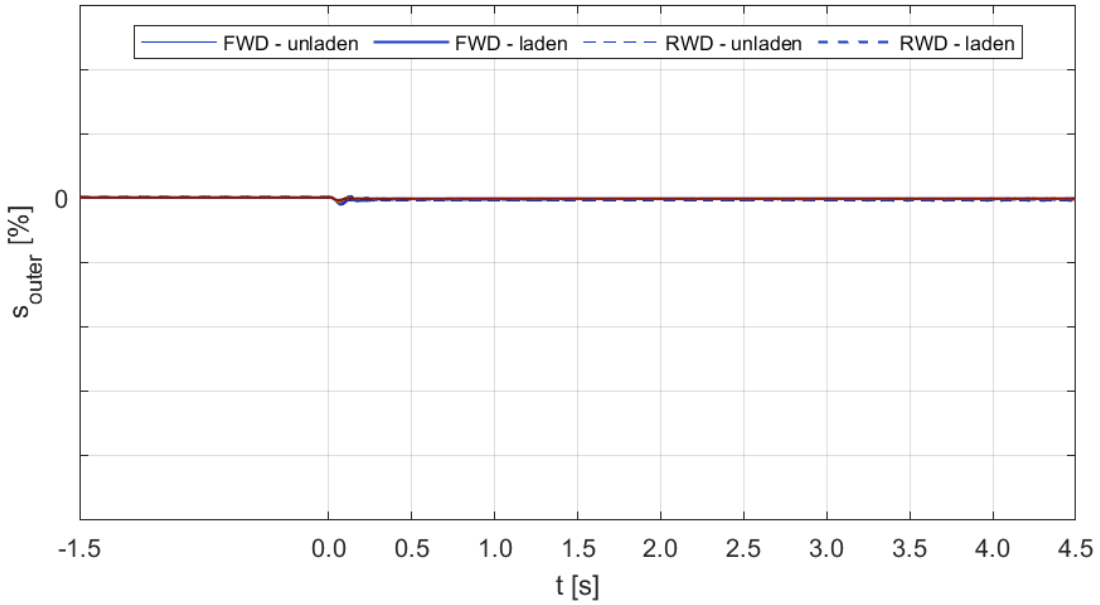

Figure 6.72: Power-Off Cornering - Minimum Path Radius - outer slip vs time.

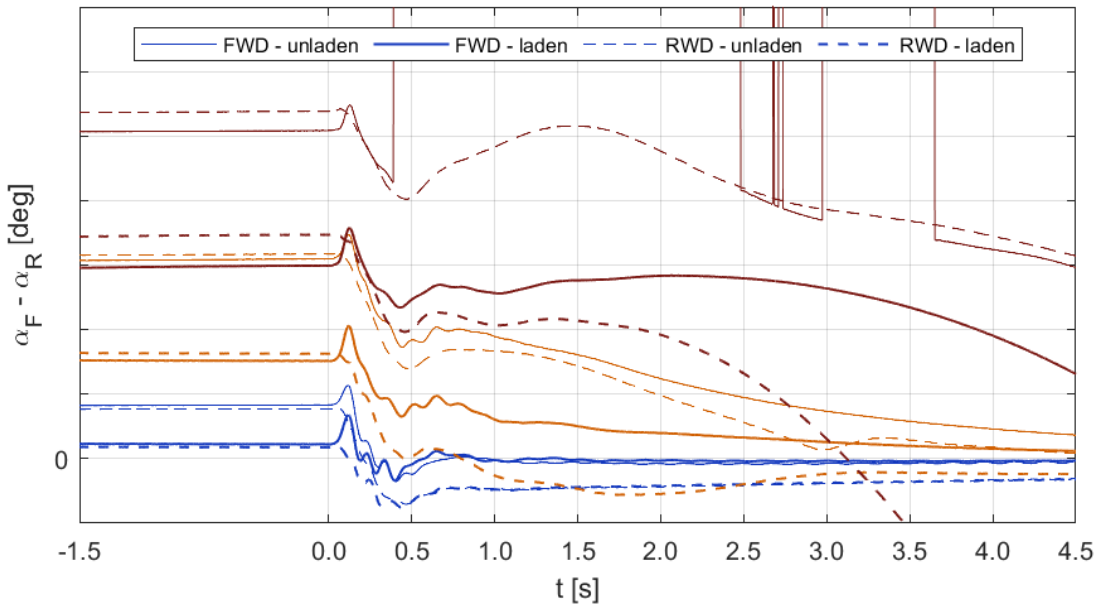

Figure 6.73: Power-Off Cornering - Minimum Path Radius - understeer gradient vs time.

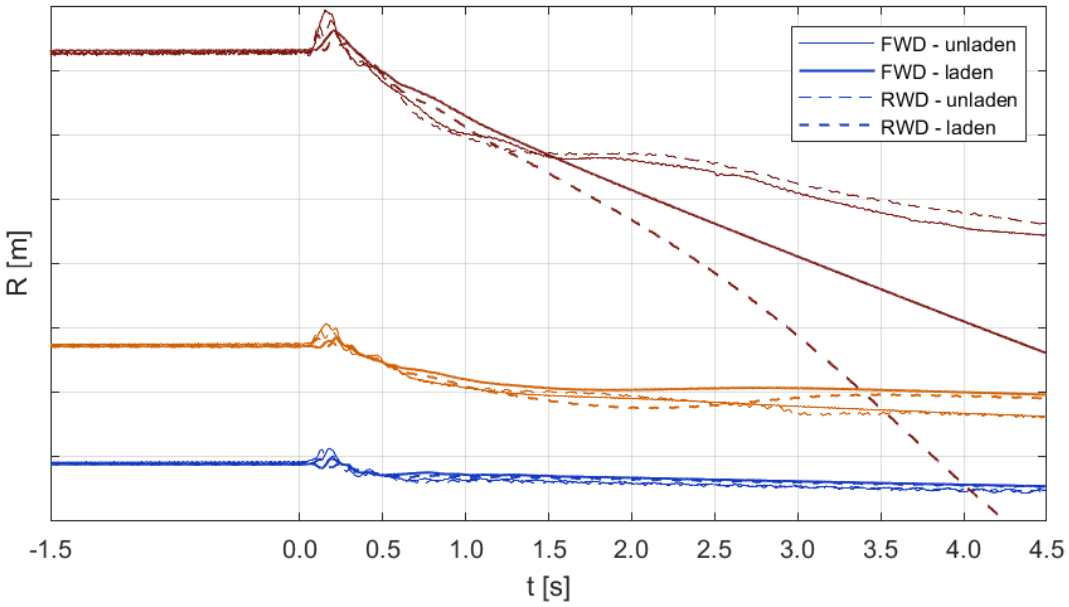

Figure 6.74: Power-Off Cornering - Minimum Path Radius - path radius vs time.

Figure 6.74 reports the path radius time history, which helps understanding the transient following power-off. RWD vehicles show a greater reactivity to the maneuver, meaning that a sudden, yet moderate, increase in path radius takes place, before starting the decreasing trend. Instead, FWD vans are less reactive, because they take a longer time before experiencing this jump, which has a greater amplitude. The peak in path radius corresponds to the one in understeer gradient, while RWD is already closing its trajectory. This means that FWD experiences a temporary reduction in its ability to steer, as the front wheels lose directionality for a very short time. The time delay, which is more pronounced in laden configuration, is likely to be caused by the wheels being forced by the engine to revert their longitudinal force. After this short transient, FWD maintains its more understeering behaviour, which is more noticeable in laden condition.

6.2.4 Steering System

Figures from 6.75 to 6.77 show the steering wheel torque, front wheels total self-aligning moment and steering rack stroke time histories. According to the sign conventions used in Adams/Car, a negative steering wheel torque is directed counterclockwise from the driver's viewpoint, thus coherent with a left turn. Instead, the self-aligning moment is negative when directed clockwise, thus effectively providing an aligning action during a left turn. Finally, the steering rack stroke is measured as the travel with respect to the neutral position.

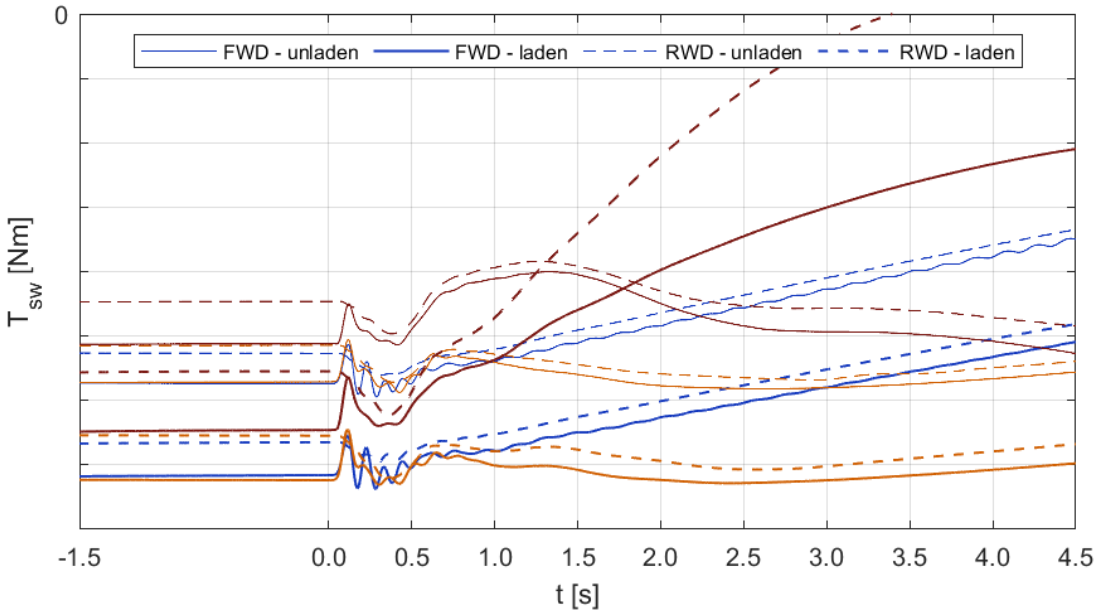

Figure 6.75: Power-Off Cornering - Minimum Path Radius - steering wheel torque vs time.

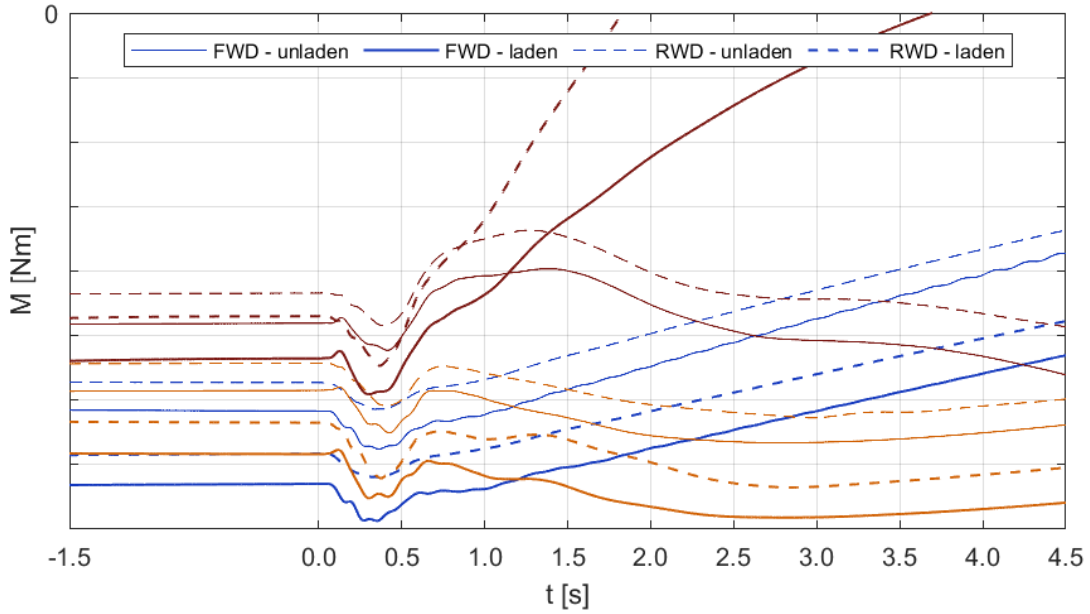

Figure 6.76: Power-Off Cornering - Minimum Path Radius - self-aligning moment vs time.

The steering wheel torque confirms the results of the previous set of tests, since FWD requires a greater torque in both steady-state and transients. The sudden drop after power-off is enhanced by this limit maneuvers and is confirmed by the increase in rack stroke, meaning that the effect of a braking torque on the front wheels is to induce an additional steer angle, which explains the temporary increase in the front wheels slip angles. In other words, the inner wheel is assuming a toe-out and the outer one is enhancing its toe-in, which result in a quick and short loss of directionality due to combined slip. In 2nd gear, despite the medium value of lateral acceleration, the steering system of FWD is subject to relevant transient vibrations in both loading conditions. These are likely to be generated by the elastic response of the torsional spring to a sudden variation in the equilibrium of forces exchanged between the tyres and ground. In 4th gear, the instabilities taking place on the laden vehicles are confirmed by the drop in steering wheel torque, which happens considerably faster on RWD and is associated with a drop in self-aligning moment until its sign reverts. This quantity is always greater on FWD vehicles and suggests that a longitudinal force always acts as a stabilizer, making the tyres more likely to recover their straight position and resist an incoming instability.

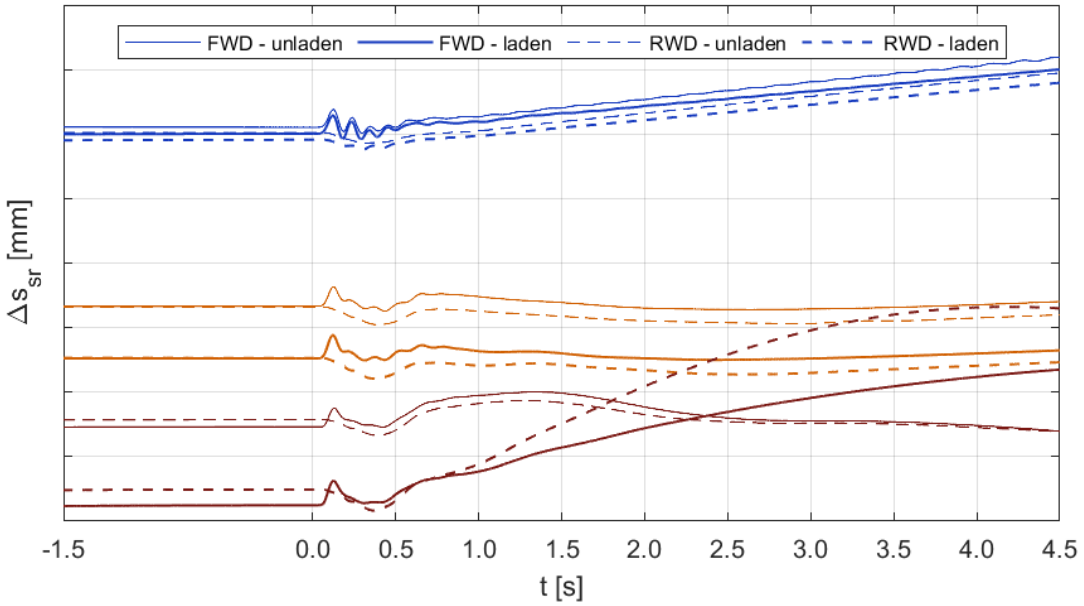

Figure 6.77: Power-Off Cornering - Minimum Path Radius - rack stroke vs time.

6.3 Conclusions

6.3.1 Standard Path Radius

Power-Off Cornering allows to highlight several features of each vehicle configuration. One of the first differences between Front and Rear-Wheel-Drive is represented by how their differential box is mounted. Rear-Wheel-Drive has the typical packaging where the differential is embedded in the rigid axle, thus contributing to the unsprung mass and suffering the reaction torque due to the spinning propeller shaft, giving asymmetric results for the whole field of lateral accelerations. Front-Wheel-Drive has a differential mounted on the chassis, meaning that it contributes to the sprung mass and does not load directly the wheels, preventing the asymmetric response due to the reaction torque. Another interesting aspect is how the tyres react to a limit maneuver. Specifically, the unladen configuration proves to be critical for the rear inner wheel, which is prone to saturation or even loss of contact, respectively in Rear and Front-Wheel-Drive. The latter manifests a slightly better ability to decelerate, mainly due to the longitudinal load transfer which is beneficial to the front axle. When considering the driver's point of view, Rear-Wheel-Drive is taken as the reference to assess which kind of changes a Front-Wheel-Drive can imply in terms of response of the steering system. The results suggest that the driver will generally feel Front-Wheel-Drive as slightly more understeering, therefore less prone to close its trajectory. Moreover, in the field of usual driving, there will be some vibrations starting from a sudden sensation of lighter steering wheel, which require a few seconds to completely disappear. Instead, when driving the vehicle to its limit, the laden configuration will give a completely different feedback depending on the drivetrain. Specifically, Rear-Wheel-Drive will provide a sensation of empty steering wheel, while dangerously steering its front wheels and providing a strong oversteering effect. Instead Front-Wheel-Drive will maintain its lower reactivity and prevent anomalous phenomena. From the point of view of the vehicle dynamics, the most critical condition is represented by the laden Rear-Wheel-Drive, which manifests a strong oversteering response when it is close to its limit, while its Front-Wheel-Drive counterpart reveals a more stable behaviour. The already mentioned vibrations taking place in 2nd gear, mainly on Front-Wheel-Drive, are source of discomfort to the driver and reflect a greater yaw sensitivity, especially in the unladen configuration. Overall, Front-Wheel-Drive displays a more understeering and less reactive response, but the phenomena involving the steering system suggest that a possible optimization of the front suspension should be investigated.

6.3.2 Minimum Path Radius

This additional set of Power-Off Cornering tests is meant to stress the tyres to the limit and assess how the drivetrain affects saturation. It is realized minimizing the path radius achievable at the maximum allowed engine rotational speed. This maneuver might be critical for Front-Wheel-Drive vehicles, because a combination of huge longitudinal and lateral forces would eventually make the front tyres unable to steer. Indeed, the results suggest that this version of the van experiences a temporary loss of directionality. A limit maneuver involves the rear inner wheel leaving the ground due to load transfer, which obviously turns into additional understeer, but does not affect the ability of the front tyres to brake effectively the vehicle. Overall, Front-Wheel-Drive displays lower reactivity and a reduced tendency to close the trajectory as a consequence of throttle release, even in the laden condition, which is able to delay and soften the incoming oversteer. Rear-Wheel-Drive does not stress the front tyres, which are devoted to steering, but consistently shows a greater reactivity to the pedal release and a tendency to close more the trajectory, with the unladen configuration still understeering at the cost of reduced braking performance, while the laden condition enters oversteer quickly.

7 Throttle-On In-Turn

7.1 Throttle @ 50%

7.1.1 Test Setup

While the accelerator pedal release is regulated by a standard, the throttle modulation is not. For this reason, ISO 9816:2018 is taken as reference to build a simulation that is as close as possible to Power-Off Cornering, except for the action on the throttle pedal. On Adams/Car, there is a test called Throttle-On In-Turn which represents the counterpart of Power-Off Cornering, but it does not provide a full control over the accelerator pedal. Therefore, the function Event Builder is exploited to create a new cornering event with the desired characteristics. The test is made of two mini-maneuvers, where the first one is a steering pad with path radius equal to 100 m, necessary to establish the initial condition and the second one is a pushing action on the throttle while keeping the steering wheel locked. While in Power-Off Cornering the accelerator was released according to a step function from its initial value to the null value in a time equal to 0.1s, here the pedal is pushed following a step function whose time interval is 1.0s and its final value is set to 50% for initial lateral accelerations up to 0.35g, in the assumption of negligible influence of aerodynamic resistance and variations in rolling resistance. Instead, above that working point an extra throttling is estimated to compensate for the aerodynamic resistance in the two loading conditions. These data are provided by the manufacturer, to replicate a real possible action exerted by the driver. *Table 7.1* resumes the parameters adopted for this test, as well as the final positions of the accelerator pedal. The values of initial lateral acceleration are modified with respect to Power-Off Cornering, because the useful starting condition consists in the engine entering its constant torque region at around 1600 rpm, while the field close to 4000 rpm is avoided, since it would correspond to over-revving, where the engine suddenly experiences a dramatic drop in torque and power. At the same time, the region below 1600 rpm is not exploited, because the engine is still increasing its torque and in case of less reactive gears, it would be difficult to reach the constant torque field. To build a consistent comparison, the quantities reported are inherited from Power-Off Cornering, both in terms of time histories and functions of initial lateral acceleration.

Sampling Time Interval		0.001s	
Throttle Step Time Interval		1.0s	
Path Radius		100 m	
		Unladen	Laden
2nd Gear	0.035g - 0.05g	50%	50%
3rd Gear	0.085g - 0.25g		
4th Gear	0.275g - 0.35g		
	0.40g	53%	54%
	0.45g	54%	55%
	0.50g	55%	57%
	0.55g	56%	59%
	0.60g	58%	52%
	0.65g	61%	66%
	0.70g	65%	70%
Power Steering		Inactive	

Table 7.1: Throttle-On In-Turn - Throttle @ 50% - test setup.

Figures from 7.1 to 7.6 show the engine rotational speed time history and the corresponding torque. Overall, similar responses are provided by FWD and RWD, while the unladen configuration obviously allows a faster increase in the engine rotational speed. With respect to Power-Off Cornering, this maneuver does not show oscillatory responses after the throttle-on time instant, due to its smoother nature.

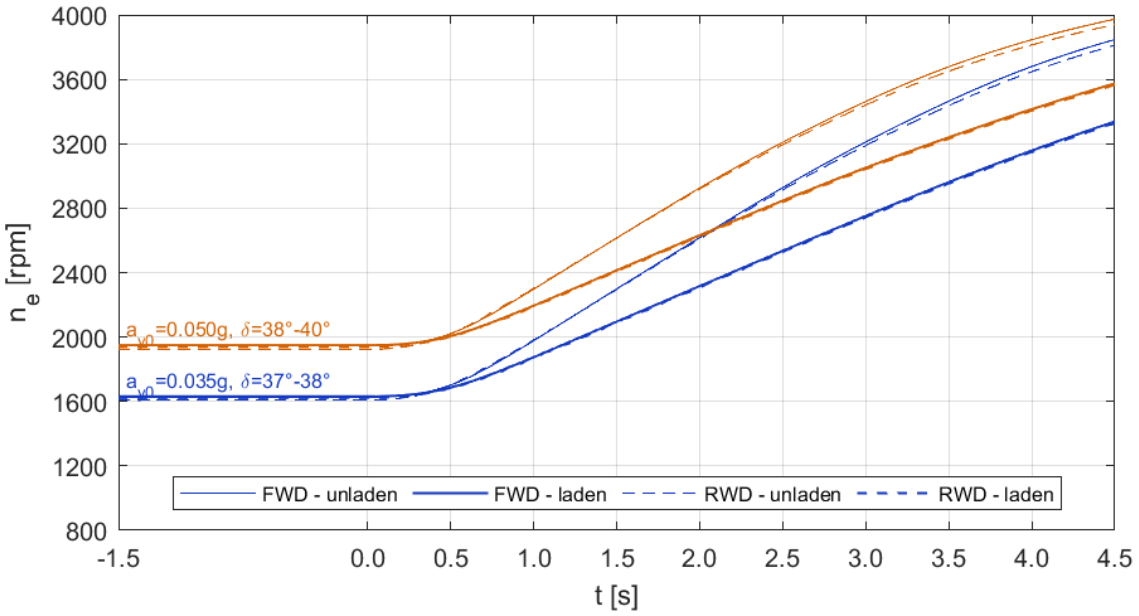

Figure 7.1: Throttle-On In-Turn - Throttle @ 50% - 2nd Gear - engine speed vs time.

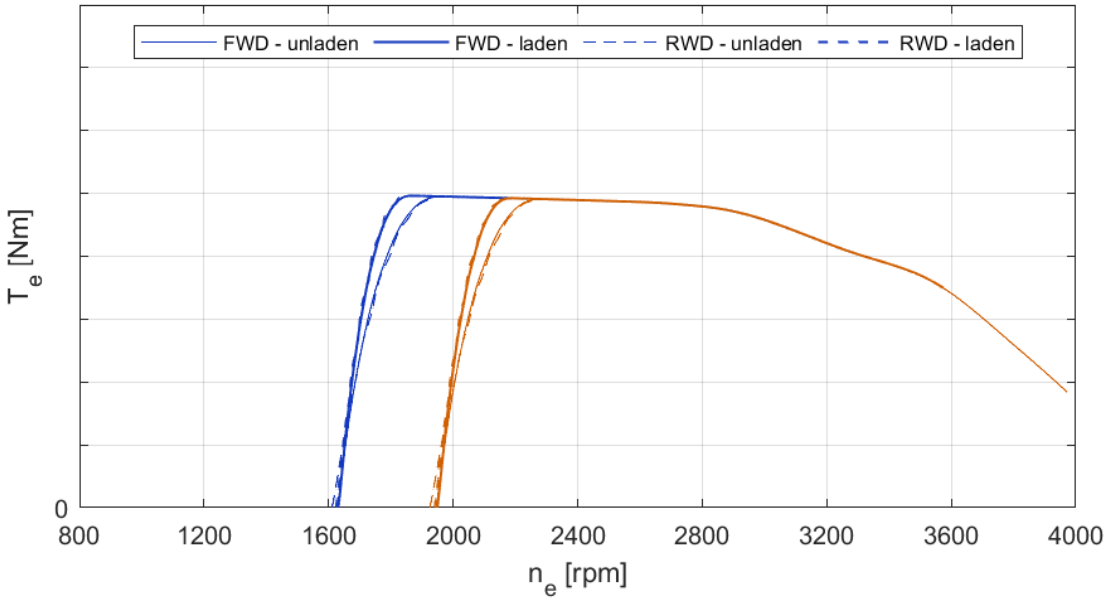

Figure 7.2: Throttle-On In-Turn - Throttle @ 50% - 2nd Gear - engine torque vs speed.

Obviously, the 2nd and 3rd gears have a quite limited range of available lateral accelerations, before reaching the upper revolutions limit of 4000 rpm. The engine characteristic (torque vs speed) clearly shows the ability to start from the constant torque region and later evolve to the constant power field, without reaching the above mentioned limit. The slope of the step in the engine characteristic is representative of the reactivity of each gear ratio, as in 2nd gear the engine increases its rotational speed by around 200 rpm before reaching the constant torque region, while in 4th gear its initial acceleration is barely visible.

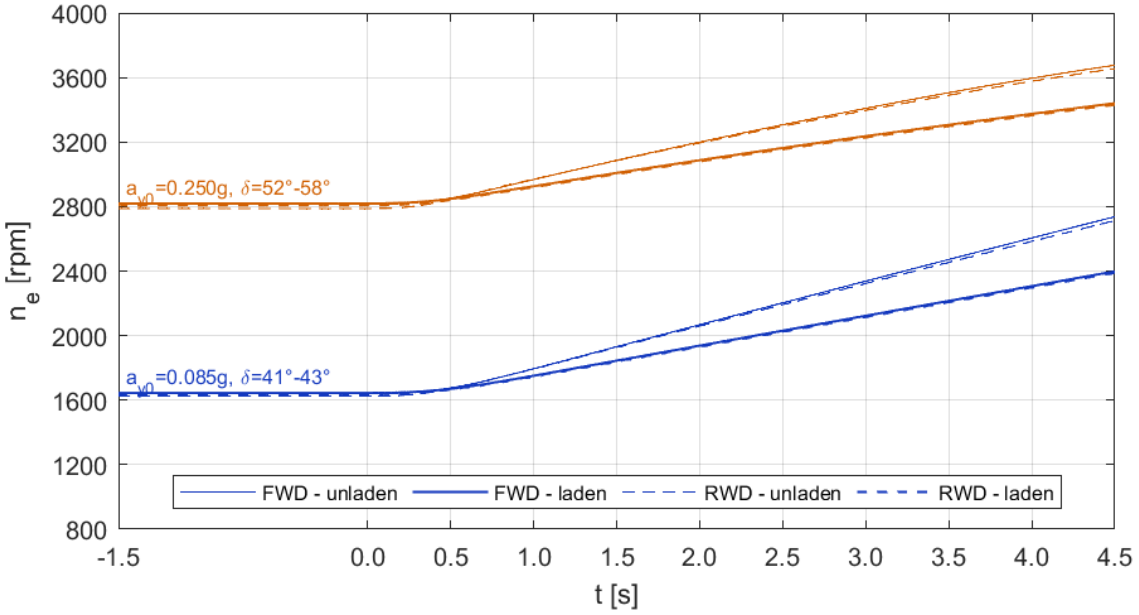

Figure 7.3: Throttle-On In-Turn - Throttle @ 50% - 3rd Gear - engine speed vs time.

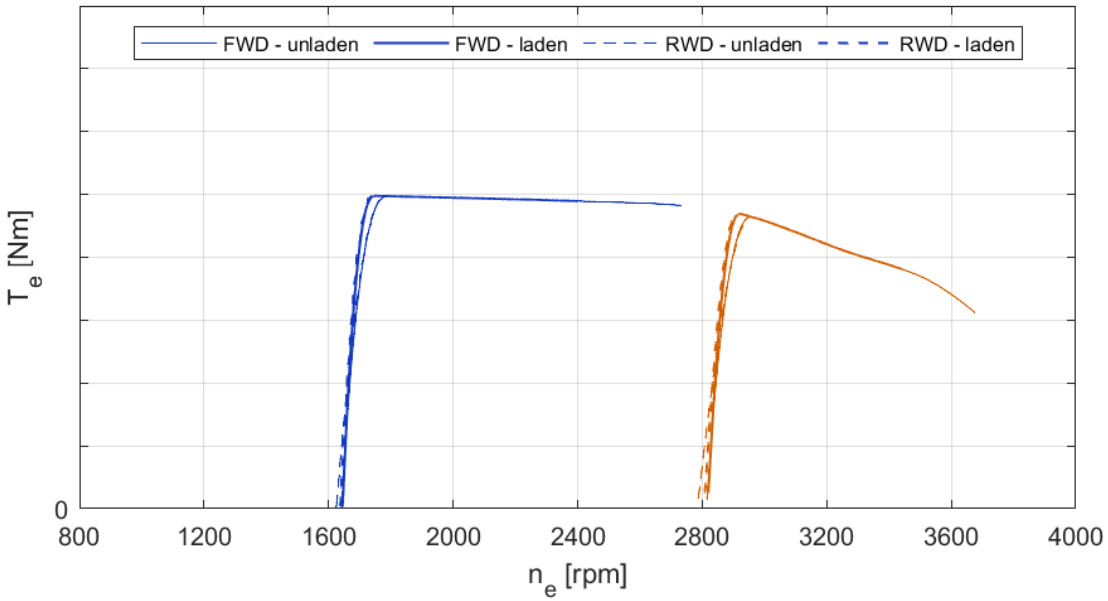

Figure 7.4: Throttle-On In-Turn - Throttle @ 50% - 3rd Gear - engine torque vs speed.

In 4th gear, an interesting discrepancy between FWD and RWD takes place close to the limit, indicating that RWD is accelerating the engine more. This response suggests that a slipping phenomenon might be taking place during the step. Moreover, the engine characteristic in 4th gear better highlights the differences between loading conditions. Specifically, the unladen van reaches lower torque peaks and wider engine accelerations, because of its reduced inertia.

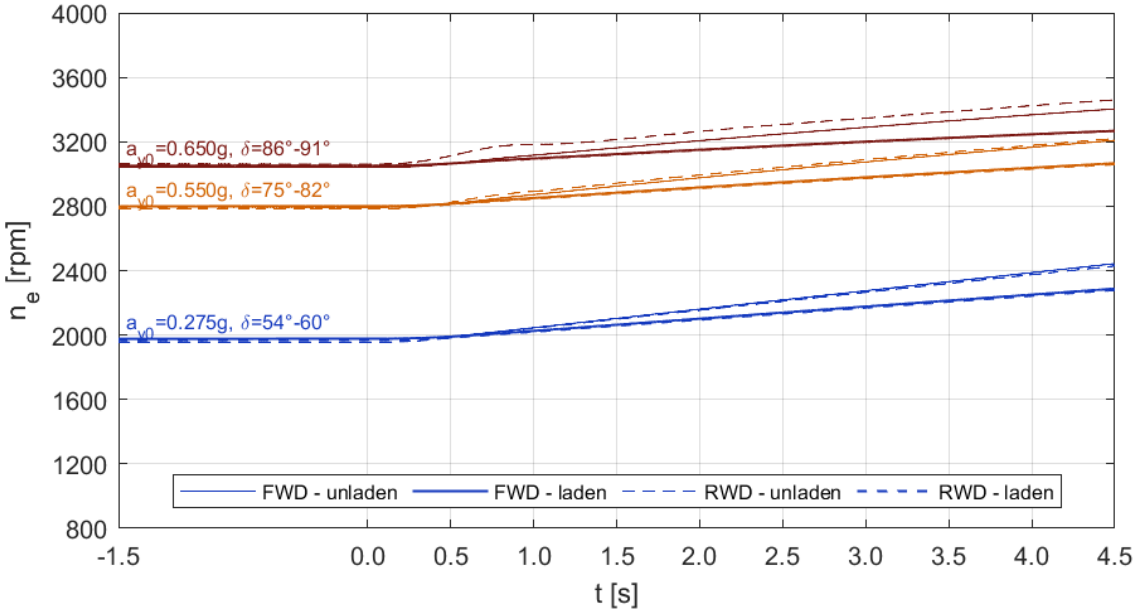

Figure 7.5: Throttle-On In-Turn - Throttle @ 50% - 4th Gear - engine speed vs time.

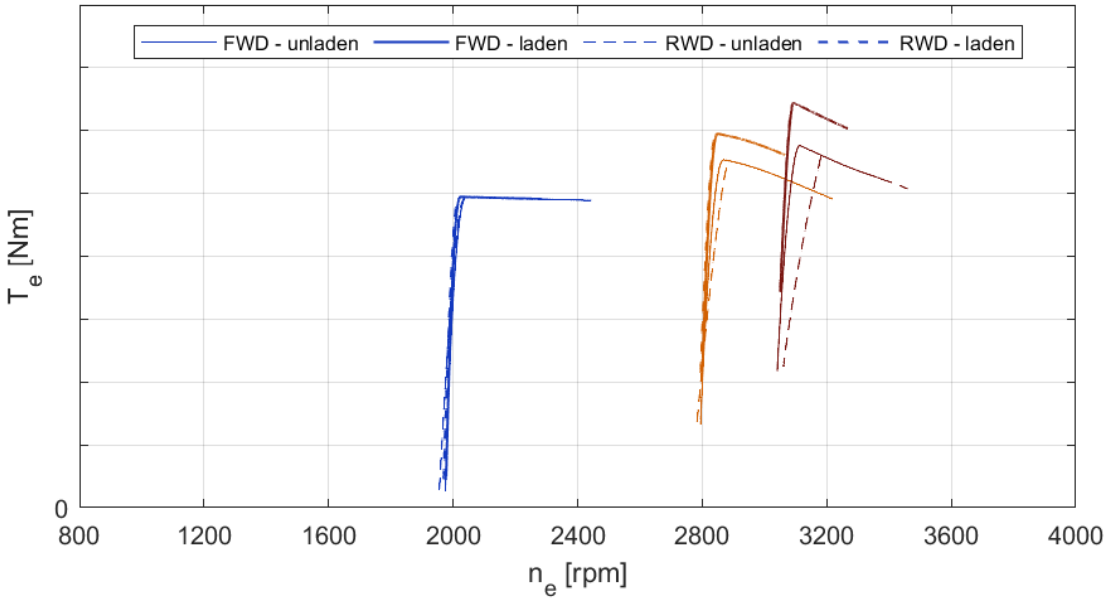

Figure 7.6: Throttle-On In-Turn - Throttle @ 50% - 4th Gear - engine torque vs speed.

7.1.2 Vehicle Dynamics

As in Power-Off Cornering, the same quantities are now reported in terms of time histories. *Figures from 7.7 to 7.9* show the lateral acceleration time history. With respect to the previous test, Throttle-On In-Turn shows a smoother transition, due to the longer time step in the accelerator function. In the field of low and middle lateral accelerations, the response is predictable, as the van reacts increasing its lateral acceleration almost linearly.

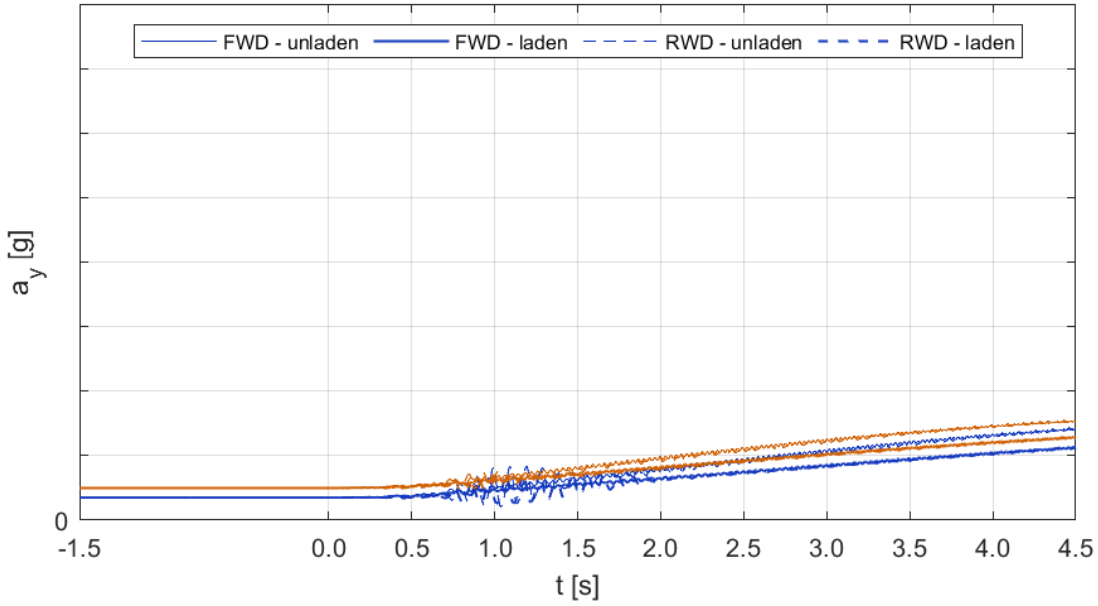

Figure 7.7: Throttle-On In-Turn - Throttle @ 50% - 2nd Gear - lat. acc. vs time.

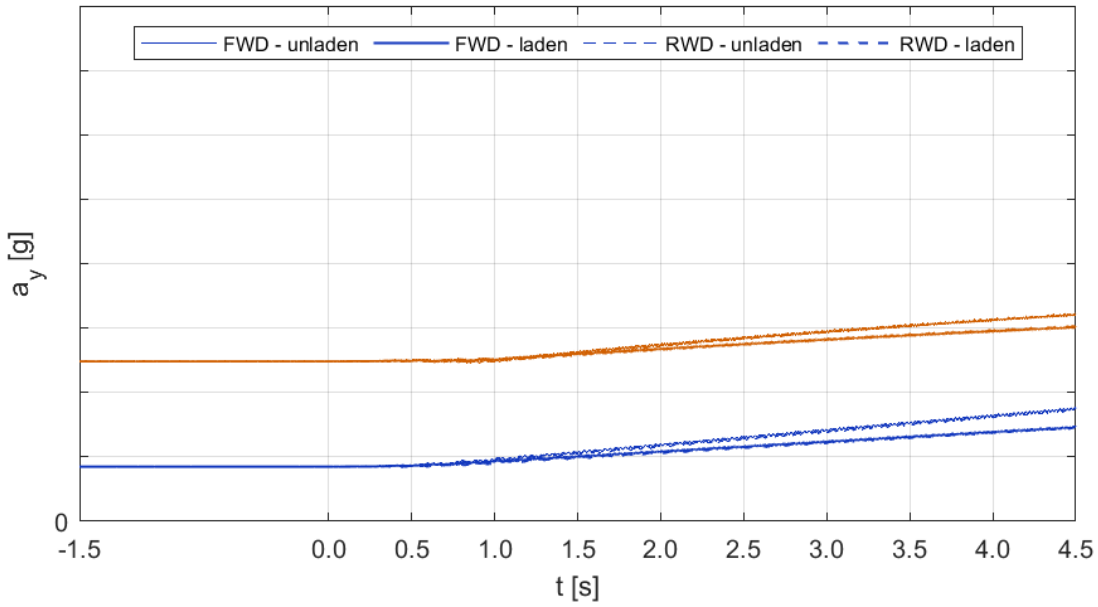

Figure 7.8: Throttle-On In-Turn - Throttle @ 50% - 3rd Gear - lat. acc. vs time.

Instead, at higher lateral accelerations, a transient occurs, where the lateral acceleration slightly decreases before entering the linear increase. RWD seems a little more sensitive to this phenomenon. Overall, it is clear that the unladen vehicle is more reactive due to its lower inertia. The differences between the two loading configurations lose relevance when running the vehicle in 4th gear. FWD and RWD generally share similar responses throughout the entire range of lateral accelerations, excluding 2nd gear, where RWD undergoes some oscillatory phenomena.

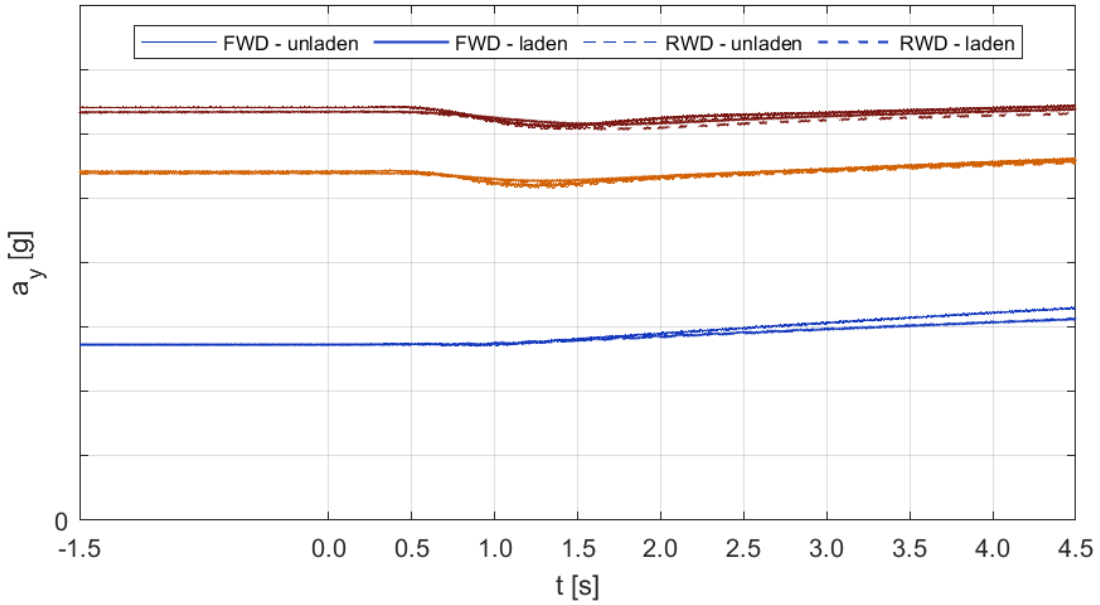

Figure 7.9: Throttle-On In-Turn - Throttle @ 50% - 4th Gear - lat. acc. vs time.

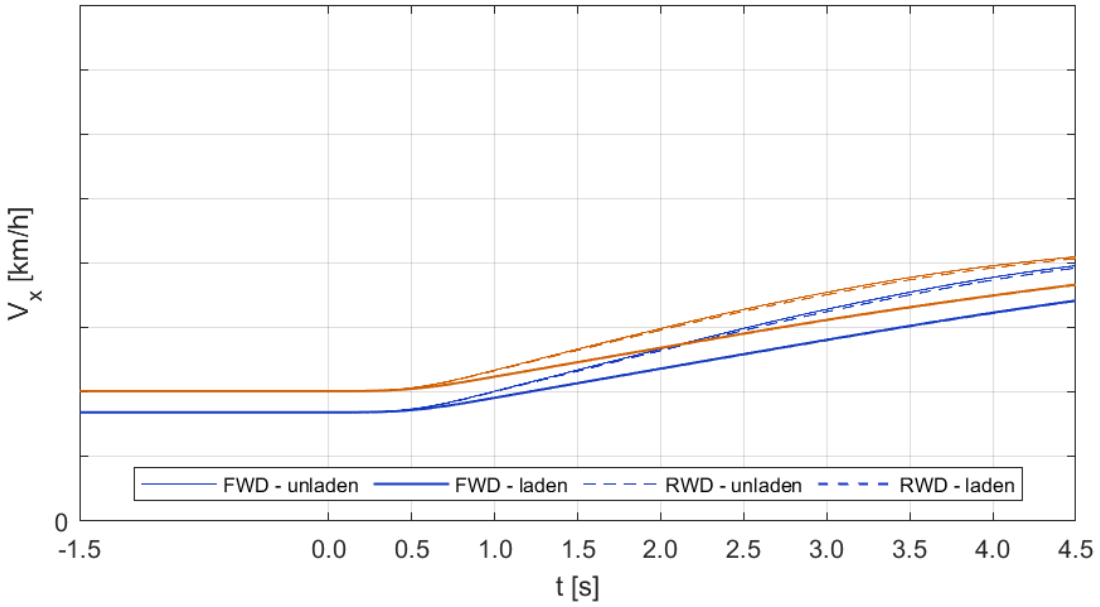

Figure 7.10: Throttle-On In-Turn - Throttle @ 50% - 2nd Gear - long. velocity vs time.

Figures from 7.10 to 7.12 show the longitudinal velocity time history. FWD and RWD share almost identical responses, while the loading condition obviously affects the vehicle inertia, thus making the laden van less sensitive to an increase in velocity. In 4th gear the loading condition becomes less relevant, as already suggested by the lateral acceleration time history.

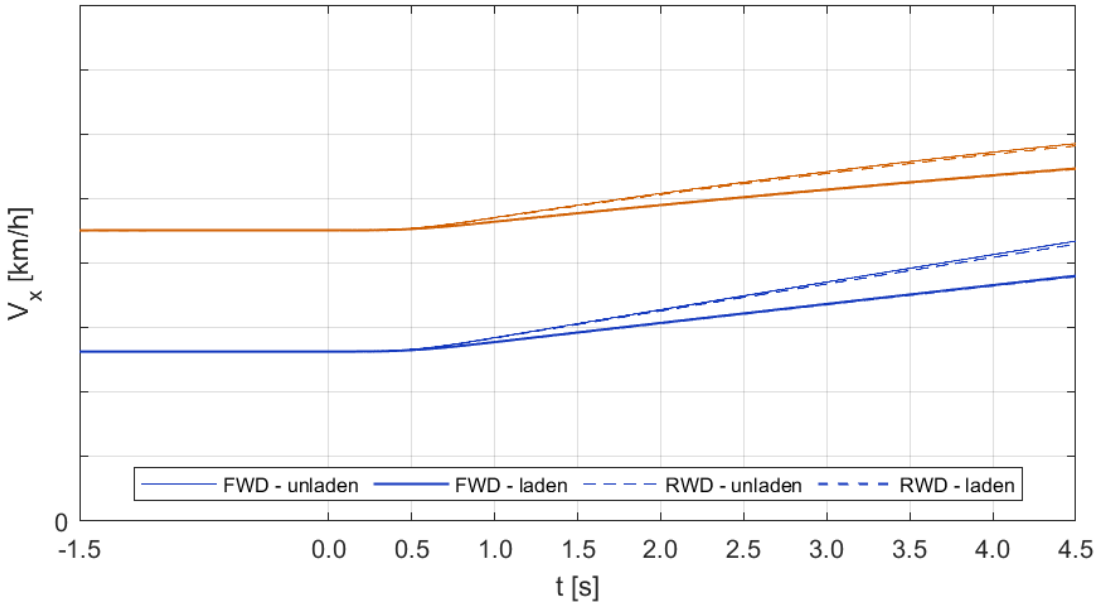

Figure 7.11: Throttle-On In-Turn - Throttle @ 50% - 3rd Gear - long. velocity vs time.

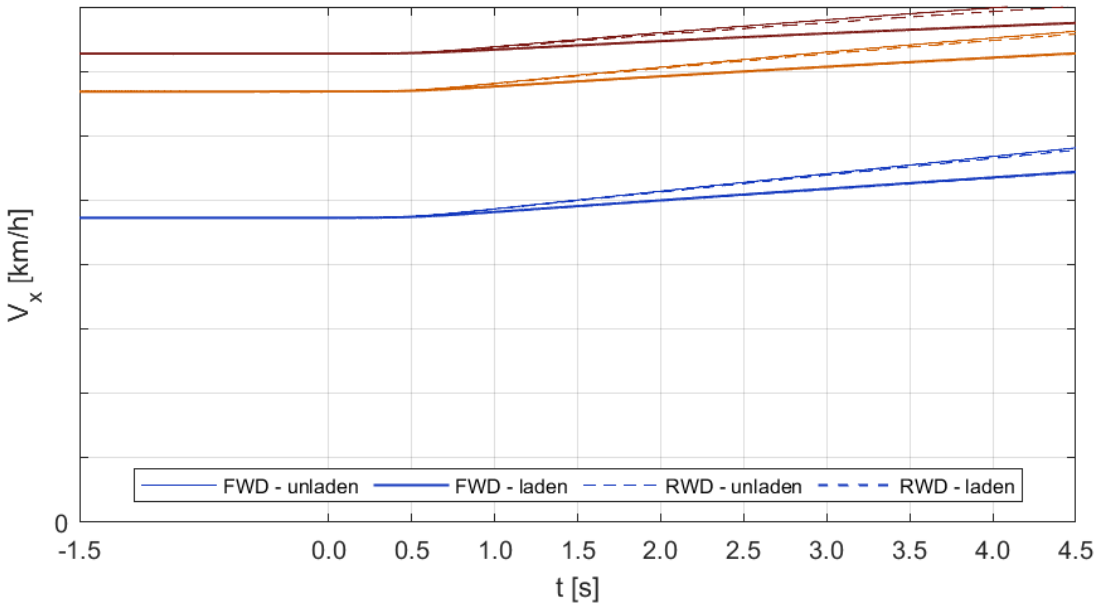

Figure 7.12: Throttle-On In-Turn - Throttle @ 50% - 4th Gear - long. velocity vs time.

Figures from 7.13 to 7.15 show the sideslip angle time history. Clearly, an increase in longitudinal velocity implies that the vehicle moves from a "nose-out" to a "nose-in" configuration, or at least a neutral condition. At lower lateral accelerations, there is no noticeable effect related to the loading condition, which gains relevance especially in 4th gear. Here, in the field close to the limit, the vehicle provides a different response, since it temporarily reduces its sideslip angle, before restoring the initial configuration. This phenomenon is linked to the transient seen in lateral acceleration. FWD and RWD keep showing similar behaviours, the latter being slightly more sensitive to some variations in the angle.

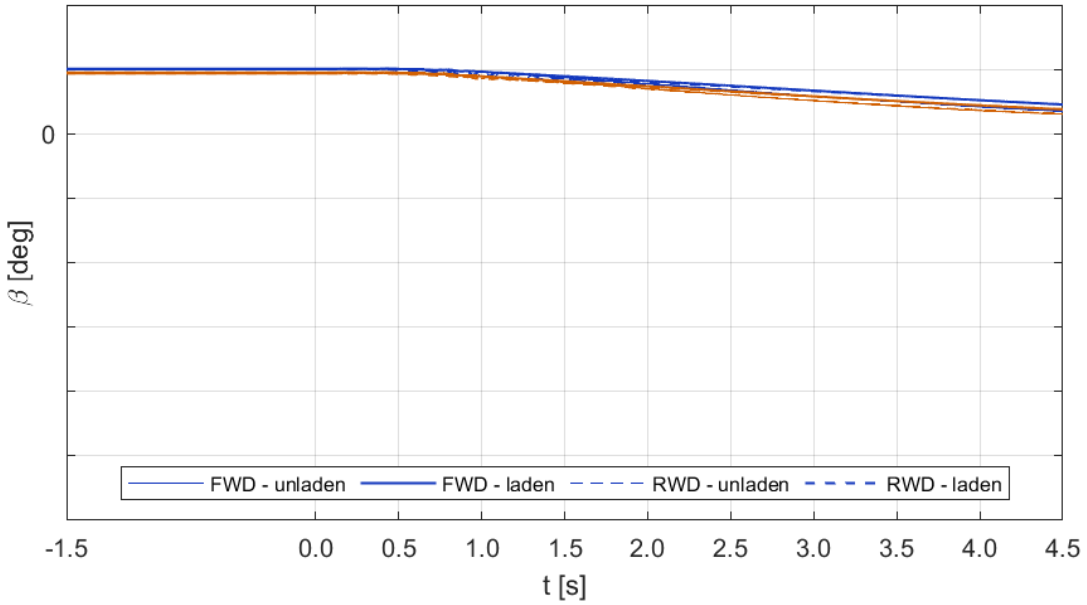

Figure 7.13: Throttle-On In-Turn - Throttle @ 50% - 2nd Gear - sideslip angle vs time.

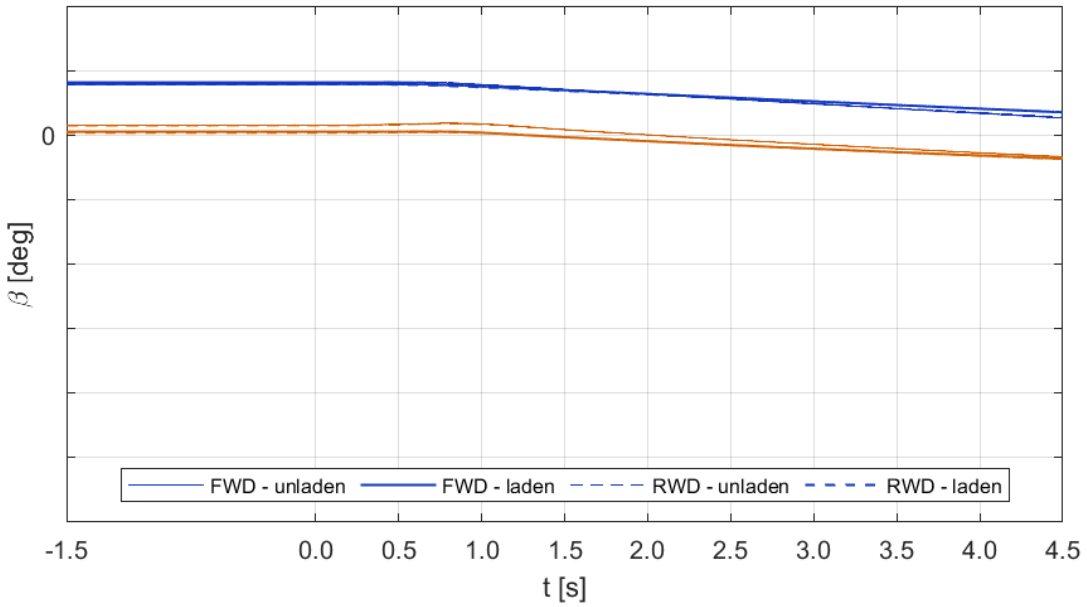

Figure 7.14: Throttle-On In-Turn - Throttle @ 50% - 3rd Gear - sideslip angle vs time.

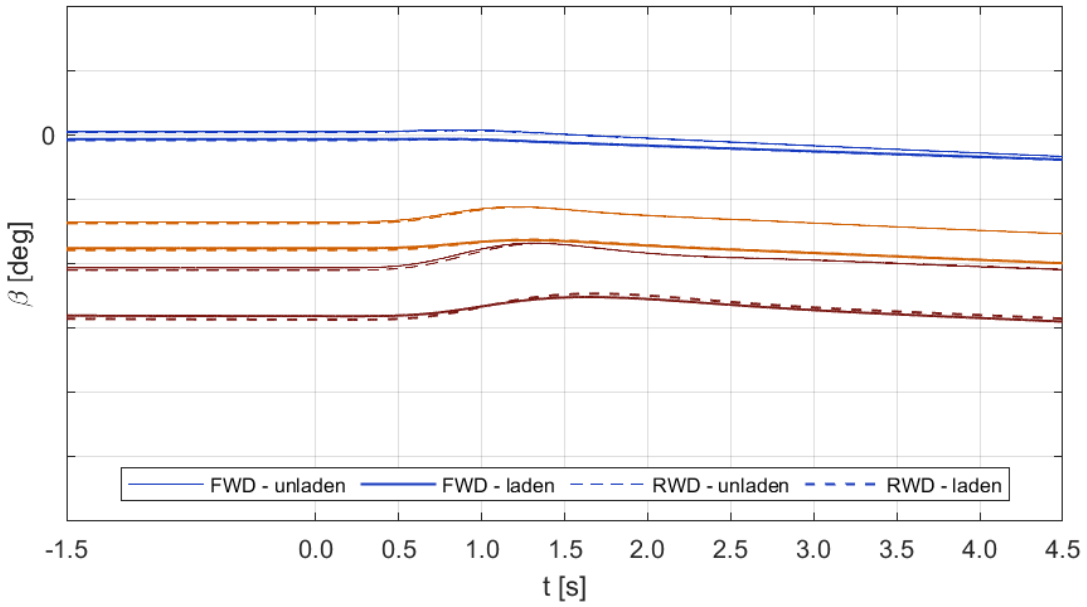

Figure 7.15: Throttle-On In-Turn - Throttle @ 50% - 4th Gear - sideslip angle vs time.

Figures from 7.16 to 7.18 show the yaw velocity time history. This variable resumes the considerations previously drawn. At low lateral accelerations, the maneuver forces the vehicle to increase its yaw velocity, therefore the acceleration is prevailing over the widening trajectory. RWD confirms the vibrations previously seen in lateral acceleration, but the overall response is similar to FWD. At greater lateral accelerations and close to the limit, a transient followed by a decrease takes place, meaning that the path radius is increasing more with respect to the longitudinal velocity. This understeering behaviour is justified by the response in terms of lateral accelerations and sideslip angle previously discussed.

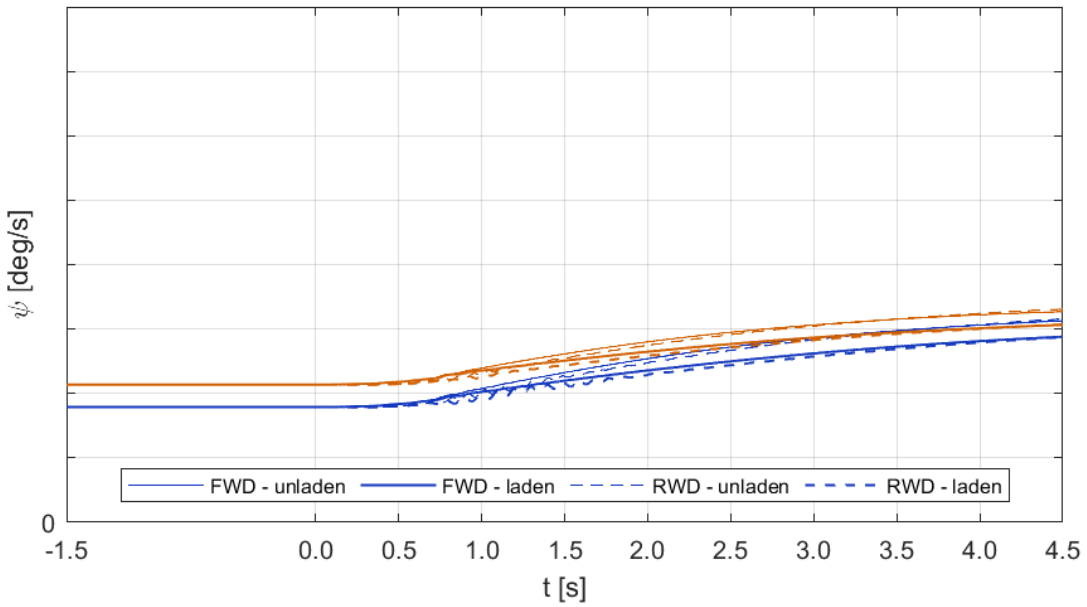

Figure 7.16: Throttle-On In-Turn - Throttle @ 50% - 2nd Gear - yaw velocity vs time.

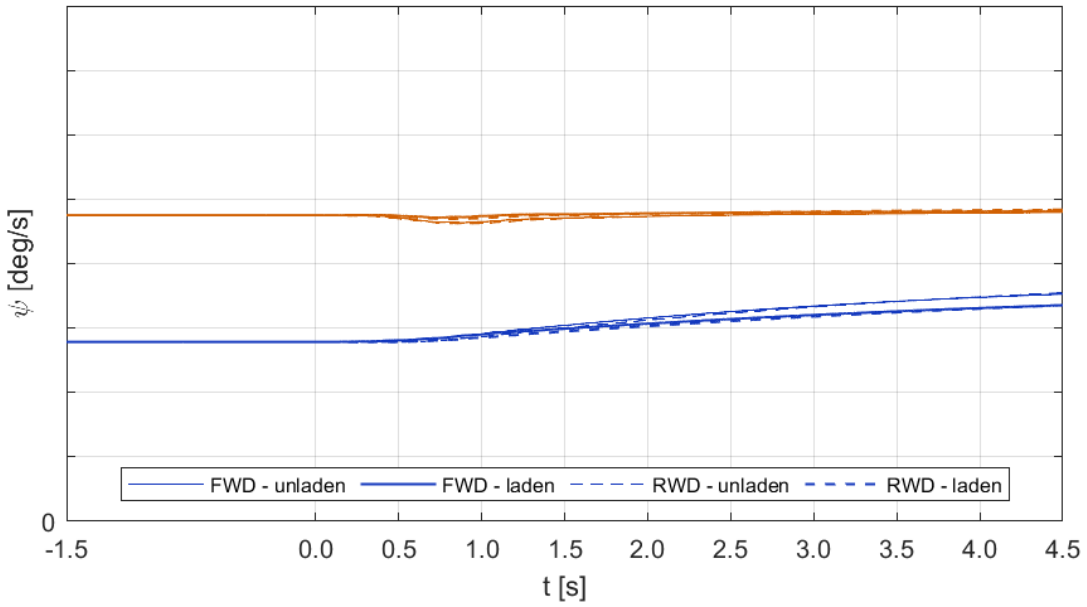

Figure 7.17: Throttle-On In-Turn - Throttle @ 50% - 3rd Gear - yaw velocity vs time.

The unladen configuration is always more prone to achieve a greater yaw velocity, as a result of its lower inertia, hence a greater ability to accelerate and a more understeering behaviour. Globally, FWD and RWD share similar responses, the latter being more subject to a decrease in yaw velocity at great lateral accelerations during the transient.

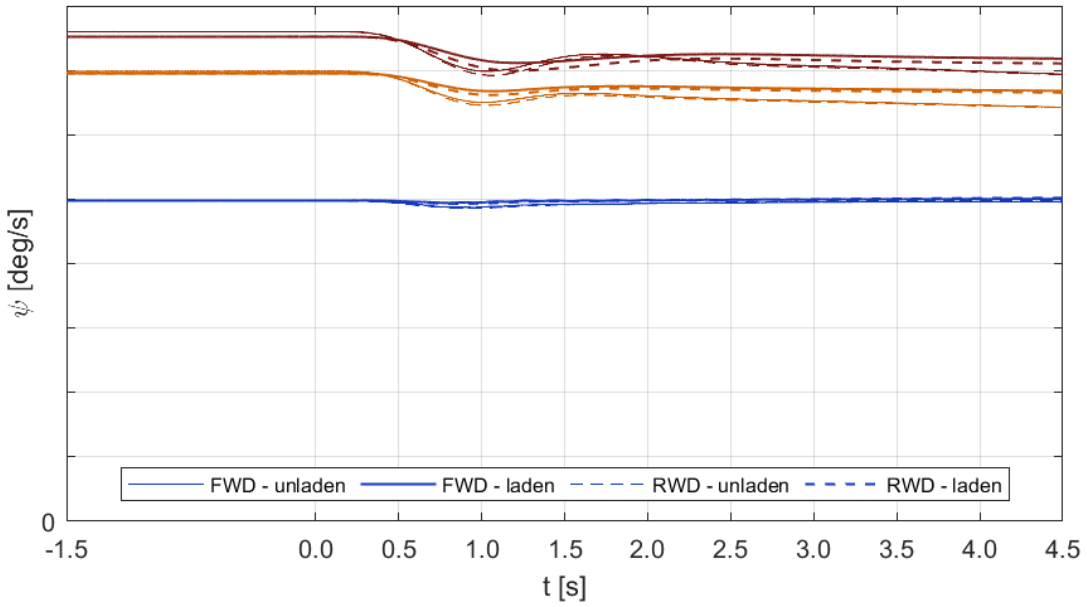

Figure 7.18: Throttle-On In-Turn - Throttle @ 50% - 4th Gear - yaw velocity vs time.

In addition to the previous prescribed quantities, *Figures from 7.19 to 7.21* report the longitudinal acceleration time history. The response in 2nd gear highlights how the engine torque evolves during the test, without reaching a null acceleration, which would happen in case of over-revving. Instead, 3rd and 4th gears confirm their lower reactivity and result in generally constant engine torque, thus a constant acceleration.

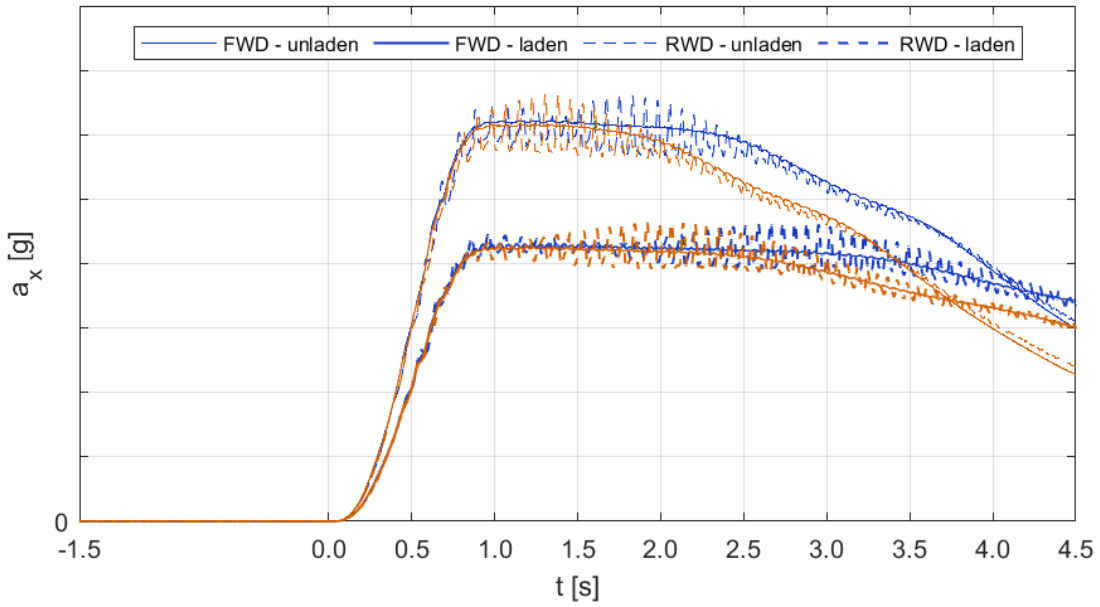

Figure 7.19: Throttle-On In-Turn - Throttle @ 50% - 2nd Gear - long. acceleration vs time.

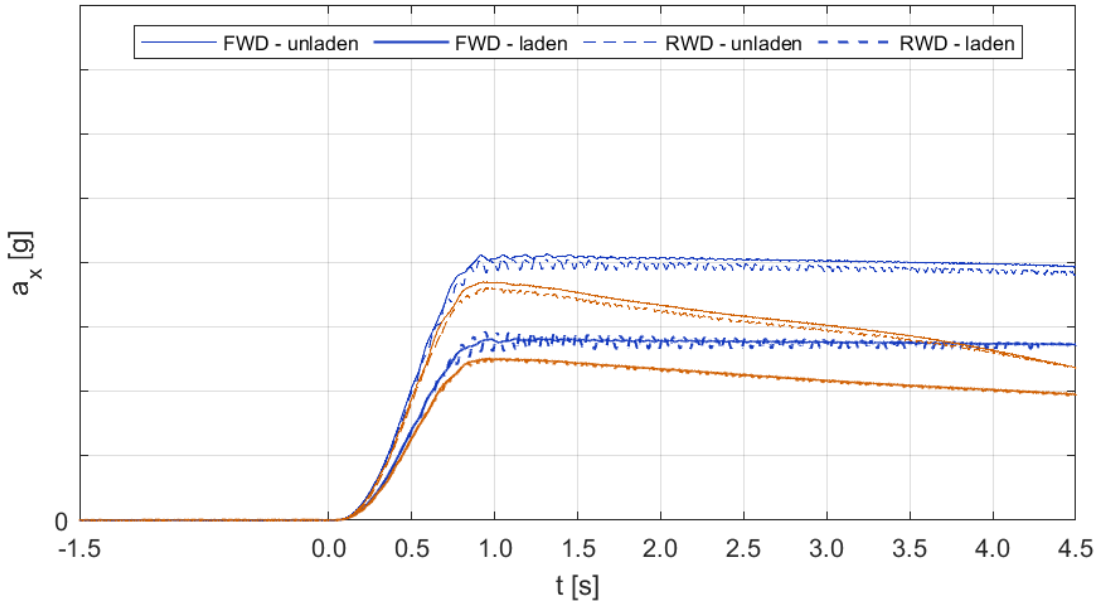

Figure 7.20: Throttle-On In-Turn - Throttle @ 50% - 3rd Gear - long. acceleration vs time.

In 2nd gear, RWD shows some vibrations with amplitude and duration depending on the loading configuration and the initial lateral acceleration. Even in 3rd gear, some minor vibrations take place, but only at lower lateral accelerations. These phenomena never appear in FWD. Interestingly, FWD seems to impress a slightly greater longitudinal acceleration, especially in the unladen configuration in 4th gear. This result might seem in contrast with the expectations, since the front axle should lose some grip due to the longitudinal load transfer, leading to a reduced ability to accelerate. The maneuver here defined proves not to be such critical, suggesting that the static load distribution is still more influential than the longitudinal load transfer. Since the front axle is remarkably more loaded in the unladen configuration, FWD takes advantage of the static load acting on the fron wheels and is able to impress a greater acceleration, while RWD suggests the possibility of a partial slippage at greater lateral accelerations, confirming that the rear axle is not gaining additional grip and is suffering the lower static weight. The slight difference in longitudinal acceleration becomes negligible in the laden configuration, because this time the load distribution is closer to 50% on each axle. This, along with a further reduction of the longitudinal load transfer due to the lower ability to accelerate the vehicle, indicates that no axle is gaining a considerable advantage, thus making the two versions display similar longitudinal dynamics.

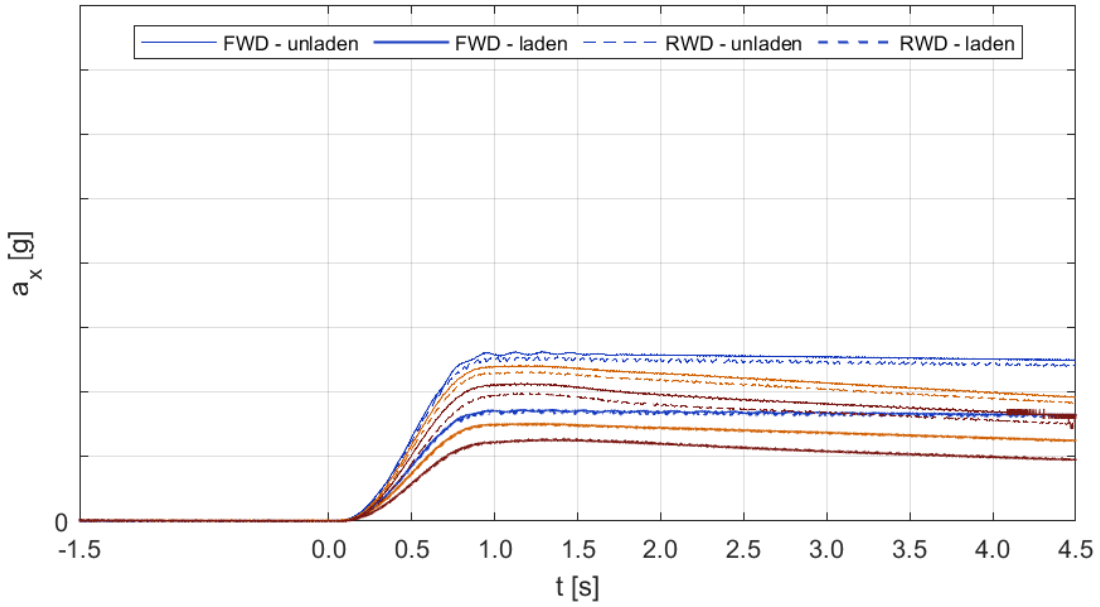

Figure 7.21: Throttle-On In-Turn - Throttle @ 50% - 4th Gear - long. acceleration vs time.

In terms of driver's comfort, the previously discussed longitudinal and lateral accelerations are now investigated by computing their power spectral density. *Figures 7.22 and 7.23* show the results to identify the frequency of excitation transmitted to the human body when the vehicle is cornering in 2nd gear, which already proved to be more stressful during Power-Off Cornering. However, this time RWD is mainly interested by the phenomenon. Apart from the excitation close to 1 Hz, which might be influenced by a not proper filtering of the overall trend, the frequency of interest is around 10 Hz, hence the field of resonance of the back.

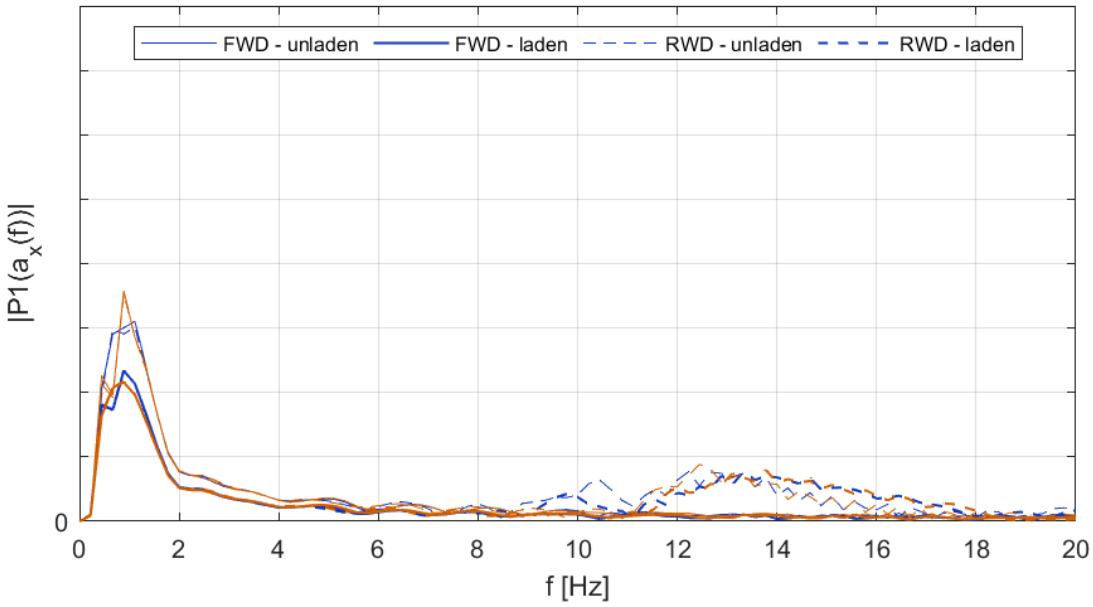

Figure 7.22: Throttle-On In-Turn - Throttle @ 50% - 2nd Gear - PSD of long. acceleration.

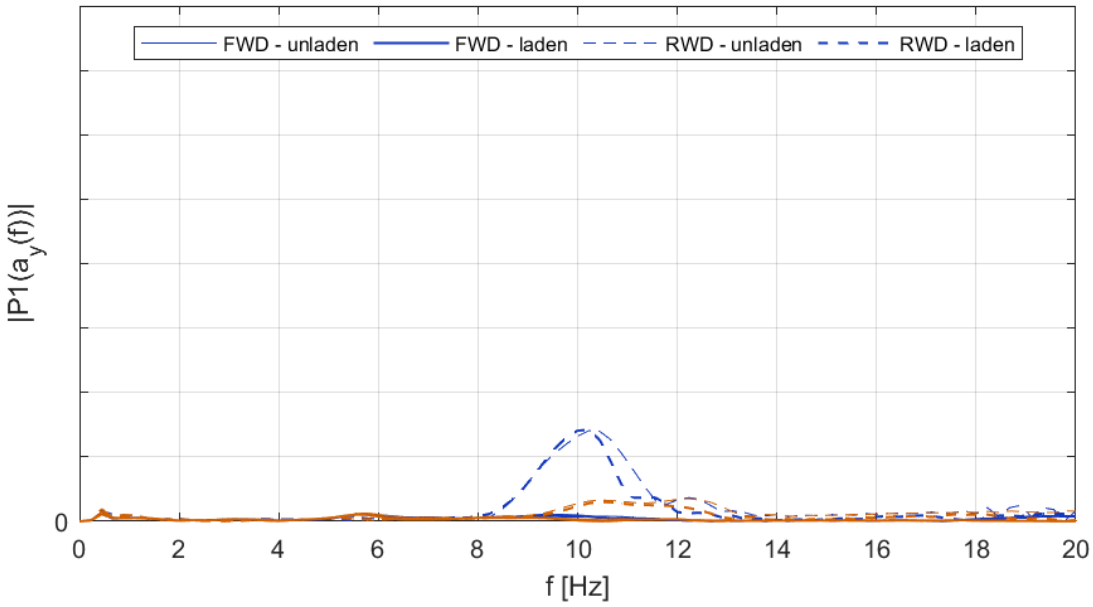

Figure 7.23: Throttle-On In-Turn - Throttle @ 50% - 2nd Gear - PSD of lat. acc.

7.1.3 Tyres Dynamics

Figures from 7.24 to 7.29 show the lateral load transfer on front and rear axles, with respect to their initial steady-state value. This definition allows to isolate the contribution to load transfer due to the cornering event, without taking into account the steady-state lateral acceleration. As in the previous test, the main difference between FWD and RWD is represented by the reaction torque. During a left turn, the propeller shaft supplies a torque to the rear axle, loading more the inner wheel. For this reason, RWD shows a lateral load transfer towards the inner wheel.

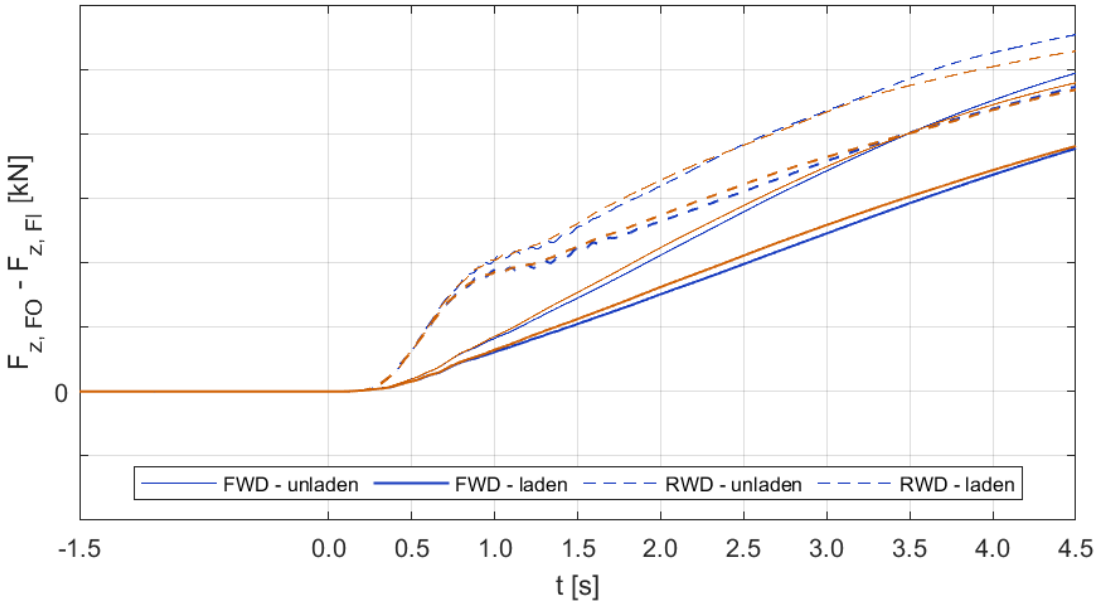

Figure 7.24: Throttle-On In-Turn - Throttle @ 50% - 2nd Gear - front lateral transfer vs time.

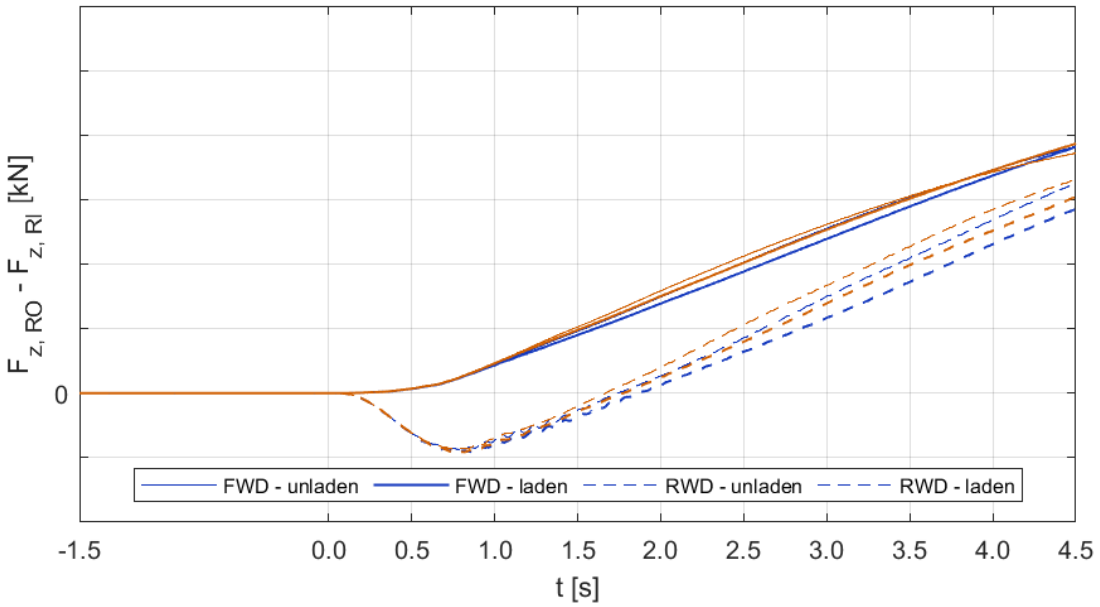

Figure 7.25: Throttle-On In-Turn - Throttle @ 50% - 2nd Gear - rear lateral transfer vs time.

Consequently, the front axle reacts loading more the outer wheel. FWD clearly shows similar responses on both axles, confirming the absence of a reaction torque. With respect to Power-Off Cornering, a smoother response is here presented and there are no critical peaks. After the transient, RWD keeps a moderate load transfer on the rear axle with respect to FWD and a greater one on the front axle. The loading condition is more influential on the front axle, which is subject to a greater load transfer in case of unladen vehicle.

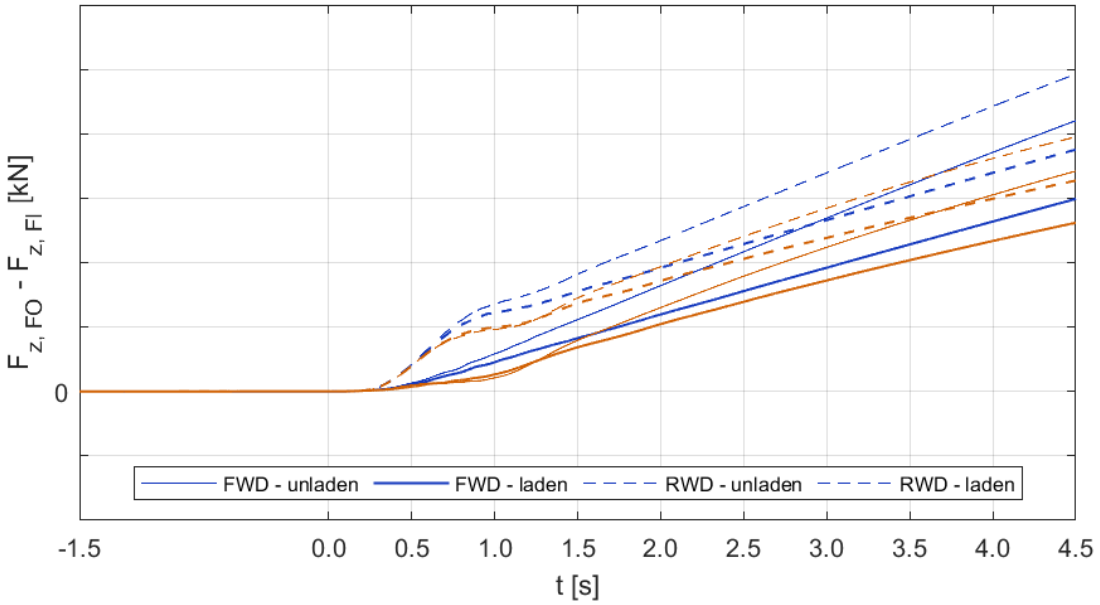

Figure 7.26: Throttle-On In-Turn - Throttle @ 50% - 3rd Gear - front lateral transfer vs time.

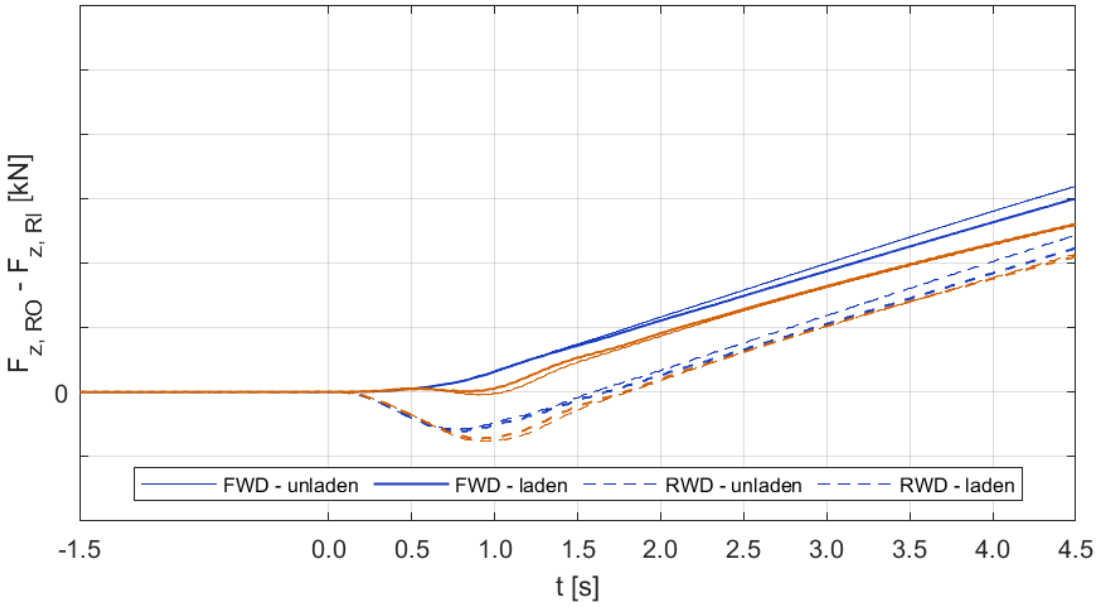

Figure 7.27: Throttle-On In-Turn - Throttle @ 50% - 3rd Gear - rear lateral transfer vs time.

In 4th gear, the contribution given by the reaction torque becomes less relevant, especially at greater lateral accelerations. Close to the limit, FWD and RWD provide similar responses, where both vehicles load more the inner side. This is in agreement with the transient previously observed on the lateral acceleration itself, which suggested an understeering response and a temporary load transfer to the inner wheels. Clearly, RWD shows a slightly greater load transfer on the rear axle due to the above mentioned reaction torque.

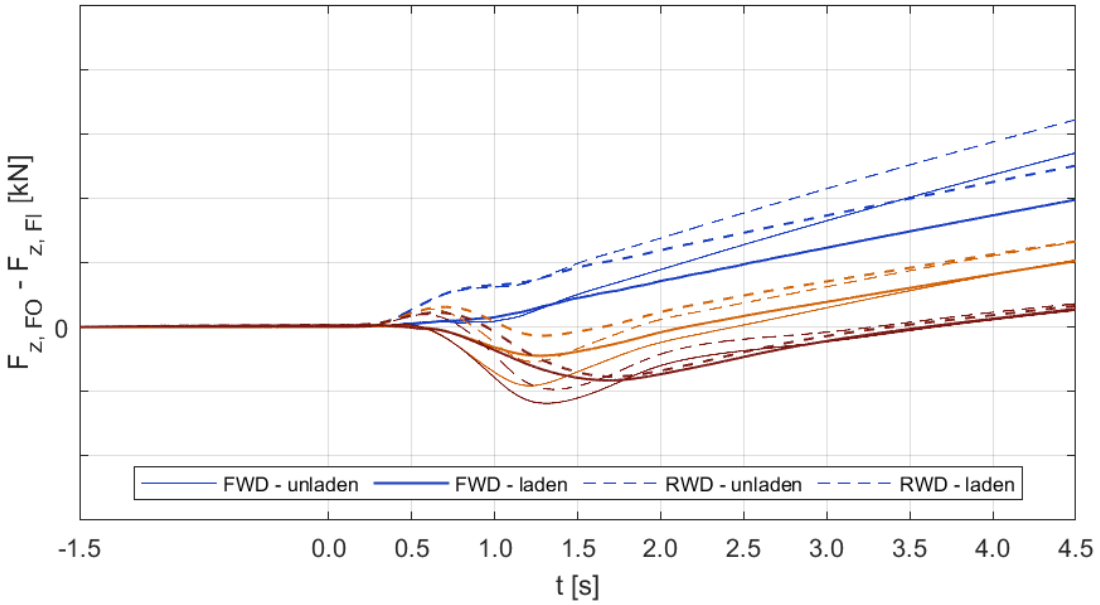

Figure 7.28: Throttle-On In-Turn - Throttle @ 50% - 4th Gear - front lateral transfer vs time.

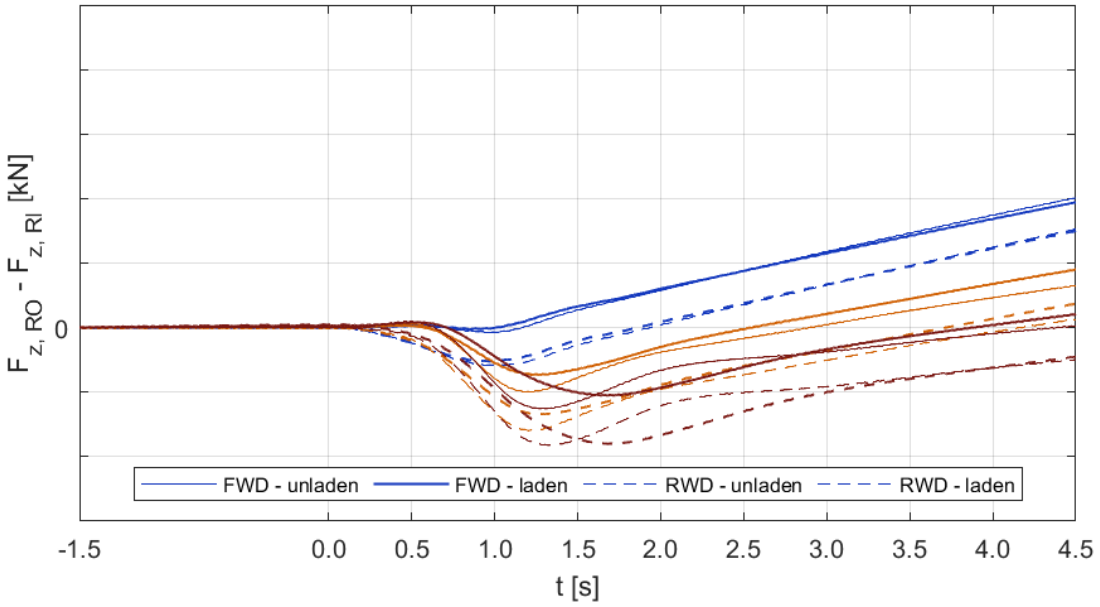

Figure 7.29: Throttle-On In-Turn - Throttle @ 50% - 4th Gear - rear lateral transfer vs time.

Figures 7.30 and 7.31 resume the lateral load transfer as function of the initial lateral acceleration at time instant t_1, hence at the conclusion of the accelerator step. FWD confirms the symmetry seen in Power-Off Cornering and the sensitivity to load transfer typical of the unladen configuration. In the field of low and middle lateral accelerations, the outer side is more loaded as a consequence of the increased lateral acceleration, while approaching the limit makes the inner side more loaded. Instead, RWD highlights the presence of a reaction torque on the rigid axle and shows some significant asymmetries in 2nd and 3rd gears.

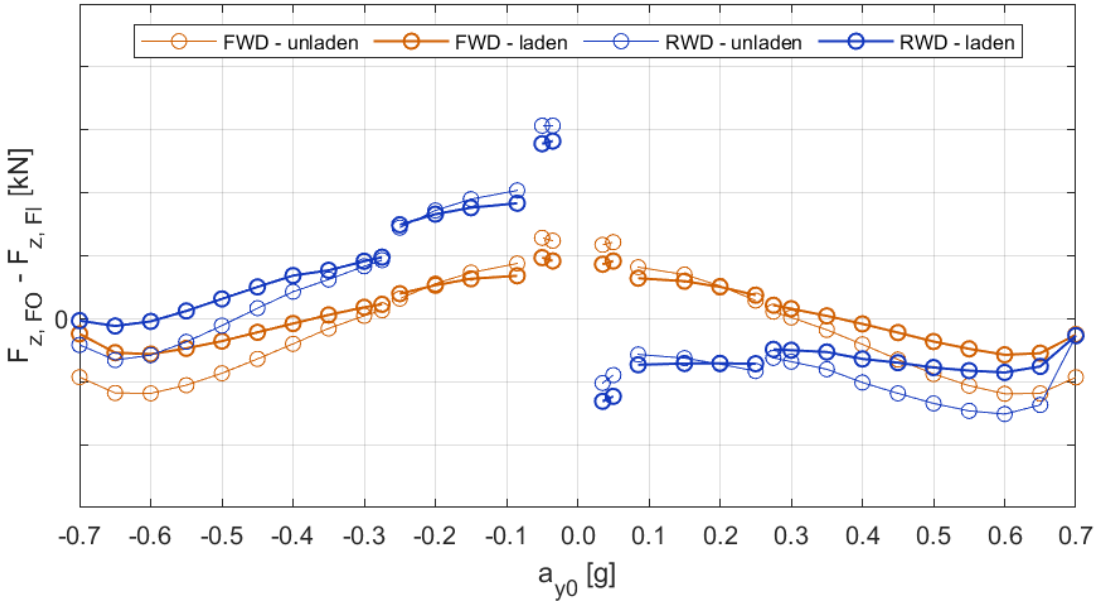

Figure 7.30: Throttle-On In-Turn - Throttle @ 50% - front lateral transfer vs in. lat. acc. @ t_1.

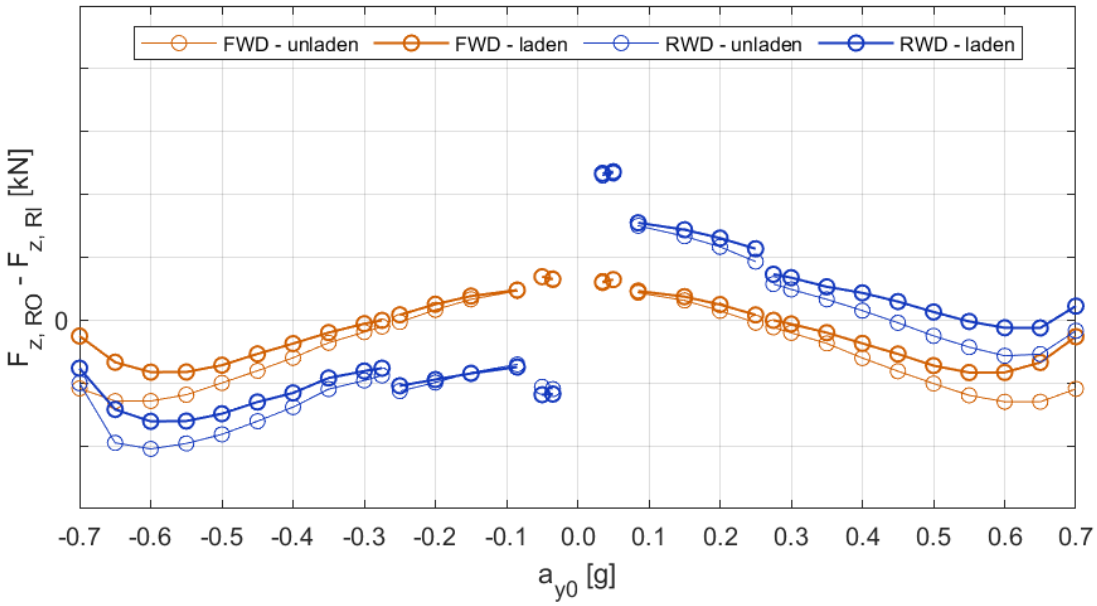

Figure 7.31: Throttle-On In-Turn - Throttle @ 50% - rear lateral transfer vs in. lat. acc. @ t_1.

Figures from 7.32 to 7.34 show the longitudinal load transfer time history, defined as the difference between rear and front axles loads, with respect to their initial steady-state value. This time, the only steady-state load transfer to be excluded is the static weight distribution. The longitudinal load transfer follows a qualitative trend similar to the longitudinal acceleration and is directly influence by the engine torque time evolution. Clearly, the longitudinal load transfer is enhanced in 2nd gear due to the greater reactivity and is generally greater in the unladen vehicle, since this configuration opposes a lower inertia.

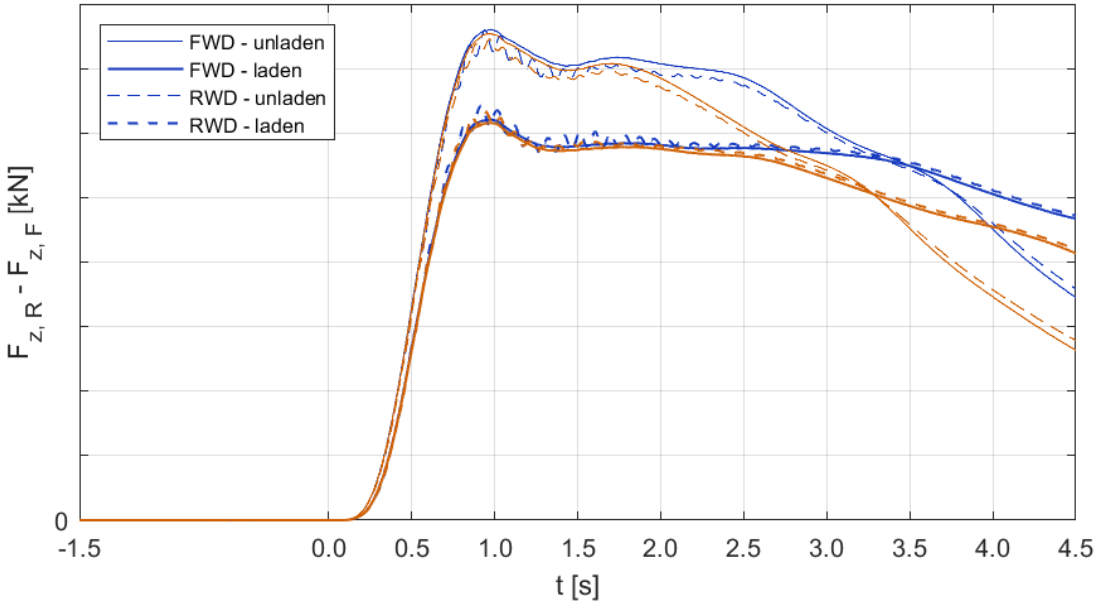

Figure 7.32: Throttle-On In-Turn - Throttle @ 50% - 2nd Gear - long. transfer time.

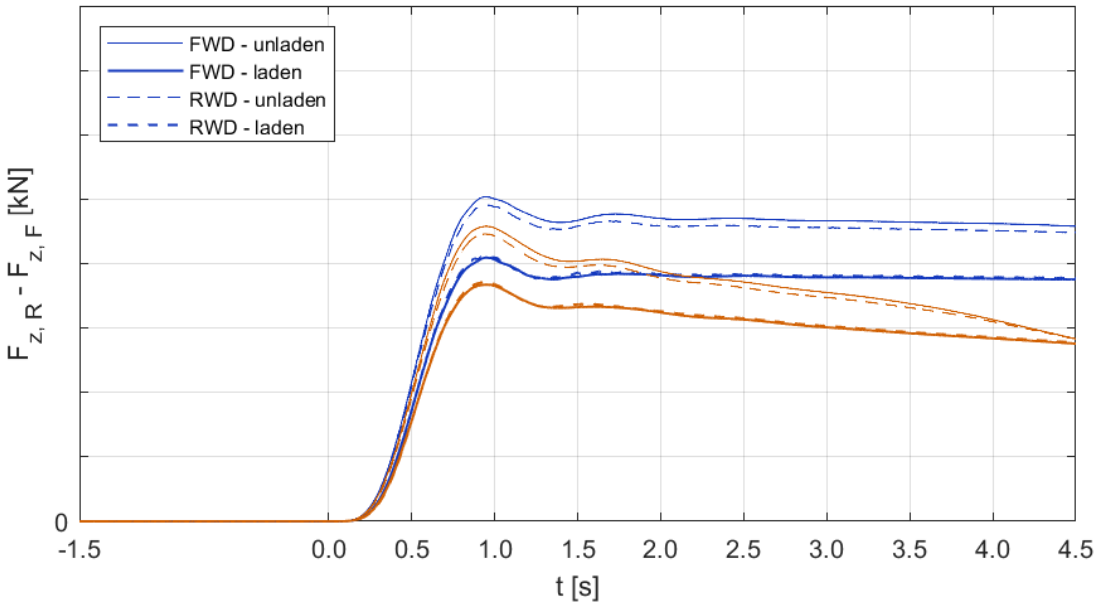

Figure 7.33: Throttle-On In-Turn - Throttle @ 50% - 3rd Gear - long. transfer time.

Overall, the unladen FWD seems slightly more subject to a longitudinal load transfer, as previously suggested by the longitudinal acceleration time history. The considerations previously drawn about the vehicle longitudinal dynamics are here confirmed. *Figure 7.35* reports the longitudinal load transfer as function of the initial lateral acceleration at time instant t_1. FWD shows its slightly increased load transfer in the unladen configuration throughout the whole range of lateral accelerations, while both vehicles behave similarly in the laden condition. The unladen RWD shows an anomalous drop at 0.7g, suggesting a partial tyre slippage, in agreement with the previous considerations about the increase in the engine rotational speed.

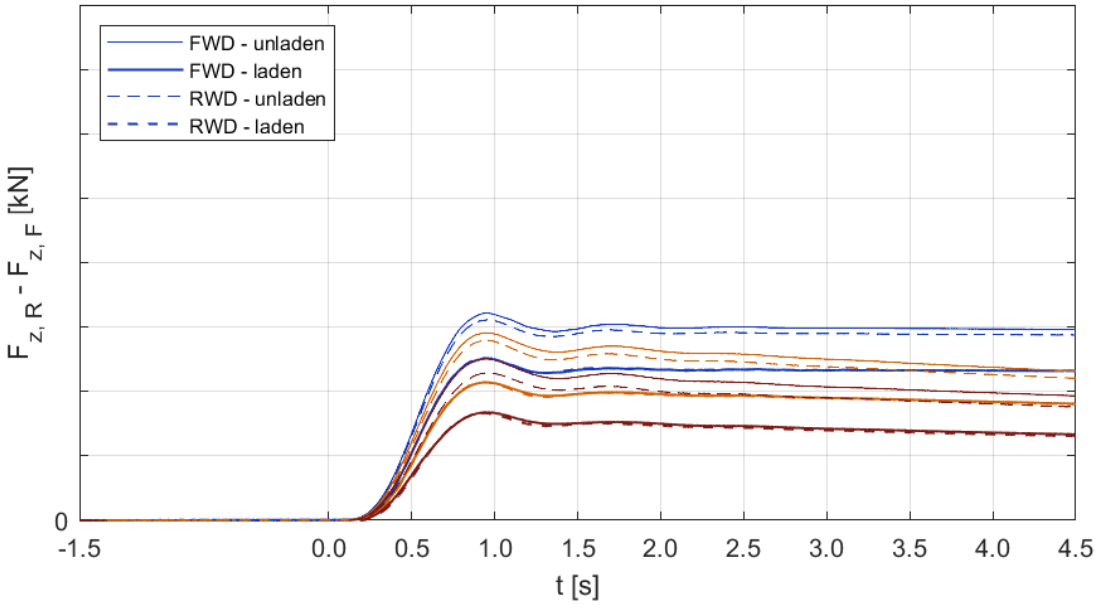

Figure 7.34: Throttle-On In-Turn - Throttle @ 50% - 4th Gear - long. transfer time.

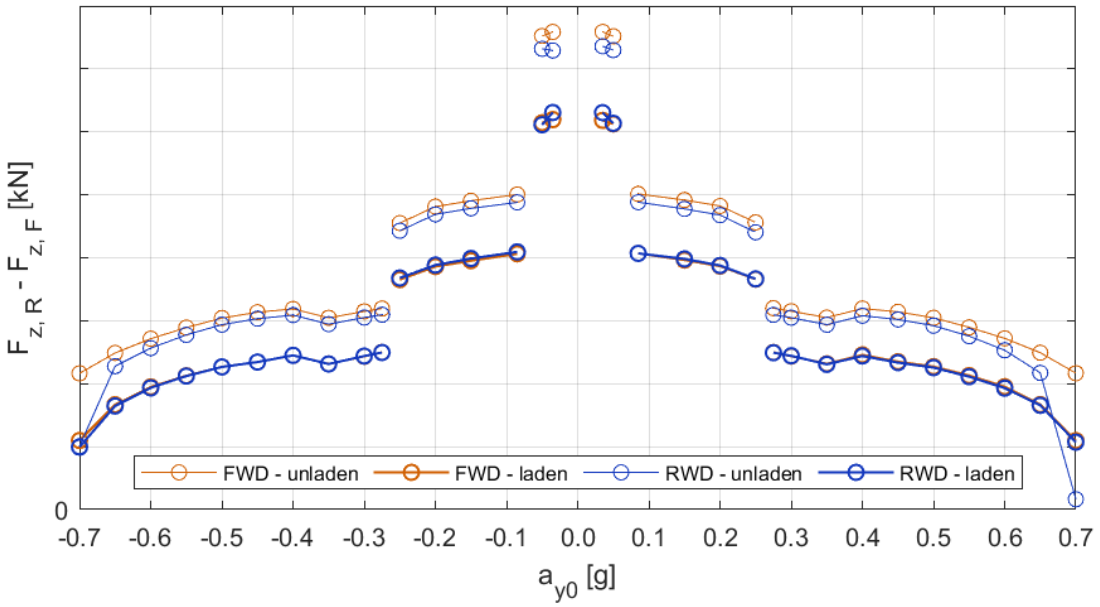

Figure 7.35: Throttle-On In-Turn - Throttle @ 50% - long. transfer vs in. lat. acc. @ t_1.

Figures 7.36 and 7.37 show the slip achieved on the drivetrain as a function of the initial lateral acceleration, at time instant t_1. As in Power-Off Cornering, the outer wheel is never subject to slippage. Concerning the inner wheel, the critical condition is represented by the unladen RWD, which achieves a remarkable slip at great lateral accelerations, without reaching saturation. A right turn is more stressful, because the reaction torque loads more the left wheel during an acceleration maneuver, leaving the right one less loaded and more prone to slip. The anomalous increase in the engine rotational speed is a direct consequence of this phenomenon.

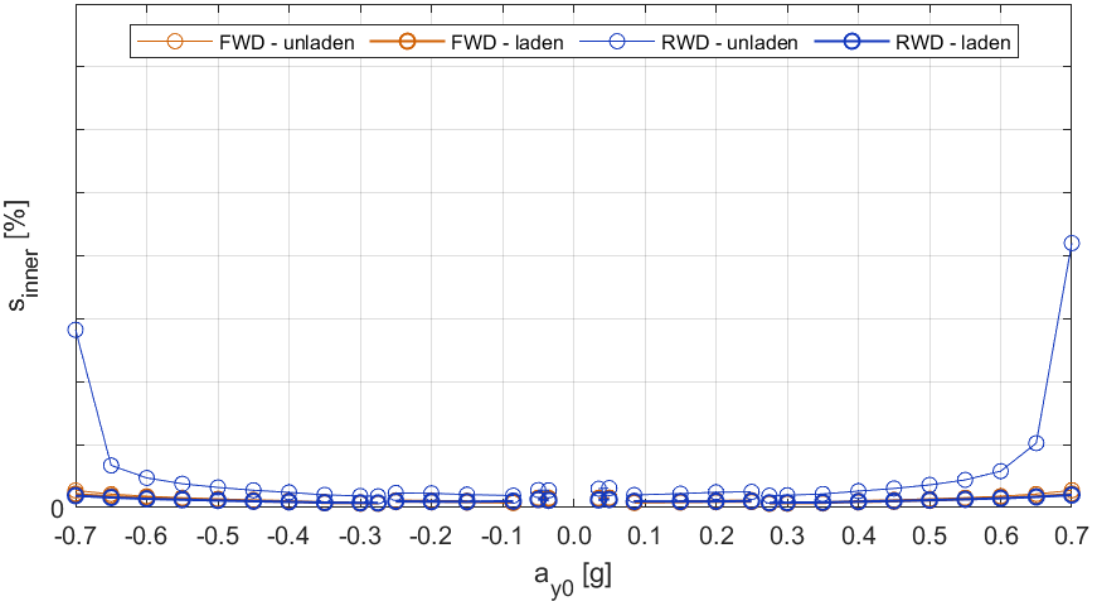

Figure 7.36: Throttle-On In-Turn - Throttle @ 50% - inner slip vs in. lat. acc. @ t_1.

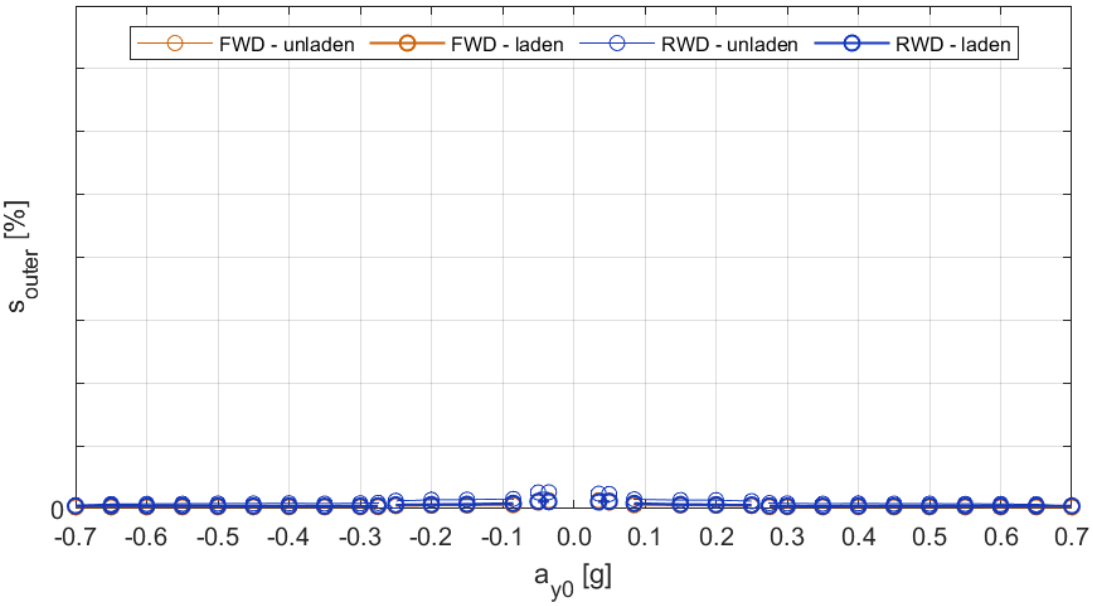

Figure 7.37: Throttle-On In-Turn - Throttle @ 50% - outer slip vs in. lat. acc. @ t_1.

Figures from 7.38 to 7.41 report the slip angle achieved on each wheel as function of the initial lateral acceleration at time instant t_1. Overall, FWD and RWD show similar results, the latter tending to slightly greater angles when approaching the limit. Obviously, the front inner wheel shows the greatest slip angle, due to its steering angle. Similarly, on the rear axle the inner wheel has a slightly greater slip angle, due to its lower turning radius with respect to the outer wheel.

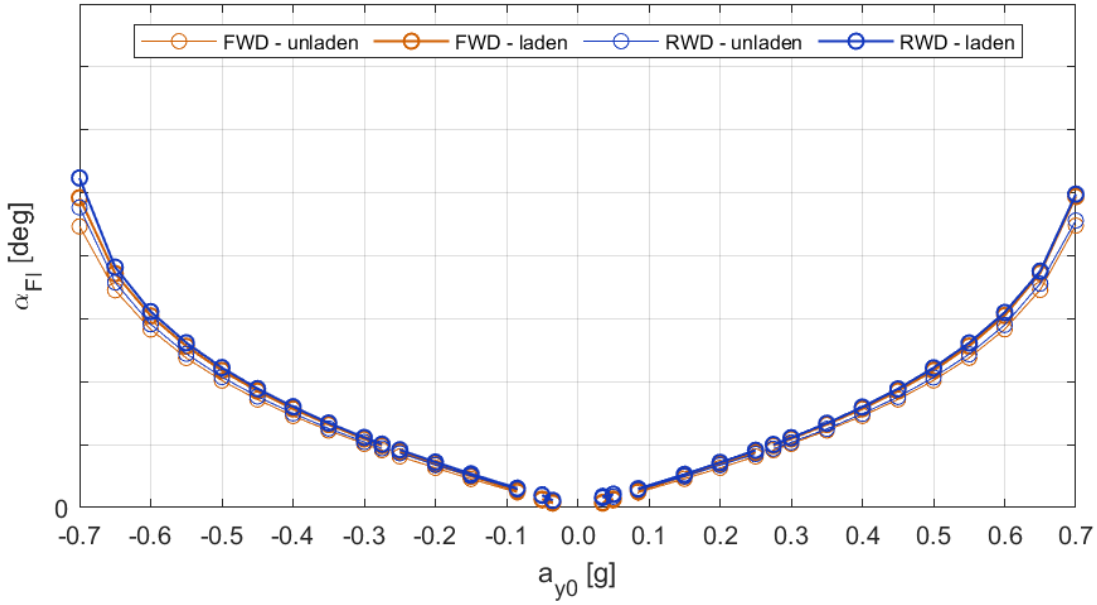

Figure 7.38: Throttle-On In-Turn - Throttle @ 50% - fr. in. slip angle vs in. lat. acc. @ t_1.

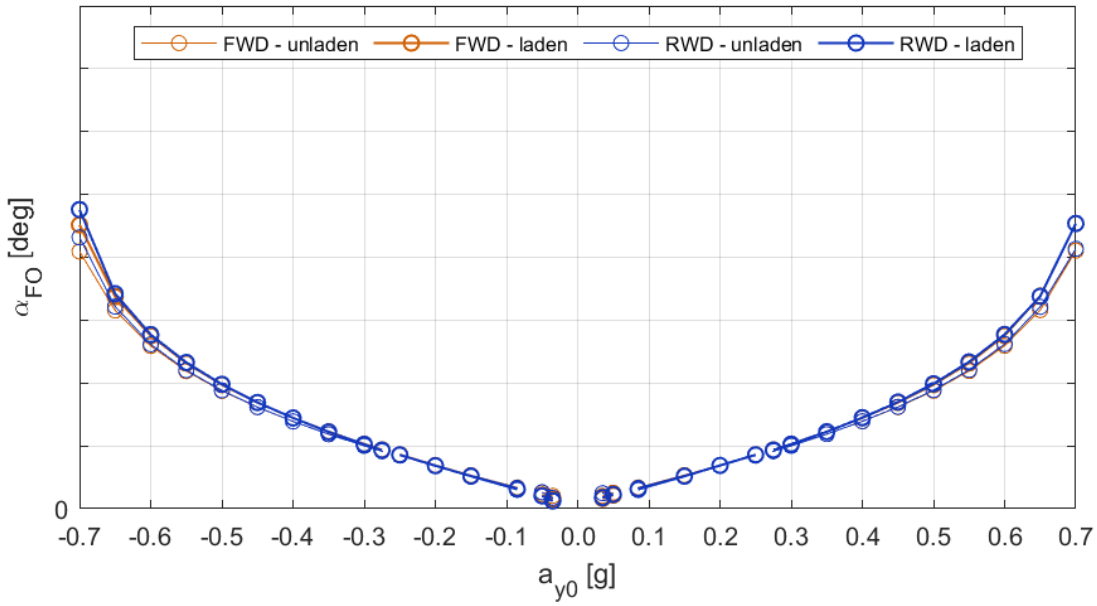

Figure 7.39: Throttle-On In-Turn - Throttle @ 50% - fr. out. slip angle vs in. lat. acc. @ t_1.

With respect to Power-Off Cornering, no critical phenomena are taking place, provided the smoother nature of this maneuver. FWD provides symmetric results, while RWD shows slightly greater slip angles on the front axle when turning to the left.

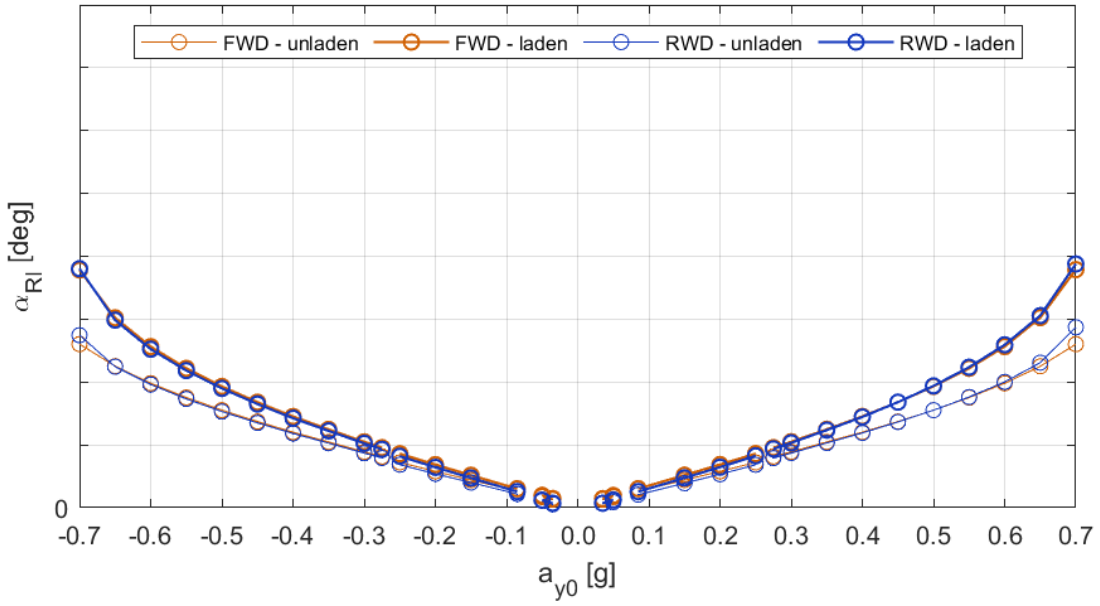

Figure 7.40: Throttle-On In-Turn - Throttle @ 50% - rr. in. slip angle vs in. lat. acc. @ t_1.

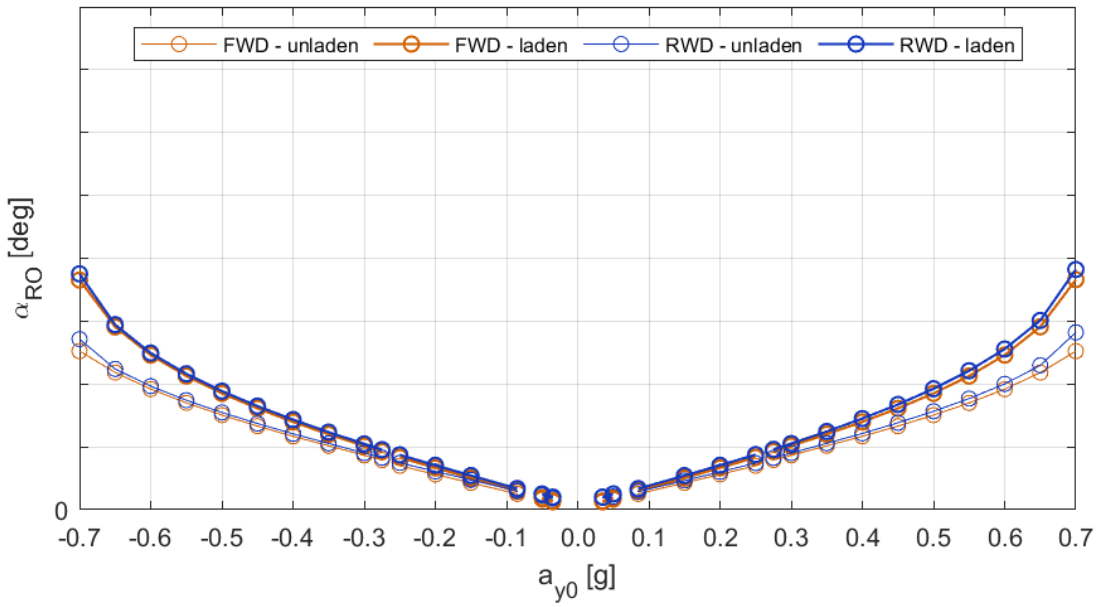

Figure 7.41: Throttle-On In-Turn - Throttle @ 50% - rr. out. slip angle vs in. lat. acc. @ t_1.

Figure 7.42 shows the handling characteristic, defined as the difference between the average front and rear slip angles as function of the initial lateral acceleration, at time t_1. Overall, the unladen configuration displays a more understeering response, meaning that it is more sensitive to an increase in its path radius. With respect to Power-Off Cornering, FWD and RWD show closer responses and it is not possible to make univocal statements. Actually, RWD seems slightly more understeering when turning to the left, while less understeering during a right turn. The reaction torque being a discriminant confirms how the two versions behave closely.

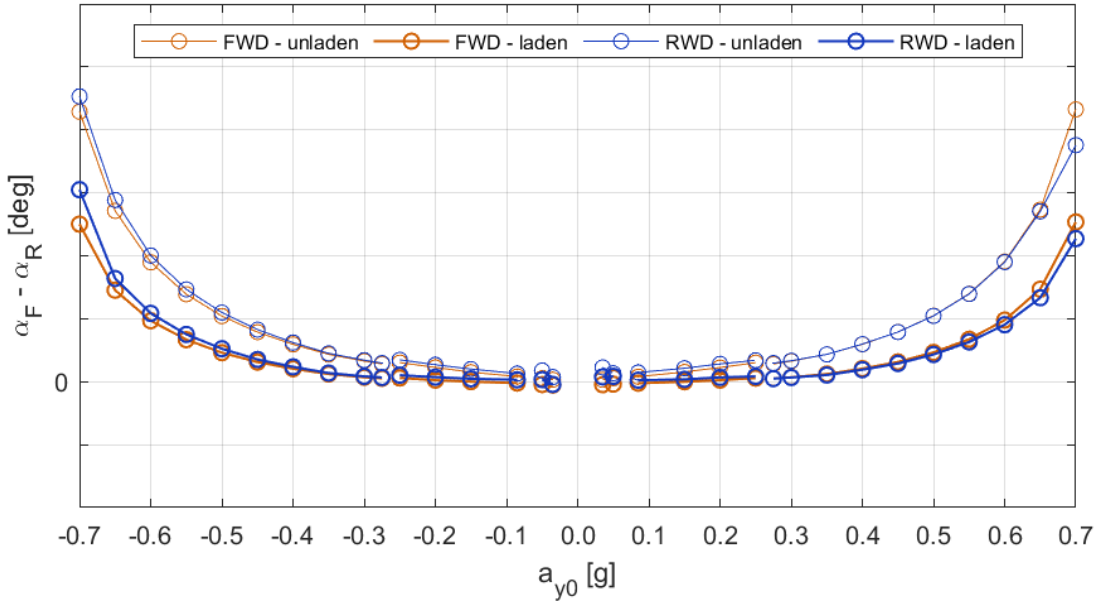

Figure 7.42: Throttle-On In-Turn - Throttle @ 50% - understeer gradient vs in. lat. acc. @ t_1.

7.1.4 Steering System

Figures from 7.43 to 7.51 show the steering wheel torque, front wheels total self-aligning moment and steering rack stroke time histories. According to the sign conventions used in Adams/Car, a negative steering wheel torque is directed counterclockwise from the driver's viewpoint, thus coherent with a left turn. Instead, the self-aligning moment is negative when directed clockwise, thus effectively providing an aligning action during a left turn. Finally, the steering rack stroke is measured as the travel with respect to the neutral position.

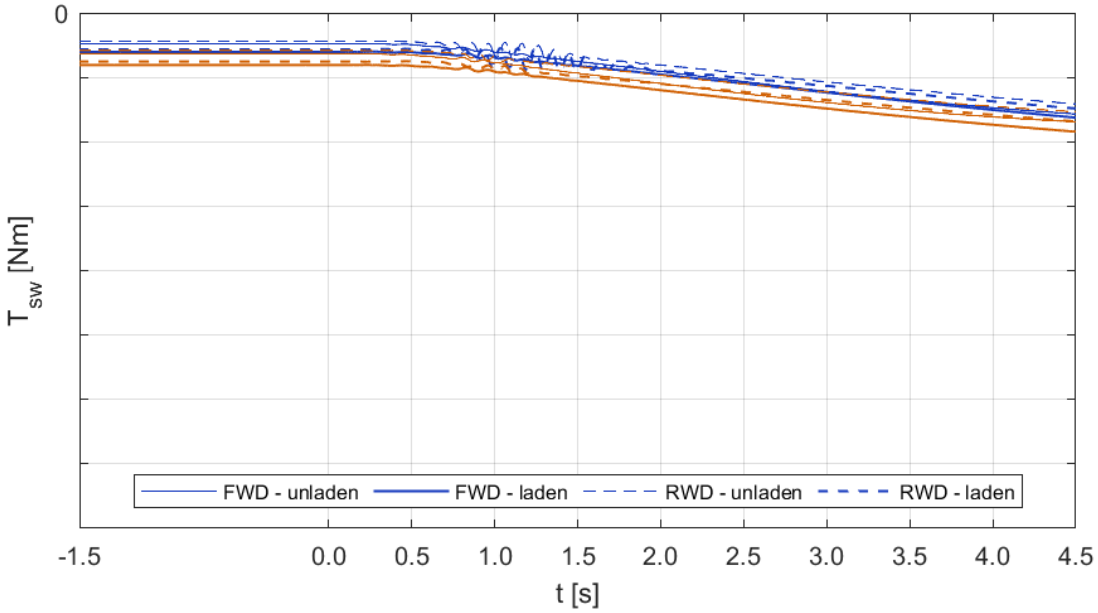

Figure 7.43: Throttle-On In-Turn - Throttle @ 50% - 2nd Gear - steering wheel torque vs time.

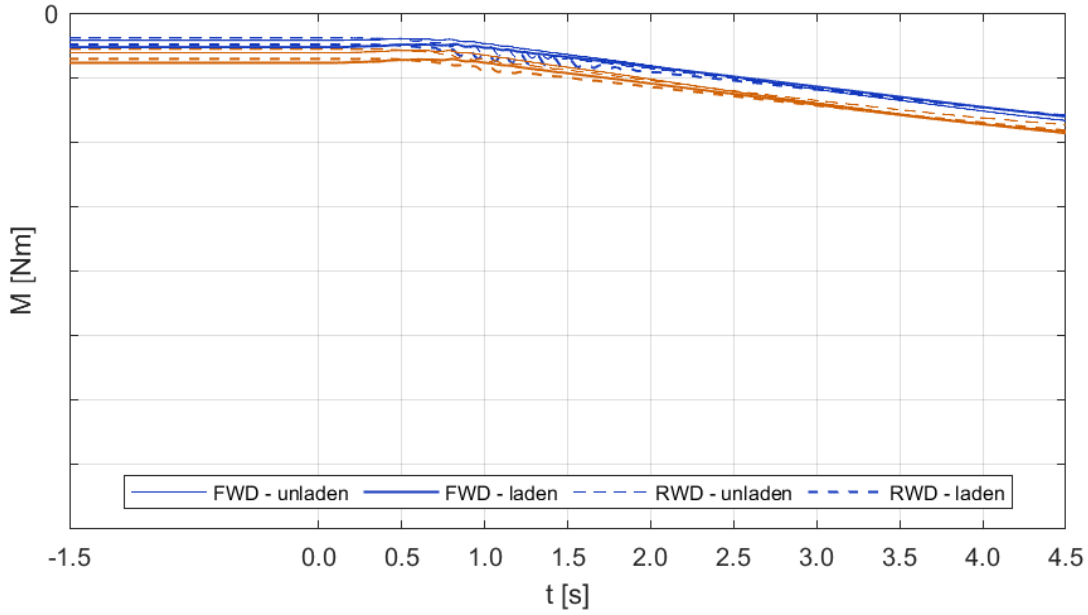

Figure 7.44: Throttle-On In-Turn - Throttle @ 50% - 2nd Gear - self-aligning moment vs time.

As already seen in Power-Off Cornering, during the steady-state maneuver, FWD is slightly more understeering than RWD, as confirmed by these three quantities. In 2nd gear, RWD

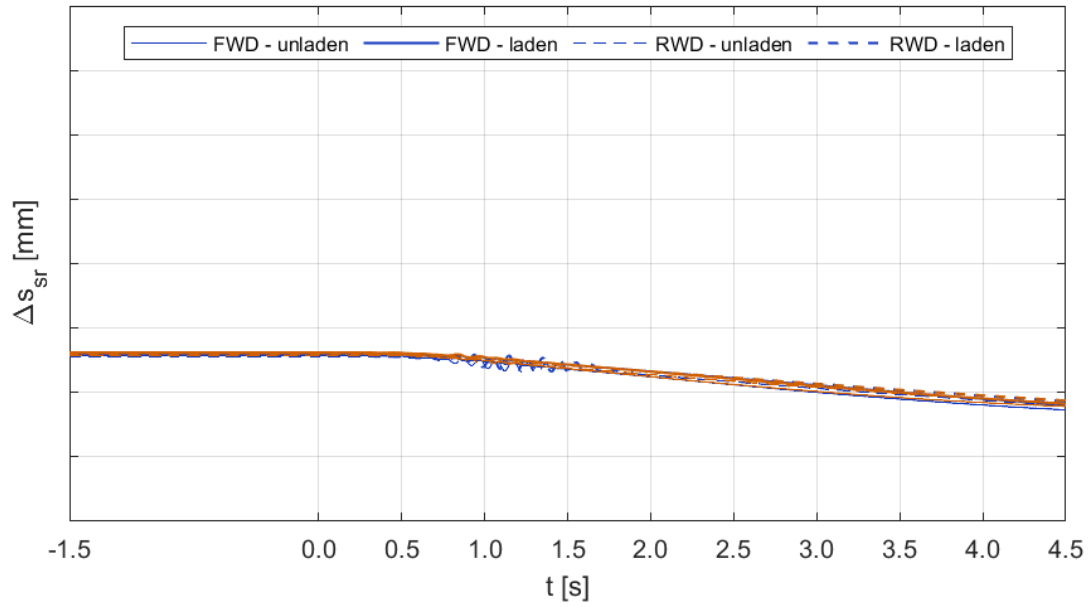

Figure 7.45: Throttle-On In-Turn - Throttle @ 50% - 2nd Gear - rack stroke vs time.

experiences some vibrations through the entire steering system, corresponding to the ones seen in the vehicle dynamics. Provided the reduced lateral accelerations here involved, there are no remarkable differences concerning the loading condition and the drivetrain.

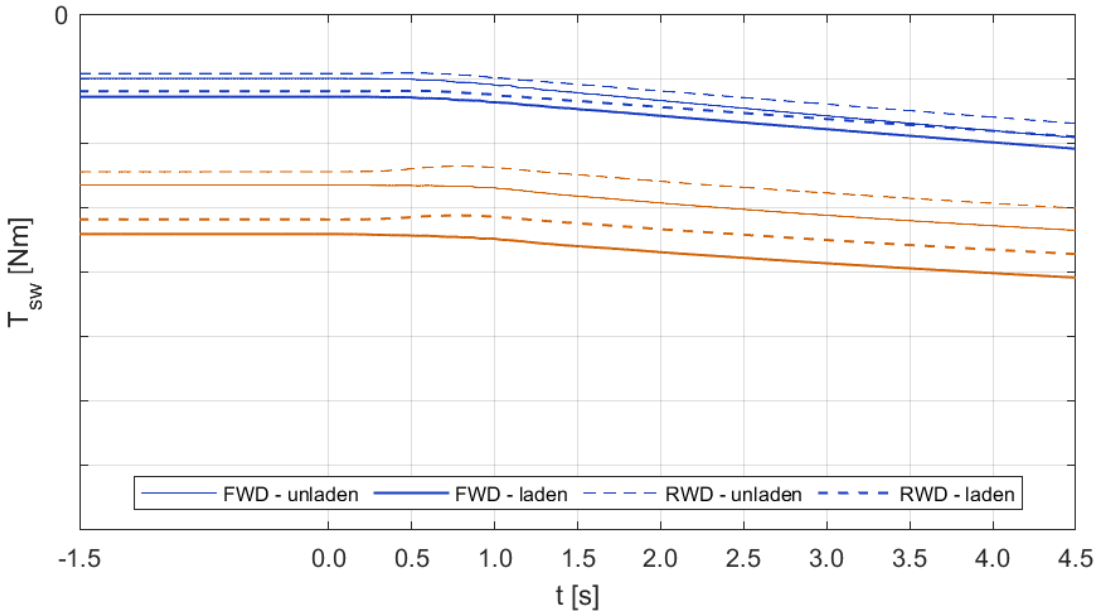

Figure 7.46: Throttle-On In-Turn - Throttle @ 50% - 3rd Gear - steering wheel torque vs time.

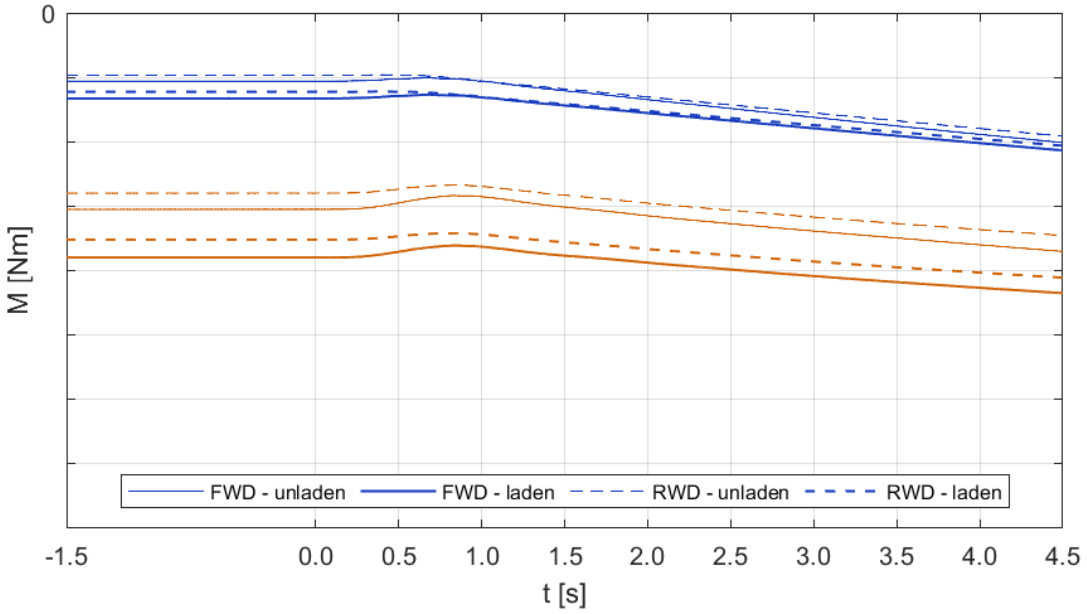

Figure 7.47: Throttle-On In-Turn - Throttle @ 50% - 3rd Gear - self-aligning moment vs time.

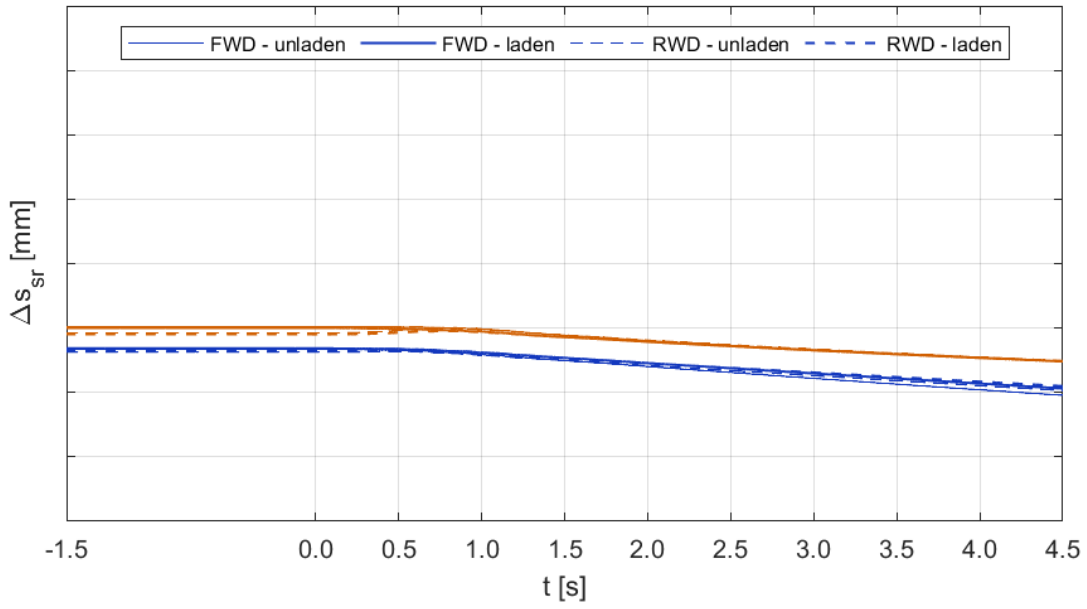

Figure 7.48: Throttle-On In-Turn - Throttle @ 50% - 3rd Gear - rack stroke vs time.

Instead, in 3rd gear some slightly different responses are achieved. The laden configuration requires a greater steering wheel torque, necessary to balance the increased self-aligning moment. The differences between FWD and RWD are less appreciable with respect to Power-Off Cornering, but it is possible to notice that FWD experiences a temporary reduction in the wheels self-aligning moment during the acceleration step. Yet, there are no interesting differences in the steering rack stroke.

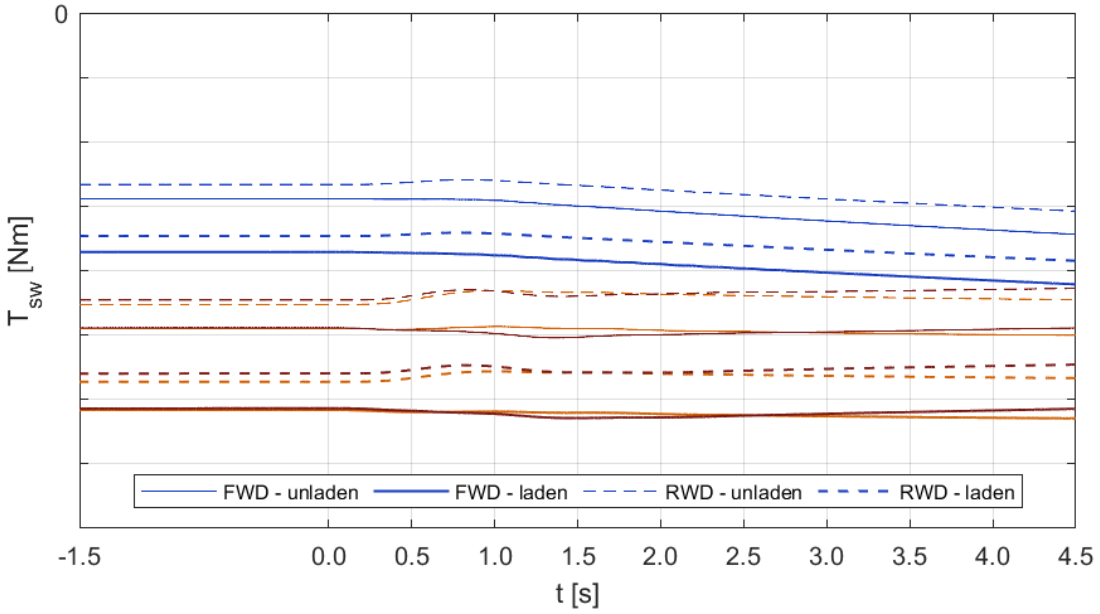

Figure 7.49: Throttle-On In-Turn - Throttle @ 50% - 4th Gear - steering wheel torque vs time.

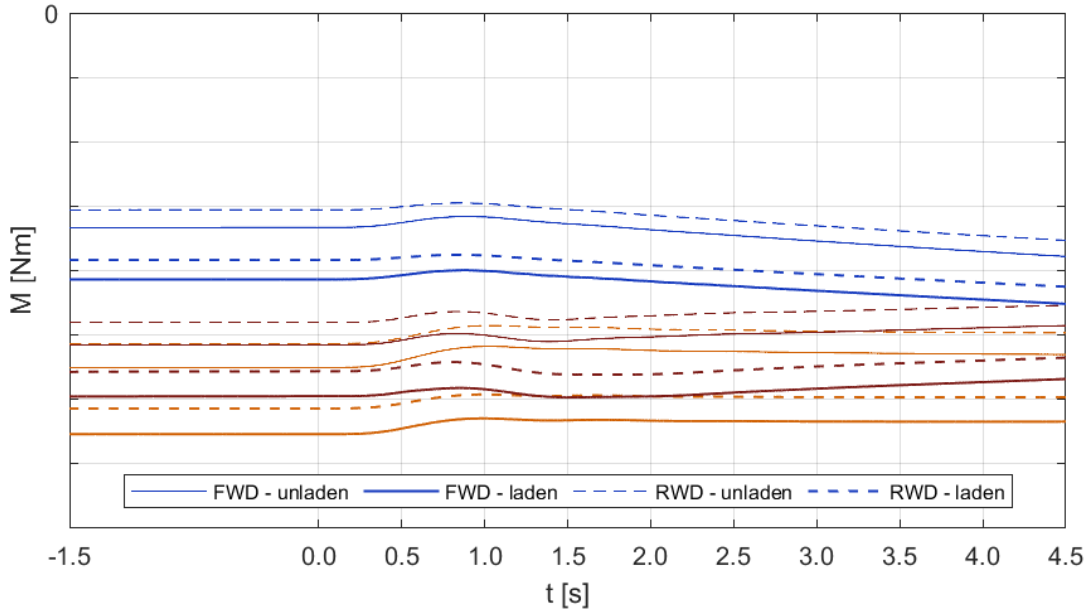

Figure 7.50: Throttle-On In-Turn - Throttle @ 50% - 4th Gear - self-aligning moment vs time.

In 4th gear, FWD confirms a more understeering response, along with a slightly different trend in the steering wheel torque. While RWD displays a little temporary decrease, FWD keeps it almost constant. Concerning the self-aligning moment, FWD manifests the slight decrease previously seen, but at higher lateral accelerations RWD behaves similarly. Interestingly, the maneuvers at 0.55g and 0.65g both show close steering wheel torques, but a reduction in the wheels self-aligning moment when the vehicle approaches its limit. In terms of rack stroke, FWD and RWD tend to homogenize their trends after the transient. Therefore, the maneuver induces almost identical steer angles on the wheels, but on FWD the self-aligning moment generated by the tyres is slightly greater and leads to an increased steering wheel torque.

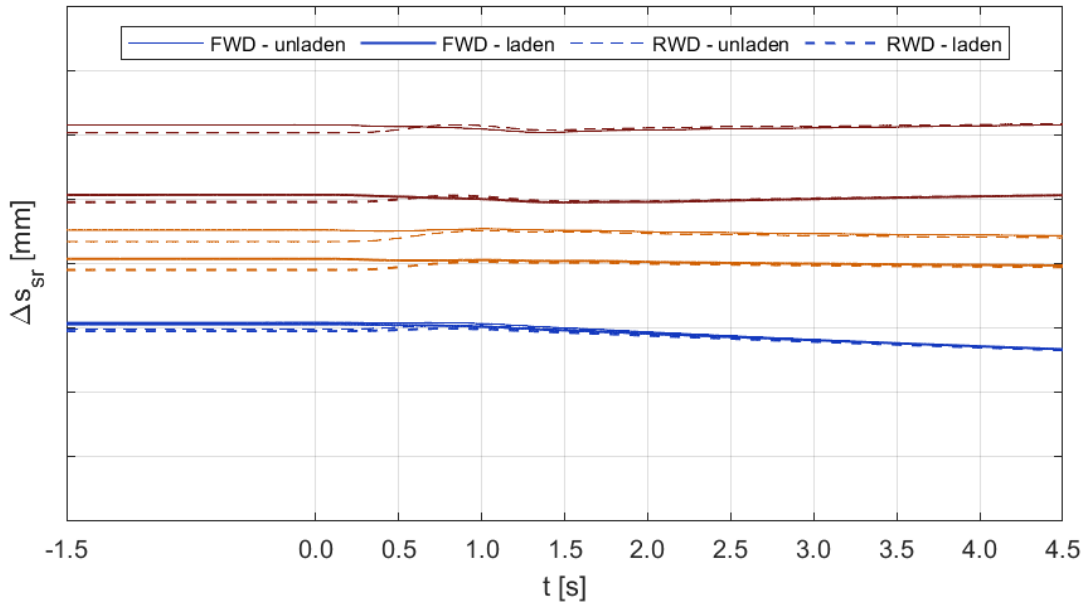

Figure 7.51: Throttle-On In-Turn - Throttle @ 50% - 4th Gear - rack stroke vs time.

7.1.5 Functions of Initial Lateral Acceleration

A few functions of initial lateral acceleration are reported, to highlight the differences occurring during the transient. The two reference time instants are t_1 and t_2, respectively 1.0s and 2.0s after the beginning of the acceleration maneuver. Specifically, t_1 coincides with the accelerator reaching its final value, while t_2 should be a time sufficient to settle to the new steady-state.

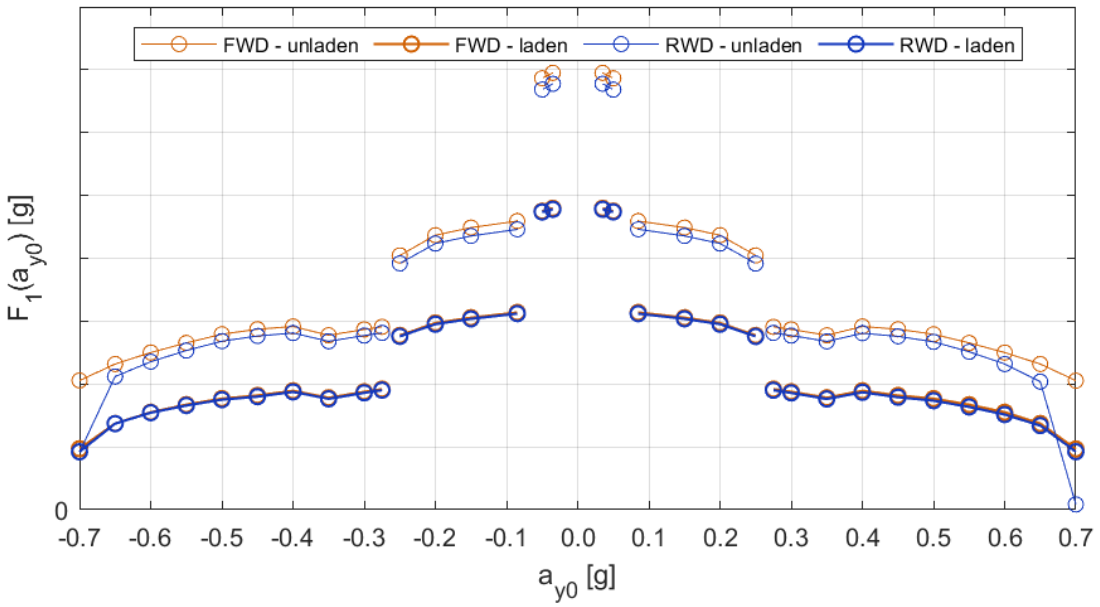

Figure 7.52: Throttle-On In-Turn - Throttle @ 50% - F_1 vs in. lat. acc.

Equation 7.1 defines the mean longitudinal acceleration in the time range of interest for the test, hence 2.0s starting from the throttle-on instant. It is shown in *Figure 7.52*.

$$f_1(a_{y0}) = a_{x,t_2} = -\frac{V_{x,t_0} - V_{x,t_2}}{t_2 - t_0} \tag{7.1}$$

This function basically reports the same information provided by the longitudinal load transfer. The unladen FWD expresses a slightly greater acceleration, while both versions behave similarly in the laden configuration. As previously seen, the unladen RWD leads the inner driving wheel to partial slippage at 0.7g, reducing its ability to accelerate. *Equation 7.2* defines the ratio between yaw velocity and reference yaw velocity, defined as the yaw velocity the vehicle would have if it maintained the initial path radius with its actual velocity, both at time t_2. It is shown in *Figure 7.53*.

$$f_2(a_{y0}) = \frac{\dot{\Psi}_{t_2}}{\dot{\Psi}_{ref,t_2}} \qquad \dot{\Psi}_{ref,t_2} = \frac{V_{x,t_2}}{R_0} \tag{7.2}$$

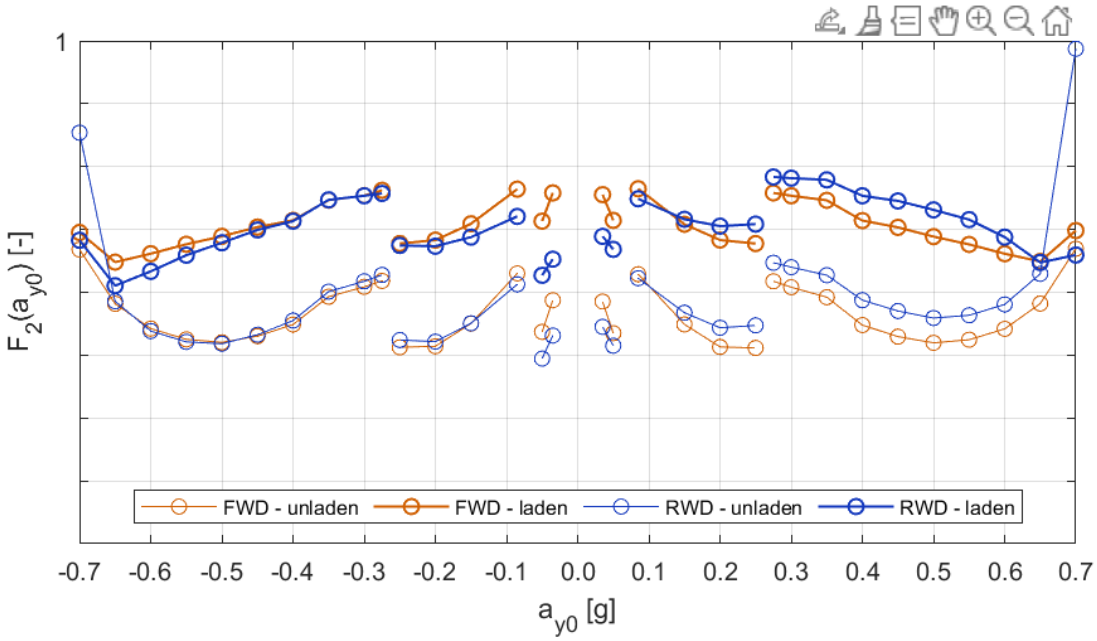

Figure 7.53: Throttle-On In-Turn - Throttle @ 50% - F_2 vs in. lat. acc. @ t_2.

Clearly, an acceleration maneuver makes the vehicle trajectory wider, but the variation is not as noticeable as in Power-Off Cornering, which is a sharper maneuver. Obviously, the unladen van has a more understeering response, meaning that it is more subject to a widening in its trajectory. RWD provides asymmetric responses for left and right turns. Particularly, when turning to the right, the outer wheel is more loaded by the reaction torque, making the vehicle more resistant to an increase in the path radius in both loading conditions. The limit case is reached at 0.7g, where the vehicle is keeping its initial trajectory due to the slip on the inner wheel. Instead, during a left turn, FWD and RWD generally show comparable results, the latter still being subject to tyre slip at 0.7g resulting in a partial insensitivity to a trajectory widening. Another interesting result is the behaviour in 2nd gear, which is similar for all vehicles. FWD is less prone to an understeering response, meaning that is is more likely to maintain the initial trajectory.

Equation 7.3 defines the ratio between maximum yaw velocity and reference yaw velocity at the time instant corresponding to the maximum yaw velocity. It is shown in *Figure 7.54*.

$$f_3(a_{y0}) = \frac{\dot{\Psi}_{max}}{\dot{\Psi}_{ref,t_{max}}} \tag{7.3}$$

This function provides two qualitatively different results. In the field of low and middle lateral accelerations, the vehicle is increasing its yaw velocity right after the acceleration maneuver, therefore its path radius is far from the reference and leads to a lower ratio. Instead, at higher lateral accelerations, the yaw velocity is kept constant or eventually decreased. For this reason, the maximum value is at the beginning of the maneuver and close to the reference. The unladen configuration looks more sensitive in the first case, with FWD showing a lower ratio in the field of 2nd and 3rd gears, meaning that it is increasing its final yaw velocity more than RWD, confirming its slightly more understeering tendency at moderate lateral accelerations. *Equation 7.4* defines the difference between yaw velocity and reference yaw velocity, both evaluated at time t_2. It is shown in *Figure 7.55*.

$$f_4(a_{y0}) = \dot{\Psi}_{t_2} - \dot{\Psi}_{ref,t_2} \tag{7.4}$$

Equation 7.5 defines the maximum difference between yaw rate and reference yaw rate through the time range of the test. It is shown in *Figure 7.56*.

$$f_5(a_{y0}) = \Delta\dot{\Psi}_{max} = (\dot{\Psi}_t - \dot{\Psi}_{ref,t})_{max} \tag{7.5}$$

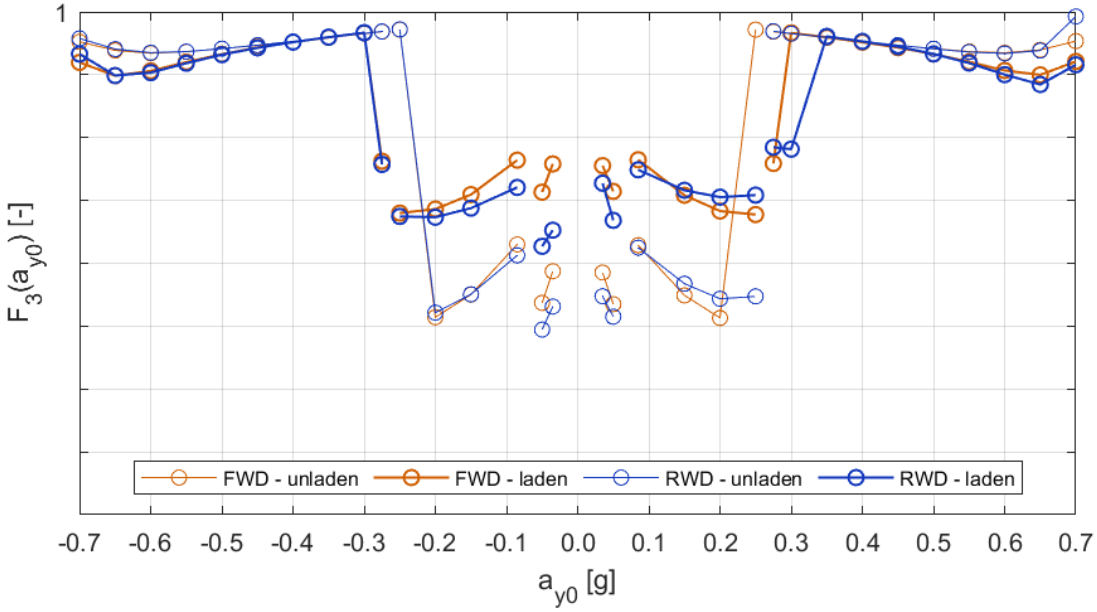

Figure 7.54: Throttle-On In-Turn - Throttle @ 50% - F_3 vs in. lat. acc.

Both functions are qualitatively similar to f_2 and f_3 respectively, as they communicate the same information in terms of differences, instead of ratios. *Equation 7.6* defines the instantaneous yaw acceleration, 1.0s after the throttle-on instant. It is shown in *Figure 7.57*.

$$f_6(a_{y0}) = \ddot{\Psi}_{t=1.0s} = \left(\frac{d\dot{\Psi}}{dt}\right)_{t=1.0s} \tag{7.6}$$

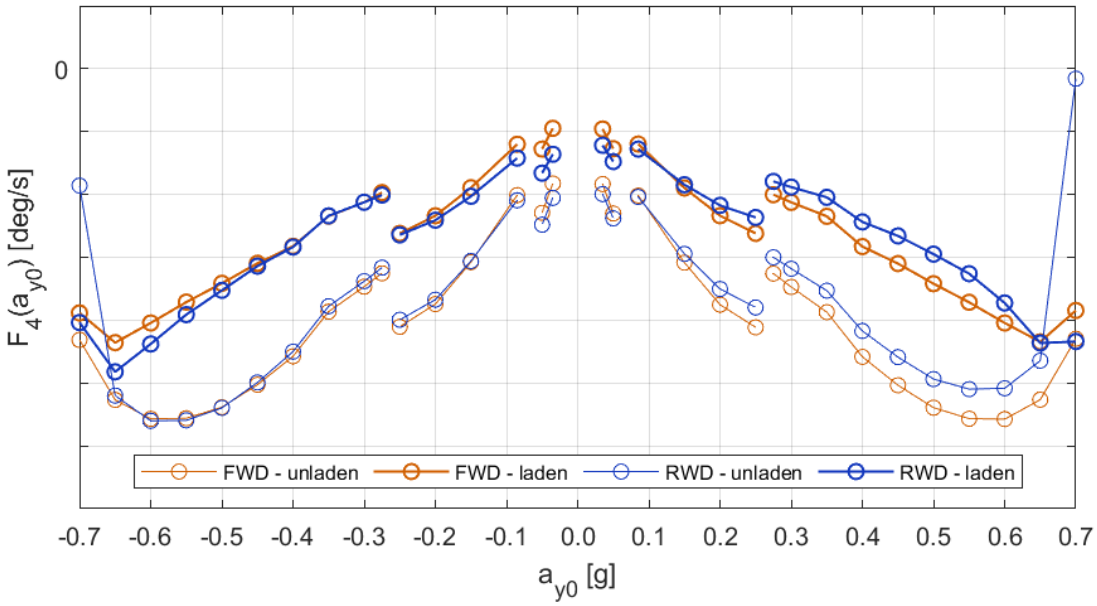

Figure 7.55: Throttle-On In-Turn - Throttle @ 50% - F_4 vs vs in. lat. acc. @ t_2.

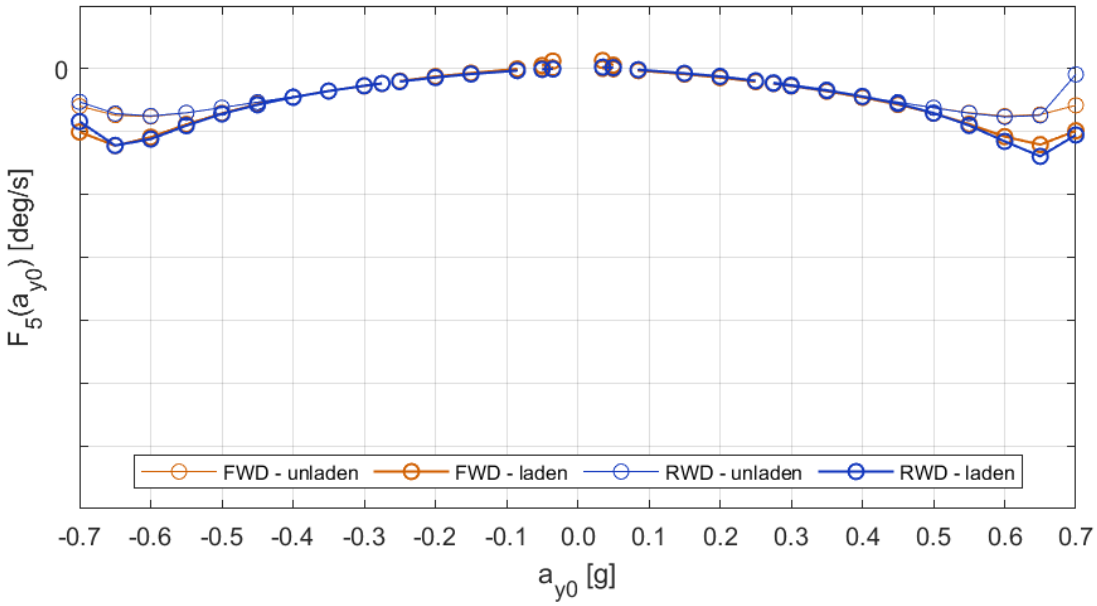

Figure 7.56: Throttle-On In-Turn - Throttle @ 50% - F_5 vs in. lat. acc.

Similarly to Power-Off Cornering, the yaw acceleration looks almost null in the field of 3rd and 4th gears, due to the low slope of the yaw velocity. The main exception is represented by RWD, which displays some vibrations here reflected by a chaotic response in 2nd gear. Instead, close to the limit there is a sign inversion between unladen and laden configurations, as in the previous test, as the laden configuration takes a longer time to extinguish the transient. Function f_7 represents the ratio between ideal and actual curvature radii. Its definition is given by *Equation 7.7*.

$$f_7(a_{y0}) = \frac{a_{y,t_2}}{a_{y,ref,t_2}} = \frac{R_0}{R_{t_2}} \qquad a_{y,ref,t_2} = \frac{V_{x,t_2}^2}{R_0} \tag{7.7}$$

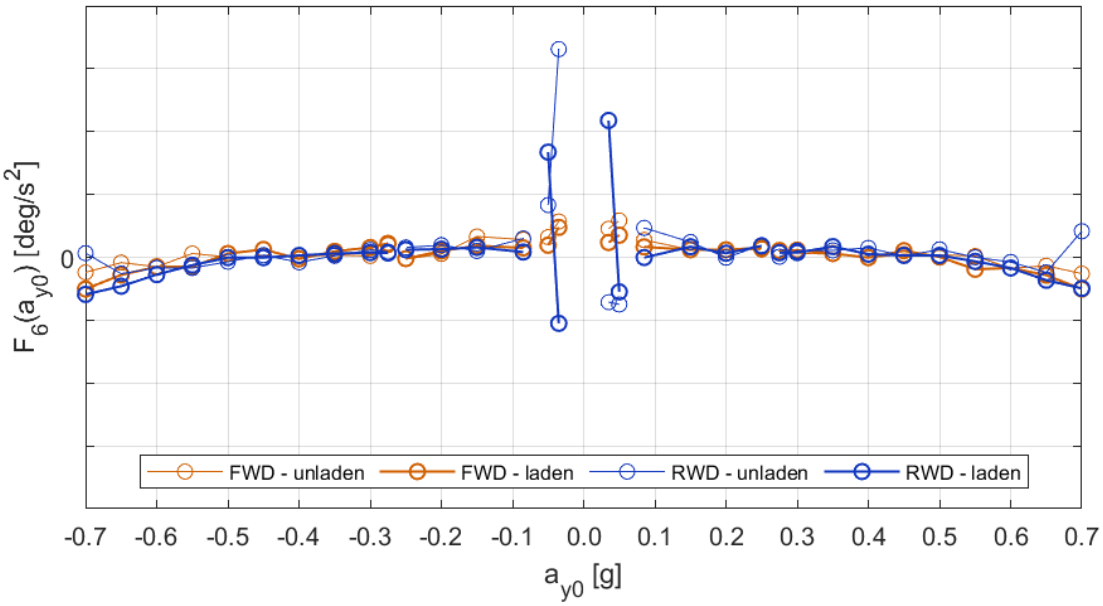

Figure 7.57: Throttle-On In-Turn - Throttle @ 50% - F_6 vs in. lat. acc. @ t_1.

The meaning of this function is similar to f_2. The main differences with the latter take place in 2nd and 3rd gears. Both FWD and RWD provide some asymmetric responses, the former confirming the more understeering response in 2nd gear. *Equation 7.8* defines the maximum absolute value of sideslip angle and the corresponding time instant at which it is achieved. These twin functions are evaluated in the time range from t_0 to t_2 as usual and are shown in *Figures 7.59 and 7.60*.

$$f_{8-1}(a_{y0}) = |\beta_{max}| \qquad f_{8-2}(a_{y0}) = t_{\beta_{max}} \tag{7.8}$$

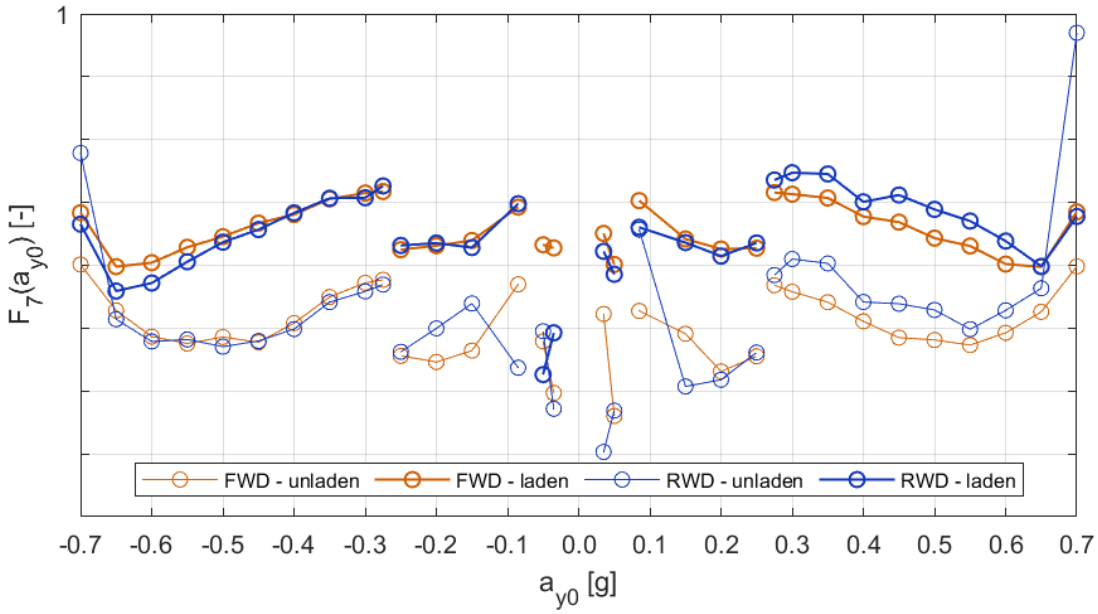

Figure 7.58: Throttle-On In-Turn - Throttle @ 50% - F_7 vs in. lat. acc. @ t_2.

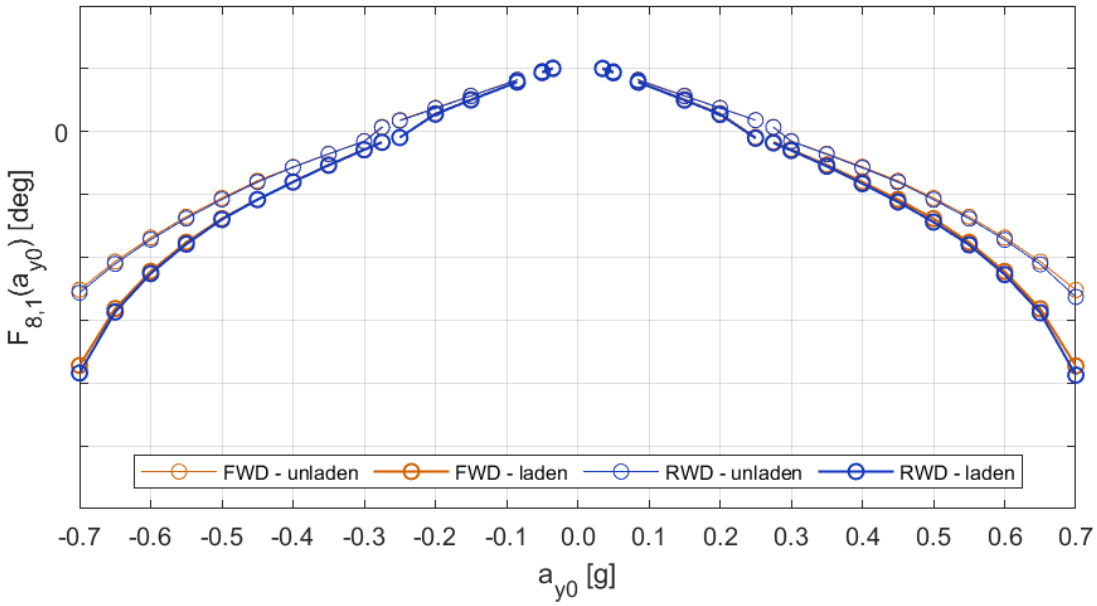

Figure 7.59: Throttle-On In-Turn - Throttle @ 50% - $F_{8,1}$ vs in. lat. acc.

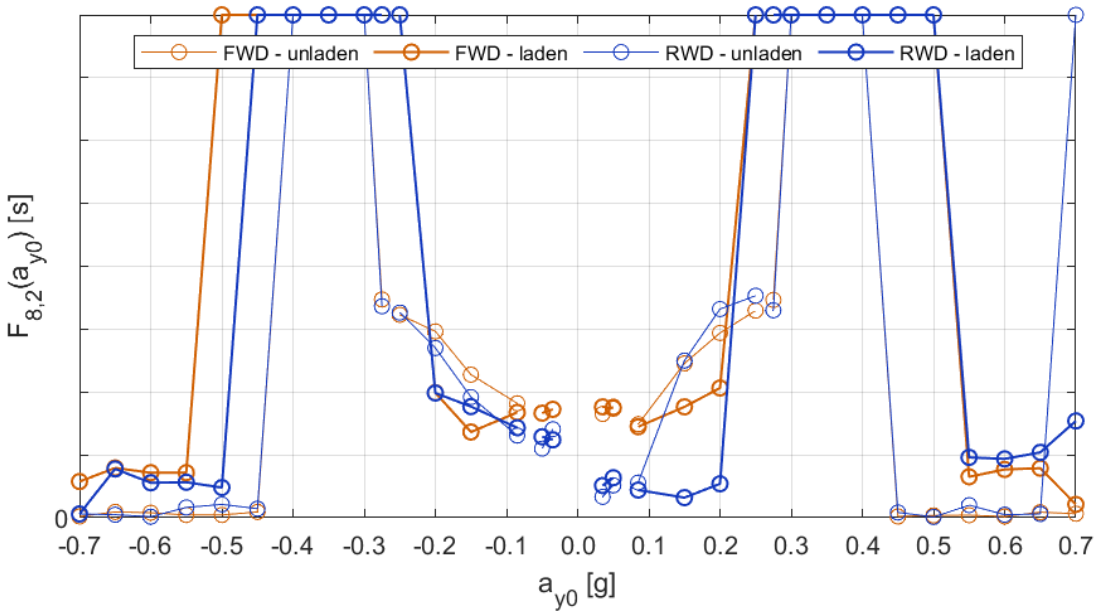

Figure 7.60: Throttle-On In-Turn - Throttle @ 50% - $F_{8,2}$ vs in. lat. acc.

The former function shows almost identical responses between FWD and RWD in both loading conditions. Clearly, the acceleration maneuver leads to an increase in longitudinal velocity, which makes the vehicle settle to a more "nose-in" configuration. With respect to the previous test, there are no critical responses in terms of sideslip angle, confirming that this maneuver is overall less demanding from the point of view of the vehicle stability. The latter function resumes the presence of a transient in the sideslip angle. At low lateral accelerations, the maximum absolute value of the angle is achieved close to the beginning of the maneuver, because it later decreases and tends to a neutral position. Instead, in the middle field, the maximum is achieved at t_2 because the vehicle moves from a neutral to a "nose-in" configuration, thus to a greater angle in absolute value.

Finally, at high lateral accelerations, the angle temporarily decreases, meaning that the vehicle tries to restore the neutral position, thus making the maximum close to the beginning of the acceleration maneuver. Overall, FWD and RWD react similarly, while the unladen condition generally shows a greater variance.

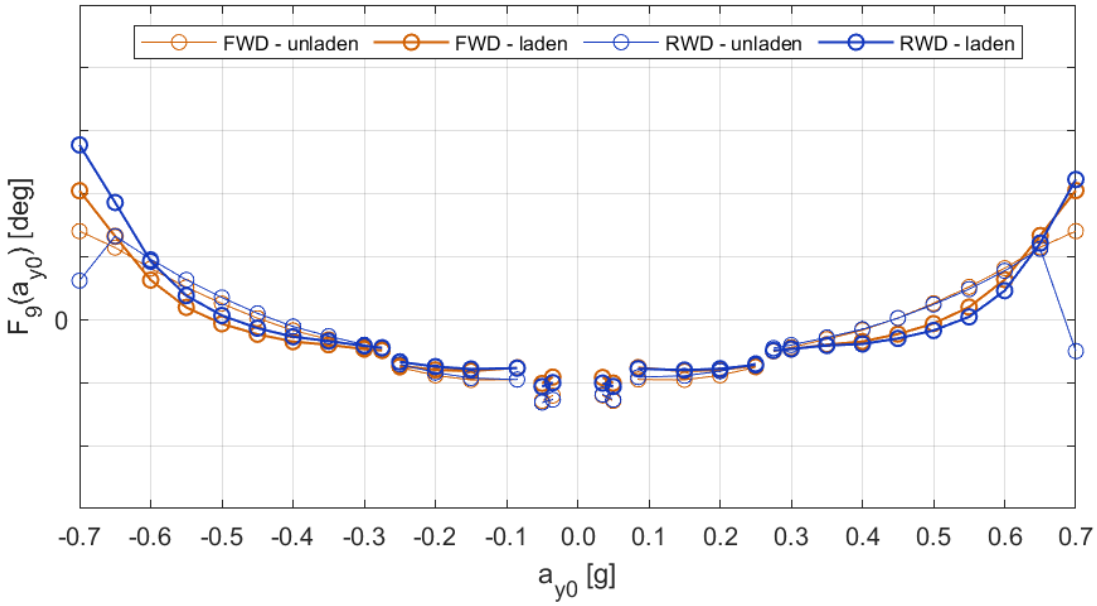

Figure 7.61: Throttle-On In-Turn - Throttle @ 50% - F_9 vs in. lat. acc. @ t_2.

Equation 7.9 defines the difference between sideslip angle 2.0s after the power-off instant and initial steady-state sideslip angle. It is shown in *Figure 7.61*.

$$f_9(a_{y0}) = \beta_{t_2} - \beta_0 \tag{7.9}$$

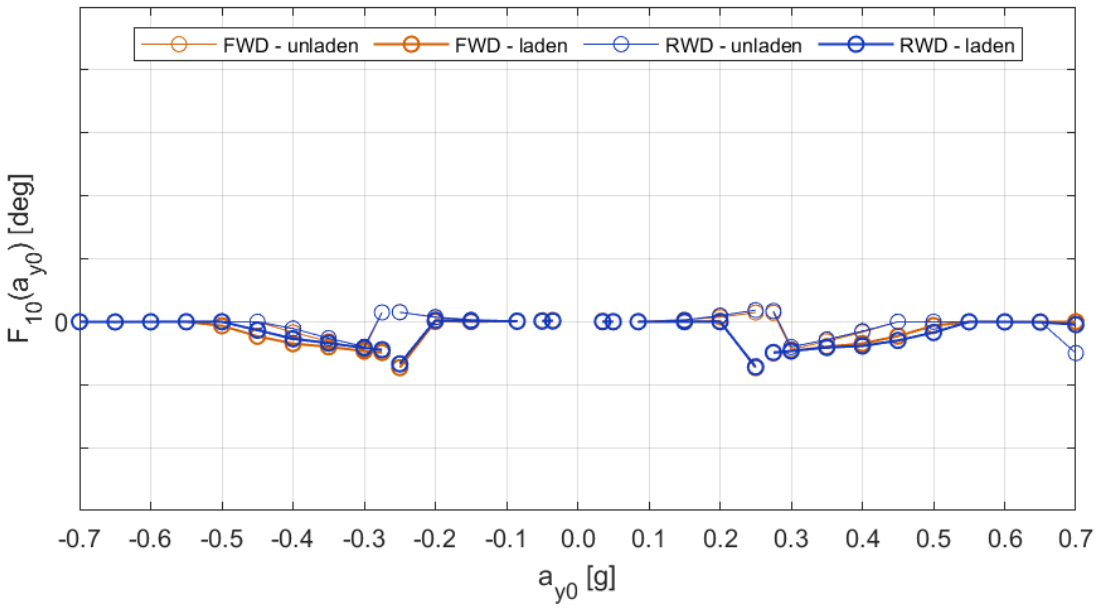

Figure 7.62: Throttle-On In-Turn - Throttle @ 50% - F_{10} vs in. lat. acc.

Equation 7.10 defines the difference between maximum sideslip angle and initial steady-state sideslip angle. It is shown in *Figure 7.62*.

$$f_{10}(a_{y0}) = \beta_{max} - \beta_0 \tag{7.10}$$

The former function effectively highlights the presence of a transient at greater lateral accelerations, while it generally assumes moderate values, meaning that the sideslip angle is slowly changing during the maneuver. Function f_{10} confirms that the acceleration usually makes the vehicle get far from its initial configuration and tend towards a neutral condition, apart from the middle field, where it is moving from neutral to "nose-in".

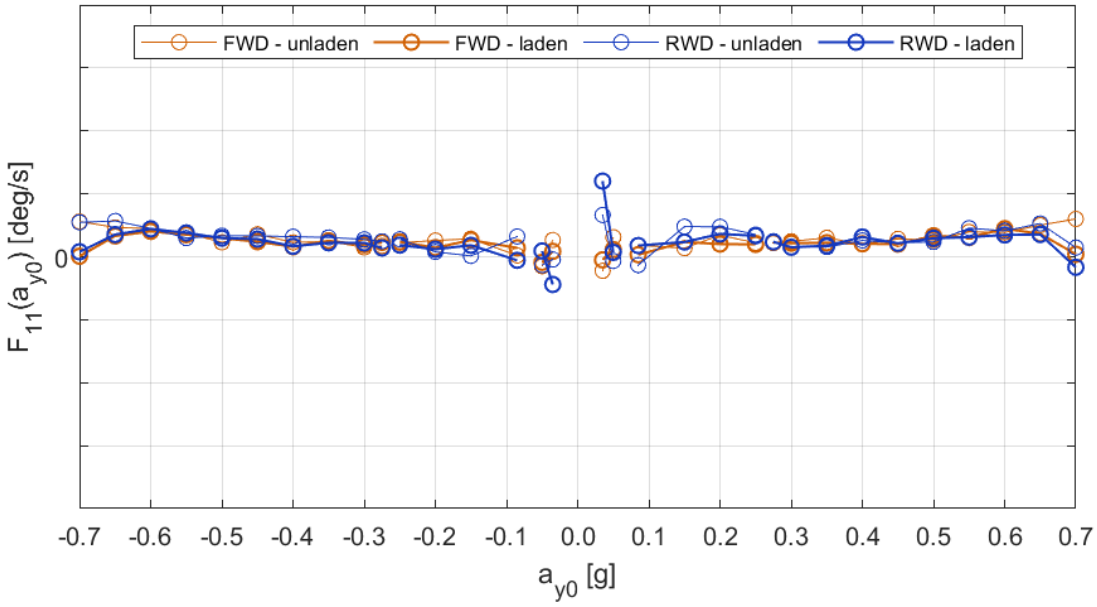

Figure 7.63: Throttle-On In-Turn - Throttle @ 50% - F_{11} vs in. lat. acc. @ t_2.

Equation 7.11 defines the difference between yaw velocity and calculated yaw velocity, both 2.0s after the throttle-on instant. It is shown in *Figure 7.63*.

$$f_{11}(a_{y0}) = \dot{\beta}'_{t_2} = \dot{\Psi}_{t_2} - \frac{a_{y,t_2}}{V_{x,t_2}} \tag{7.11}$$

This function represents the sideslip angle velocity uncorrected for the effects of the sideslip angle itself and the deceleration. It gains relevance in 2nd gear, where RWD feels some oscillatory phenomena, while it generally shows values that are one order of magnitude smaller than the absolute value of yaw velocity. The slower nature of this maneuver makes the yaw sensitivity less critical with respect to Power-Off Cornering. *Equation 7.12* defines the percentage deviation as the radial distance between vehicle reference point and initial circular path, 2.0s after the throttle-on instant. It is shown in *Figure 7.64*.

$$f_{12}(a_{y0}) = \Delta s_{y,t=2.0s} = \frac{R_0 - R_{t_2}}{R_0} \tag{7.12}$$

As previously stated, the unladen vehicle is more sensitive to a widening trajectory through the entire working range. The discriminant between FWD and RWD is only represented by the reaction torque on the rigid axle of RWD, confirming how the two versions behave closely. The exception is represented by the unladen RWD close to the limit, which experiences some slippage, leading to the inability to open its trajectory.

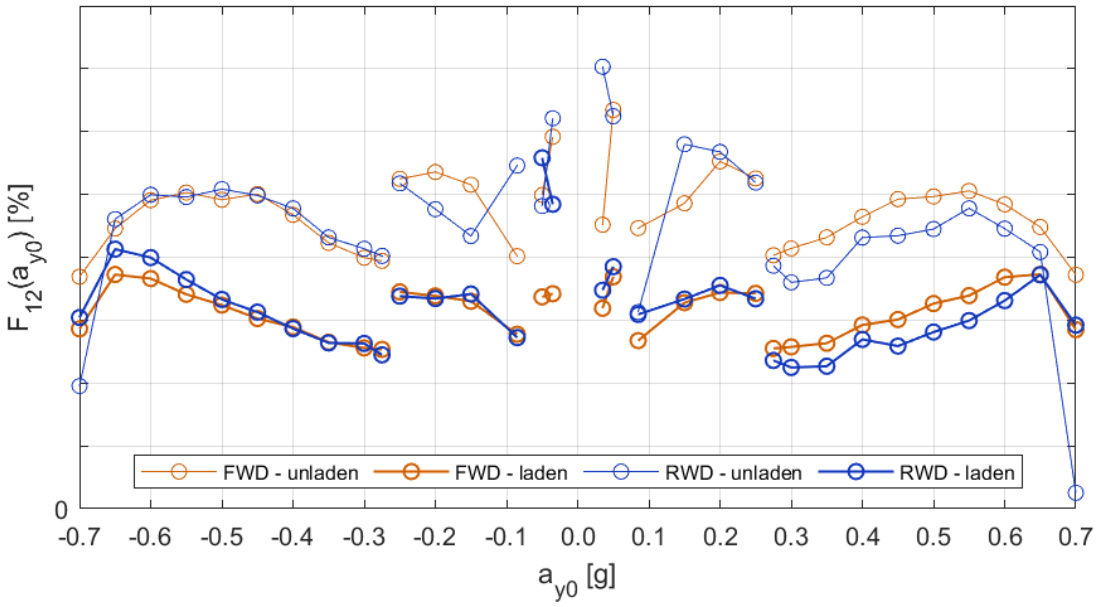

Figure 7.64: Throttle-On In-Turn - Throttle @ 50% - F_{12} vs in. lat. acc. @ t_2.

7.2 Throttle @ 100%

7.2.1 Test Setup

This additional set of Throttle-On In-Turn tests simulates the condition of maximum acceleration, which is achieved pushing the accelerator pedal to its maximum in a time equal to 1.0s. The criterion here adopted is to start with the engine entering its constant torque region (around 1600 rpm), so that the throttle step determines a torque increase not due to the raise in rotational speed, but only because the engine curve is shifting upwards, until the maximum torque is reached. The path radius is not set uniquely to the standard value, instead it is adjusted to the estimates previously adopted in Power-Off Cornering when trying to minimize it. However, in Throttle-On In-Turn these values are not necessarily indicative of maximum cornering forces, because the engine is initially running at a slower speed, meaning that the vehicle has a lower longitudinal velocity and lateral acceleration. The choice of path radii is therefore guided by the corresponding Power-Off Cornering test, not only to have a direct comparison, but also because the previous values represent realistic values for each gear. In other words, a Throttle-On In-Turn test in 4th gear could be run with a path radius equal to 30 m, as the initial lateral acceleration would still be within the grip limit, but the maneuver would be meaningless and extreme. As all cornering events explored up to now, the gear positions of interest are from 2nd to 4th. The addition of further tests at upper gears (5th and 6th) is not interesting, provided the reduced reactivity of these ratios. *Table 7.2* resumes the parameters adopted for this test.

Sampling Time Interval		0.001s
Throttle Step Time Interval		1.0s
2nd Gear	Path Radius	30 m
	Lateral Acceleration	0.10g
3rd Gear	Path Radius	50 m
	Lateral Acceleration	0.15g
4th Gear	Path Radius	100 m
	Lateral Acceleration	0.175g
Turn Direction		Left
Power Steering		Inactive

Table 7.2: Throttle-On In-Turn - Throttle @ 100% - test setup.

7.2.2 Vehicle Dynamics

Figures 7.65 and 7.66 report the lateral acceleration and longitudinal velocity time histories. The latter quantity gives an important indication of how the longitudinal load transfer is expected to affect traction. While in 2nd gear RWD is able to accelerate faster, thus suggesting that the rear wheels are finally experiencing an improved grip, in 3rd and 4th gears FWD is still more advantaged, especially in the unladen configuration. These observations are confirmed by the lateral acceleration, with RWD also showing some great vibrations in 2nd gear.

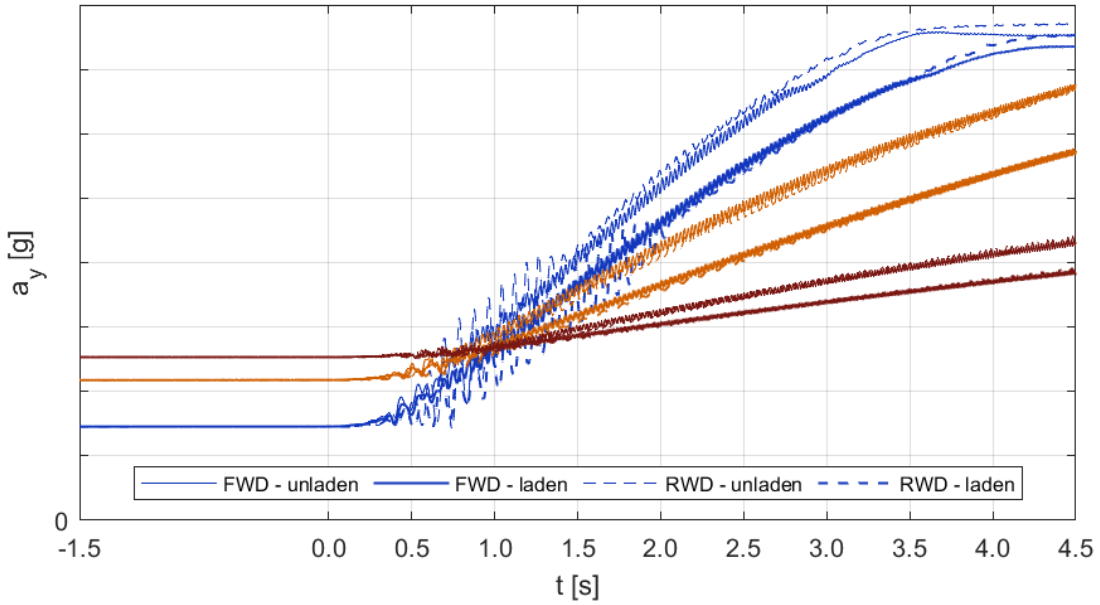

Figure 7.65: Throttle-On In-Turn - Throttle @ 100% - lat. acc. vs time.

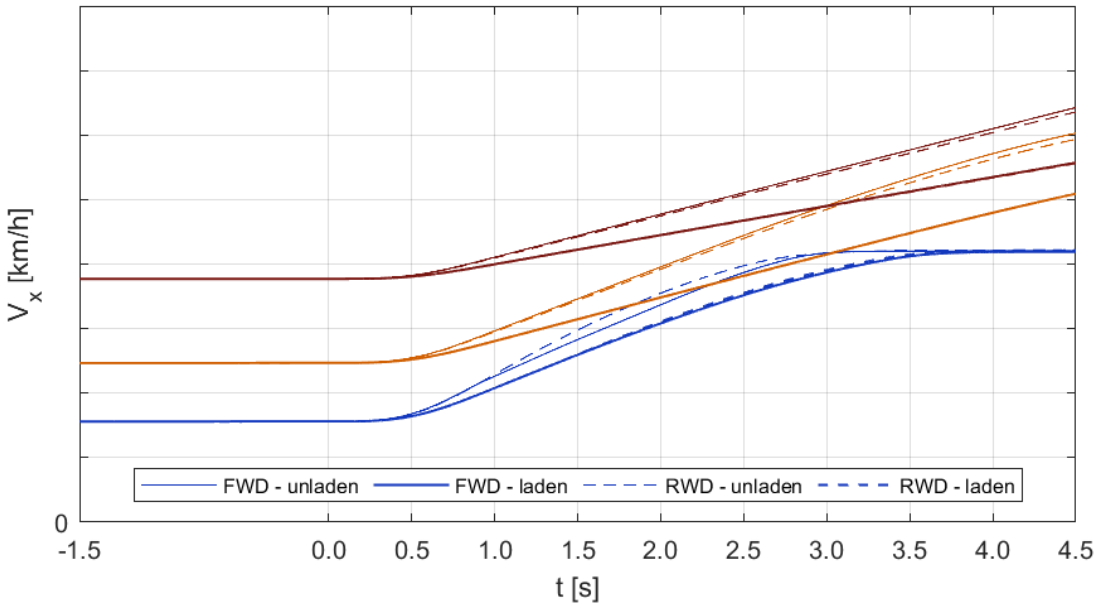

Figure 7.66: Throttle-On In-Turn - Throttle @ 100% - long. velocity vs time.

Figure 7.67 shows the sideslip angle time history. The more noticeable differences involve 2nd gear, where RWD is clearly more likely to reduce the "nose-out" configuration due to its faster longitudinal acceleration. Instead, at upper gears FWD confirms the greater grip on the front axle, which results in a faster acceleration accompanied by a slight reduction in sideslip angle. *Figure 7.68* shows the yaw velocity time history. Interestingly, FWD seems to achieve a greater yaw rate during the transient, which suggests a lower tendency to widen the trajectory with respect to RWD, although this situation reverts near the end of the test, where RWD confirms its less understeering behaviour. This response is probably the result of an improved ability to accelerate for RWD, which finally increases its speed and path radius faster at low gears.

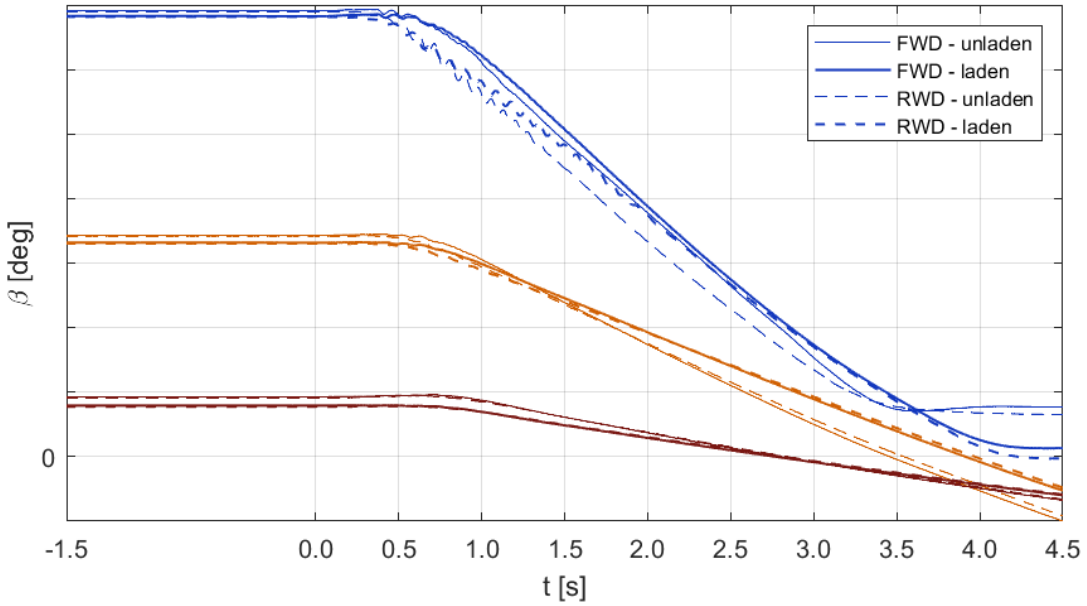

Figure 7.67: Throttle-On In-Turn - Throttle @ 100% - sideslip angle vs time.

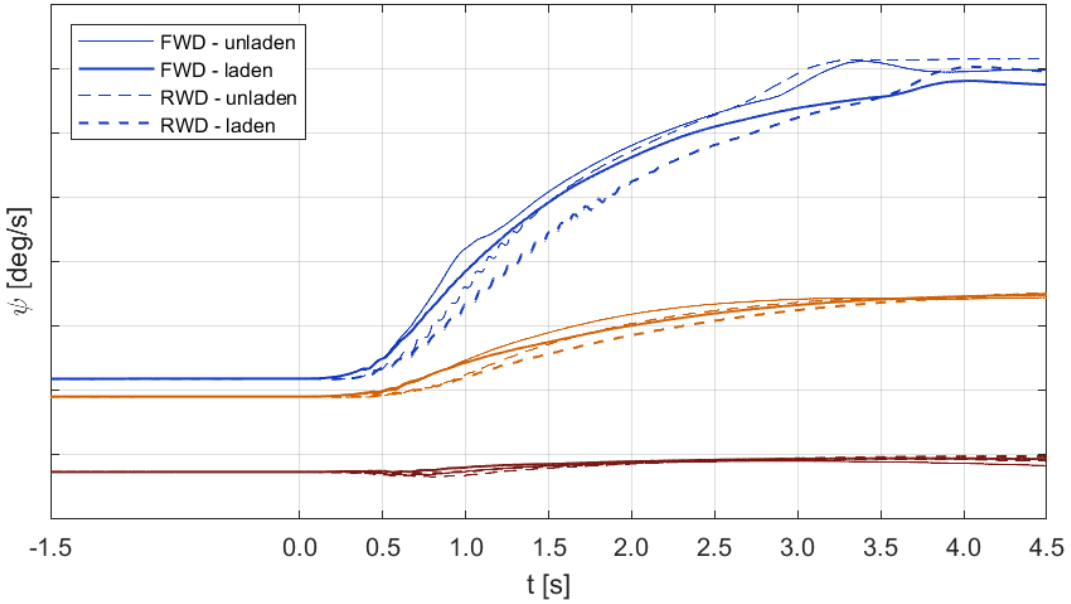

Figure 7.68: Throttle-On In-Turn - Throttle @ 100% - yaw velocity vs time.

7.2.3 Tyres Dynamics

Figures 7.69 and 7.70 show the lateral load transfer on front and rear axles, with respect to their initial steady-state value. On the rear wheels, RWD exhibits the presence of a reaction torque which loads more the inner wheel, in case of a left turn. Clearly, a right turn would further unload the inner wheel and possibly emphasize a slippage phenomenon involving that tyre. As in all previous tests, FWD does not show this issue and immediately loads the outer side of both axles as the result of an increase in lateral acceleration.

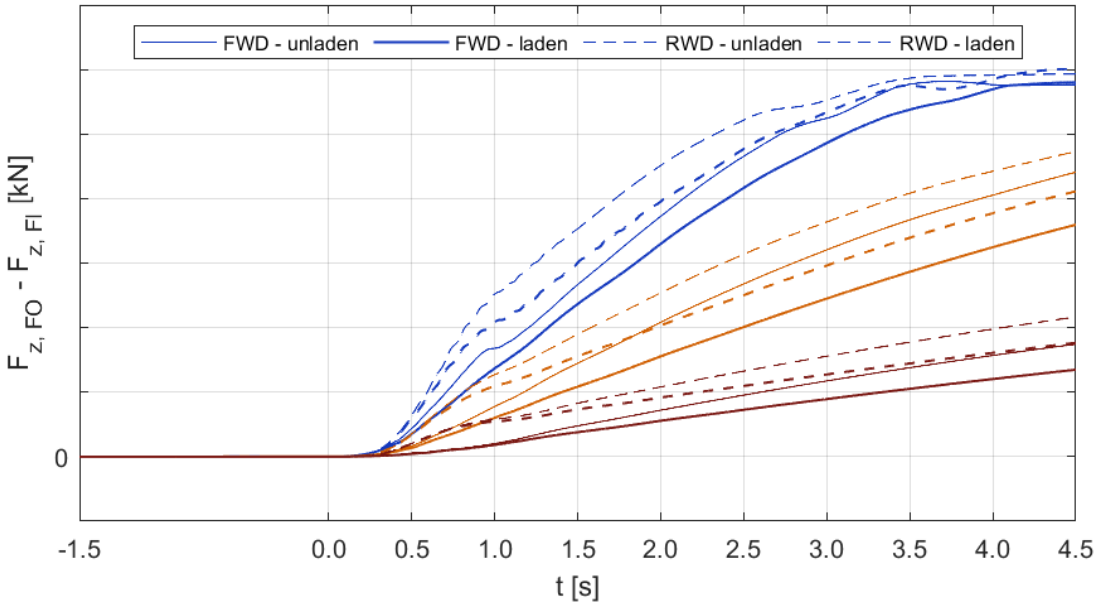

Figure 7.69: Throttle-On In-Turn - Throttle @ 100% - front lateral transfer vs time.

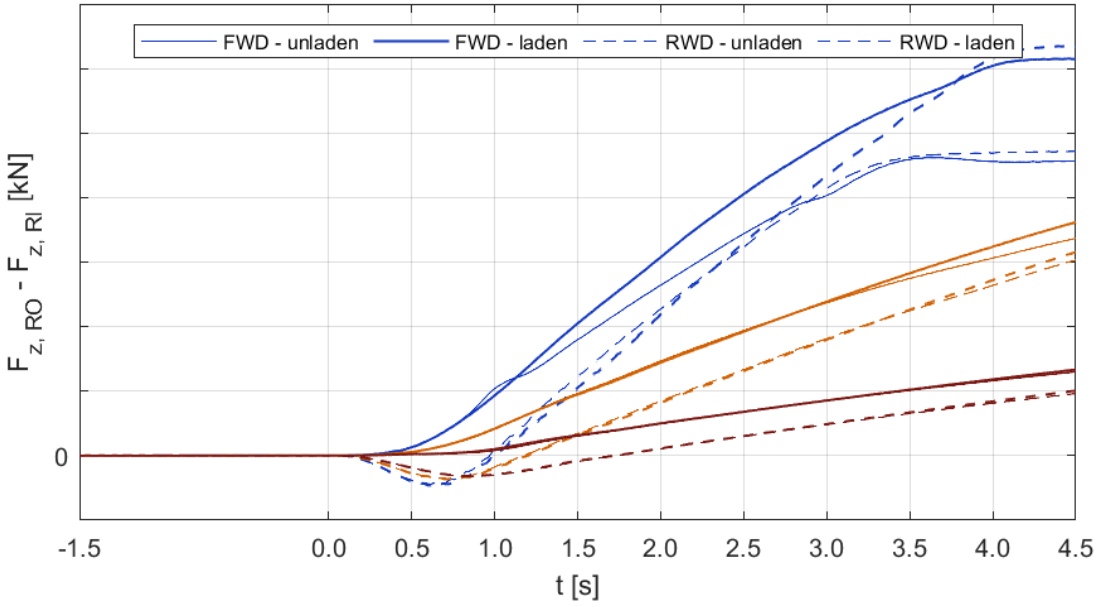

Figure 7.70: Throttle-On In-Turn - Throttle @ 100% - rear lateral transfer vs time.

Figure 7.71 shows the longitudinal load transfer time history, defined as the difference between rear and front axles normal loads, with respect to their initial steady-state value. This quantity confirms the previous assumptions made looking at the vehicle speed. Actually, in 2nd gear RWD is achieving a noticeable increase in longitudinal transfer, hence grip on the rear tyres, which allows it to accelerate faster and reach the engine over-revving limit sooner, especially in the unladen condition. Instead, in 3rd and 4th gears all vehicles are comparable, with the unladen FWD able to slightly enhance the grip on front tyres, thanks to the static load distribution which is still prevailing with respect to the longitudinal transfer induced by an acceleration.

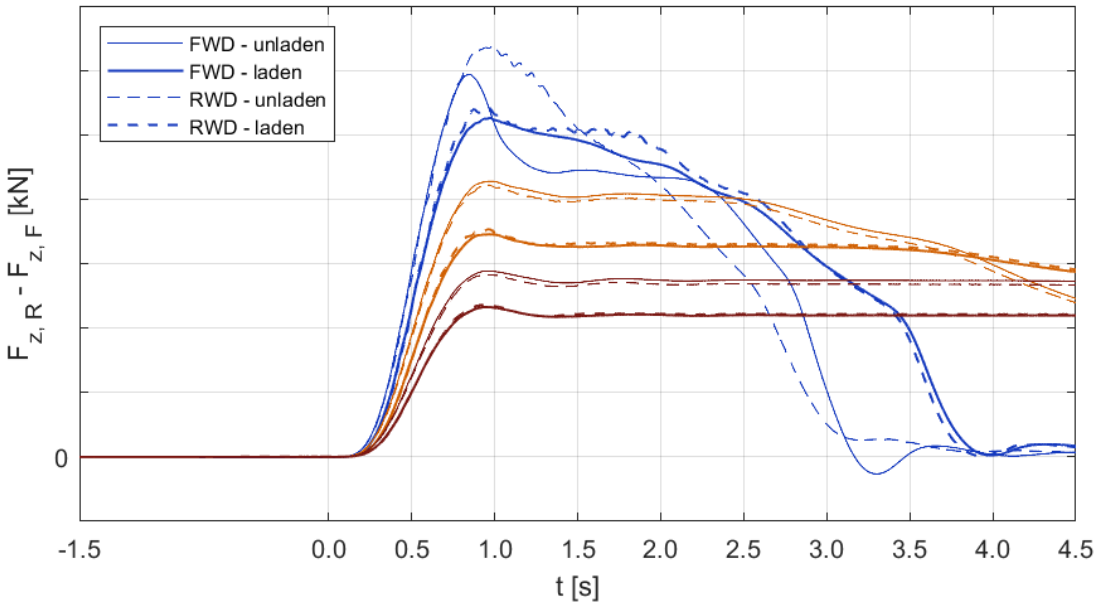

Figure 7.71: Throttle-On In-Turn - Throttle @ 100% - long. transfer time.

Figures 7.72 and 7.73 report the slip achieved on the driving wheels as function of time. With respect to the previous set of Throttle-On In-Turn tests, this time the combination of longitudinal and lateral forces proves to be sufficient to stress the tyres, at least in 2nd gear. Here, the unladen FWD is experiencing a complete saturation of the inner wheel corresponding to the end of the accelerator step, which is limiting the total available torque on the ground and reduces the vehicle ability to accelerate. A partial slippage takes place in the laden condition as well. The unladen RWD is subject to a moderate slippage on the inner tyre, which is present on the outer wheel as well, although in a reduced amount. These results suggest that RWD is close to its limit longitudinal acceleration in combined conditions and the situation might get a little more critical during a right turn, due to the above mentioned reaction torque. At upper gears, the driving wheels experience small or negligible slip on both sides, mainly due to the lower torques associated with these ratios, which make the maneuver smoother.

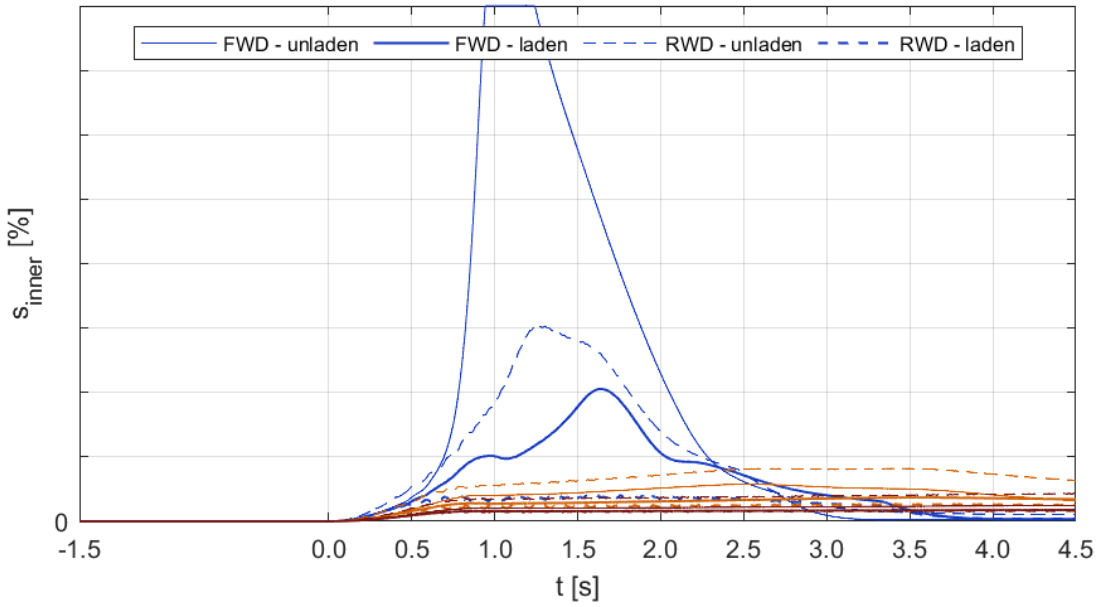

Figure 7.72: Throttle-On In-Turn - Throttle @ 100% - inner slip vs time.

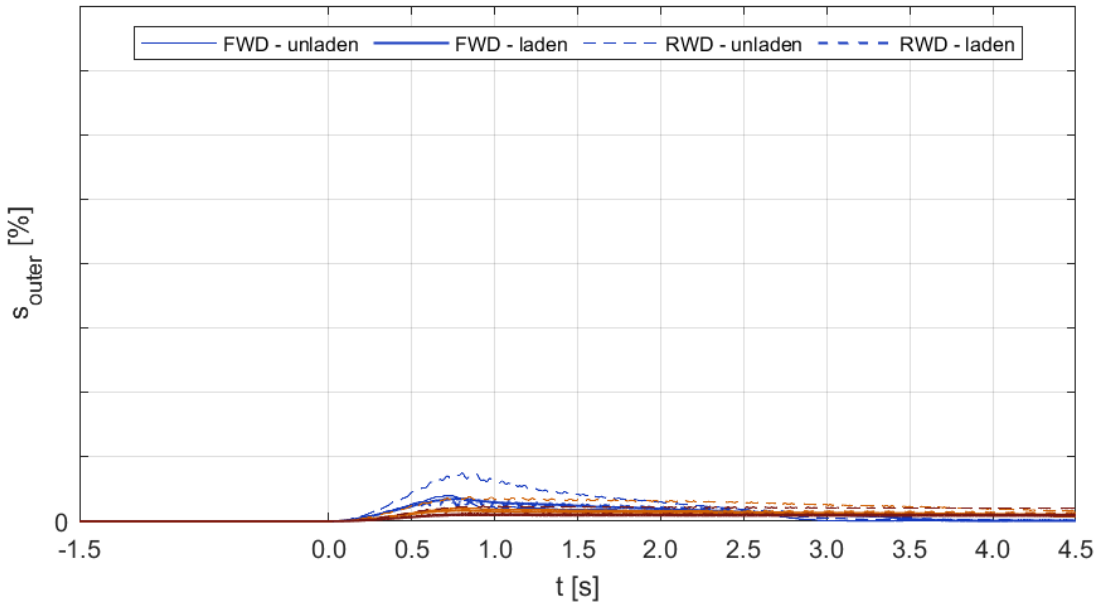

Figure 7.73: Throttle-On In-Turn - Throttle @ 100% - outer slip vs time.

Figure 7.74 shows the understeer gradient time history. The results are deeply affected by the behaviour of the steering rack, which reacts to the drivetrain differently and affects the front wheels steer angles, which ultimately determine their slip angles as well. Therefore, it is difficult to make predictions looking at this quantity alone. RWD seems more understeering not only during the transient, but also when approaching the test conclusion, which is not in agreement with the previous quantities.

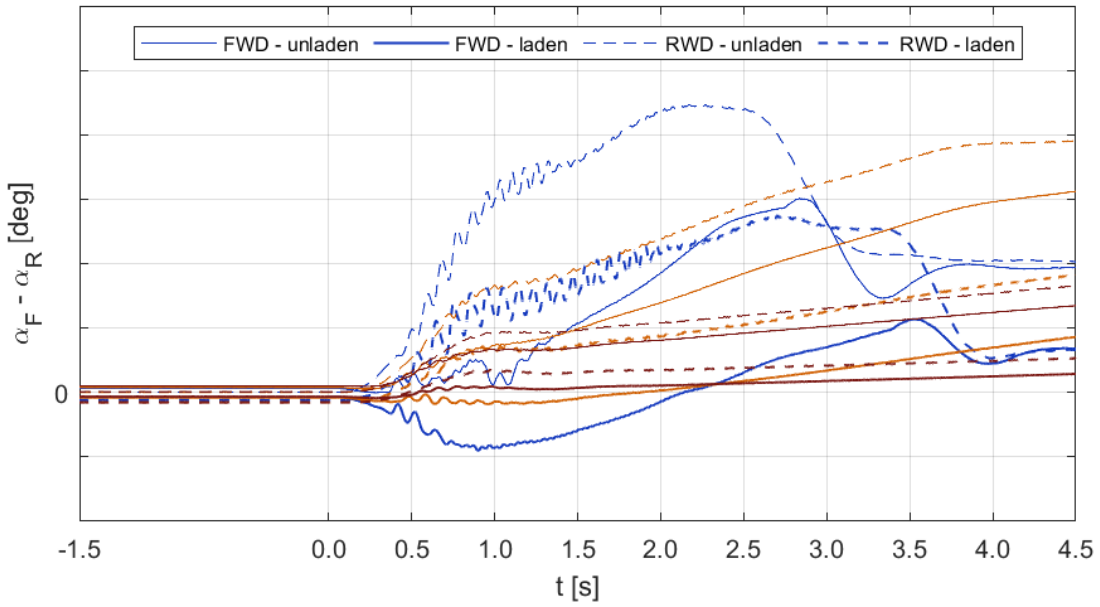

Figure 7.74: Throttle-On In-Turn - Throttle @ 100% - understeer gradient vs time.

Figure 7.75 reports the path radius time history. In 2nd gear, RWD temporarily increases the radius more than FWD, due to the improved ability to accelerate, but later settles to a slightly lower radius, as in 3rd and 4th gears. Therefore, the apparently greater understeer already detected in the yaw rate graph is actually the result of a faster longitudinal acceleration. The truth is shown near the end of the test, where RWD reaches a lower radius with respect to FWD and confirms its less understeering behaviour already detected in the previous tests.

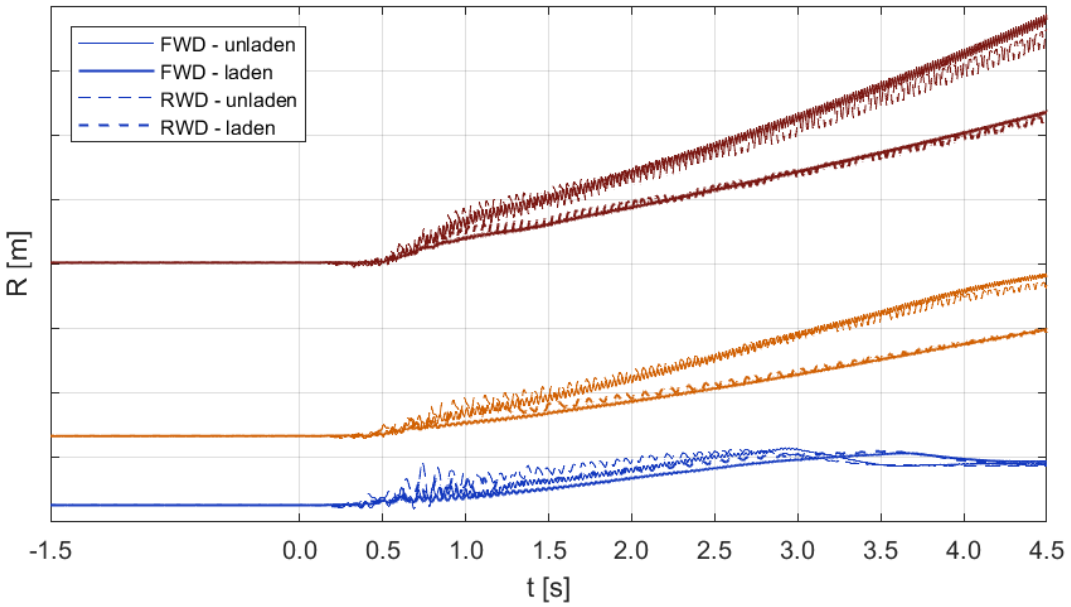

Figure 7.75: Throttle-On In-Turn - Throttle @ 100% - path radius vs time.

7.2.4 Steering System

Figures from 7.76 to 7.78 show the steering wheel torque, front wheels total self-aligning moment and steering rack stroke time histories. According to the sign conventions used in Adams/Car, a negative steering wheel torque is directed counterclockwise from the driver's viewpoint, thus coherent with a left turn. Instead, the self-aligning moment is negative when directed clockwise, thus effectively providing an aligning action during a left turn. Finally, the steering rack stroke is measured as the travel with respect to the neutral position.

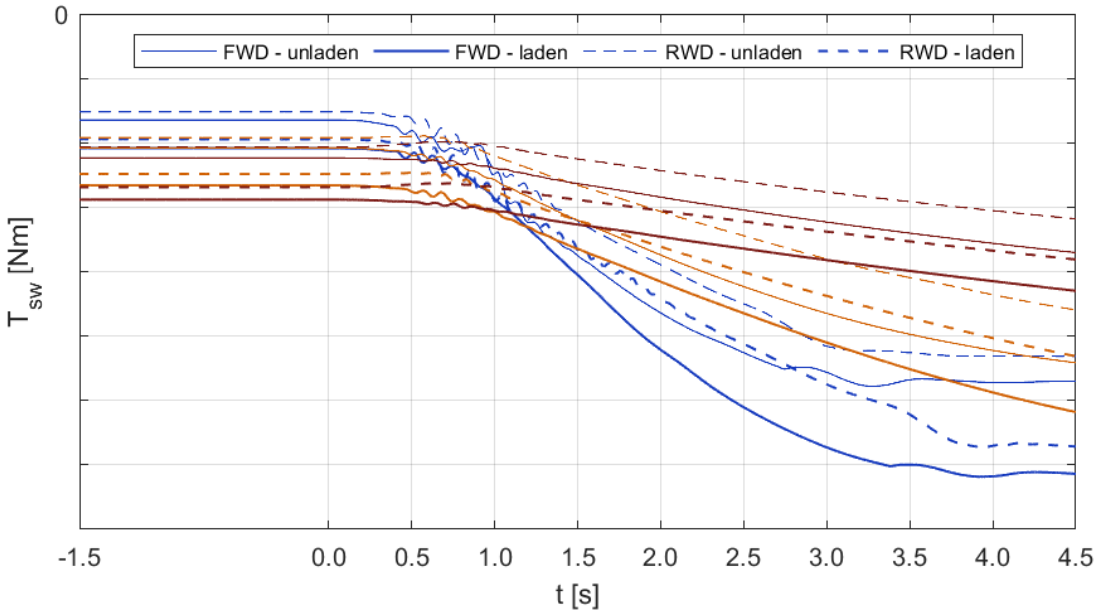

Figure 7.76: Throttle-On In-Turn - Throttle @ 100% - steering wheel torque vs time.

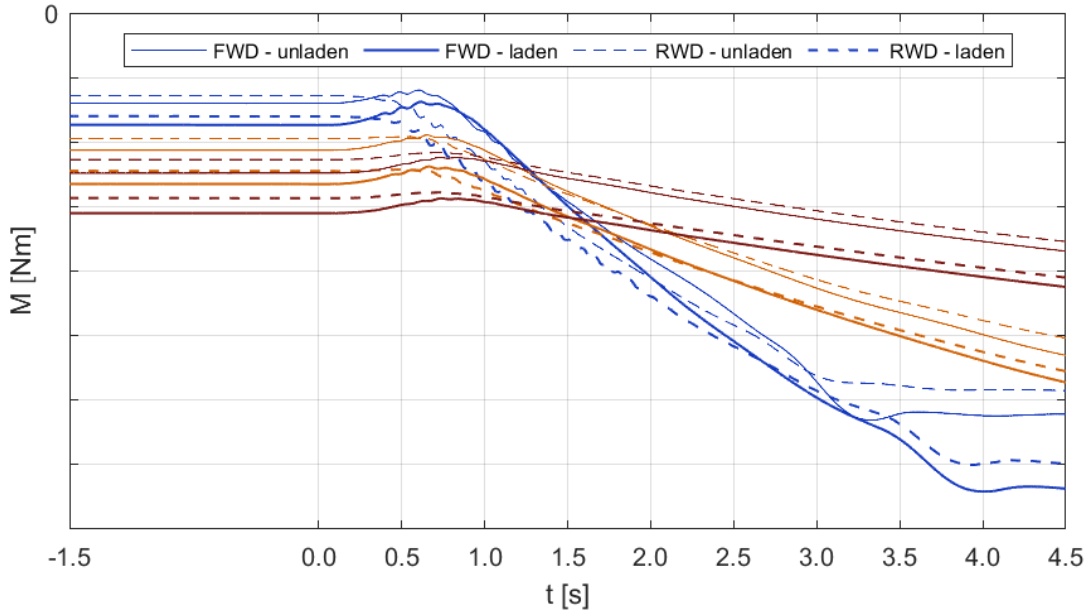

Figure 7.77: Throttle-On In-Turn - Throttle @ 100% - self-aligning moment vs time.

With respect to the previous set of tests, here some additional considerations about the steering system can be drawn. First of all, FWD confirms its slightly more understeering tendency in steady-state, as shown by the three quantities. During the transient, in 2nd gear FWD displays a huge increase in steering wheel torque required to prevent the wheels self-aligning action, which shows a temporary decrease followed by a steeper increase with respect to RWD. The rack stroke decreases more sharply as well, so that the wheels end up having smaller steer angles on FWD. This behaviour justifies the handling curve shown above, where RWD apparently behaves significantly more understeering than FWD. Comparing the loading conditions, the rack stroke in laden configuration starts from a slightly greater value, but ends up being smaller than the one achieved on the unladen van, meaning that the wheels steer angles are greater on the unladen vehicle at the test conclusion. This result is not reflected by the steering wheel torque, which is still lower, along with the self-aligning moment exerted by the wheels. Moving to 3rd and 4th gears, the rack stroke shows again a steeper slope on FWD, suggesting that the wheels decrease more their steer angles with respect to RWD. This response is accompanied by a greater self-aligning moment, which passes through a temporary decrease almost absent on RWD. On the other hand, the steering wheel torque on FWD shows some vibrations before increasing more with respect to RWD. This means that on FWD the wheels have a lower steer angle and yet a greater tendency to return straight, forcing the driver to exert a greater torque.

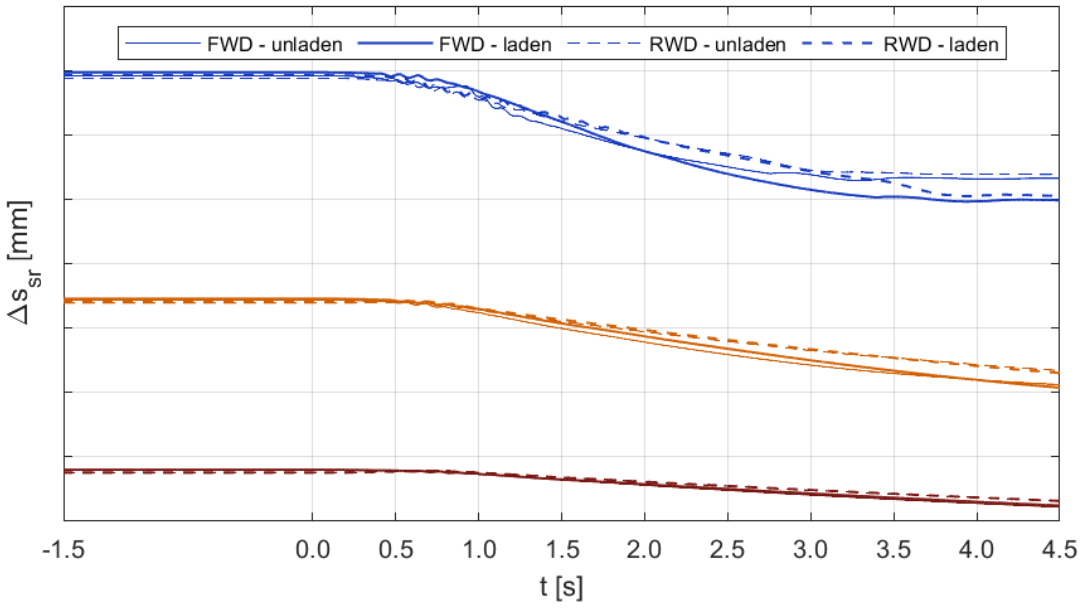

Figure 7.78: Throttle-On In-Turn - Throttle @ 100% - rack stroke vs time.

7.3 Conclusions

7.3.1 Throttle @ 50%

Throttle-On In-Turn proves to be a less critical maneuver and generally provides similar results between Front and Rear-Wheel-Drive. In terms of vehicle dynamics, both versions experience an increase in lateral acceleration, along with an evolution in the sideslip angle towards a neutral or a "nose-in" configuration. The path radius gets wider, especially for the unladen van, which shows a greater reactivity to the maneuver. When the vehicle works at greater lateral accelerations, it experiences a transient decrease in lateral acceleration, corresponding to a remarkable understeering response, before restoring its initial steady-state condition. Rear-Wheel-Drive experiences some vibrations in 2nd gear, suggesting a greater yaw sensitivity at low lateral accelerations. Concerning the tyre dynamics, the main difference between Front and Rear-Wheel-Drive is still represented by the reaction torque taking place on the rigid axle of the latter version. This phenomenon results in asymmetric behaviours for left an right turns and eventually forces the inner wheel to slip remarkably, without reaching saturation, thus affecting the ability of the unladen Rear-Wheel-Drive to accelerate close to the limit. Another interesting difference lies in the longitudinal load transfer and acceleration, which are slightly greater in the unladen Front-Wheel-Drive. This result suggests that the maneuver, as here defined and accomplished, is giving more importance to the static load distribution among axles, rather than to the acceleration itself, which should be expected to be advantageous to the rear drivetrain. Concerning the handling performance, it is impossible to state uniquely that Front-Wheel-Drive is more understeering than Rear-Wheel-Drive, because the two vehicles behave similarly enough to make the reaction torque a discriminant between left and right turns. Looking at the steering system, the maneuver itself induces almost identical rack strokes, meaning similar steer angles on the front wheels, but Front-Wheel-Drive requires a sightly greater steering wheel torque to balance an extra self-aligning moment coming from the wheels. Overall, provided the difficulty in stressing the vehicles to the limit, an additional Throttle-On In-Turn maneuver is required.

7.3.2 Throttle @ 100%

This complementary set of Throttle-On Turn-In maneuvers is intended to make the longitudinal acceleration more relevant than the static load distribution, at least at lower gears. The adoption of different path radii allows to operate in the field of low initial lateral accelerations and positive sideslip angles. The tyres are stressed more due to combined slip in Front-Wheel-Drive vans, which eventually suffer saturation and show a decreased ability to accelerate at low gears. During the transient, Rear-Wheel-Drive vehicles seem more likely to increase understeer, because they are able to transfer huge accelerations to the ground. There is no indication of power oversteer occurring at low gears, at least according to the testing method here adopted. It is important to notice that, after Rear-Wheel-Drive loses its enhancement in longitudinal acceleration, it gets back to a lower understeer with respect to Front-Wheel-Drive. Looking at the steering system, Front-Wheel-Drive displays a transient almost absent on Rear-Wheel-Drive and later tends to further restore the straight position of the front wheels, thus forcing the driver to oppose a greater torque to maintain the steering wheel locked. Combining the results of this and the previous set of Throttle-On In-Turn tests, it is possible to state that Front-Wheel-Drive is more understeering, but the degree of reactivity of both drivetrains strongly depends on the amount of acceleration impressed. Both vehicles can experience tyre saturation depending on how the longitudinal load transfer and static load distribution are related one to each other. Front-Wheel-Drive is more reactive to moderate accelerations, while it loses grip for extreme maneuvers. The opposite happens on Rear-Wheel-Drive vehicles.

8 Front Suspension Optimization

8.1 Alternative Geometries

The overall idea provided by the tests performed in the previous Sections is that a Front-Wheel-Drive vehicle directly derived from the actual Rear-Wheel-Drive does not show critical issues that might affect its dynamic behaviour when negotiating a curve. Consequently, the actual front suspension mounted on Rear-Wheel-Drive can be taken as a reference to eventually develop an optimization. Since Front-Wheel-Drive does not show any evident loss of performance with respect to Rear-Wheel-Drive, the main field of interest where some possible alternative suspension layouts might be investigated is represented by the feeling perceived by the driver. Assuming that a usual driver is not meant to keep the steering wheel locked, the different sensations provided by Front-Wheel-Drive might eventually lead to unsafe reactions by the driver, who is perceiving that something different is happening. This Chapter explores different ways to optimize a double wishbone, with special reference to the steering system response. The front suspension geometry affects the steering wheel feedback perceived by a driver. The parameters involved in determining the steering feel are caster moment arm and scrub radius. These two quantities are interchangeable with caster and kingpin angles, as they represent the arms between tyre contact point and projection of the steering axis on the ground, in longitudinal and lateral directions. The optimization here considered only involves caster moment arm, which is traditionally a discriminant among suspensions designed for Front and Rear-Wheel-Drive vehicles. Usually, the latter category requires greater mechanical trails to ensure stability when driving, because the front wheels only exert cornering forces. Instead Front-Wheel-Drive vehicles, as seen in the previous Chapters, provide a "self-stabilizing" effect to the front wheels because of the longitudinal forces acting together with the lateral components. This is the reason why these vehicles usually feature smaller caster moment arms, especially when equipped with McPherson suspensions. A shorter mechanical trail implies a lower torque around the kingpin axis, hence a reduction in the steering wheel torque required to the driver, but also an increased sensitivity to any road irregularity, which explains why the arm should never be null. Concerning scrub radius, it is not investigated in this Thesis, because its effects are mainly related to the vehicle stability in straight driving, not only relatively to the presence of road irregularities, but also in terms of safety in split-μ braking. Going back to caster moment arm, the hardpoints object of optimization are the two spherical joints connecting the suspension control arms to the upright. In the Adams/Car model, they are called:

- Point 10: upper control arm to upright
- Point 5: lower control arm to upright

The intervention on caster moment arm consists in a reduction to 1/3 of its initial value. Among the possible solutions which can be implemented, the following two alternatives are considered:

- Solution 1: Point 10 is translated forward in the longitudinal direction, Point 5 is unvaried. This alternative implies a strong reduction in caster angle. It is shown in *Figure 8.1b*
- Solution 2: Points 10 and 5 are translated backward in the longitudinal direction. This alternative allows to preserve the initial caster angle. It is shown in *Figure 8.1c*

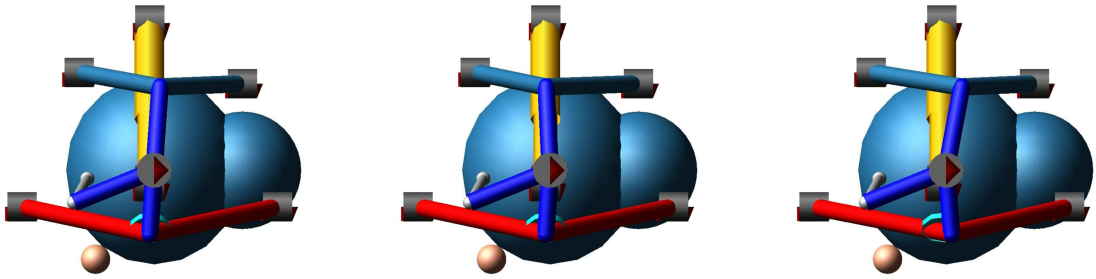

(a) Initial. *(b) Solution 1.* *(c) Solution 2.*

Figure 8.1: Optimization - Front Suspension - Lateral View.

The coordinates of Points 10 and 5 for all suspension geometries are resumed in *Table 8.1*. It is clear that both y and z components are not modified, resulting in a unique rear projection of the suspension, here shown in *Figure 8.2* to highlight the kingping axis position with respect to the constant velocity joint on the wheel side.

		Point 10	Point 5
Initial	x	-10.184	-27.668
	y	-732.782	-789.891
	z	208.011	-42.028
Solution 1	x	-26.688	-27.668
	y	-732.782	-789.891
	z	208.011	-42.028
Solution 2	x	6.296	-10.828
	y	-732.782	-789.891
	z	208.011	-42.028

Table 8.1: Optimization - Front Suspension - Points 10 and 5.

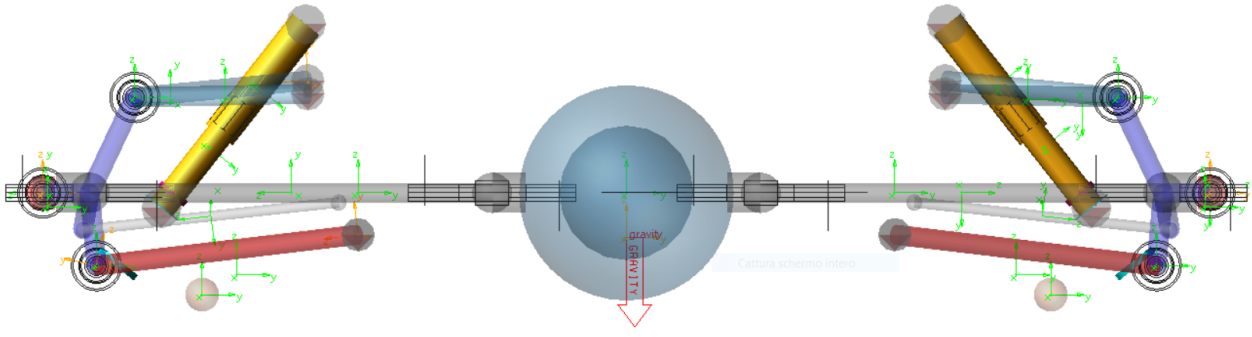

Figure 8.2: Optimization - Front Suspension - Rear View.

The above mentioned geometries are achieved in a 2-steps optimization. The first step consists in a rough modification of the hardpoints by trial-and-error to reach some first guess values before implementing the second step, which is a refined tuning using Adams/Insight. This tool operates together with Adams/Car, according to the following workflow:

1. Parallel Wheel Travel: on Adams/Car, the initial suspension is tested to determine its design condition. The original values of mechanical trail and caster angle are measured

2. Design Objectives: the already mentioned caster moment arm and caster angle of both sides are taken as design objectives, meaning that they are the goals of the optimization

3. Export: the test just performed is exported to Adams/Insight, so that it can later be repeated using a set of trial values to fit the model behaviour with a statistical tool

4. Factors: on Adams/Insight, the longitudinal coordinates of Points 10 and 5 are selected as factors. Each simulation corresponds to one value for each factor. The first guess values already found are used to reduce the range of optimization. Specifically, each coordinate is enclosed in boundaries of $\pm 1mm$

5. Responses: these are the results required to the optimization, obviously the caster moment arm and the caster angle. The former is present on both solutions, the latter is used as a constraint only on Solution 2, where caster angle should remain constant

6. Design Specification: this toolbar allows to set the criteria used by the software to fit the simulations results. The following setup is selected:

   - Investigation Strategy: DOE Response Surface
   - Model: Cubic
   - DOE Design Type: Latin Hypercube
   - Number of Runs: 20 (conceptually, one run per each tenth of mm)

7. Simulation: Adams/Insight sends to Adams/Car 20 simulations, each one with a set of factors values, meaning a corresponding set of diversified responses. The results are processed to build a response surface, valid for the boundaries previously specified

8. Optimization: the desired values for both mechanical trail and caster angle are given as input to the model, which returns the estimated hardpoints longitudinal coordinates

9. Validation: Parallel Wheel Travel is repeated for each Solution to ensure that the new hardpoints are effectively giving the desired suspension parameters. Clearly, the result is affected by an error, because the optimization is based on a response surface. The selection of narrow boundaries around the first guess values allows to reduce the number of runs necessary to establish a sufficiently good fit

Table 8.2 resumes the values achieved on Factors and Responses for both Solutions. In the Adams/Car model, points 10 and 5 indicate the spherical joints connecting the upright respectively to the upper and lower control arms.

	Initial	Solution 1	Solution 2
$x_{pt.10}$ (mm)	-10.184	-26.688	6.296
$x_{pt.5}$ (mm)	-27.668	-27.668	-10.828
CMA (mm)	24.38	8.02	8.02
CA (°)	4.08	0.16	4.13

Table 8.2: Optimization - Front Suspension - results of optimization.

The new suspension geometries can be installed on the Adams/Car model and tested in both steady-state and transient maneuvers, to assess how caster moment arm and caster angle affect the behaviour of a Front-Wheel-Drive vehicle and the steering feedback to the driver. Power steering is activated for all tests performed in the following Sections, provided that the main focus of the optimization concerns the steering feedback perceived by the driver.

8.2 Steering

Since caster moment arm and caster angle play a huge influence over the steering system, the comparison starts with a Steering test. The results are plotted as functions of the steering wheel angle, adopting a convention where a positive angle corresponds to a right turn. *Figures 8.3 and 8.4* show the wheels steer angle and camber angle. The former suggests that Solution 2 has a greater steering ratio, meaning that to achieve a target steer angle, a greater steering wheel angle is required. Instead, Solution 1 behaves similarly to the initial suspension, with a slightly lower steering ratio.

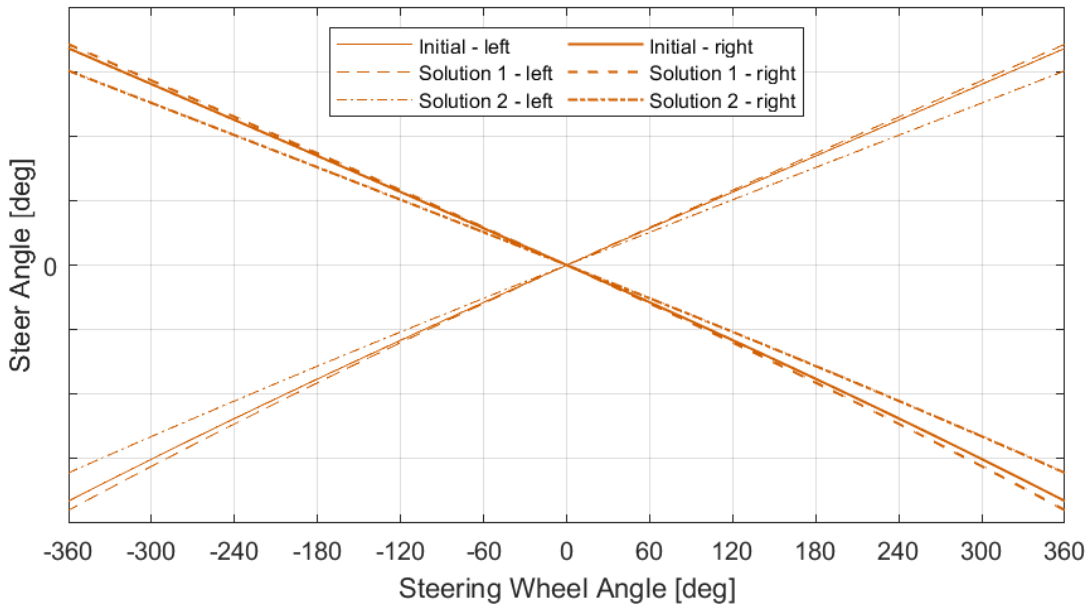

Figure 8.3: Optimization - Steering - steer angle vs steering wheel angle.

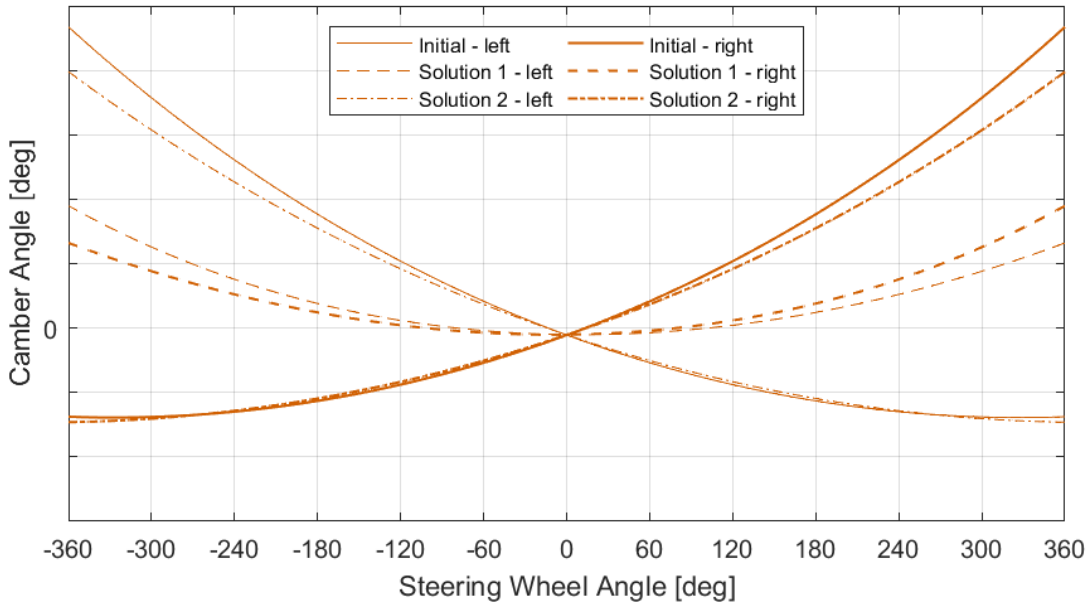

Figure 8.4: Optimization - Steering - camber angle vs steering wheel angle.

Concerning the latter quantity, Solution 1 shows poor camber recovery, meaning that camber angle is less sensitive to the steering wheel angle. This effect comes from the strong reduction in caster angle and is not desirable because, while cornering, the wheels are likely to follow the body roll, hence to keep a small camber angle and increase the inclination angle with respect to the ground, resulting in a loss of grip, especially on the outer wheel, which is the most loaded. *Figure 8.5* reports the roll-camber coefficient, defined as the ratio between the vehicle body roll angle and the wheels camber angle. Solution 1 shows a greater and quite constant coefficient, representative of a reduced camber recovery. Instead, Solution 2 resembles the initial suspension and is less sensitive to the steering wheel angle.

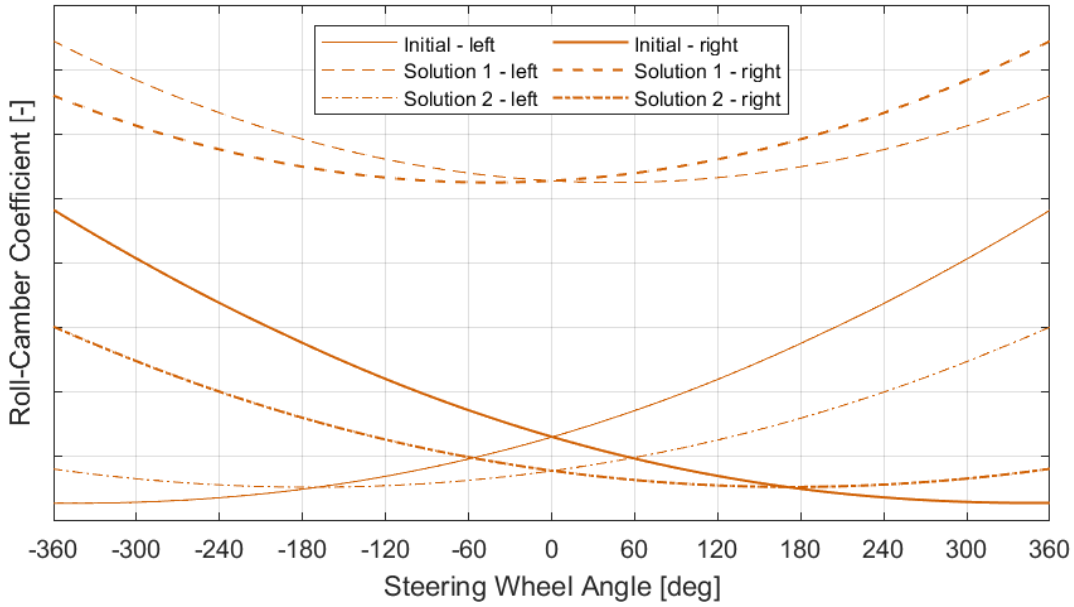

Figure 8.5: Optimization - Steering - roll-camber coefficient vs steering wheel angle.

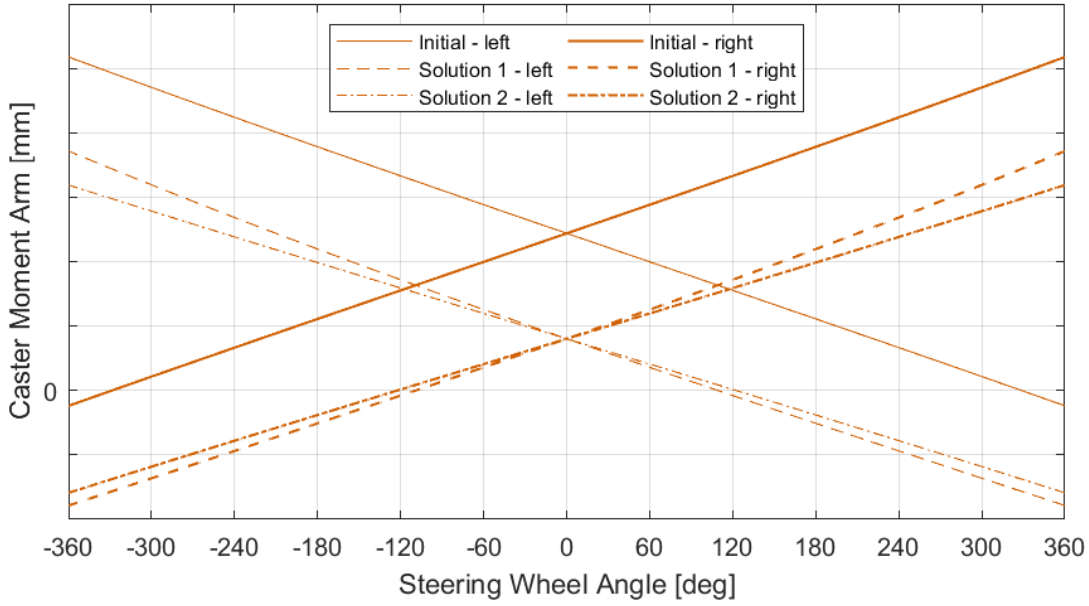

Figure 8.6: Optimization - Steering - caster moment arm vs steering wheel angle.

Figures 8.6 and 8.7 show the caster moment arm and the roll-caster coefficient, defined as the ratio between the vehicle body roll angle and the wheels caster angle. Obviously, both Solutions show an offset with respect to the initial geometry, since their caster moment arm is about 1/3 of the reference. Both graphs suggest that Solution 2 is less sensitive to the steering wheel angle, while Solution 1 is more sensitive. At last, *Figure 8.8* reports scrub radius. Even though this is not the focus of optimization, it is interesting to notice how changing a suspension geometry affects not only the parameters of interest, but some others as well. In this specific case, while the static value of scrub radius is almost preserved, both Solutions display a reduced sensitivity to the steering wheel angle.

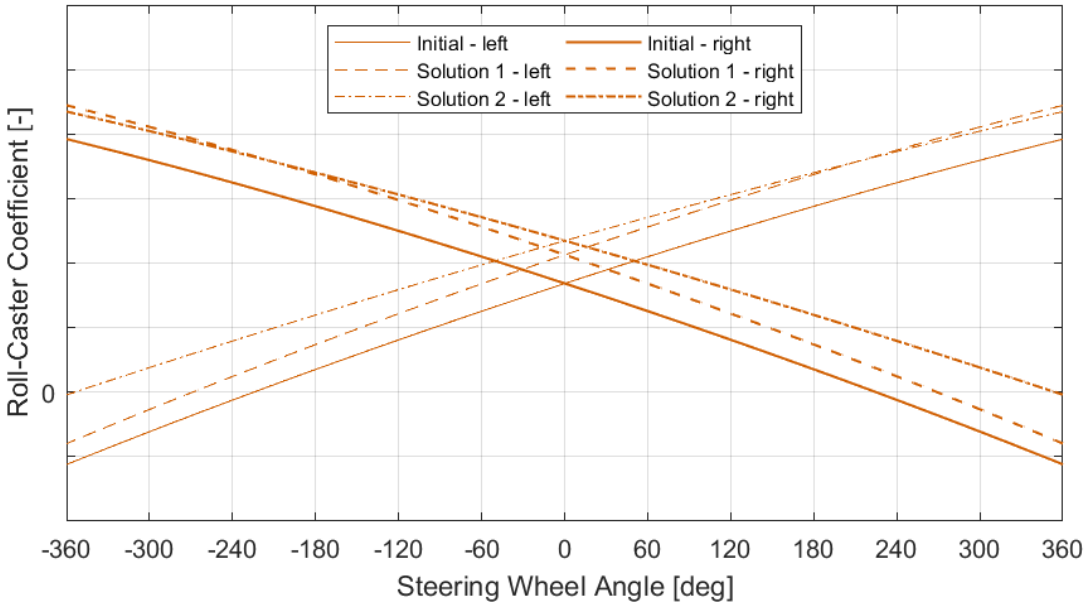

Figure 8.7: Optimization - Steering - roll-caster coefficient vs steering wheel angle.

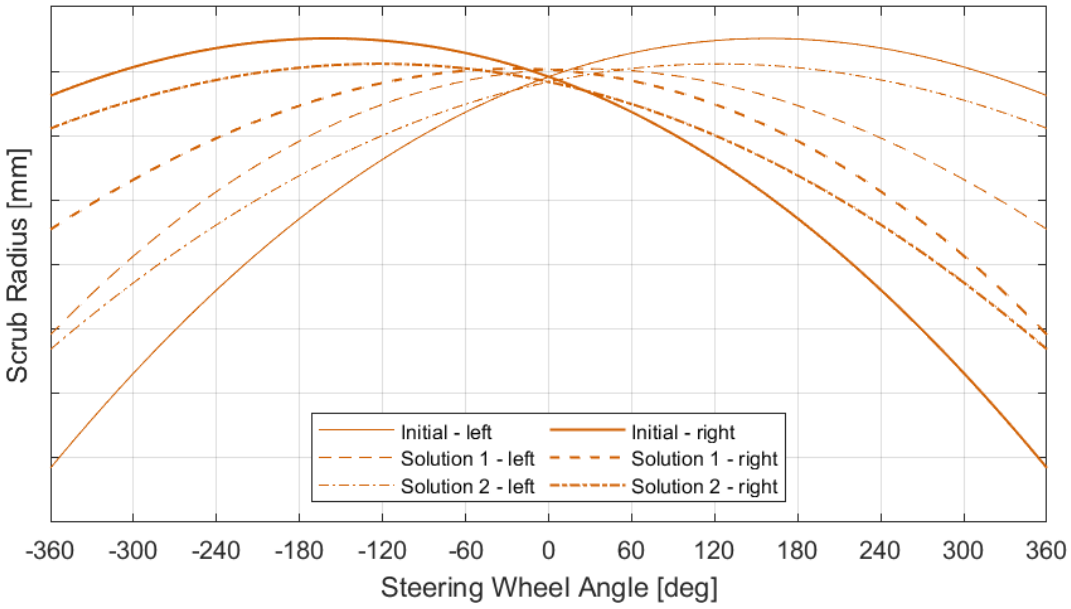

Figure 8.8: Optimization - Steering - scrub radius vs steering wheel angle.

8.3 Ramp Steer

The second test to compare the initial suspension to both Solutions is a Ramp Steer, which is performed using the same parameters previously adopted, here reported in *Table 8.3*.

Ramp	60 °/s
Longitudinal Velocity	100 km/h
Gear Position	4th
Power Steering	Active

Table 8.3: Optimization - Ramp Steer - test setup.

The roll, sideslip and steering wheel angles, along with the understeer gradient, are reported as functions of lateral acceleration in *Figures from 8.9 to 8.12*. The roll angle achieved by the two Solutions shows negligible differences with respect the initial geometry, with Solution 1 having a slightly lower roll gradient and Solution 2 almost identical to the initial suspension. Reminding that both points 10 and 5 are translated in the longitudinal direction only, obviously their transversal and vertical coordinates provide the same initial geometry in the front plane. Consequently, the roll centre height of the front suspension is nearly insensitive to the variations introduced in this study. Clearly, mechanical trail and caster angle could be modified with a combined optimization of both longitudinal and vertical coordinates of Points 10 and 5, thus implying a variation in the roll centre height, which is not desired, because the purpose of this study is to isolate the effect of a reduced caster moment arm.

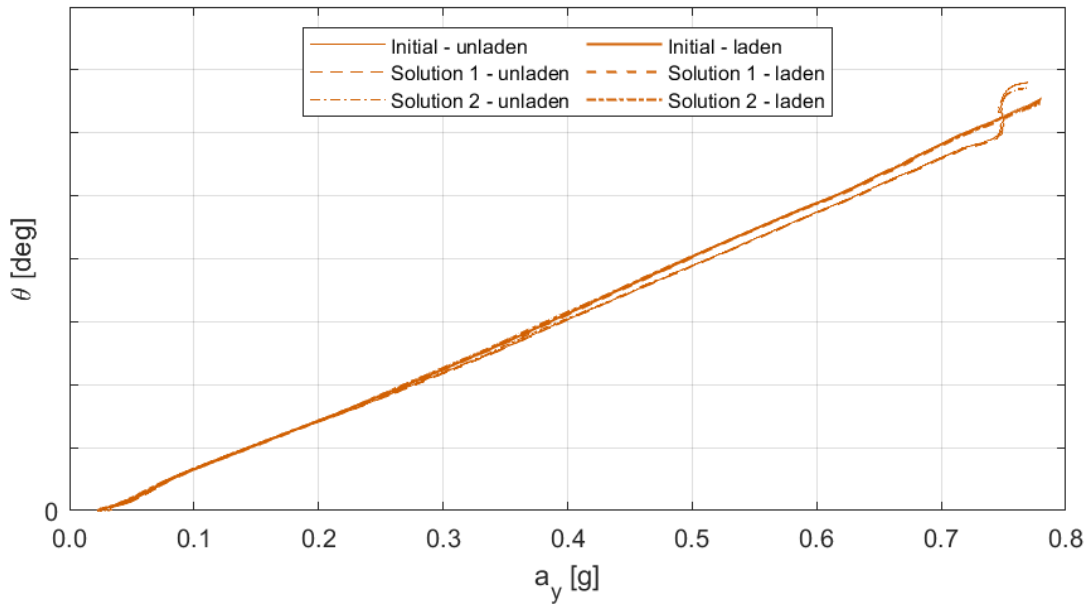

Figure 8.9: Optimization - Ramp Steer - roll angle vs lat. acc.

Looking at the sideslip angle, no noticeable changes take place, even in the field close to the limit, because this quantity is mainly affected by the rear axle, which is identical on all vehicles. A little difference involves Solution 2, which makes the vehicle slightly more prone to "nose-in".

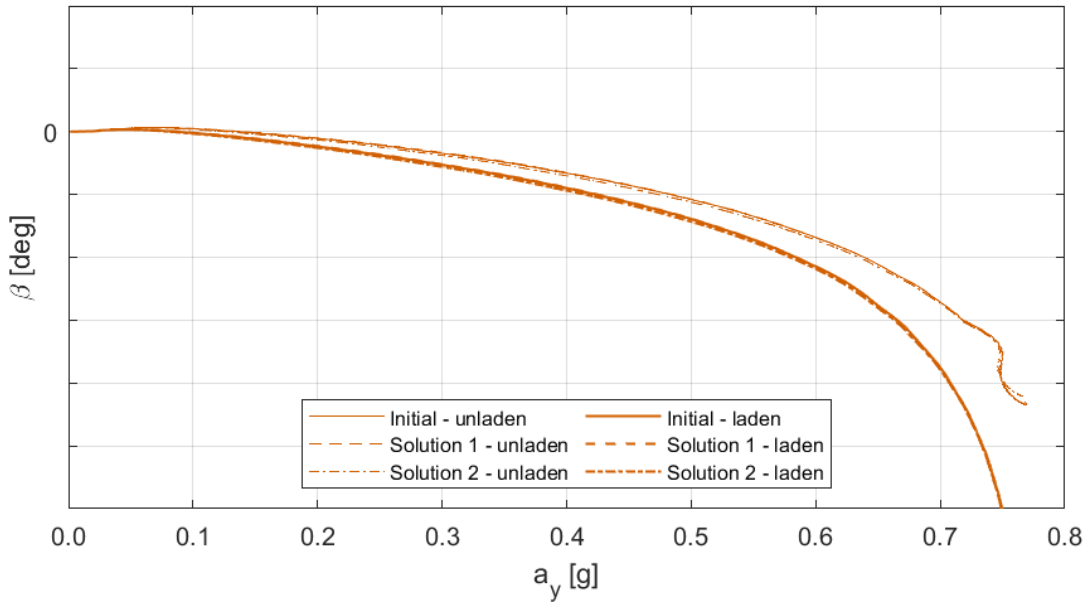

Figure 8.10: Optimization - Ramp Steer - sideslip angle vs lat. acc.

Instead, the steering wheel angle shows some differences. Particularly, Solution 1 requires the lowest steering wheel angle in both loading conditions, while Solution 2 requires an additional steering wheel angle with respect to the initial geometry. These different responses are explained by the steering ratios previously detected in the Steering test. Solution 2 shows the greatest steering ratio, which justifies the greater values of steering wheel angle required in a Ramp Steer maneuver to achieve a certain value of lateral acceleration. Opposite considerations explain why Solution 1 apparently looks less understeering. Approaching the vehicle limit, all suspensions tend to converge to the initial geometry.

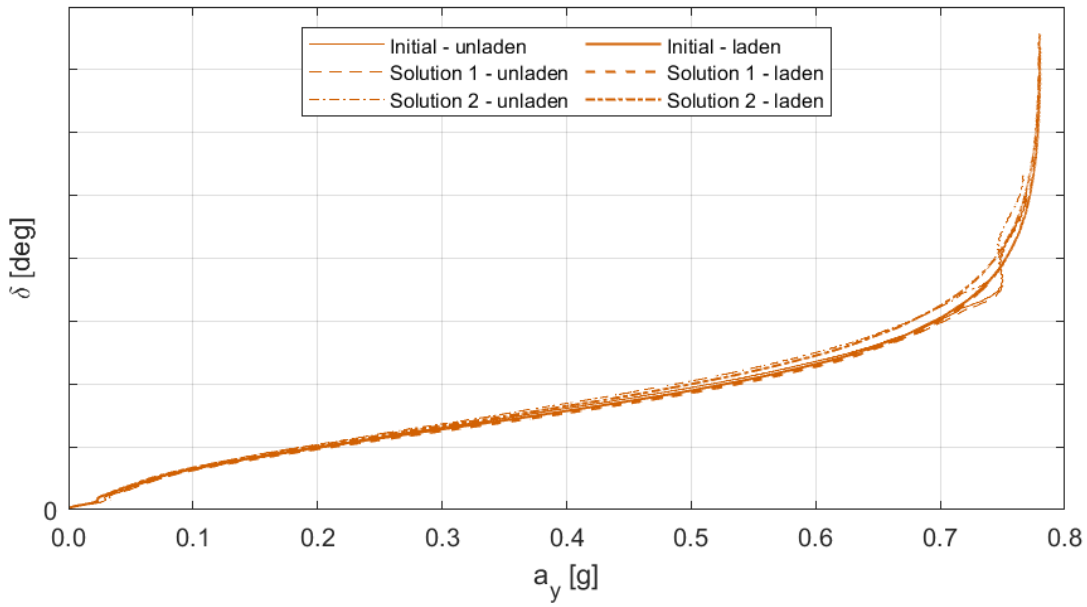

Figure 8.11: Optimization - Ramp Steer - steering wheel angle vs lat. acc.

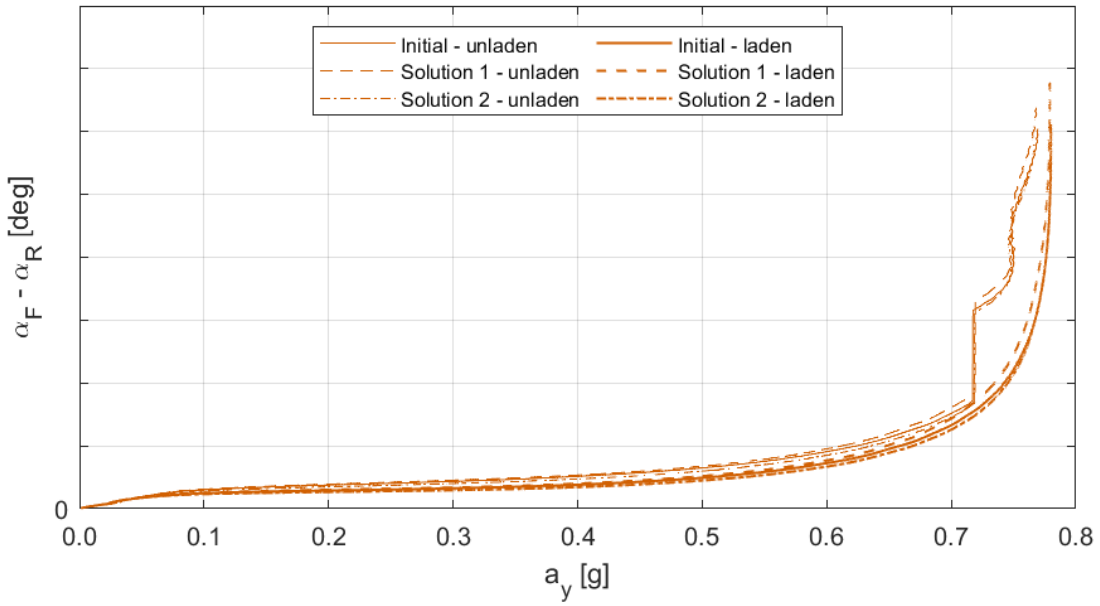

Figure 8.12: Optimization - Ramp Steer - understeer gradient vs lat. acc.

Looking at the understeer gradient, Solution 1 looks more understeering than the initial geometry, while Solution 2 is slightly less understeering, in both loading configurations. At high lateral accelerations, Solution 1 emphasizes its more understeering behaviour, while Solution 2 converges to the initial geometry. In the unladen configuration, the loss of contact between the rear inner wheel and the ground is always present and highlights these differences. Anyway, the three geometries tend to conform when they reach their maximum lateral acceleration, as previously observed. The understeer gradient provides results that seem in opposition with steering wheel angle. However, reminding the definition of understeer gradient:

$$\alpha_F - \alpha_R = \delta_{sw} - \delta_0 = \left(\frac{m_F}{C_{yF}} - \frac{m_R}{C_{yR}}\right) \cdot a_y = K_{us} \cdot a_y \tag{8.1}$$

It is clear that the kinematic value is subtracted to the actual steering wheel angle. Since this optimization is affecting the steering ratio, the kinematic value changes as well. In other words, the steering wheel angle diagram is not truly representative of handling, when different suspensions are compared. For this reason, the correct behaviour is represented by the understeer gradient. *Figures 8.13 and 8.14* show the steering wheel torque and the front wheels resulting self-aligning moment as functions of lateral acceleration. Concerning the steering wheel torque, it is worth noticing that the order of magnitude is remarkably lower due to the activation of power steering. Both Solutions allow a further reduction with respect to the initial geometry, with Solution 2 able to minimize the driver's effort. The differences are more noticeable in the field of medium lateral accelerations, while another interesting phenomenon occurs close to the limit in the laden configuration. Here, while the initial geometry is dramatically decreasing the steering wheel torque but still keeping it negative, both Solutions show a premature sign change, meaning that the driver has to prevent the steering wheel from overturning. Looking at the wheels self-aligning moment, the differences are less noticeable because this quantity is primarily affected by pneumatic trail. For low and medium lateral accelerations, Solution 1 exhibits a slightly greater moment, while Solution 2 decreases it with respect to the initial geometry. At greater lateral accelerations the situation reverts.

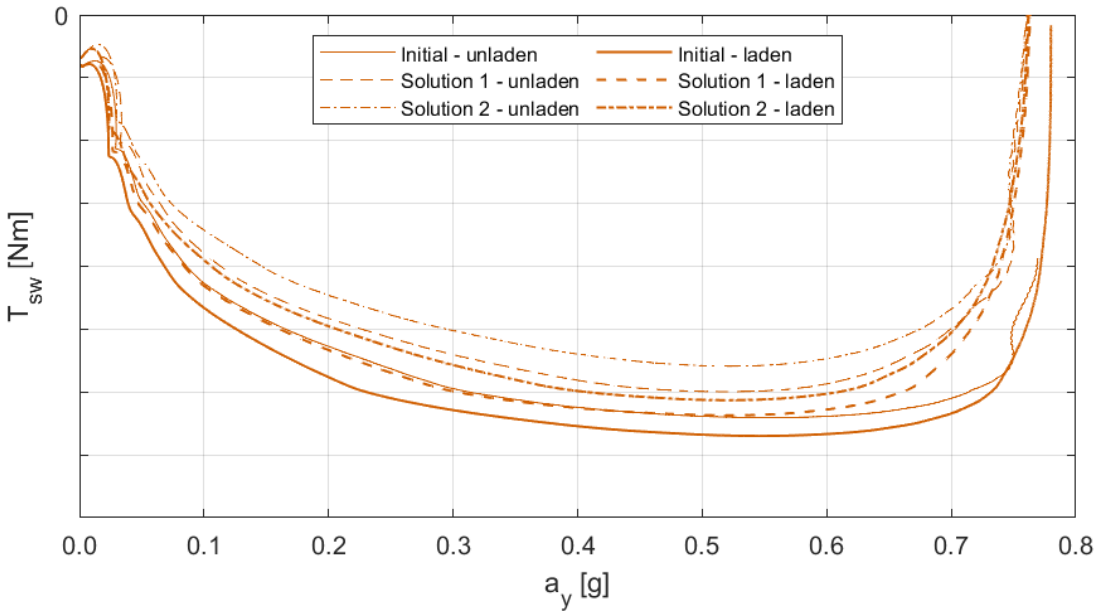

Figure 8.13: Optimization - Ramp Steer - steering wheel torque vs lat. acc.

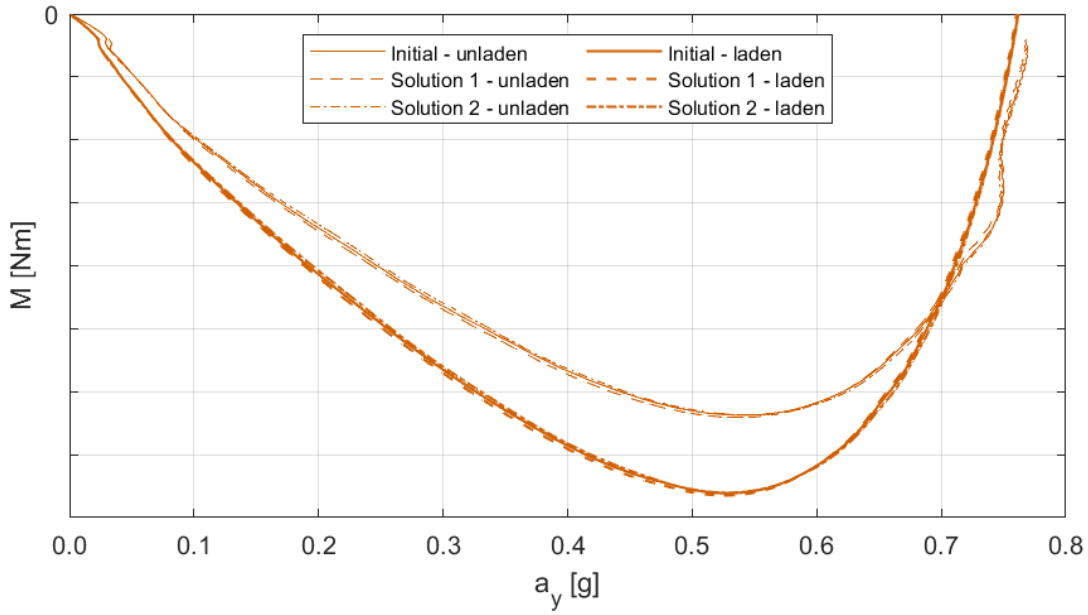

Figure 8.14: Optimization - Ramp Steer - self-aligning moment vs lat. acc.

8.4 Power-Off Cornering

8.4.1 Test Setup

A limited set of Power-Off Cornering tests is performed on both Solutions, to build a comparison with the initial suspension geometry and understand how the transient response is affected by caster moment arm and caster angle. The path radius is always set equal to the standard value, while the lateral accelerations correspond to the maximum engine rotational speed allowed. This way the braking torque is maximized, while the cornering forces in 2nd and 3rd gears are not. Avoiding the minimum path radius prevents any critical response and provides general information without exploring limit phenomena. *Table 8.4* reports the test parameters.

Sampling Time Interval	0.001s
Throttle Release Time Interval	0.1s
Path Radius	100 m
2nd Gear	0.15g
3rd Gear	0.35g
4th Gear	0.65g
Turn Direction	Left
Power Steering	Active

Table 8.4: Optimization - Power-Off Cornering - test setup.

8.4.2 Vehicle Dynamics

Figures from 8.15 to 8.17 show the lateral acceleration, sideslip angle and yaw velocity time histories. Looking at the first quantity, Solution 2 generally shows a slight reduction, except for a temporary increase in 4th gear when the vehicle is laden. Instead, Solution 1 provides either a slight increase or a response similar to the initial suspension. These preliminary considerations should indicate Solution 1 as slightly more prone to close the trajectory.

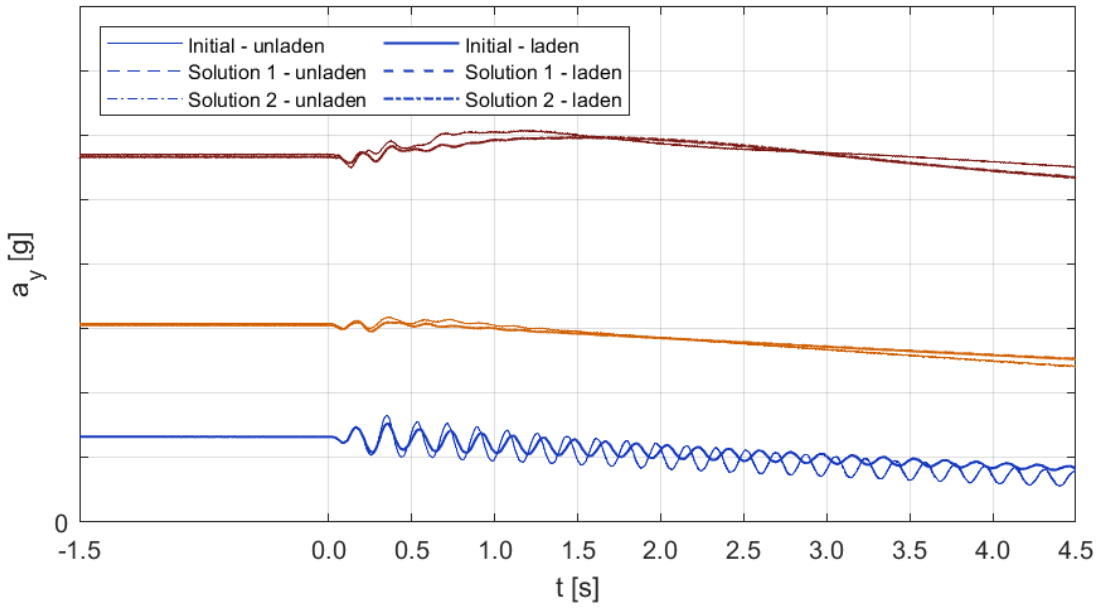

Figure 8.15: Optimization - Power-Off Cornering - lat. acc. vs time.

Looking at the sideslip angle, all vehicles behave similarly in 2nd and 3rd gear, while in 4th gear Solution 2 experiences a slightly greater tendency to a "nose-in" configuration, already detected in Ramp Steer. Similar conclusions are suggested by the yaw velocity, which is a little higher in Solution 2, before converging to the initial geometry in steady-state. Interestingly, the vehicle dynamics during the transient immediately following the power-off instant is almost insensitive to the modifications of the suspension parameters. Some minor differences take place only approaching the vehicle limit and involve the long lasting transient before the vehicle is able to restore the initial condition.

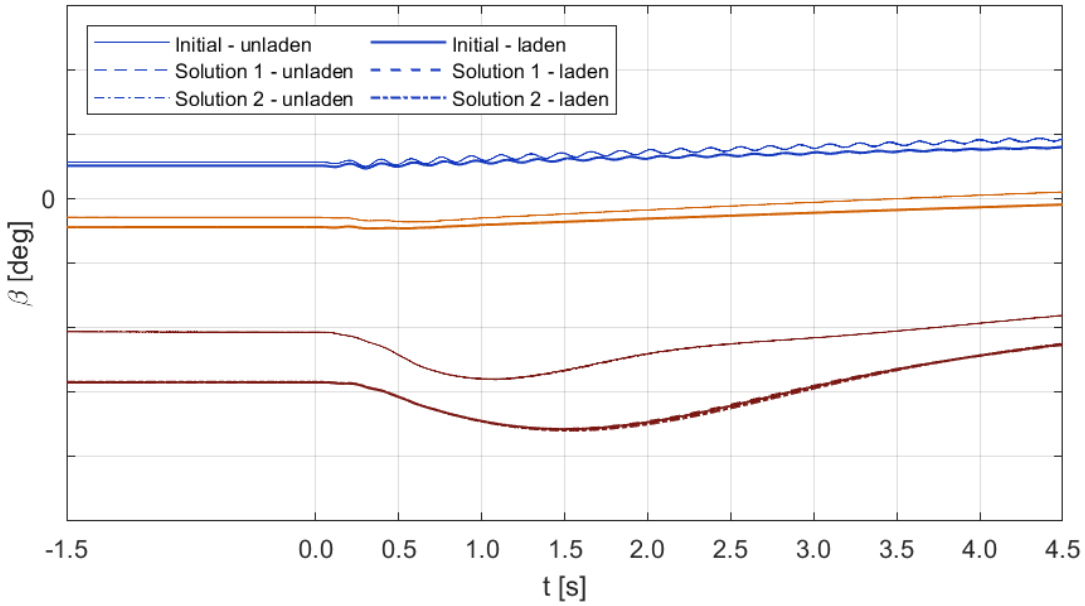

Figure 8.16: Optimization - Power-Off Cornering - sideslip angle vs time.

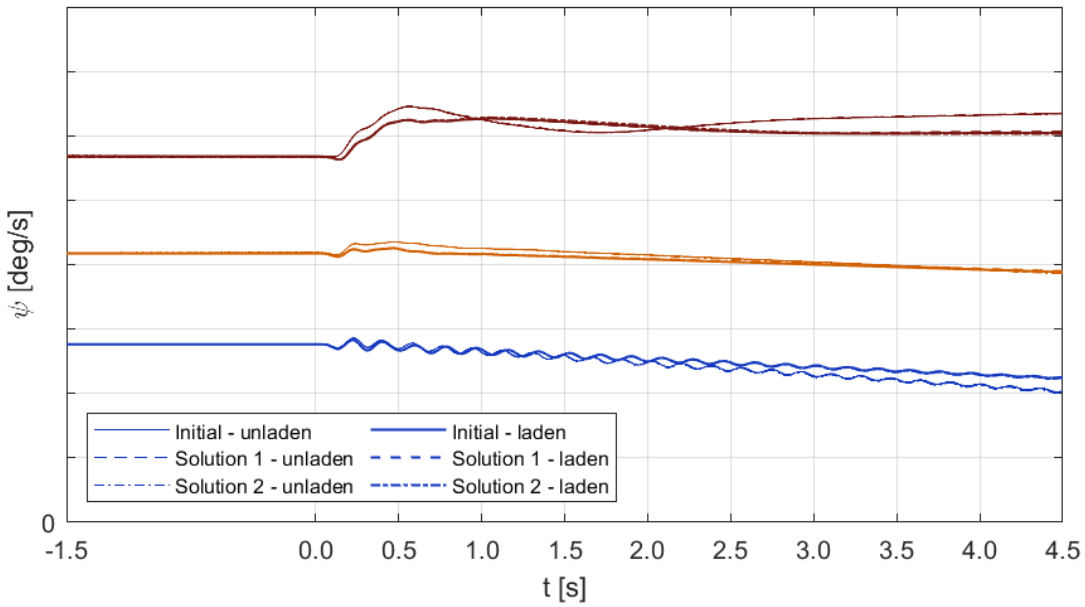

Figure 8.17: Optimization - Power-Off Cornering - yaw velocity vs time.

8.4.3 Tyre Dynamics

Figures 8.18 and 8.19 show the lateral load transfers on both axles, adopting the same definitions seen in the previous Sections. In terms of lateral load transfer, in 2nd and 3rd gears the differences are barely noticeable, with Solution 1 loading the outer side more than Solution 2. Instead, in 4th gear Solution 2 shows a slightly greater lateral load transfer on both axles, while Solution 1 keeps close to the initial geometry. Anyway, once the transient is extinguished, all geometries tend to converge. The response seen on Solution 2 is again coherent with the previous quantities involving the vehicle dynamics, giving the idea that this geometry provides a slightly greater tendency to close the trajectory at high lateral accelerations.

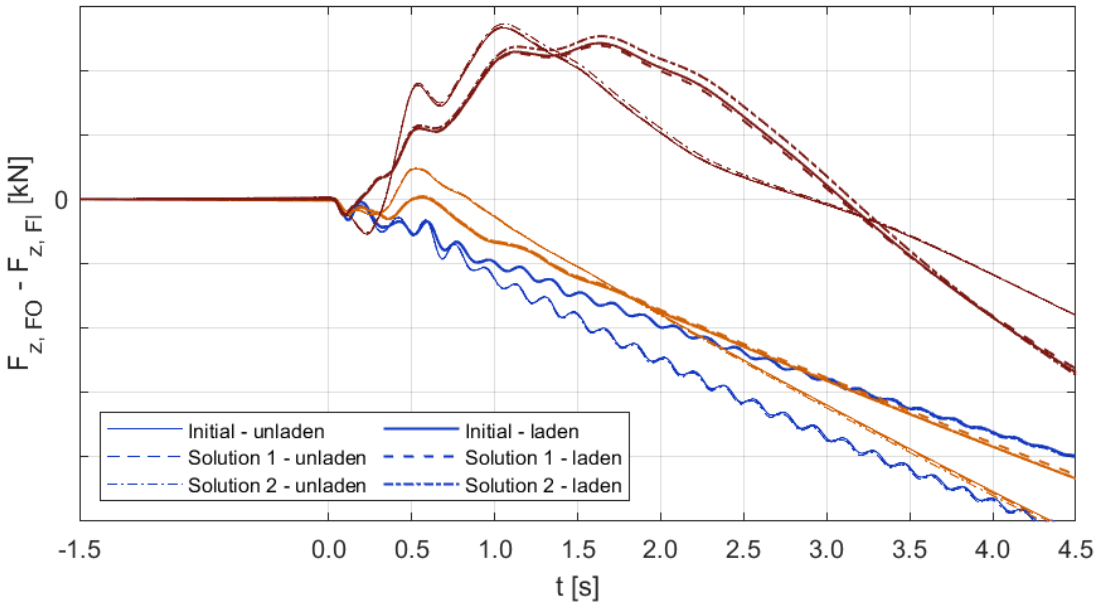

Figure 8.18: Optimization - Power-Off Cornering - front lateral transfer vs time.

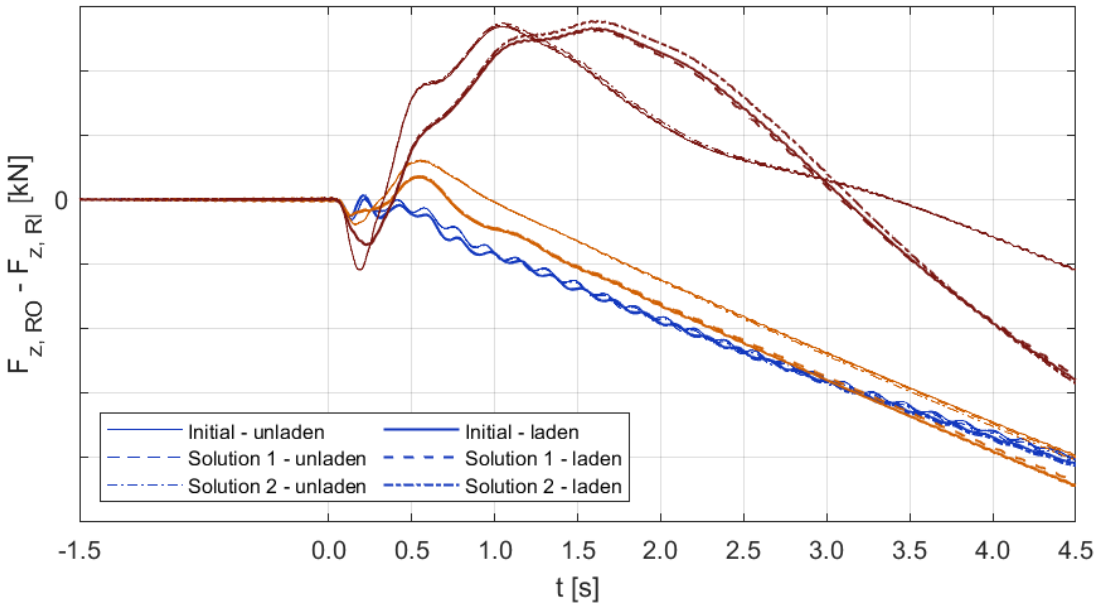

Figure 8.19: Optimization - Power-Off Cornering - rear lateral transfer vs time.

Figure 8.20 shows the understeer gradient time history. This quantity is affected by the different steering ratios of the three suspensions, which can explain why Solution 1 shows such a greater gradient. Some considerations on handling can be drawn looking at the path radius reported in *Figure 8.21*. Solution 2 generally looks less prone to close the trajectory, apart from the temporary decrease in understeer already detected in 4th gear when the vehicle is laden. Instead, Solution 1 displays a consistent tendency to decrease the path radius in its laden configuration, while it behaves closer to the initial geometry in the unladen condition.

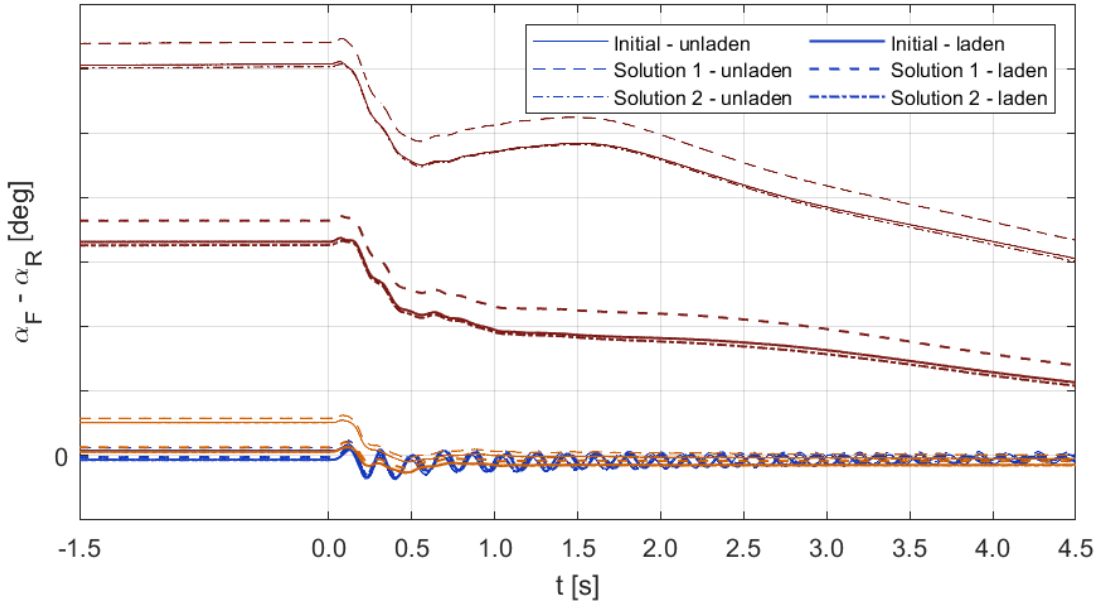

Figure 8.20: Optimization - Power-Off Cornering - understeer gradient vs time.

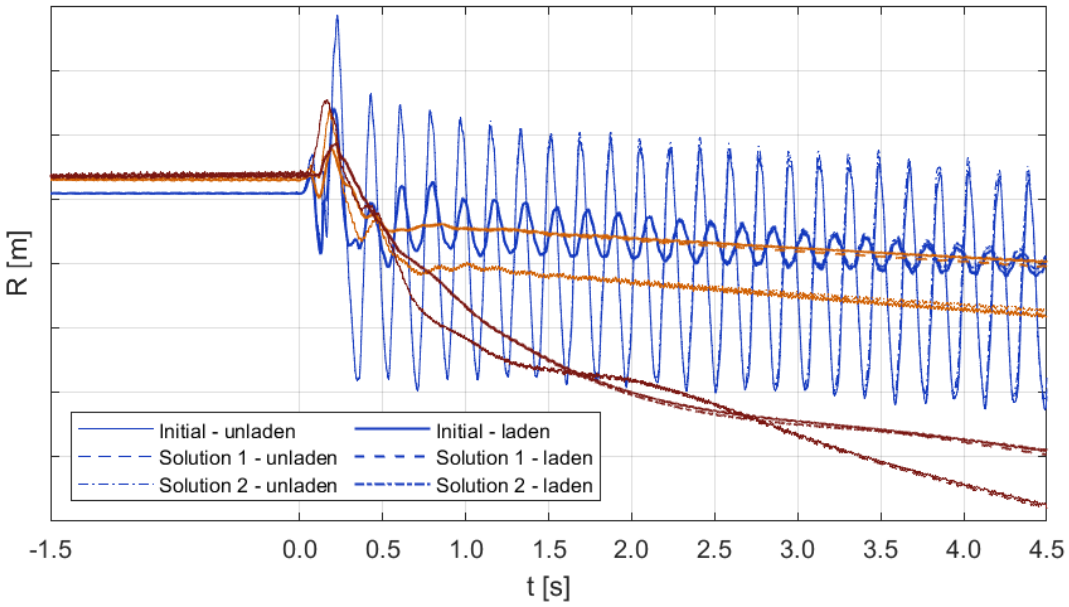

Figure 8.21: Optimization - Power-Off Cornering - path radius vs time.

8.4.4 Steering System

Figures from 8.22 to 8.24 show the steering wheel torque, self-aligning moment on the front wheels and steering rack stroke time histories. Looking at the first quantity, it is immediately noticeable that the activation of power steering allows a dramatic reduction in the steering wheel torque required to the driver. A side effect of power steering is an overall flattening of the curves, also in terms of rack stroke, which looks almost constant.

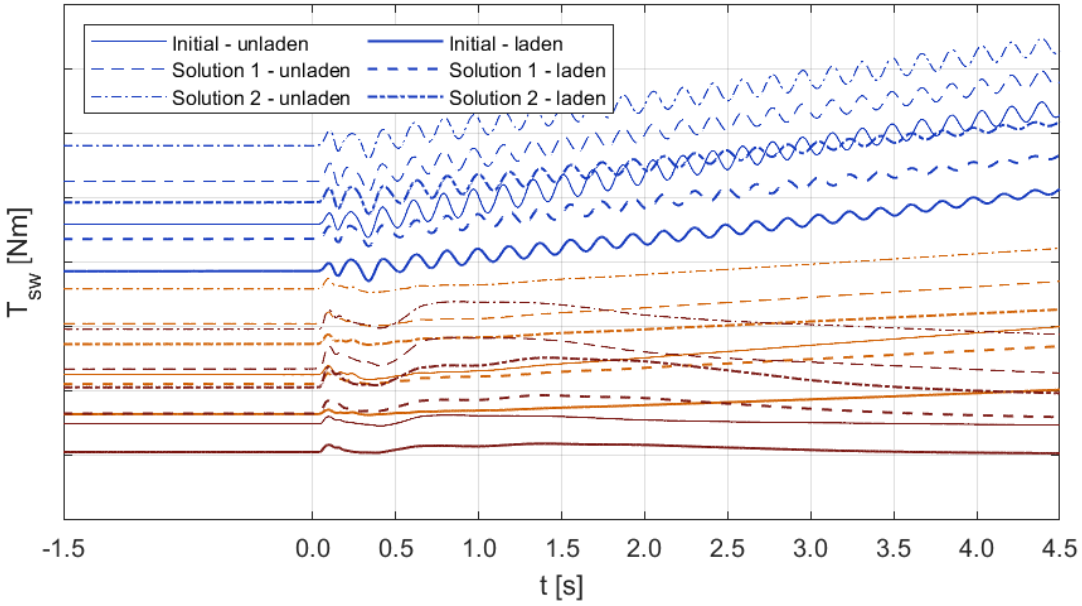

Figure 8.22: Optimization - Power-Off Cornering - steering wheel torque vs time.

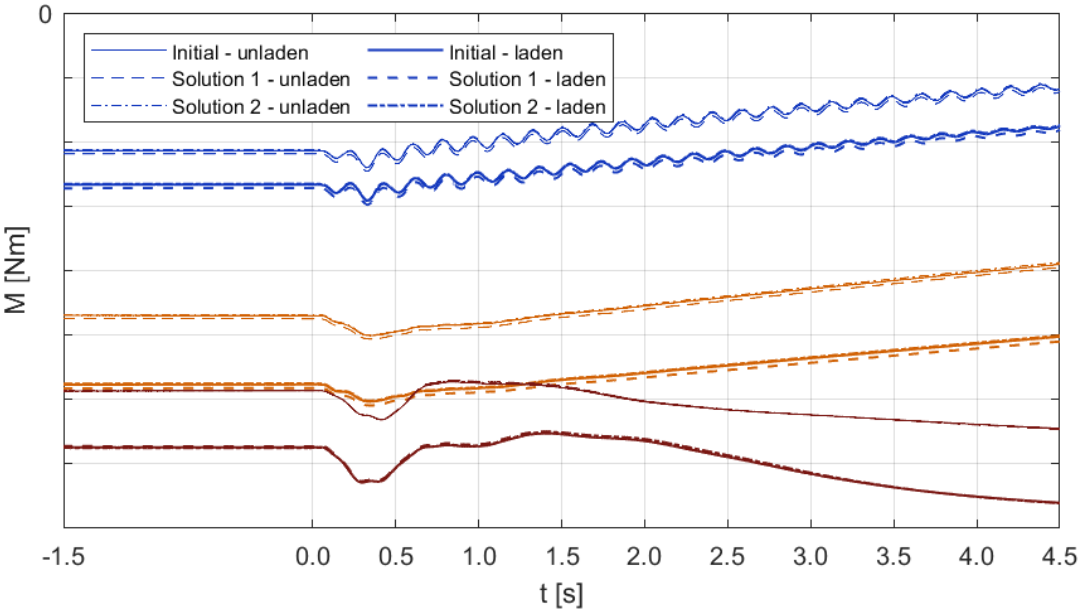

Figure 8.23: Optimization - Power-Off Cornering - self-aligning moment vs time.

In terms of rack stroke, the only difference between the three suspensions is represented by its mean value, which is greater for Solution 2, where the steering ratio is increased. Instead, Solution 1 has a slightly lower rack stroke, as a consequence of its lower steering ratio. The initial geometry requires the greatest torque, which is minimized by the reduction in caster moment arm, especially on Solution 2, as already observed in Ramp Steer. At the same time, both Solutions seem to emphasize the transient decrease following the power-off instant, in 3rd and 4th gears, while the initial geometry shows an almost constant steering wheel torque. Instead, in 2nd gear the vibrations are completely insensitive to any change in the suspension parameters. Looking at the wheels self-aligning moment, Solution 1 generally shows slightly greater values, especially in 2nd and 3rd gears, where the wheels breaking torque is greater. Anyway, the overall trend is almost identical on all geometries and the differences are modest, provided the dependency mainly on pneumatic trail and not on caster moment arm.

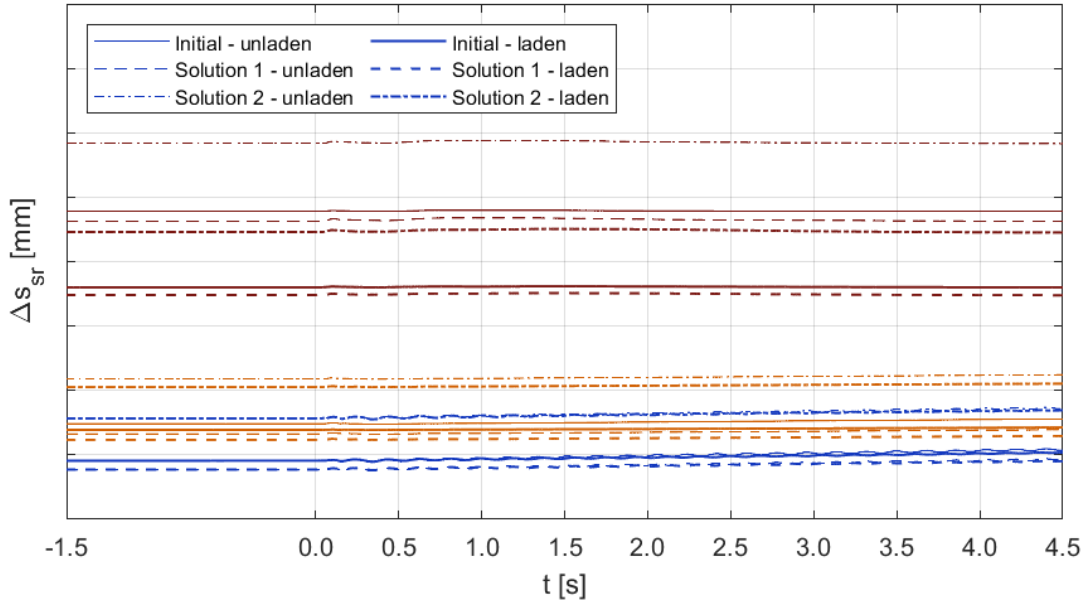

Figure 8.24: Optimization - Power-Off Cornering - rack stroke vs time.

8.5 Throttle-On In-Turn

8.5.1 Test Setup

The last set of tests to compare these three suspensions is made of a few Throttle-On In-Turn maneuvers performed at the standard path radius with maximized longitudinal acceleration. These tests are selected as the most representative of a generic acceleration maneuver, without changing path radius as previously done in the comparison between Front and Rear-Wheel-Drive vehicles, to exclude tyre saturation and any limit phenomena and provide general information about the different suspension layouts. The testing parameters are reported in *Table 8.5*.

Sampling Time Interval	0.001s
Throttle Step Time Interval	1.0s
Path Radius	100 m
2nd Gear	0.035g
3rd Gear	0.085g
4th Gear	0.175g
Turn Direction	Left
Power Steering	Active

Table 8.5: Optimization - Throttle-On In-Turn - test setup.

8.5.2 Vehicle Dynamics

Figures from 8.25 to 8.27 show the lateral acceleration, sideslip angle and yaw velocity time histories. A close look indicates that Solution 2 tends to increase its lateral acceleration slightly more with respect to the other two suspension geometries, revealing a likeliness to reduce understeer. Solution 1 shows a barely noticeable increase as well, especially in 2nd gear. As in Power-Off Cornering, the short transient is insensitive to the suspension layout and the differences are located only in the region close to the new steady-state.

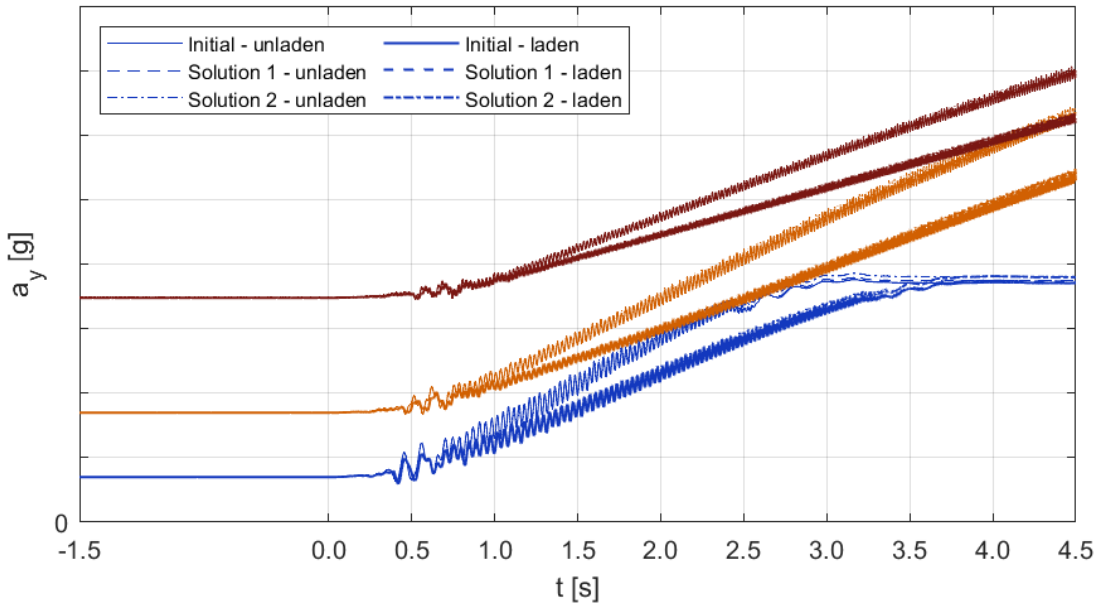

Figure 8.25: Optimization - Throttle-On In-Turn - lat. acc. vs time.

Looking at the sideslip angle, all vehicles behave similarly and the differences become negligible, with Solution 2 keeping slightly more "nose-out" than the other two vehicles. Instead, the yaw velocity provides results similar to the lateral acceleration, since Solution 2 is again slightly more prone to an increase in yaw rate. Overall, provided that the initial transient does not stress the differences in suspension parameters, this test suggests that Solution 2 is generally less likely to widen its trajectory due to the acceleration maneuver, while Solution 1 behaves closely to the initial vehicle. The laden configuration emphasizes this different response between Solution 2 and the other two vehicles.

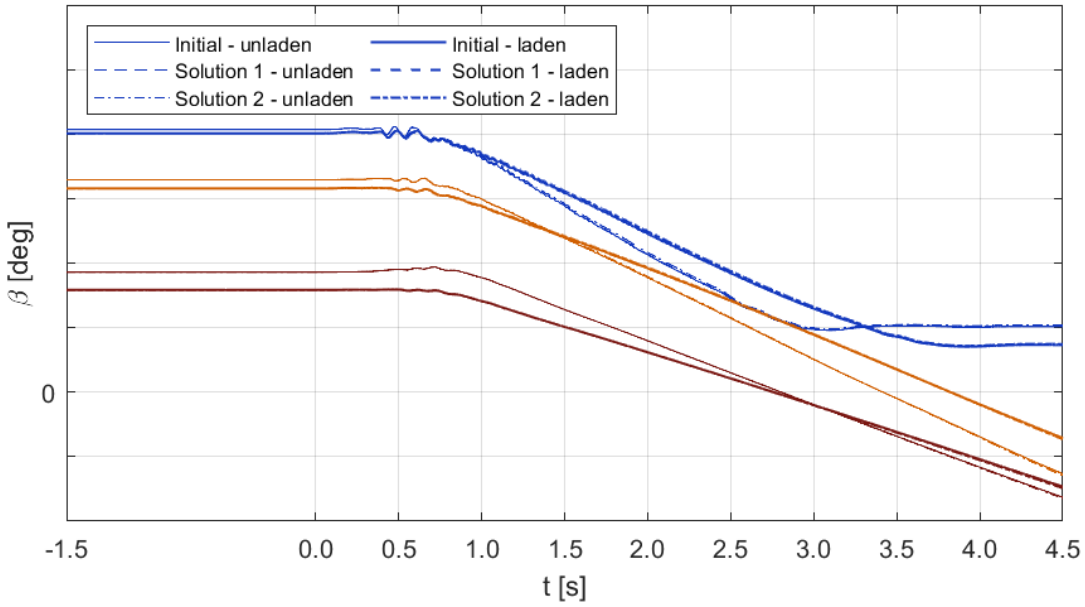

Figure 8.26: Optimization - Throttle-On In-Turn - sideslip angle vs time.

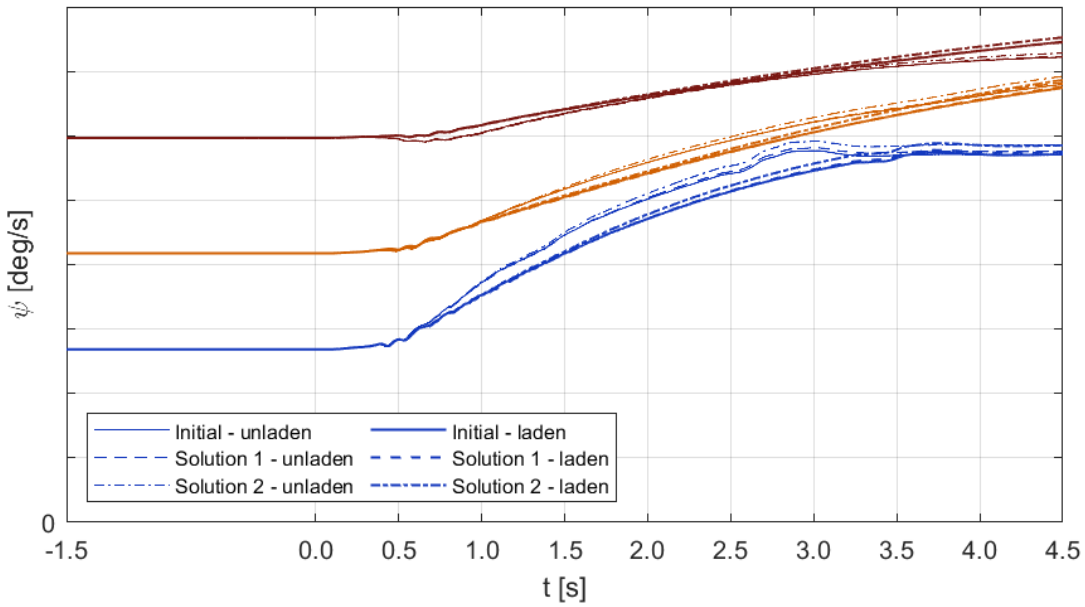

Figure 8.27: Optimization - Throttle-On In-Turn - yaw velocity vs time.

8.5.3 Tyre Dynamics

Figures 8.28 and 8.29 show the lateral load transfers on both axles, adopting the same definition seen in the previous Sections, which allows to isolate the contribution of the maneuver. As in Power-Off Cornering, Solution 2 displays an increased load transfer to the outer wheel on both axles. This response, shared by both loading conditions, further confirms the tendency to increase its yaw rate and reduce the path radius.

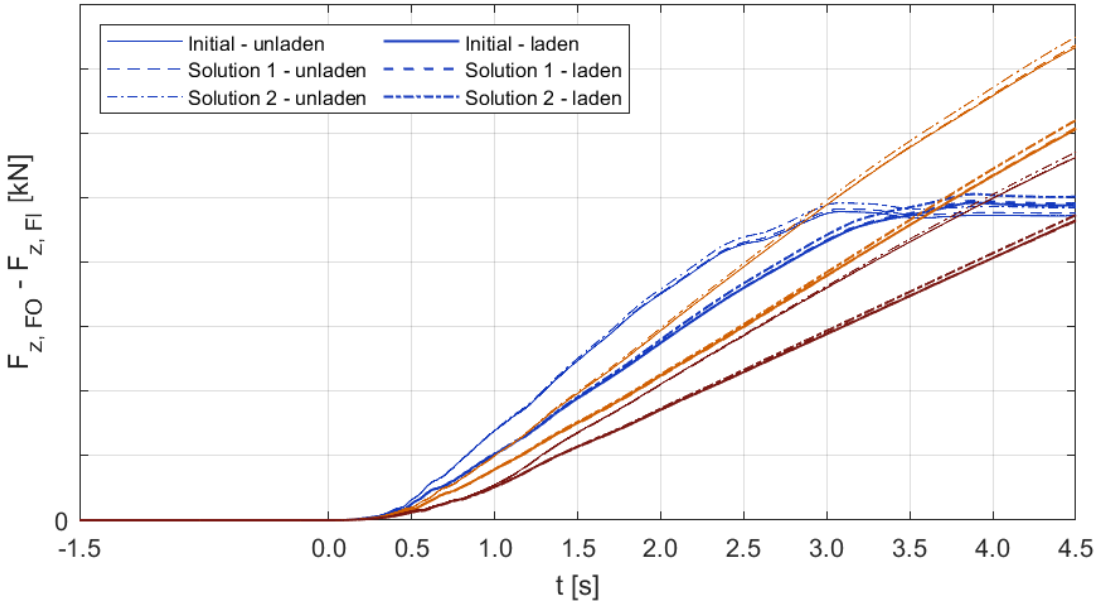

Figure 8.28: Optimization - Throttle-On In-Turn - front lateral transfer vs time.

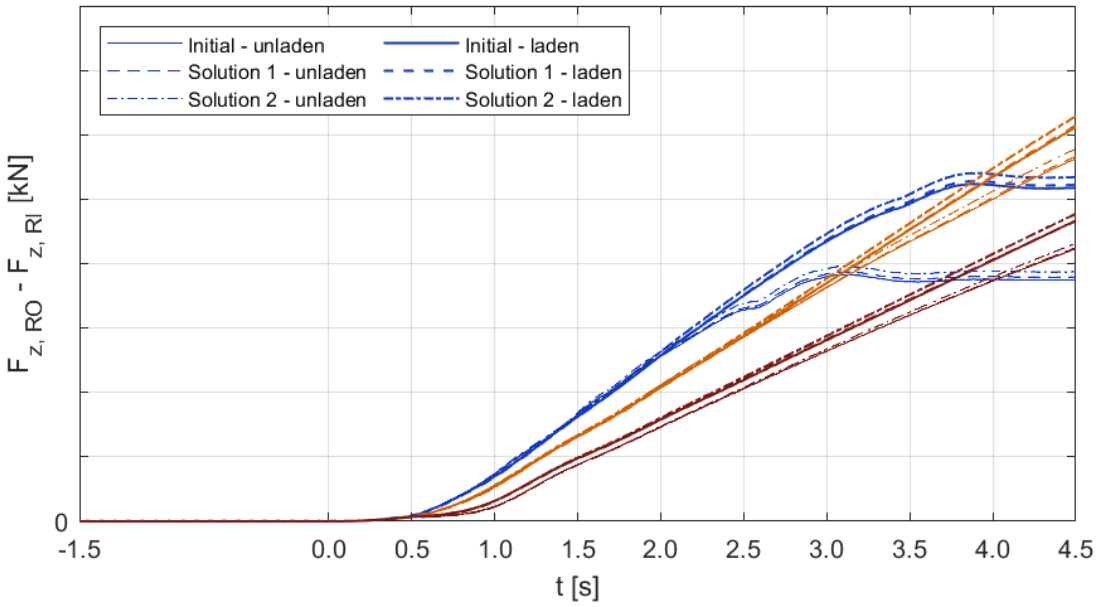

Figure 8.29: Optimization - Throttle-On In-Turn - rear lateral transfer vs time.

Figure 8.30 shows the understeer gradient time history. Solution 1 displays a greater gradient both in steady-state and transients, while Solution 2 gets close to the initial suspension geometry and does not manifest any noticeable difference, despite the previous suggestions. Interestingly, both Solutions seem more understeering during the accelerator step, but then Solution 2 converges to the initial vehicle. This results contradict the path radius shown in *Figure 8.31*, where Solution 2 shows an evidently narrower trajectory, with Solution 1 slightly less understeering with respect to the initial geometry as well, as previously suggested by the other quantities. The understeer gradient is clearly affected by the different steering ratios of each suspension layout, as previously seen in Ramp Steer.

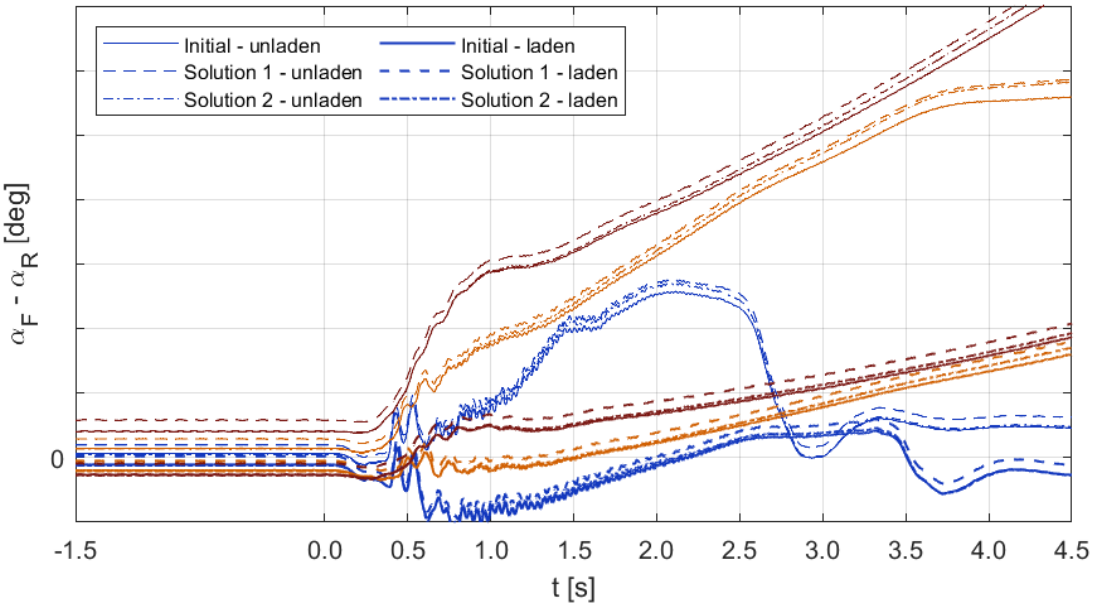

Figure 8.30: Optimization - Throttle-On In-Turn - understeer gradient vs time.

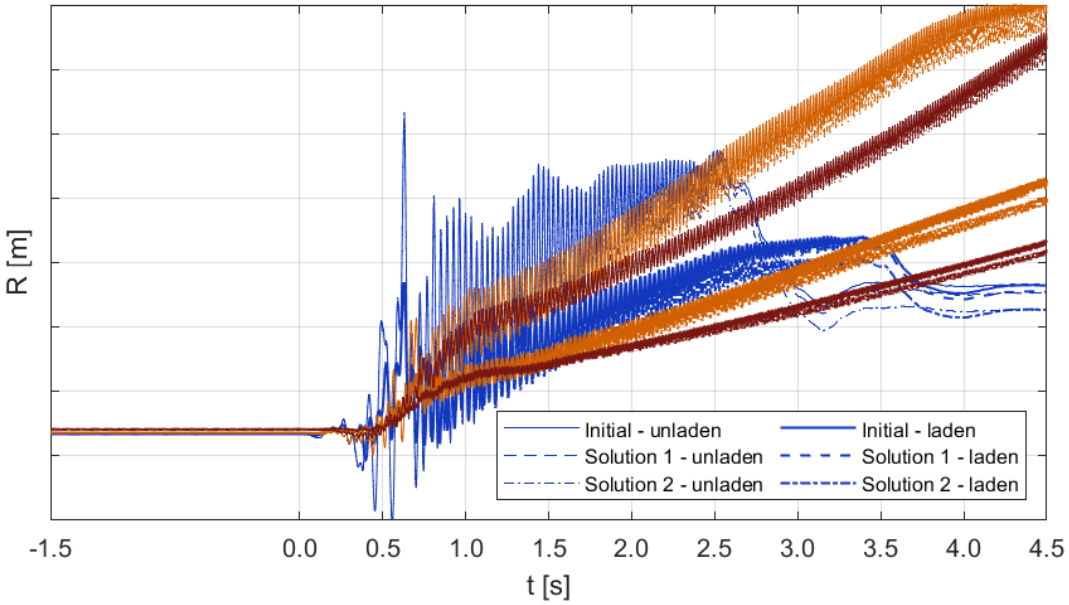

Figure 8.31: Optimization - Throttle-On In-Turn - path radius vs time.

8.5.4 Steering System

Figures from 8.32 to 8.34 show the steering wheel torque, self-aligning moment on the front wheels and steering rack stroke time histories. As in Power-Off Cornering, the response of the steering wheel torque is mainly affected in its mean value, meaning a vertical offset, with Solution 2 providing the minimum torque required to the driver. Both Solutions provide a little reduction in the amplitude of the transient oscillations and a slightly lower slope in the region following the oscillations, before the new steady-state is reached. Concerning the wheels self-aligning moment, it is enhanced by Solution 1, while it is slightly reduced on Solution 2.

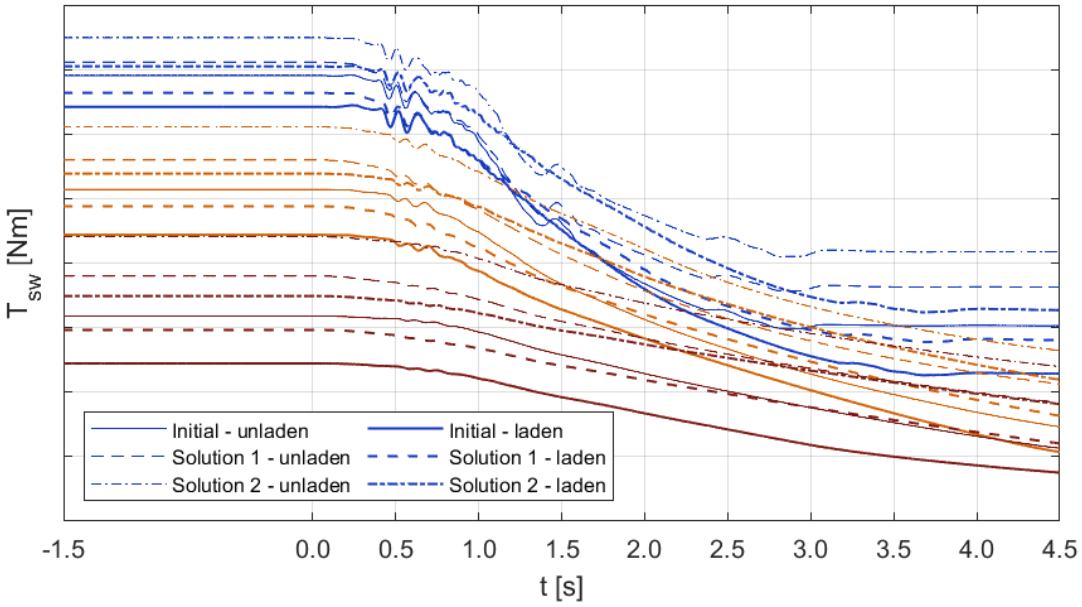

Figure 8.32: Optimization - Throttle-On In-Turn - steering wheel torque vs time.

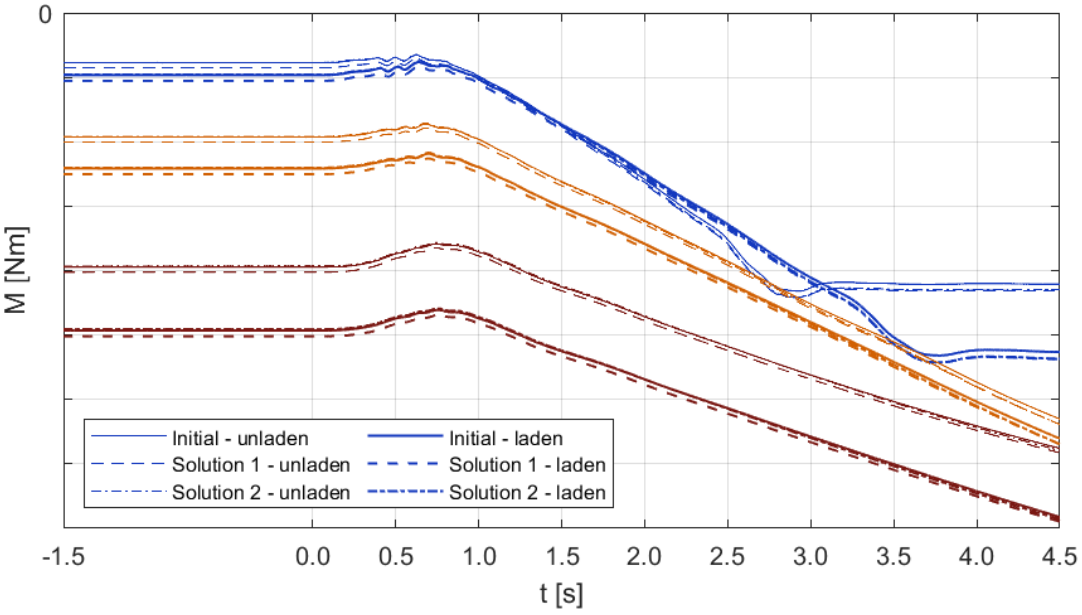

Figure 8.33: Optimization - Throttle-On In-Turn - self-aligning moment vs time.

Looking at the steering rack stroke, the influence of the suspension layout in terms of steering ratio is evident. Solution 1 has a slightly lower steering ratio, which turns into a reduced rack stroke, while Solution 2 displays a huge increase in stroke, associated with a significantly greater steering ratio. Nevertheless, the suspension layout affects primarily the mean value of rack stroke, but not its trend, which is common to all vehicles, as in the two previous quantities.

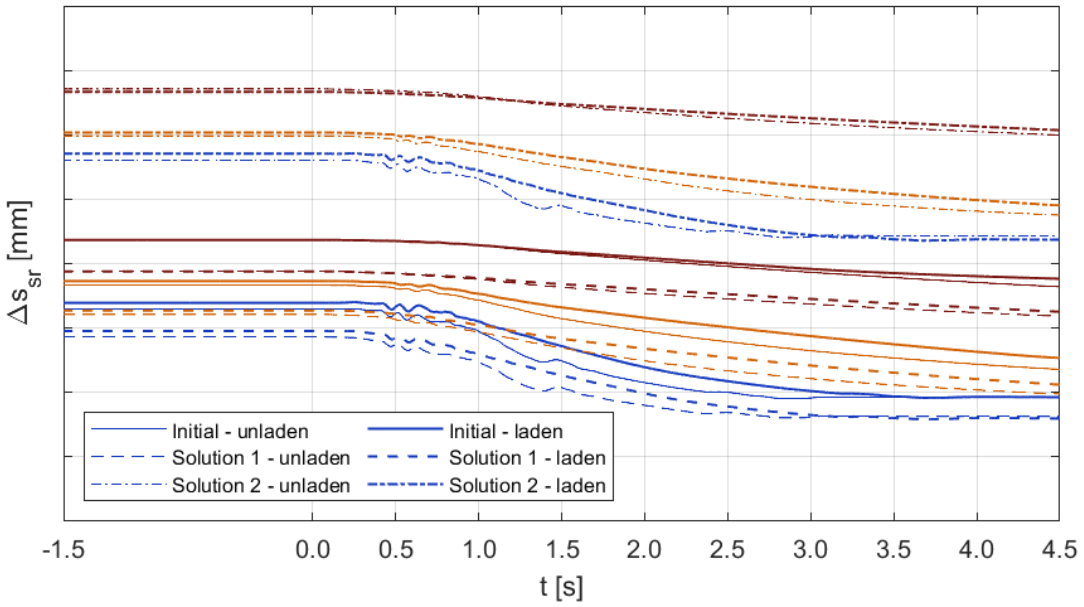

Figure 8.34: Optimization - Throttle-On In-Turn - rack stroke vs time.

8.6 Conclusions

Scaling the mechanical trail down to 1/3 of its initial value firstly results in a significant reduction in the steering wheel torque required to the driver. At the same time, it implies a variation in steering ratio, especially on Solution 2, thus heavily affecting the rack stroke. In terms of steady-state handling, Solution 1 is more understeering, while Solution 2 displays a lower understeer with respect to the initial suspension. The response on Solution 1 is potentially affected by the drop in camber recovery, which might also result in severe tyre wear. During transient maneuvers instead, Solution 1 seems to be at least as much sensitive as the initial suspension, with the laden condition generally more prone to emphasize understeer during accelerations and oversteer when decelerating. On the other hand, Solution 2 is more likely to emulate the neutral vehicle condition, meaning that its trajectory is less affected by any action on the accelerator pedal while negotiating a curve. Adopting a global perspective, although Solution 1 requires the modification of a lower number of mechanical components, namely the upper control arm and upright, it looks less applicable due to the drop in caster angle, which affects many aspects of a suspension setup and makes the vehicle farther from the neutral condition. Instead, the implementation of Solution 2 seems more challenging from the industrial viewpoint, because the lower control arm is modified as well, but allows to preserve the initial caster angle, with a slight overall tendency towards a neutral behaviour.

9 Conclusions

This Thesis investigates the influence of the drivetrain over a front double wishbone suspension and its effects in terms of handling in both steady-state and transient cornering maneuvers.
The first step consists in the development of a working Adams/Car Front-Wheel-Drive model derived from the Rear-Wheel-Drive vehicle provided by the manufacturer, previously adapted to two different loading configurations. The conversion is based on reverting the driveline to transfer the torque to the front wheels. Specifically, the front suspension is equipped with a pair of drive shafts, the tripods and a differential box. The rear suspension instead is deprived of these elements to obtain an idle axle, while the propeller shaft is shortened and oriented towards the front axle. The Adams/Car model just obtained is not meant to be representative of a real Front-Wheel-Drive vehicle, since the Thesis is part of a wider study and only concerns how the drivetrain is involved in the van road-holding ability and handling.
The second step consists in a comparison between the Adams/Car Rear-Wheel-Drive model and the available experimental data, for both suspension and full-vehicle tests. The model shows some differences that can be ascribed mainly to the front double wishbone suspension modelling, which implies some assumptions letting the model be less faithful to the reality. Anyway, provided the comparative nature of this Thesis, which investigates the behaviours displayed by Front and Rear-Wheel-Drive models, this is not a major drawback.
The third step is a set of simulations of Cornering Events, which are setup according to the existing ISO standard and run through the full range of lateral accelerations achievable by the case study. The results generally suggest a comparable behaviour between Front and Rear-Wheel-Drive vehicles. The different responses taking place in Power-Off Cornering and Throttle-On In-Turn indicate that the actual double wishbone suspension installed on Rear-Wheel-Drive vehicles can be taken as a reference when optimizing it for Front-Wheel-Drive.
The last step provides some guidelines concerning the optimization of the above mentioned double wishbone suspension. This preliminary study does not concern packaging, nor how Front-Wheel-Drive should be implemented on the van, instead it investigates how a reduction in caster moment arm, along with a reduction or preservation of caster angle, affects the handling performance and steering feedback of the hypothetical Front-Wheel-Drive vehicle. The examined solutions show some variations in both fields of interest and affect both steady-state and transient responses, allowing the van to either emphasize its sensitivity to such maneuvers or approach the neutral vehicle condition. Some additional considerations such as tyre wear and manufacturability are obviously complementary to the guidelines here provided.

10 References

[1] *Road vehicles - Types - Terms and definitions*. Standard ISO 3833:1977(E). Vernier, Geneva, Switzerland: International Organization for Standardization, Dec. 1977.

[2] *IVECO S.p.A.* `https://www.iveco.com/italy`. Accessed: 20-04-2023.

[3] Genta G. Morello L. *The Automotive Chassis Volume 2: System Design*. Ed. by Springer. II Edition. 2020.

[4] *Road vehicles - Vehicle dynamics and road-holding ability - Vocabulary*. Standard ISO 8855:2011(E). Vernier, Geneva, Switzerland: International Organization for Standardization, Dec. 2011.

[5] Guiggiani M. *The Science of Vehicle Dynamics*. Ed. by Springer. II Edition. 2018.

[6] Genta G. Morello L. *The Automotive Chassis Volume 1: Components Design*. Ed. by Springer. II Edition. 2020.

[7] Hexagon MSC Software. *Adams/Car*. Adams Help.

[8] Candela A. *Analisi numerica e sperimentale delle caratteristiche elastocinematiche delle sospensioni di un veicolo commerciale leggero*. Master's Thesis. Politecnico di Torino, A.Y.2021/2022.

[9] Romano F. *Multi-Body modelling and mathematical analysis of a steering system adopted on a light-duty commercial vehicle*. Master's Thesis. Politecnico di Torino, A.Y.2021/2022.

[10] *Passenger cars - Steady-state circular driving behaviour - Open-loop test methods*. Standard ISO 4138:2021(E). Vernier, Geneva, Switzerland: International Organization for Standardization, Sept. 2021.

[11] *Passenger cars - Vehicle dynamic simulation and validation - Steady-state circular driving behaviour*. Standard ISO 19364:2016(E). Vernier, Geneva, Switzerland: International Organization for Standardization, Oct. 2016.

[12] *Passenger cars - Power-off reaction of a vehicle in a turn - Open-loop test method*. Standard ISO 9816:2018(E). Vernier, Geneva, Switzerland: International Organization for Standardization, Apr. 2018.

11 Appendix

11.1 Cornering Events

Both Power-Off Cornering and Throttle-On In-Turn tests are built according to ISO 9816:2018. The former is the one described in the standard and Adams/Car offers a rich setup wizard with many options, even though in this Thesis the test is formulated to be fully compliant with the prescriptions. The latter is not standardized and Adams/Car offers a quite poor setup wizard, therefore it is developed using the Event Builder tool, taking Power-Off Cornering as reference.

11.1.1 Power-Off Cornering

Figure 11.1 shows the setup wizard accessible in Adams/Car selecting *Simulate/Full-Vehicle Analysis/Cornering Events/Power-Off Cornering*. A few considerations to get a test setup compliant with ISO 9816:2018:

- *Step Size*: it is set equal to 0.001s. Bigger steps allow a reduction in the computational effort, however some oscillatory phenomena are not properly simulated
- *Road Data File*: it is the default flat road file implemented in the software
- *Gear*, *Lateral Acceleration*, *Turn Direction*: they are set depending on the specific test and determine the initial vehicle speed and steering wheel angle
- *Turn Radius*: it can be set equal to 100 m or decreased down to 30 m, which are respectively the standard and minimum permissible values prescribed in ISO 9816:2018
- *Steering Input*: it is set to *lock steering during Power-Off*. There is another option which allows the steering wheel motion to maintain the initial path radius, but it is not compliant with the standard, which specifies to keep the steering wheel locked
- *Disengage Clutch during Power-Off*: it is not selected, because the standard explicitly prescribes to maintain the clutch engaged
- *Throttle Delay*: it represents the power-off instant. It is set equal to 5.0s to have a time long enough to ensure a steady-state initial condition. The results can be cut in the Adams/PostProcessor to consider only 1.5s before the power-off instant
- *Throttle Step Duration*: it is set equal to 0.1s, which is the default value, assumed as reasonable to simulate a sudden accelerator pedal release

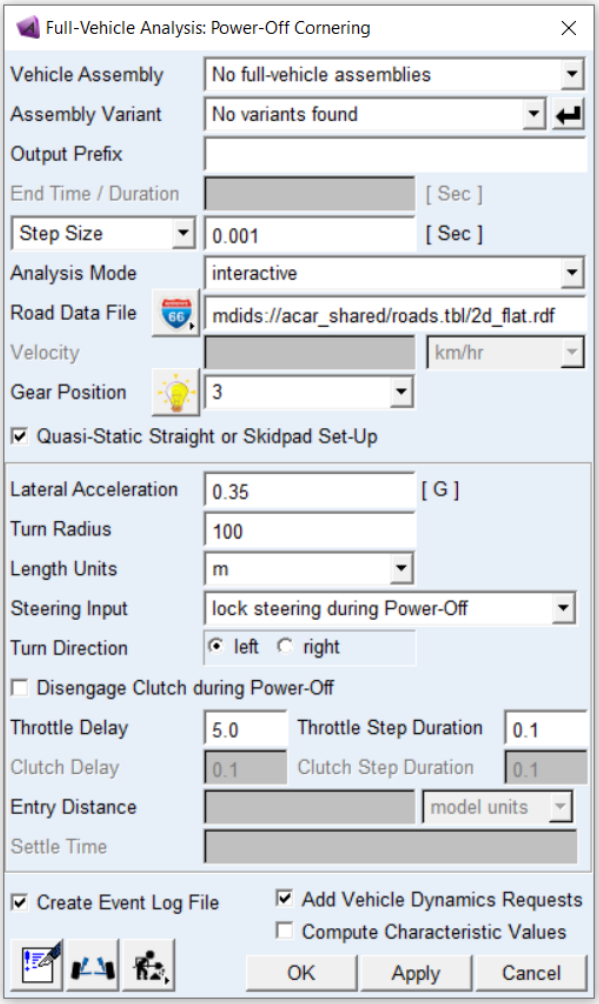

Figure 11.1: Appendix - Power-Off Cornering - setup wizard.

11.1.2 Throttle-On In-Turn

As explained in the dedicated Chapter, Throttle-On In-Turn is the name given to another cornering event in Adams/Car. However, its setup wizard has a limited control over the accelerator pedal, because it only allows to define the vehicle longitudinal acceleration and its time duration. To overcome these limitations, the tool accessible selecting *Simulate/Full-Vehicle Analysis/Event Builder* is exploited. *Figure 11.2* shows the first page page of the Event Builder. The upper part of the wizard includes *Static Setup* which corresponds to the steady-state in Power-Off Cornering. A few considerations:

- *Speed*: it is not modified and is automatically computed basing on the other parameters
- *Gear*: it is selected depending on the initial lateral acceleration, as in Power-Off Cornering
- *Task*: it is set to *skidpad*
- *Turn Direction*, *Radius* and *Lat. Acc.*: they are set as in Power-Off Cornering. The only difference lies in the lateral acceleration, here expressed in m/s^2

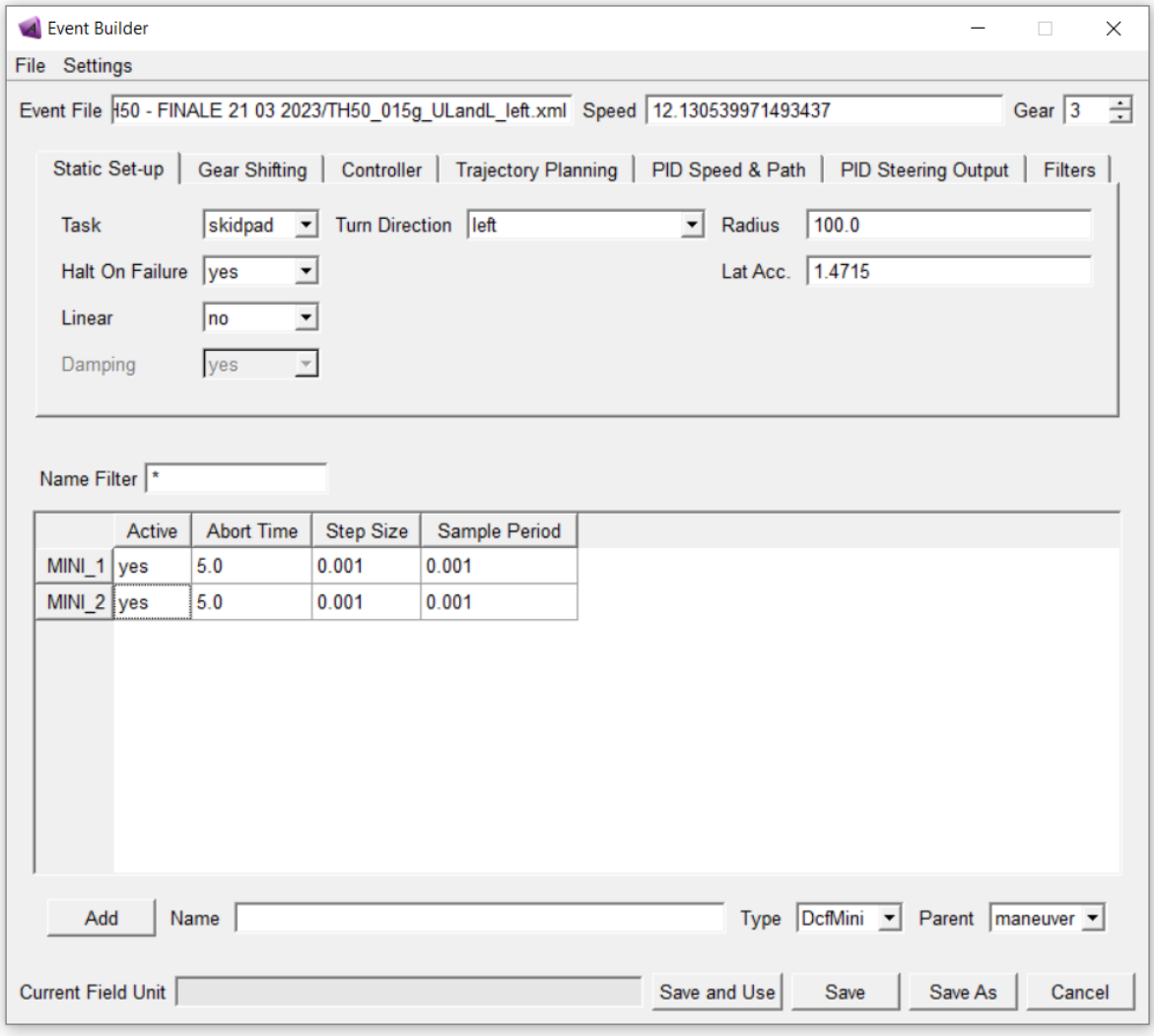

Figure 11.2: Appendix - Event Builder - setup wizard.

The lower part of the wizard contains the mini-maneuvers, each one defined by an *Abort Time* and a *Step Size*. The two mini-maneuvers are defined as follows:

1. Maintaining the skidpad steady-state. Main details shown in *Figure 11.3*:
    - *Abort Time*: it is set equal to 5.0s, because it corresponds to *Throttle Delay* in Power-Off Cornering
    - *Step Size*: it is set equal to 0.001s as in Power-Off Cornering
    - *Steering*: to lock the steering wheel, the parameters are set so that its *rotation* has a null *Relative Control Value*, meaning that it is not rotated with respect to its initial position, previously defined by the *Static Setup*
    - *Throttle*: it is controlled so that the vehicle *maintains* its *initial target* velocity, in agreement with the prescriptions in ISO 9816:2018
    - *Gear*: it is managed similarly to *Steering*, because the test never contemplates a gear shift, as in Power-Off Cornering
    - *Clutch*: it is managed similarly to *Steering*, because the test resembles Power-Off Cornering, where the clutch is always engaged

2. Accelerating the vehicle. Main details shown in *Figure 11.4*:

   - *Abort Time*: it is set equal to 5.0s, because the total duration of the release maneuver in Power-Off Cornering automatically lasts around 5.0s
   - *Step Size*: it is set equal to 0.001s as in Power-Off Cornering
   - *Steering*: it is managed as in the first mini-maneuver
   - *Throttle*: it is controlled so that it reaches its *Absolute Final Value* through a *step* function whose *Duration* is 1.0s. For lateral accelerations up to 0.35g, the accelerator reaches 50% for both loading configurations, while above 0.35g the two conditions feature different values, which are listed in the dedicated Chapter
   - *Gear*: it is managed as in the first mini-maneuver
   - *Clutch*: it is managed as in the first mini-maneuver

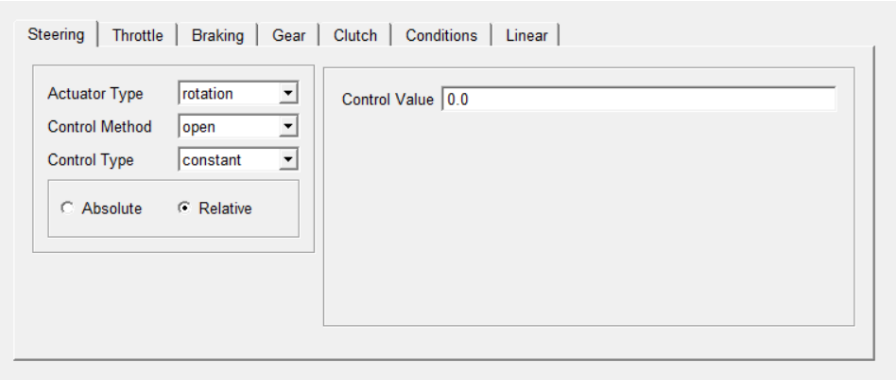

(a) Steering.

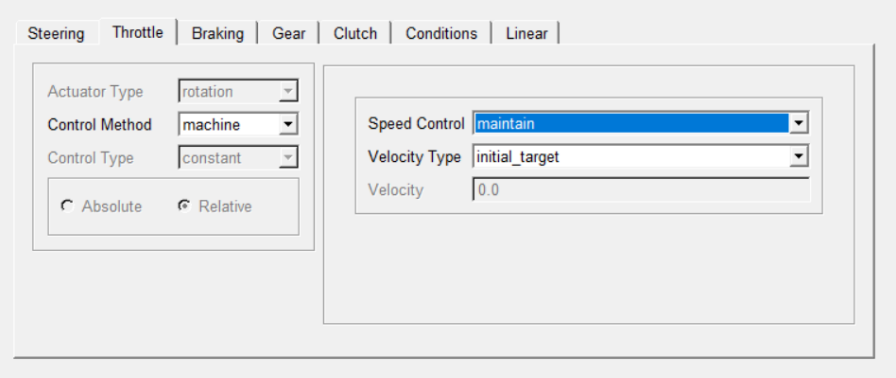

(b) Throttle.

Figure 11.3: Appendix - Event Builder - mini-maneuver 1.

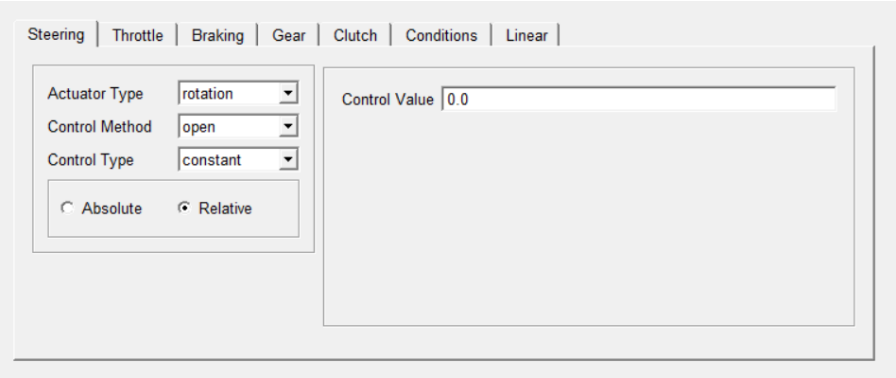

(a) Steering.

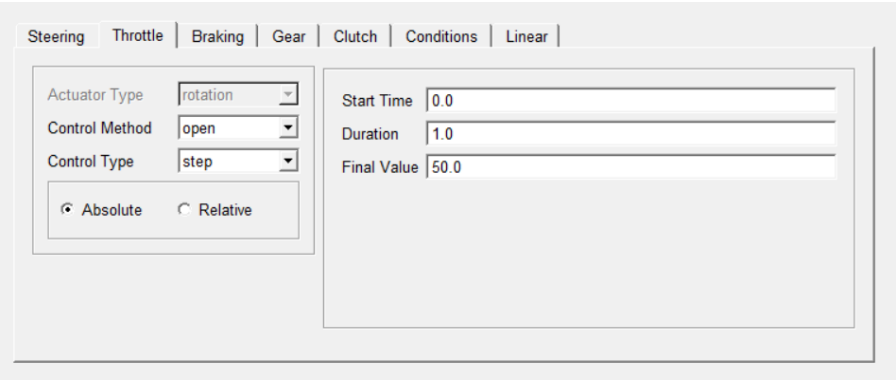

(b) Throttle.

Figure 11.4: Appendix - Event Builder - mini-maneuver 2.

Once the Throttle-On In-Turn files are created in the *Event Builder*, they are loaded and used to run simulations selecting *Simulate/Full-Vehicle Analysis/File Driven Events*. The *Road Data File* is again the default flat road file implemented in the software.

11.2 Problems Encountered

The development a Front-Wheel-Drive Adams/Car model was accompanied by a few issues needing simple but essential modifications to make the vehicle work properly and consistently.

11.2.1 Steering Rack Resonance

While simulating both Power-Off Cornering and Throttle-On In-Turn, an instability phenomenon used to take place when the vehicle was in the laden configuration and was working in the field of lateral accelerations between 0.15g and 0.25g. The problem involved both Rear and Front-Wheel-Drive models, therefore it could not be ascribed to the transition from one drivetrain to another, but only to the definition of the loading conditions. The source of this instability was identified looking at the propagation of vibrations on the components of both driveline and steering system. The former did not show any anomaly, while the latter displayed some fluctuations in the forces exchanged between the tie rods and the steering rack. Going back through the entire steering chain, the problem was identified in a resonance phenomenon involving the steering rack. This phenomenon forced the front wheels to rapidly change their steer angles with an increasing amplitude, thus explaining the overall instability and the fluctuating forces on tie rods. The solution consisted in doubling the value of torsional damping present in the bushing placed between the lower shaft and the pinion. This simple intervention proved to be effective for both Front-Wheel-Drive and Rear-Wheel-Drive in the whole range of lateral accelerations and was obviously extended to the unladen configuration. *Figure 11.5* shows the steering rack stroke time history, before and after tuning.

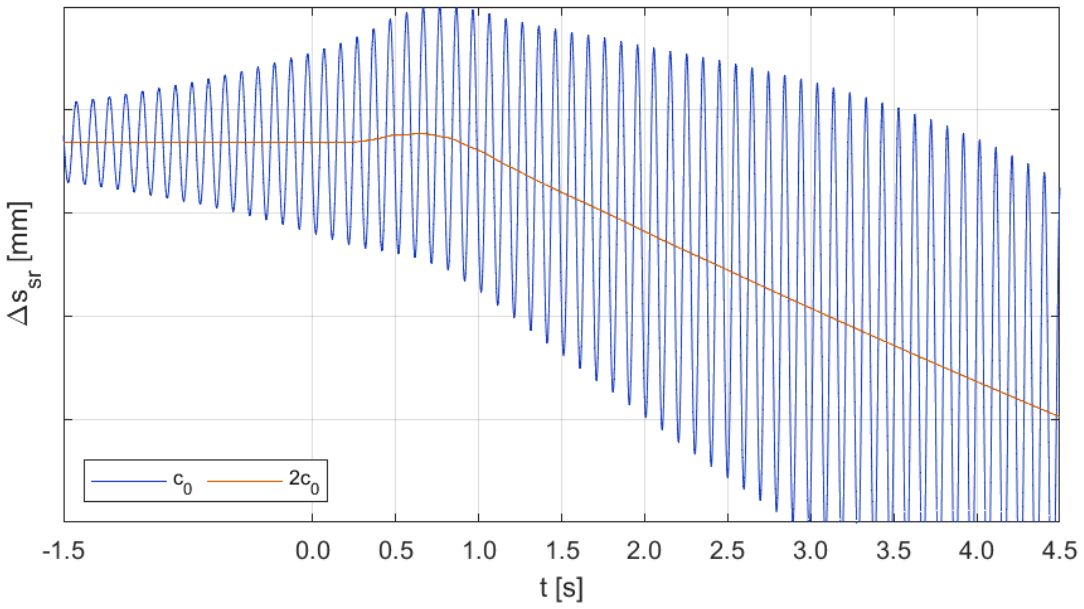

Figure 11.5: Appendix - Throttle-On In-Turn - rack stroke vs time.

11.2.2 Propeller Shaft Inclination

The first problem detected when passing from Rear to Front-Wheel-Drive looked like a torque fluctuation on the front wheels. The huge vibrations were monitored going from the spindles back to the beginning of the driveline, precisely the propeller shaft. Since the whole transmission was interested by this phenomenon, the source was at the beginning, specifically on the universal joint connecting the gearbox to the shaft itself. Provided the infinitely rigid modelling of this component, the problem came from the fact that the shaft had been shortened to connect the gearbox to the differential box on the front axle, but the hardpoints z coordinates were inherited from Rear-Wheel-Drive. Therefore, due to the remarkably shorter length of the new shaft, some greater phase angles on both universal joints were generated and resulted in a torque fluctuation already present at the output of the powertrain, which obviously propagated and reached the front wheels. The problem was solved putting all driveline hardpoints at the same height, so that the propeller shaft was horizontal and parallel to the vehicle longitudinal axis. This solution obviously resulted in a vertical translation of the reference point of connection between the gearbox and the shaft, but it was one of the few really feasible, because the shaft input end was modelled so that it was always oriented parallel to the gearbox. Therefore, even putting a straight shaft inclined from the gearbox down to the differential box, would have provided the same issue. The only alternative was a vertical translation of the straight shaft, so that the initial point of connection with the gearbox was preserved, but this solution would have implied a translation of the differential box as well, to prevent the formation of a phase angle on the output end of the shaft. Anyway, the former approach was preferred, to make the model simpler and maintain the drive shafts coaxial with the front wheels and parallel to the vehicle transversal axis. The new driveline resulted in a clean torque signal and a working Front-Wheel-Drive model. *Figure 11.6* shows the propeller shaft evolution.

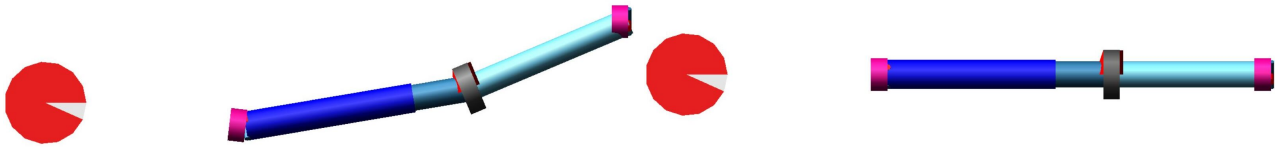

(a) Inclined. *(b) Straight.*

Figure 11.6: Appendix - Front-Wheel-Drive - driveline.

11.2.3 Differential Box Mounting

Another issue detected during the definition of the Front-Wheel-Drive model was the presence of excessive vibrations during Throttle-On In-Turn, which started during the acceleration step and later disappeared. This response was linked to the initial modelling consisting in the differential box mounted to the engine subsystem in three non-aligned points. This approach resulted in great oscillatory phenomena whenever the maneuver was based on a huge raise in the engine rotational speed. Basically, the engine transmitted its undamped vibrations to the differential, which forced the drive shafts to experience the same accelerations, thus affecting the torque supplied to the wheels. The solution consisted in connecting the differential box to the chassis, part of the body subsystem, in three non-aligned points as before. Clearly, the engine vibrations were filtered by the three bushings connecting it to the chassis, making the differential box immune to the propagation of vibrations. This phenomenon was not a problem affecting the model functioning, but it was a symptom of not optimal modelling.

Ringraziamenti

Desidero ringraziare le persone che mi hanno sostenuto durante il mio percorso universitario e supportato nello svolgimento di questa Tesi, che ne rappresenta la naturale conclusione.
Ringrazio il prof. Enrico Galvagno per avermi dato l'opportunità di svolgere questa Tesi e per la disponibilità, tempestività e professionalità manifestate nel corso del suo intero sviluppo.
Ringrazio Angelo Casolo, Daniele Catelani e Mauro Vesco di Hexagon MCS Software per il supporto all'apprendimento di Adams/Car e i preziosi spunti offerti.
Ringrazio l'ing. Vittorio Dal Col per avermi seguito costantemente durante lo svolgimento della Tesi, trasmettendomi la *forma mentis* necessaria per trascendere i risultati delle simulazioni e darvi un significato reale. Ringrazio Lorenzo Architetto, Luigi Bianco, Matteo Castellaneta, Libero Catalano, Francesco Cristiano, Michele De Rosa, Raffaele Garofalo, Marco Menichelli, Efrem Mirolo per la cordialità e gli importanti suggerimenti fornitimi. Ringrazio Iveco Group per avermi procurato il materiale utile allo svolgimento di questa Tesi.
Ringrazio in maniera speciale i miei genitori, che mi hanno sempre dato pieno sostegno e fiducia, mettendomi nelle condizioni migliori per affrontare gli anni al Politecnico di Torino.
Ringrazio infine gli amici incontrati nel corso degli studi per i momenti felici passati insieme e per essere sempre stati al mio fianco, rendendo questa esperienza universitaria indimenticabile.